SUPPLEMENTARY INFORMATION

doi:10.1038/nature10574

SECTION OVERVIEW

SECTION S1: Species distribution modelling

1.1 Introduction

Species distribution models, or SDMs, have been developed over the last three decades to address our incomplete knowledge of species distributions, a challenge described as the "Wallacean shortfall"[1]. While primarily developed to estimate the current distribution of species for which we have incomplete sampling, SDMs have also been heavily utilized over the last decade to forecast species future distributions due to modern climate change[2]. They may also be a promising tool for reconstructing the distribution of species in past time periods[3] for which varying sampling intensity and bias in the fossil record are more significant problems than in the distribution data from current ecological sampling schemes.

Species distribution models are deeply rooted in niche theory[4,5] (see also Soberón[6] for a recent study on niche theory and SDMs) and gradients analysis[7,8]. They link ecological theory and statistics under the principle that species abundance and population performance, which control species distributions, change across environmental gradients[9,10], by relating the distribution of species and the environmental conditions in which they occur in an *n*-dimensional environmental space, in which each dimension is an environmental variable, to statistically describe the environmental niche of a species (or the climatic niche if only climatic variables are used). The modelled species niche can be transferred into geographical space where each grid cell (or unit of space) is assigned specific values of the environmental parameters used to define the species niche. The methodological approach, which transfers the species niche from environmental to geographical space is rooted in the duality between Hutchinson's "niche" and "biotope"[11]. Under climate change, the spatial extent of suitable climatic conditions for a given species can increase or decrease, driving changes in the distribution of that species. For example, a large reduction in the availability of suitable climate conditions would be expected to cause a reduction in a species' realised distribution, thus contributing to a reduction of population size and a potential increase in extinction risk[12].

To relate changes in the megafauna species' (woolly rhinoceros (*Coelodonta antiquitatis*), woolly mammoth (*Mammuthus primigenius*), horse (wild *Equus ferus* and living domestic *Equus caballus*), reindeer/caribou (*Rangifer tarandus*), bison (*Bison priscus/Bison bison*) and musk ox (*Ovibos moschatus*)) distributions against estimates of effective population size from the Bayesian skyride models (see Supplementary Information section S3), we used SDMs to estimate range sizes for each

species through the late Quaternary. In practice, SDMs reconstruct species' geographic distributions by relating species' presence records (in this case, fossil locality data) to a set of environmental predictors (e.g., temperature and rainfall) to map a species' geographic range using a geographic information system (GIS)[13]. Strong enthusiasm for incorporating SDMs in a variety of biological studies has resulted in intense scrutiny of the method's theoretical assumptions[14]. Paramount is recognising the difference between a species' fundamental niche, the full set of conditions in which a species can survive long-term, and the realised niche, the subset of the fundamental niche that is actually occupied at a given time[5] and upon which SDMs are based. SDMs are generated using climatic data[15], but a species' realised niche is also determined by other factors (such as barriers to dispersal). Projecting an SDM onto past or future climate surfaces, as is common in climate change studies, may ignore those limits while assuming a species will exist in all places with favourable climatic conditions, and that the niche is static through evolutionary time—assumptions which need to be explored for many species[14]. Further, combinations of climatic variables with no analogues in other time periods may result in underestimation of a species' ecological and geographic range in past or future projections[16].

Therefore, range size estimates to be compared with the genetic data (results in Fig. 2 in main text) were modelled using only locality and climate data from the same time periods (42, 30, 21 and 6 kyr BP); SDMs from one time period were not projected onto earlier or later periods, and range measurements were restricted to regions for which fossils were used to build the models, rather than all potentially suitable Holarctic area. This approach allowed us to circumvent assumptions regarding climatic niche stasis through time, as well as the effects of dispersal limitations which might have prevented species from reaching areas of otherwise suitable habitat.

1.2 Palaeoclimate data

Late Quaternary climatic conditions are simulated using Atmospheric-Ocean coupled General Circulation Models (hereafter AOGCMs). An AOGCM is a set of equations simulating the dynamics of the ocean and the atmosphere under certain environmental conditions (i.e, CO^2 concentration, ice sheet extent) to provide estimates of past climatic parameters (e.g., rainfall or temperature). Each AOGCM differs slightly in both the absolute values of estimated climatic conditions and in the geographical distribution of those conditions. To assess the effect of AOGCM choice on species' distributions and the subsequent relationship between range size and effective population size, we simulated past climatic conditions using two different AOGCMs: GENESIS2 and HadCM3.

1.2.1 GENESIS2

Four GENESIS2 simulations were used: two for Marine Isotope Stage 3 (MIS 3), one for the Last Glacial Maximum (LGM; ~21 kyr BP) and one for the mid-Holocene (~6 kyr BP). The Marine Isotope Stage 3 (MIS 3) simulations represent the warmer middle part (~42 kyr BP) and colder later part (~30 kyr BP) of MIS 3. Carbon dioxide levels were specified at 200 ppm for the MIS 3 and LGM simulations[17] and 280 ppm for the mid-Holocene simulation[18]. Sea surface temperatures (SSTs) for the MIS 3 and LGM simulations were taken primarily from CLIMAP[19], with modifications from GLAMAP-2000 and other sources[20]. SSTs for the mid-Holocene simulation were prescribed at present-day values[21]. In all cases, insolation was calculated using orbital parameters[22,23]. All simulations were spun up to equilibrium; results are 10-year averages.

Comparison of GENESIS2 model output to proxy data shows that temperatures in Europe are accurate to within ± 1°C for the mid-Holocene and ± 2°C for the LGM[24]. For Oxygen Isotope Stage 3, [25] found that GENESIS2 temperatures in southern Europe agree well with proxy data but were 3-4°C too warm in Northern Europe. Comparison of present day GENESIS2 model output with observations suggests that variability in Europe can be extrapolated to all of northern Eurasia and North America[26]. We are unaware of any GENESIS2 model-data comparisons for palaeoprecipitation. However, for present-day northern Eurasia and North America the model is accurate to within ± 1 mm day^{-1} when compared to observations[26]. Atmospheric carbon dioxide boundary conditions are well-constrained[27,28].

1.2.2 HadCM3

A second set of climate model outputs for the same Quaternary periods, the warmer middle part (~40 kyr BP) and colder later part (~32 kyr BP) of MIS 3, LGM and the Mid-Holocene were derived from the Hadley Centre Coupled Climate Model Version 3 (HadCM3). The simulations form part of the ensemble presented in [29]. The particulars of HadCM3 are well documented[30]. HadCM3 was one of the first coupled atmosphere-ocean climate models which required no flux corrections, even for simulations of a thousand years or more[31]. The climate model consists of a linked atmospheric model, ocean model and sea ice model. In HadCM3 the horizontal resolution of the atmosphere model is 2.5 degrees latitude by 3.75 degrees longitude. This gives a grid spacing at the equator of 278 km in the north-south direction and 417 km east-west and is approximately comparable to a T42 spectral model resolution. The atmospheric model consists of 19 layers. The spatial resolution over the ocean in is 1.25˚ × 1.25˚ and the model has 20 layers. The atmospheric

model has a time step of 30 minutes and includes a radiation scheme that can represent the effects of minor trace gases[32]. A parameterization of simple background aerosol climatology is also included[33]. The convection scheme is that of [34]. A land-surface scheme includes the representation of the freezing and melting of soil moisture. The representation of evaporation includes the dependence of stomatal resistance on temperature, vapour pressure and CO^2 concentration[35].

The ocean model includes the use of the Gent-McWilliams mixing scheme[36]. There is no explicit horizontal tracer diffusion in the model. The horizontal resolution allows the use of a smaller coefficient of horizontal momentum viscosity leading to an improved simulation of ocean velocities. The sea ice model is a simple thermodynamic scheme and contains parameterizations of ice drift and leads (Polynyas[37]).

For the MIS 3, LGM and mid-Holocene, orbital parameters are taken from [23]. Atmospheric concentrations of CO_2 were taken from the Vostok ice core record[38] and CH_4, and N_2O were taken from EPICA[39]. All ice-core data were on the same EDC3 timescale[40].

Ice-sheet reconstructions are developed from the ICE5G model[41], which includes a detailed evolution of the ice thickness, extent and continental isostatic rebound for the whole period from the LGM to the modern at 500-year intervals. Using standard linear interpolation techniques, this dataset was used to calculate, at the scale of the climate model, the total continental elevation (including the direct thickness of the ice sheets plus the effects of isostatic adjustment), bathymetry (including isostatic changes), ice-area extent, and land sea mask for the LGM and mid-Holocene. To ensure consistency with pre-industrial boundary conditions an anomaly-based method was used to calculate palaeogeographic boundary conditions. In this method, for anomalies of a particular time-slice, palaeogeography minus pre-industrial ICE-5G data are then added to our model pre-industrial geographical boundary conditions. The geographical extent and heights of the major ice sheets prior to the LGM were based on [42], which included a calculation of the pre- and post-glacial ice. Singarayer and Valdes[29] used the SPECMAP[43] record of $d^{18}O$ history to constrain the evolution of the volume of land ice from the last interglacial up to the LGM.

Each simulation was integrated for approximately 200 years, a sufficient period of time to bring the surface climatology to equilibrium, with the final 30 years used to calculate the required climatological mean. The version of HadCM3 used does not include interactive vegetation, so all simulations use the same pre-industrial vegetation boundary condition. Similarly, aerosol loading in the model is unchanged and does not account for changes in dust during the cycle.

Using HadCM3, we obtain reasonable estimates of the global temperature glacial/interglacial range as well as trends in polar regions, although the magnitude of change at high latitudes is underestimated, as other similar models have found for the LGM[29]. HadCM3 produces a pattern of cooling for the LGM which are broadly consistent with the findings from simpler models and palaeoclimatic data[44]. HadCM3 performance in simulating both the LGM and mid-Holocene have been evaluated and are recognised as being either good or generally comparable with other climate models run for the same time intervals[45].

1.2.3 Palaeoclimate variables

From both AOGCM datasets, three variables (Supplementary Figure S1.1) were selected to describe the potential distribution of each species: mean temperature of the coldest month (°C), mean temperature of the warmest month (°C), and annual precipitation (mm). Temporal trends in these climatic variables are similar between the two AOGCMs (Supplementary Figure S1.2). Palaeoclimatic simulations for GENESIS2 are at a 2×2-degree spatial resolution; palaeoclimatic simulations for HadCM3 are resampled at a 2×2-degree resolution. This conservative variable set was selected to balance the number of species occurrences versus the number of climatic variables used to calibrate species' realised climatic niches. Using many climatic variables to model the potential distribution of a species using few presence records (e.g., fossil localities) is likely to lead to model over-fitting, yielding a misrepresentation of the geographical distribution of the modelled species[46]. Given the constraint of using only a small number of climatic variables, we aimed to capture the upper and lower thermal limits of each species, as well as a moisture variable. Previous applications of SMDs have used similar limited sets of climatic variables as predictors of megafauna distributions[3]. All figures presented in the main text were generated using climate variables from GENESIS2.

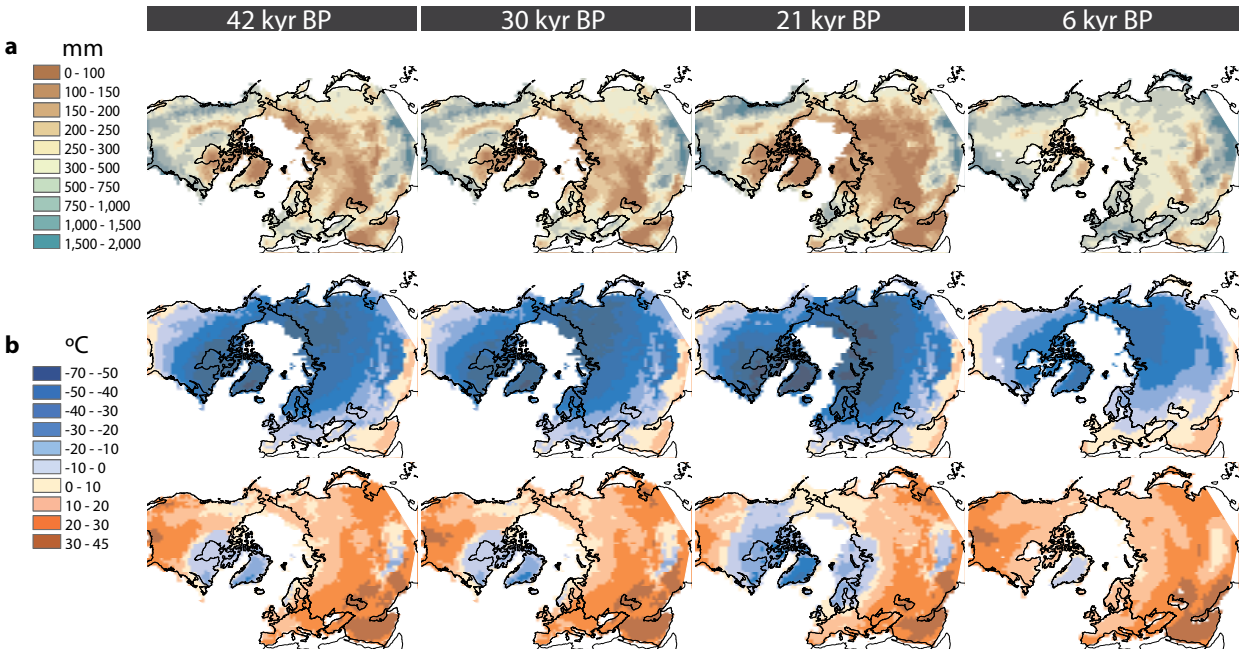

Supplementary Figure S1.1. Palaeoclimatic data (GENESIS2) for annual precipitation (mm), average temperature of the warmest month (°C), average temperature of the coldest month (°C) and the fossil record were used to estimate species potential ranges.

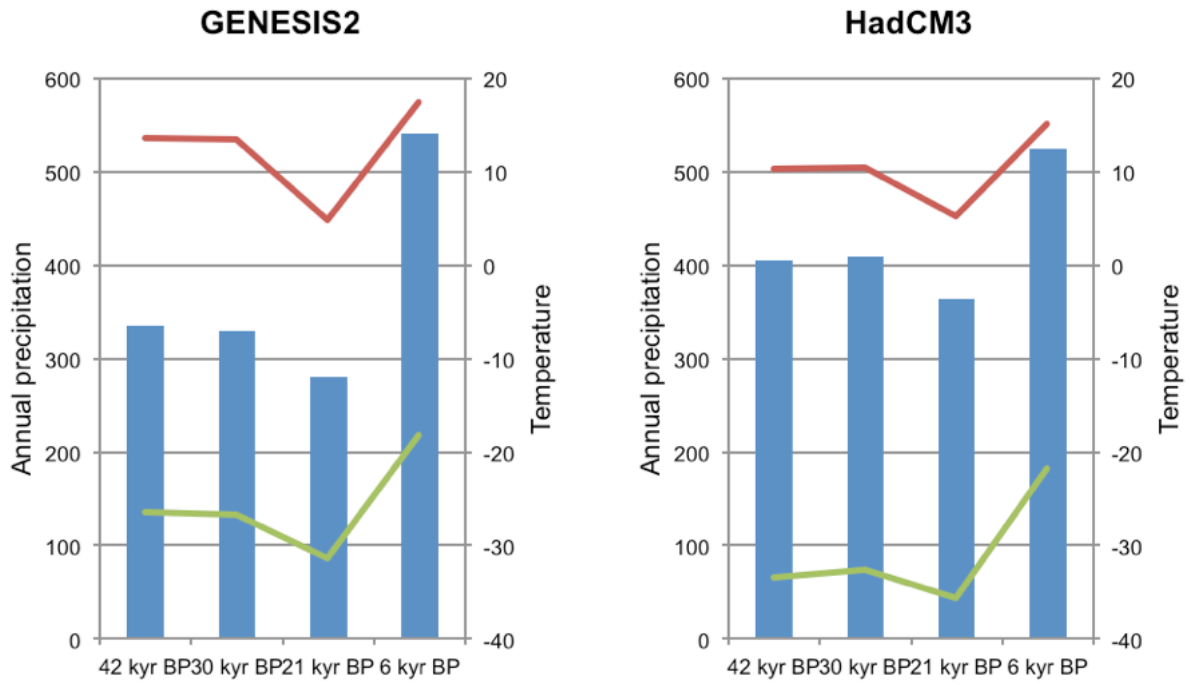

Supplementary Figure S1.2. Average climatic temporal trends across the Holartic based on GENESIS, left, and HadCM3, right, AOGCMs. Green (lower) lines indicate mean temperature of

the coldest month (°C), red (upper) lines indicate mean temperature of the warmest month (°C), and blue bars indicate annual precipitation (mm).

1.3 Megafauna locality data

For each species, ^{14}C-dated fossil localities from Eurasia and North America were obtained for the following calendar time intervals: 45–39, 33–27, 24–18 and 9–3 kyr BP. Radiocarbon dates (uncalibrated ^{14}C dates) were calibrated into calendar years using the IntCal09 calibration curve[47] using the OxCal 4.1 online calibration resource (https://c14.arch.ox.ac.uk). The 829 fossil localities included data from sequenced specimens (Supplementary TableS6.2-6.4), supplemented with fossil localities from the literature (Supplementary Table S6.1); The majority of the 829 localities used for the Species Distribution Models (SDMs) were compiled from synthetic works, rather than the original papers in which the dates were first presented, so we were unable to evaluate our data by fossil context, dated material or dating method[48]. However, the vast majority (98%) of the 829 localities used were from directly dated (standard or AMS) animal remains; thus, if we assume that most dates were from bone collagen, dung, hide or hair, we anticipate that most of our directly dated samples would rank an 11 or 12 on the scale proposed by [48] . Given the breadth of the time bins used—6,000 calibrated years—the difference between dating methods should have little impact on our results, as this is significantly greater than the differences between conventional and AMS dates observed by [48].

The list of localities is not and was not intended to be exhaustive, but was meant to cover at least those regions with genetic data to enable comparison of the estimates of potential range size and estimated effective population size. Therefore, modelled species ranges are not intended to fully represent past species distributions in great detail, and may under-represent the species' actual range in areas for which we have little data. Fossil localities are indicated in Supplementary Fig. S1.3. Data were only included where the literature contained explicit geographic coordinates or detailed site descriptions which could be located at http://toolserver.org/~geohack/. As each set of geographical coordinates relates to a specific dated fossil, localities are duplicated where more than one dated fossil has been found.

For woolly mammoth, all known fossils dating from 9–3 kyr BP are from Wrangel Island[49,50], with the exception of one known specimen from St. Paul Island[51]. This fossil distribution, consisting of two unique localities, is insufficient data with which to generate species distribution models, and so

no distribution is presented for the woolly mammoth at 6 kyr BP, even though the species was not yet extinct.

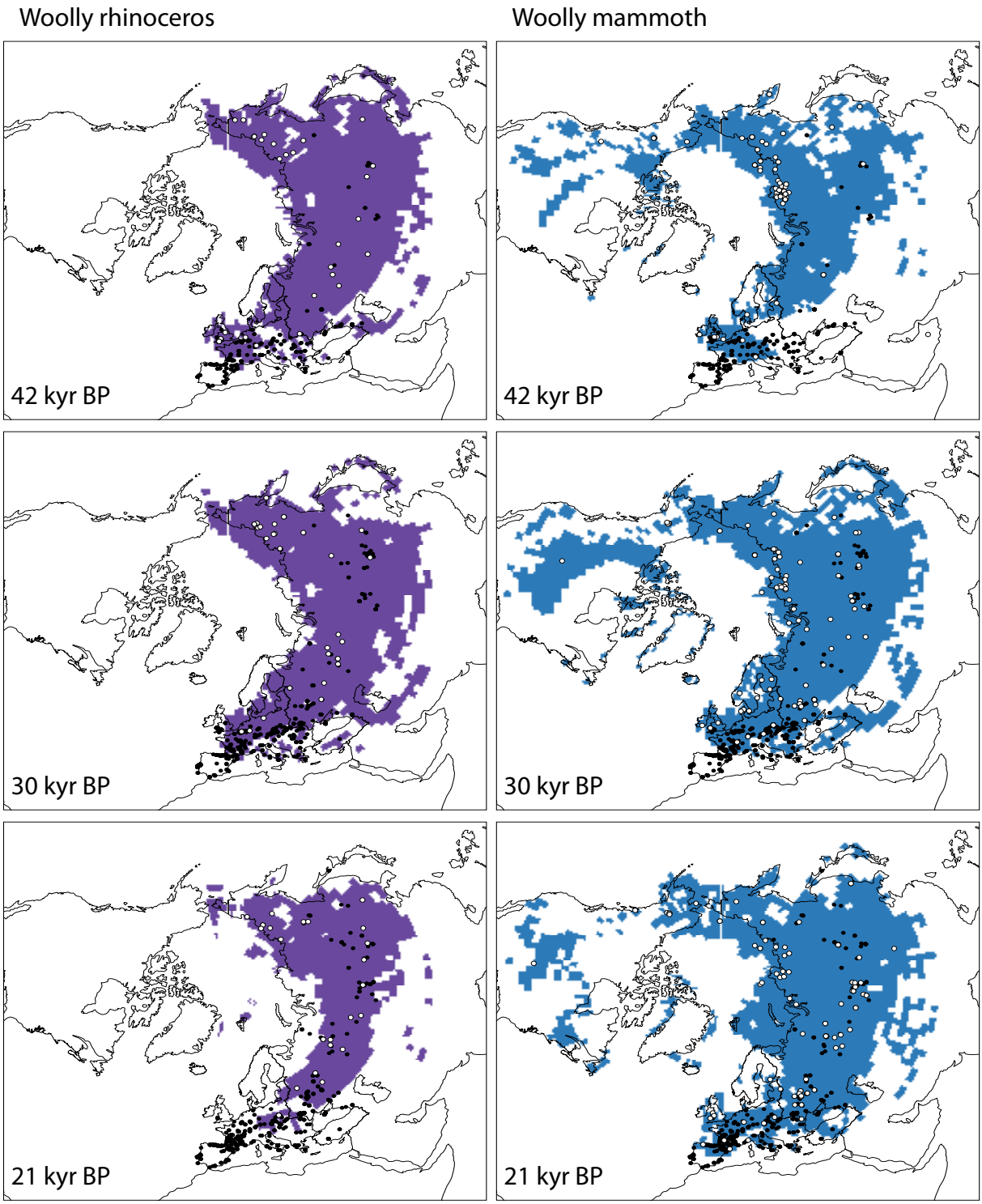

Supplementary Figure S1.3. Megafauna potential range at 42, 30, 21 and 6 kyr BP estimated from palaeoclimatic data (GENESIS2) and dated fossils for each species, represented by white dots.

Range measurements were restricted to regions for which fossils were used to build the models, rather than all potentially suitable Holarctic area. Contemporaneous Palaeolithic human sites for each period are represented by black dots. No or too few fossils were available for woolly rhinoceros and mammoth to estimate their ranges at 6 kyr BP.

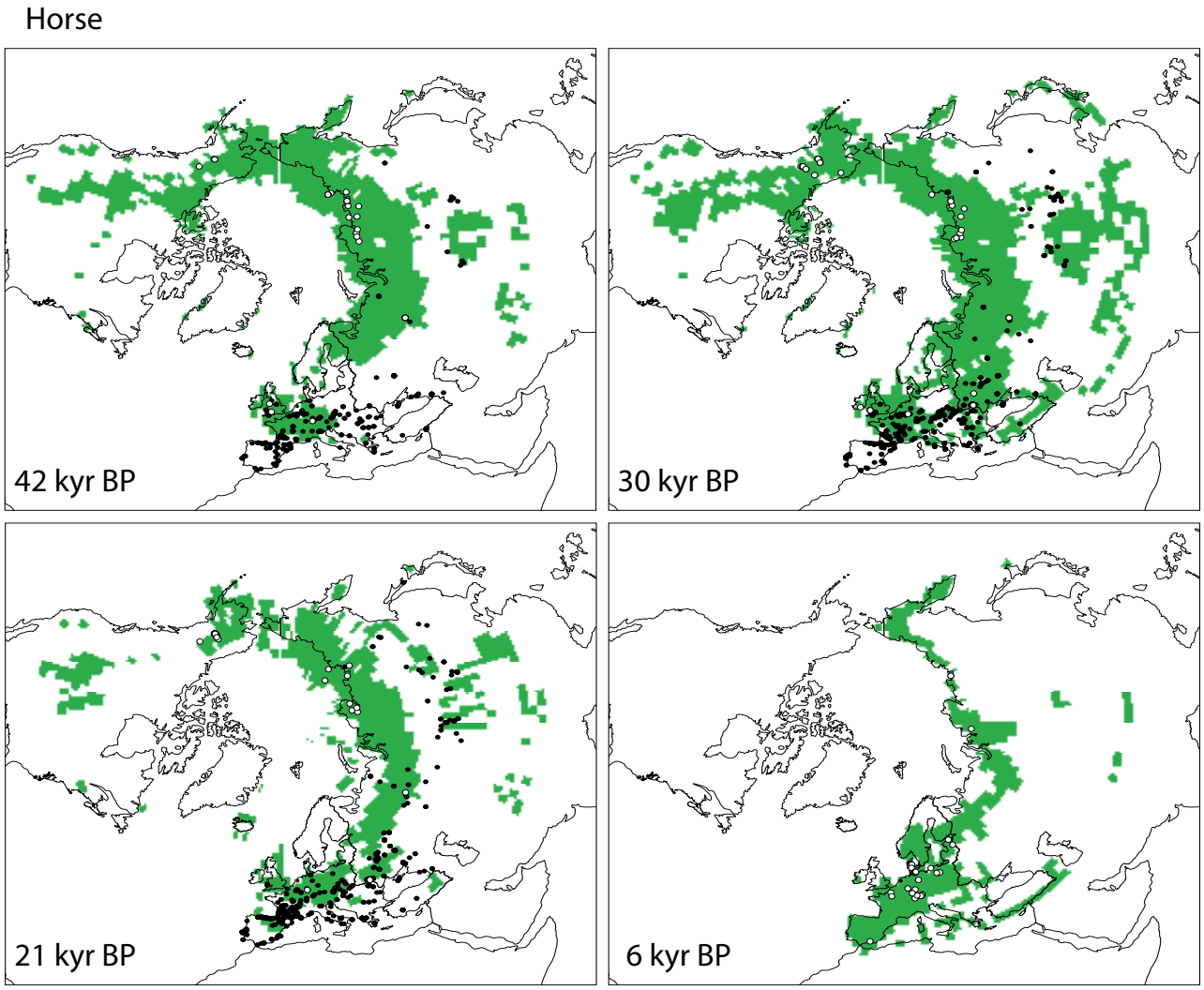

Supplementary Figure S1.3. Continued.

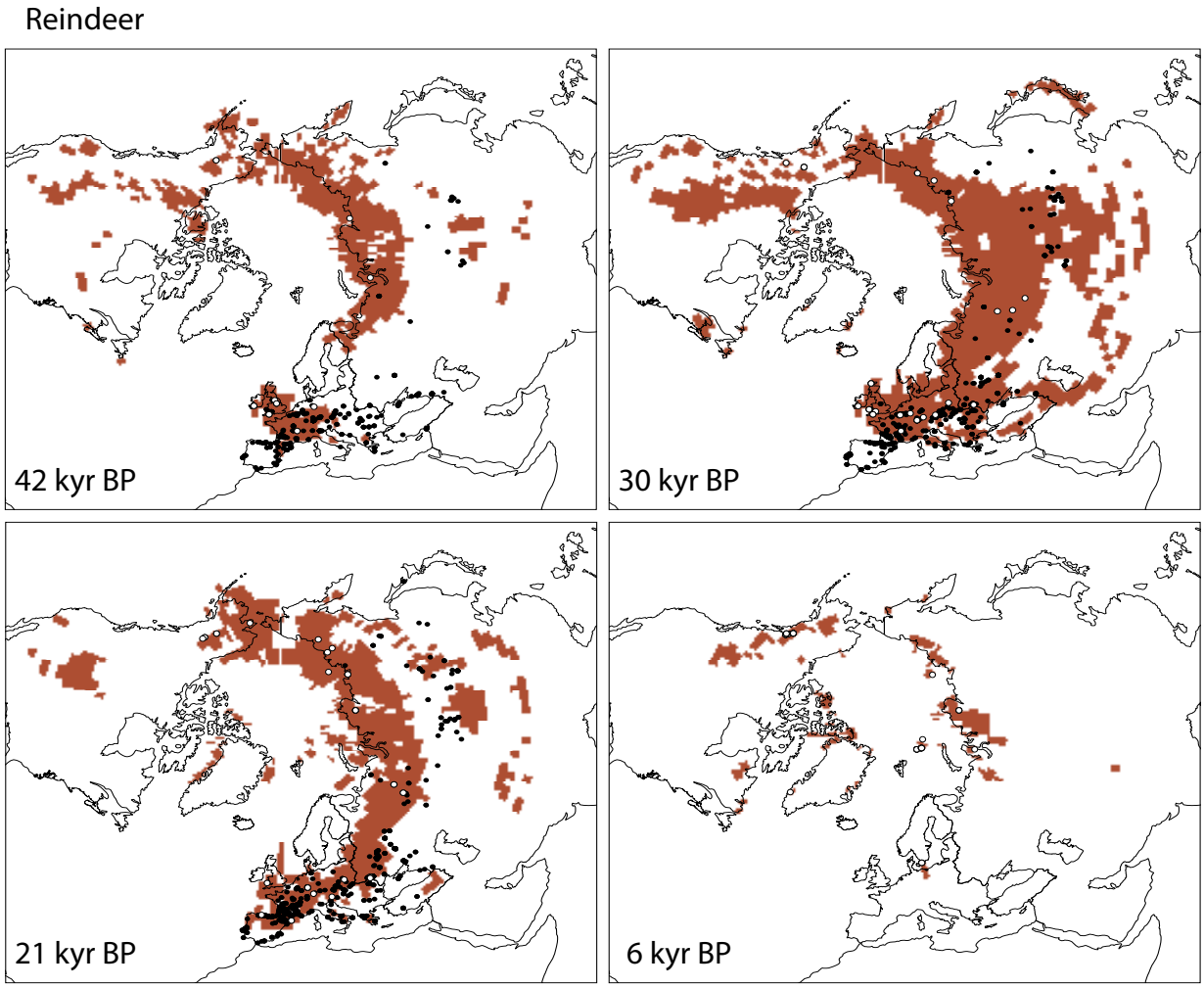

Supplementary Figure S1.3. Continued.

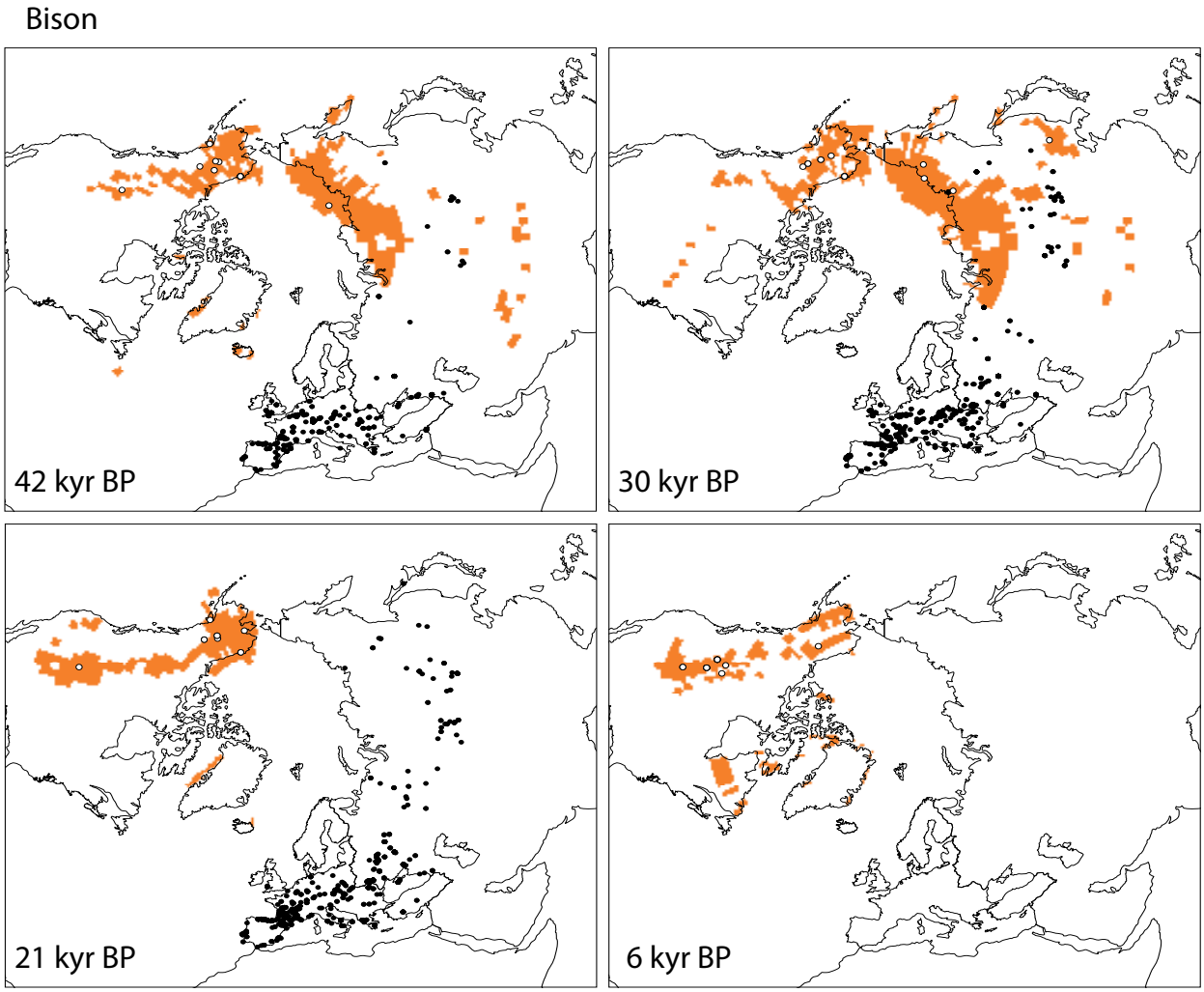

Supplementary Figure S1.3. Continued.

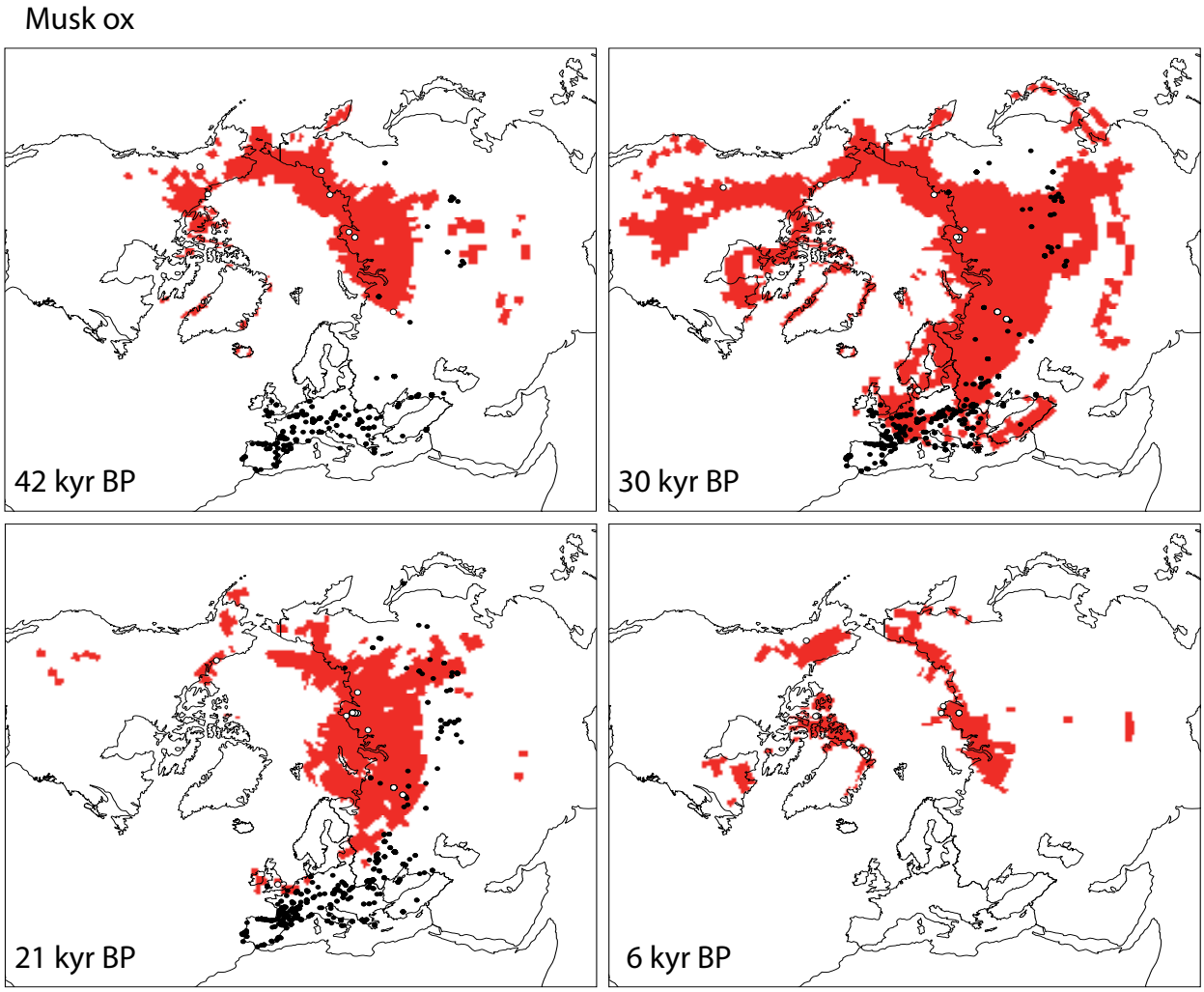

Supplementary Figure S1.3. Continued.

1.4 Species distribution modelling

1.4.1 Model algorithms

Species distribution model (SDM) projections are sensitive to the different statistical techniques used to describe and project species' potential ranges. Mahalanobis Distance (MD)[52], a strict presence-only method, was used to model the 42, 30, 21 and 6 kyr BP distributions of each species. MD is a simple envelope technique that provides a strict presence-only measure of environmental distance, which is calculated in relation to an optimum climatic point, defined as the centroid for all occurrence points in the total climatic space. The distance between this "optimum" and the observed climatic values for each species presence is inverse to the suitability of the climate at that site. MD produces an ellipsoidal envelope around the climatic optimum space by taking into account the covariance among climatic variables.

While a variety of methods are available for modelling species distributions, certain characteristics of the fossil record help to narrow the range of algorithms from which to select. First, the fossil record provides information about the presence of species, but not about their absence, and so presence-absence algorithms must be discarded. Other well-known, more complex algorithms such as GARP[53] or Maxent[54] could be used because they generate pseudo-absences against which to test the models. However, different procedures for calculating pseudo-absences can yield significantly different modelled species ranges[55,56]. In addition, bias in the fossil record is not simply a result of sampling effort, as with extant species, but of unevenly distributed geomorphological conditions affecting the fossilisation and persistence of remains through time, making selection of the study area on which to calculate pseudo-absences far more challenging for fossil data than for extant species for which the extent of the distribution is often known to some degree[55]. After these methods are discarded, the remaining suitable algorithms are restricted to simple presence-only methods based on environmental distances to a climatic optimum, which have been shown to handle bias in the fossil record better than more complex algorithms[57]. Specifically, MD has been shown to perform better than other presence-only methods in a recent comparative study[58]. It has been successfully used for palaeobiology studies[3,57,59] and is specifically recommended[57] for modelling potential species distributions using the fossil record.

1.4.2 Model implementation and performance

Species' distributions used to estimate range size (see below) were modelled using only locality and climate data from the same time periods (42, 30, 21 and 6 kyr BP). A minimum of five dated fossil localities per species/time period were used to build the models[60] (Supplementary Table S1.1). Modelling was implemented using the openModeller cross-platform modelling interface[61]. Each species/time period was modelled with both methods using all available locality data to build the model using both GENESIS2 and HadCM3.

To assess the impact of using a limited subset of the known fossil record on model performance for each species, we performed ten independent model runs in which a different randomly selected 75% of the data were used to build the model and 25% were used to test it each time. This evaluation does not assess the accuracy of model predictions—independent evaluation data (e.g., genetic data or additional fossils) would be required for this purpose. Rather, it provides a measure of internal consistency among repeated runs. Model performance was assessed using the Area Under the (Receiver Operating Characteristic) Curve (AUC; see [62] for a review on the advantages and disadvantages of using the AUC as a performance measure). Scores >0.75 are typically considered adequate for species distribution modelling[63]. Random sub-set model runs were performed using GENESIS2. Species distribution models yielded consistently high AUC values under testing, with only two species/time period yielding a coefficient of variation in AUC greater than 5% (bison and musk ox, 42 kyr BP; Supplementary Table S1.2). This suggests that model performance was relatively robust.

Supplementary Table S1.1. Total number of samples used to build the SDM for each species/ time period. Some localities had multiple dated samples, and the number of unique localities is given in parentheses.

	42 kyr BP	30 kyr BP	21 kyr BP	6 kyr BP
Woolly rhinoceros	35 (29)	34 (28)	27 (24)	n/a
Woolly mammoth	78 (50)	112 (77)	97 (78)	n/a
Wild horse	35 (21)	42 (29)	53 (24)	32 (26)
Reindeer	16 (10)	33 (23)	35 (12)	46 (18)
Bison	15 (8)	16 (9)	10 (7)	15 (7)
Musk ox	8 (7)	25 (10)	49 (10)	16 (12)

Supplementary Table S1.2. AUC scores for ten model runs using a unique 75% and 25% of the data for building and testing the model, respectively (GENESIS2). Mean AUC, standard deviation and coefficient of variation (CV) are indicated.

	Woolly rhinoceros				**Woolly mammoth**			
	42 kyr BP	30 kyr BP	21 kyr BP	6 kyr BP	42 kyr BP	30 kyr BP	21 kyr BP	6 kyr BP
run01	0.97	0.95	0.97	n/a	0.98	0.97	0.95	n/a
run02	0.96	0.97	0.97	n/a	0.98	0.98	0.96	n/a
run03	0.97	0.95	0.98	n/a	0.97	0.95	0.97	n/a
run04	0.94	0.97	0.98	n/a	0.95	0.96	0.96	n/a
run05	0.96	0.94	0.97	n/a	0.94	0.96	0.97	n/a
run06	0.96	0.96	0.98	n/a	0.9	0.96	0.96	n/a
run07	0.95	0.97	0.96	n/a	0.97	0.95	0.98	n/a
run08	0.97	0.98	0.98	n/a	0.92	0.97	0.95	n/a
run09	0.93	0.97	0.98	n/a	0.94	0.97	0.94	n/a
run10	0.96	0.97	0.99	n/a	0.98	0.96	0.95	n/a
Mean	0.96	0.96	0.98	n/a	0.95	0.96	0.96	n/a
StDev	0.01	0.01	0.01	n/a	0.03	0.01	0.01	n/a
CV	1.40%	1.30%	0.86%	n/a	2.93%	0.99%	1.25%	n/a

	Wild horse				**Reindeer**			
	42 kyr BP	30 kyr BP	21 kyr BP	6 kyr BP	42 kyr BP	30 kyr BP	21 kyr BP	6 kyr BP
run01	0.98	0.97	0.98	0.97	0.98	0.98	0.96	0.98
run02	0.99	0.98	0.94	0.99	0.96	0.97	0.98	0.98
run03	0.99	0.98	0.96	0.99	0.95	0.98	0.94	0.98

run04	0.98	0.98	0.98	0.99	0.99	0.98	0.98	1
run05	0.99	0.96	0.99	0.98	0.95	0.91	0.98	1
run06	0.98	0.97	0.96	0.96	0.96	0.97	0.97	0.99
run07	0.99	0.96	0.95	0.98	0.99	0.98	0.97	0.99
run08	0.97	0.97	0.97	0.96	0.99	0.97	0.99	0.98
run09	0.99	0.97	0.99	0.99	0.94	0.98	0.96	0.98
run10	0.99	0.97	0.96	0.99	0.98	0.97	0.97	0.99
Mean	0.99	0.97	0.97	0.98	0.97	0.97	0.97	0.99
StDev	0.01	0.01	0.02	0.01	0.02	0.02	0.01	0.01
CV	0.72%	0.76%	1.74%	1.27%	1.97%	2.20%	1.46%	0.83%

	Bison				**Musk ox**			
	42 kyr BP	30 kyr BP	21 kyr BP	6 kyr BP	42 kyr BP	30 kyr BP	21 kyr BP	6 kyr BP
run01	0.96	0.98	0.99	0.96	0.99	0.98	1	1
run02	1	0.99	0.94	0.91	0.97	0.98	0.99	1
run03	0.94	1	0.93	0.96	0.82	0.98	0.99	0.99
run04	0.82	0.99	0.87	0.95	0.98	0.99	0.99	0.93
run05	0.94	1	0.98	0.91	0.94	0.98	0.96	0.99
run06	0.95	1	0.94	0.96	0.83	0.98	0.95	0.97
run07	1	0.99	0.99	0.96	0.99	0.98	1	0.99
run08	1	0.98	0.98	0.94	0.96	1	0.94	0.98
run09	0.83	1	1	0.96	0.96	0.99	0.95	0.99
run10	0.93	0.89	0.98	0.99	0.97	0.99	0.99	0.99
Mean	0.94	0.98	0.96	0.95	0.94	0.99	0.98	0.98
StDev	0.06	0.03	0.04	0.02	0.06	0.01	0.02	0.02
CV	**6.92%**	3.39%	4.17%	2.58%	**6.69%**	0.72%	2.38%	2.09%

1.4.3 Measuring range size

To calculate modelled range size for each species/time period, the continuous suitability values mapped by openModeller were converted into deciles and the upper decile (suitability >0.9), the area of most suitable climate conditions, was used to map modelled range size (following a similar approach to [3]). Assuming that only the areas with the highest suitability constituted the potential range is a conservative approach which should prevent overestimation of range sizes. Because all species were not present throughout the Holarctic for all periods, the Holarctic was divided into 3 regions: Europe, Asia and North America. Modelled ranges were cropped to exclude non-land areas and to match those regions for which fossil localities were used to generate the models (e.g., if no fossils were available from North America for a given period, as for the woolly rhinoceros, climatically suitable range from North America was excluded from the range size estimate). This ensured that aDNA and species distribution modelling methods were testing hypotheses relating to

the geographic space actually occupied by each species at a given time as indicated by the fossil record. Cropping was conducted in R[64] using the package sp[65]. Species ranges were then measured (in square kilometres) using IDRISI Taiga (Clark Labs, Worcester, MA, USA).

Distributions for the six megafauna herbivores, reconstructed using SDMs for the periods 42, 30, 21 and 6 kyr BP, contracted in size from 30 kyr BP to the present for all species, although the severity of contraction varies substantially among taxa (Supplementary Table S1.3, Supplementary Fig. S1.3). While the absolute area of species ranges modelled using GENESIS2 and HadCM3 differ, as expected, trends of range expansion and contraction through time are consistent between AOGCMs (Supplementary Figure S1.4). Estimates of range size based on HaDCM3 also shows a significant correlation with estimated effective population size (Section S4; Supplementary Figure S4.3).

Supplementary Table S1.3. Area of potential species' range (climatic suitability ≥ 0.9.), rounded to the nearest 50,000 km^2.

Potential range modelled with GENESIS2				
	42 kyr BP	30 kyr BP	21 kyr BP	6 kyr BP
Woolly rhinoceros	34,900,000	32,600,000	19,350,000	n/a
Woolly mammoth	26,050,000	42,900,000	39,500,000	n/a
Wild horse	19,400,000	26,250,000	16,000,000	9,200,000
Reindeer	12,250,000	26,250,000	17,800,000	2,750,000
Bison	6,800,000	8,700,000	3,700,000	2,950,000
Musk ox	12,300,000	27,750,000	22,550,000	9,250,000

Potential range modelled with HadCM3				
	42 kyr BP	30 kyr BP	21 kyr BP	6 kyr BP
Woolly rhinoceros	19,400,000	18,600,000	12,650,000	n/a
Woolly mammoth	12,150,000	25,900,000	22,600,000	n/a
Wild horse	15,450,000	24,000,000	10,650,000	4,100,000
Reindeer	6,950,000	22,350,000	10,250,000	4,900,000
Bison	11,800,000	14,900,000	1,850,000	3,350,000
Musk ox	6,650,000	12,900,000	9,200,000	6,150,000

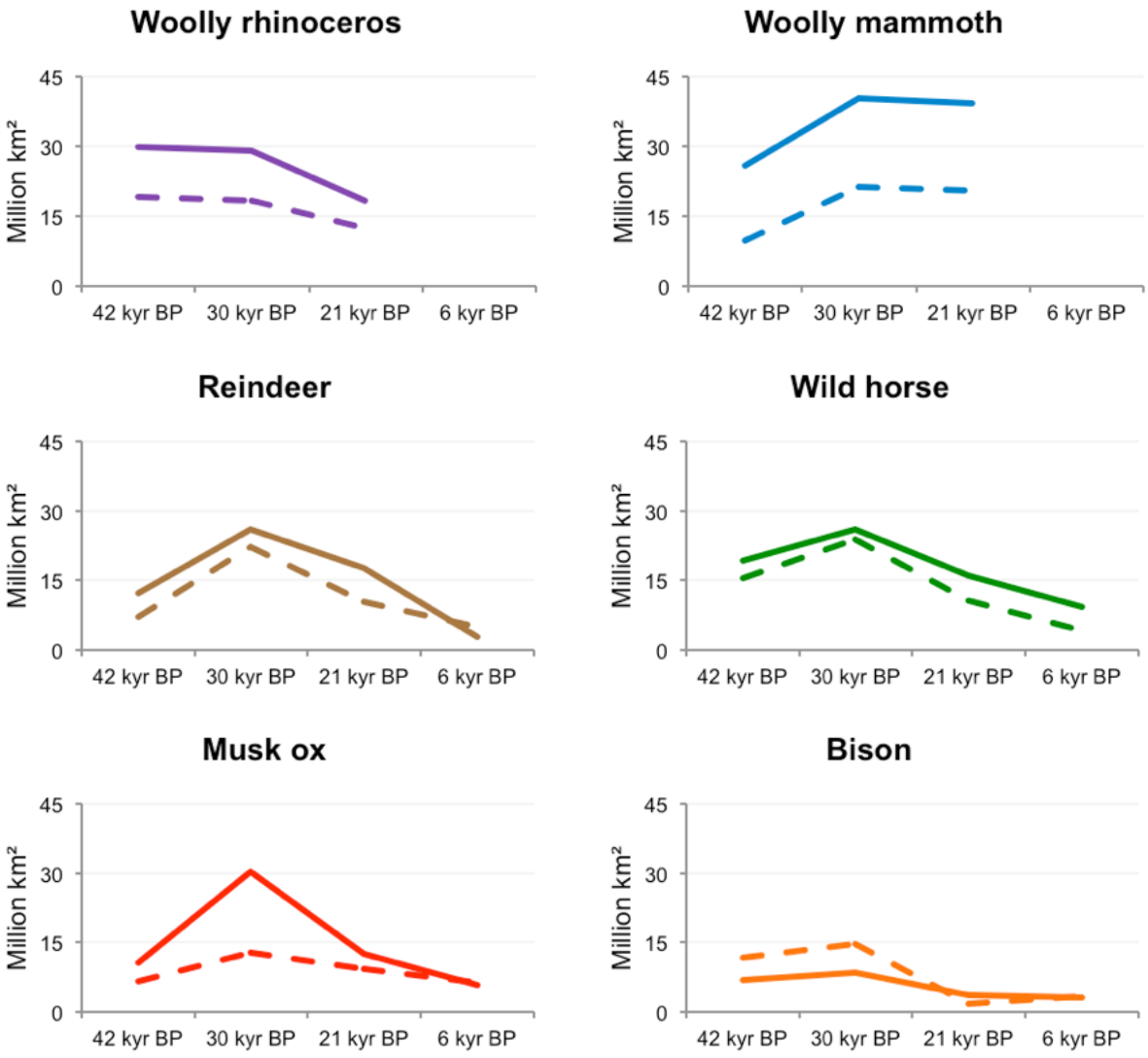

Supplementary Figure S1.4. Estimated potential range size in km^2 for all 6 species at 42, 30, 21 and 6 kyr BP, modelled using the GENESIS2 (solid line) and HadCM3 (dotted line) AOGCMs. While the absolute area of species ranges differ, temporal trends in range size are consistent between AOGCMs.

1.4.4 Sensitivity of range size estimates to fossil record uncertainty

Species Distribution Models are sensitive to the initial conditions used to calibrate the models. When modelling the past distributions of extinct and extant species, initial conditions include the historical climatic data and the distribution of the fossil record. Above we address the effect of using different AOGCMs for estimating range size, but the fossil record is an incomplete and often biased representation of the past distribution of species which can also bias our results Therefore, to incorporate this uncertainty in the estimation of potential range size into the correlation between effective population size and geographic range size (Supplementary Information section S4) we performed ten additional independent model runs using GENESIS2, in which a different randomly selected 90% set of the localities was used to build the model each time. Modelled ranges from the 90% random sub-set runs were cropped and measured as described in S1.4.2. We found a positive correlation between changes in the size of available habitat and genetic diversity for the four species for which we have range estimates spanning all four time-points (although the correlation was not statistically significant for reindeer: $p = 0.101$; Supplementary Information section S4).

1.4.5 Sensitivity of range sizes to radiocarbon dating error

Radiocarbon dates associated with indirectly-dated fossils are considered less reliable than those for which the specimen of interest itself is dated[48] although in some cases (e.g., reindeer, 21 kyr BP, Spanish localities) indirectly-dated fossils can represent important extensions of a species' geographic distribution for which directly-dated fossils are unavailable. Furthermore, for reindeer, ten indirectly-dated specimens from North America were included in the analysis, as the published DNA sequences from the samples[66] were included in the genetic analysis. To examine whether the incorporation of 16 indirectly-dated fossils (ten reindeer, six bison) is likely to have influenced the detected trends in range size through time, we re-ran the models for these species excluding the indirectly-dated specimens (from Supplementary Tables S6.1 and S6.4) using GENESIS2. While the absolute area of species ranges differ, as in the random sub-set model runs, consistent temporal trends of range expansion and contraction through time are detected with these 16 specimens included and excluded (Supplementary Figure S1.5). Incorporating these new measurements into the correlation analysis did not affect the strength of the correlation between range size and effective population size, which was still significant (Supplementary Table S4.).

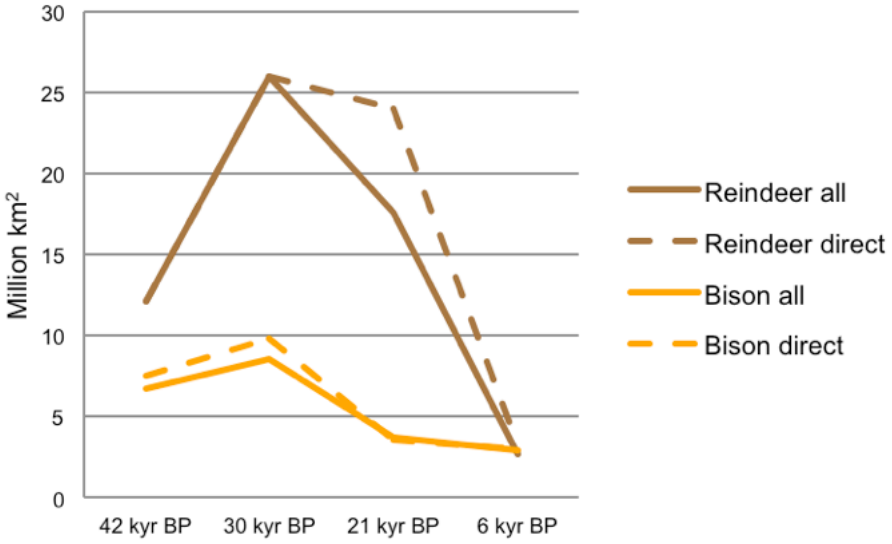

Supplementary Figure S1.5. Estimated potential range size in km^2 for reindeer and bison at 42, 30, 21 and 6 kyr BP, modelled using all (solid line) and only directly-dated (dotted line) fossil localities (GENESIS2). While the absolute area of species ranges differ, temporal trends in range size are consistent between fossil datasets used.

1.5 Human presence within modelled ranges

To calculate the density of Palaeolithic human fossil sites (bones, artefacts and charcoal) within the modelled geographic range for each species/time period, human fossil localities from the calendar time intervals 45–39, 33–27 and 24–18 kyr BP were overlaid on species' modelled ranges (GENESIS2) for 42, 30 and 21 kyr BP, respectively. Human radiocarbon data were derived from the INQUA Palaeolithic Radiocarbon Database v. 11 for Europe[67] and from [68] for Siberia. Details on these radiocarbon determinations and their selection can be found in the associated citations and in Supplementary Information section S5. The most recent period (6 kyr BP) was excluded because localities were only compiled for >9 kyr BP in some data sets.

Palaeolithic human localities (Supplementary Fig. S1.3) were mapped on top of SDM results in IDRISI Taiga to identify grid cells within each species' measured range in which humans were present. Grid cells were then converted into area (km^2) to calculate the extent of each species' range occupied by humans (Supplementary Fig. S1.6).

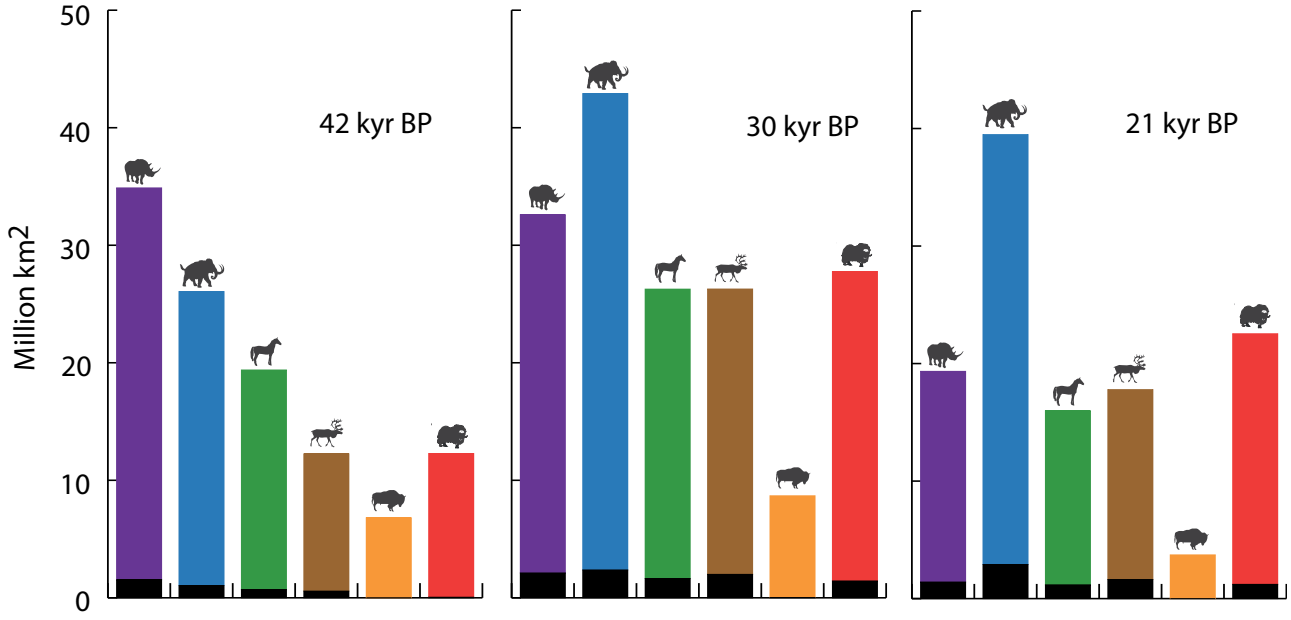

Supplementary Figure S1.6. Overlap (km^2) between megafauna and humans at 42, 30 and 21 kyr BP. Palaeolithic human localities were mapped on top of species ranges (GENESIS2), and grid cells in which humans were present were converted into area to calculate the extent of each species' range occupied by humans. Column height indicates estimates of megafauna range size; the black portion represents area of human/megafauna overlap.

1.6 Discussion

The key goal for this portion of our study was to relate changes in the megafauna species distributions to estimates of effective population size from the Bayesian skyride models (see Supplementary Information section S4). We used SDMs to estimate the potential range size for each species at four periods for which we have palaeoclimatic data, using a subset of the fossil record. The fossil list was not intended to be an exhaustive survey of all known locations for each species; rather, we targeted the fossil record for data within the same regions for which genetic data were sampled, so that SDMs and Bayesian skyride models could be explicitly compared. Modelled distributions are therefore unlikely to capture the full known distributions for some species (e.g., bison).

We have taken a conservative approach to modelling the distributions of each species; by using only contemporaneous data to build each model, rather than projecting a species' modelled climatic niche from one period to the next, we are able to avoid two potential pitfalls for SDMs: species-

climate equilibrium and climatic niche stability through time[14]. Species-climate equilibrium is the assumption that a species is in equilibrium with its climate, or that a species will exist in all places in which climatic conditions are favourable for its long-term survival[69]. However, many factors other than climate shape a species' ecological niche; these include barriers to dispersal, interactions with other species, and historical contingency[70], and any of these factors may result in a species' distribution being out of equilibrium with its climatic niche. For example, moist conditions on the Bering land bridge have been implicated as a barrier to dispersal to steppe-tundra species such as the woolly rhinoceros, which was adapted to drier conditions[71], even though suitable habitat likely existed on both sides of the strait. Likewise, niche stability through time is the assumption that a species maintains the same climatic niche, with no niche evolution (e.g., behavioural or physiological adaptation) taking place between periods of interest. While this assumption is likely to be true for some species, resulting in either extinction or tracking of suitable conditions under periods of climate change, it will not hold true for all species. Although our fossil data are limited for some species for certain periods, we maintain that building a discrete SDM for each time period, rather than projecting the distribution from those periods for which we have more data, is more relevant for comparison with the genetic data because it represents a species' realised distribution for a given time, rather than a potentially incomplete measure of the species' climatic niche.

SECTION S2: Megafauna ancient DNA extraction, amplification and sequencing

2.1 Megafauna samples

Ancient mitochondrial DNA control region (mtDNA CR) data sets were generated for woolly rhinoceros (*Coelodonta antiquitatis*), wild horse (*Equus ferus*; the fossil species *E. lambei* has been determined to be genetically indistinguishable from *E. ferus*, based upon [72], hence the latter name takes precedence), and reindeer (known as caribou in North America, *Rangifer tarandus*). Sub-fossil samples of bone, tooth and horn were collected across northern Eurasia and North America, including the Canadian Arctic Archipelago and Greenland (Supplementary Fig. S2.1, Supplementary Tables S6.2, S6.3, S6.4). Woolly rhinoceros was only sampled in Eurasia, as the species has never been found in the New World. Sequences data sets from woolly mammoth, bison and musk ox were downloaded from GenBank (Supplementary Information section S3).

2.2 Accelerator Mass Spectrometry dating

A total of 353 Accelerator Mass Spectrometry (AMS) radiocarbon dates were obtained for woolly rhinoceros (n = 136), wild horse (n = 72) and reindeer (n = 145) from the commercial facilities offered by the Oxford Radiocarbon Accelerator Unit, UK (AMS ID: OxA), AMS 14C Dating Centre, Institut for Fysik og Astronomi, Aarhus University (AMS ID: AAR), Lawrence Livermore National Laboratory's Center for Accelerator Mass Spectrometry (AMS ID: CAMS), and NSF Arizona AMS Facility, Physics Department, University of Arizona (AMS ID: AA) (Supplementary Tables S6.2, S6.3, S6.4).

All radiocarbon dates, including those already published, were calibrated using the IntCal09 calibration curve[47] and the OxCal 4.1 online calibration resource (https://c14.arch.ox.ac.uk). Samples with infinite radiocarbon dates and radiocarbon dates past the IntCal09 calibration curve (*c*. >43,000 ^{14}C years before present, depending on the error of the date) were not included in the statistical analyses. Samples where the standard error of the calibrated date fell outside the calibration curve were omitted. Of the 353 new radiocarbon dates generated for this study, 16% were omitted from further analysis as their dates lay beyond the calibration curve or had infinite dates. All samples are discussed as kyr BP throughout the text, where kyr BP is defined as calendar thousand years before the present.

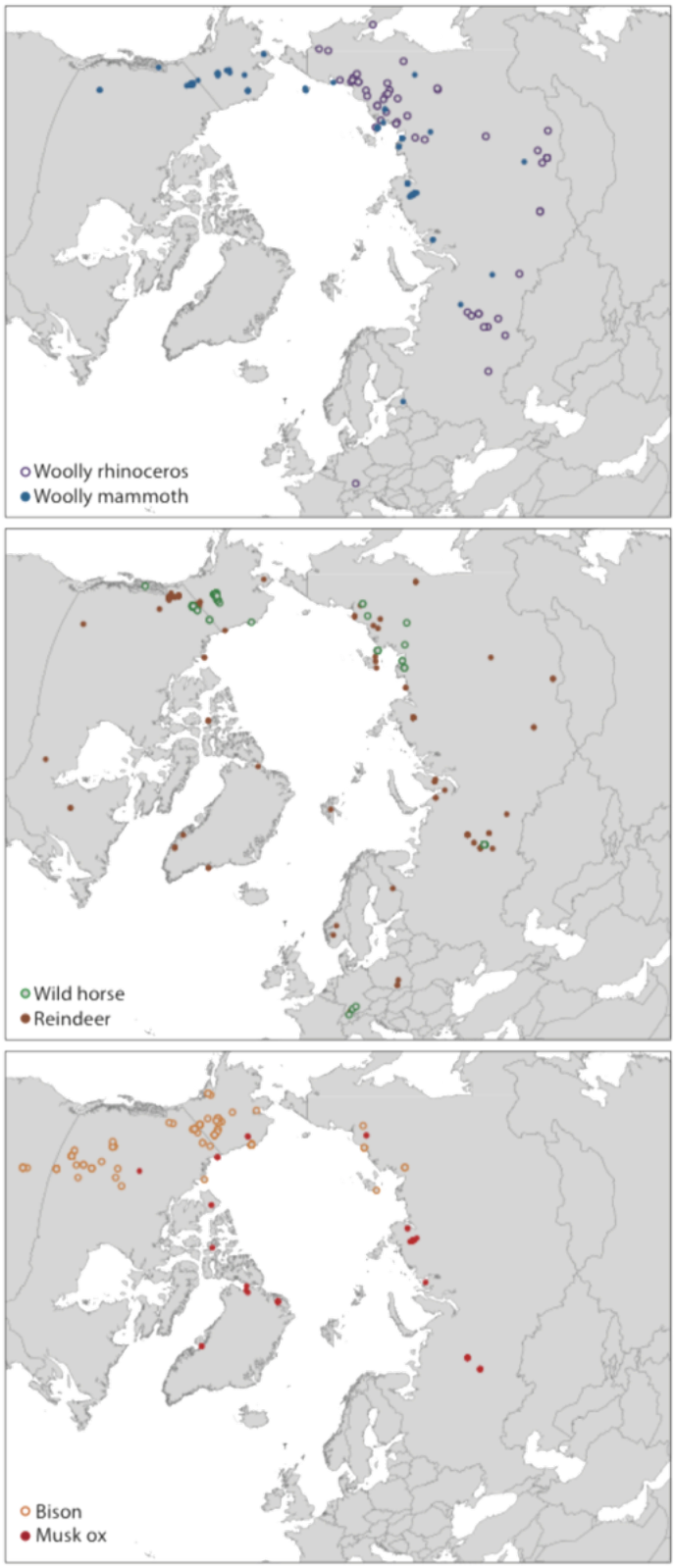

Supplementary Figure S2.1. Polar view of the Holarctic, with Eurasia to the right, indicating the DNA sample localities of the six megafauna species. New data sets were generated for woolly rhinoceros, horse and reindeer; further information in Supplementary Tables S6.2, S6.3, S6.4.

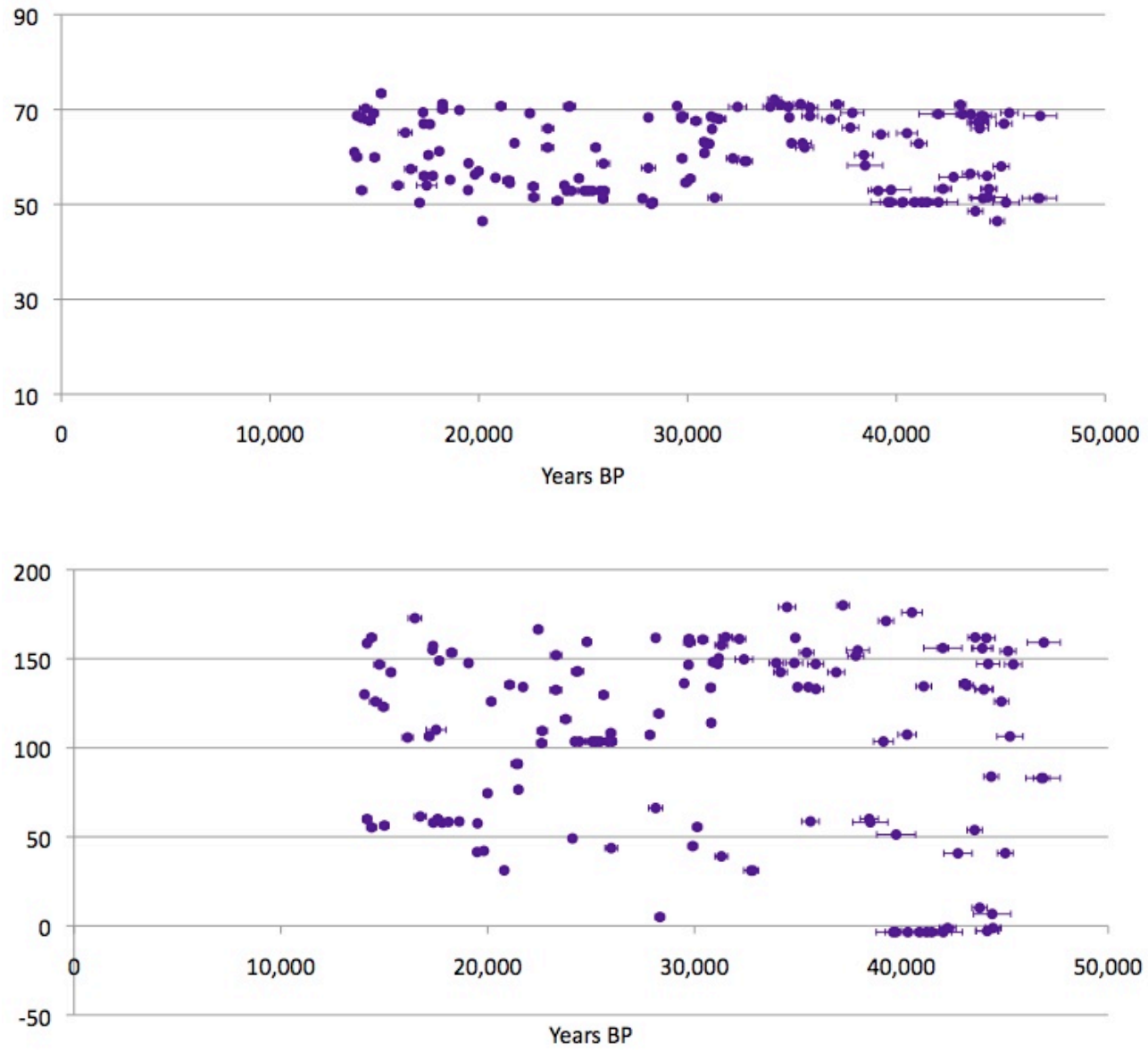

Supplementary Fig. 2.2. The woolly rhinoceros fossil record, including the 136 new radiocarbon dates generated for this study, plotted against latitude (top) and longitude (bottom) coordinates . Data are presented in Supplementary Tables S6.1 and S6.2. The species was present throughout Siberia right up until its disappearance from the fossil record. X-axis in calendar years BP, 1-sigma errors of the calibrated dates are included.

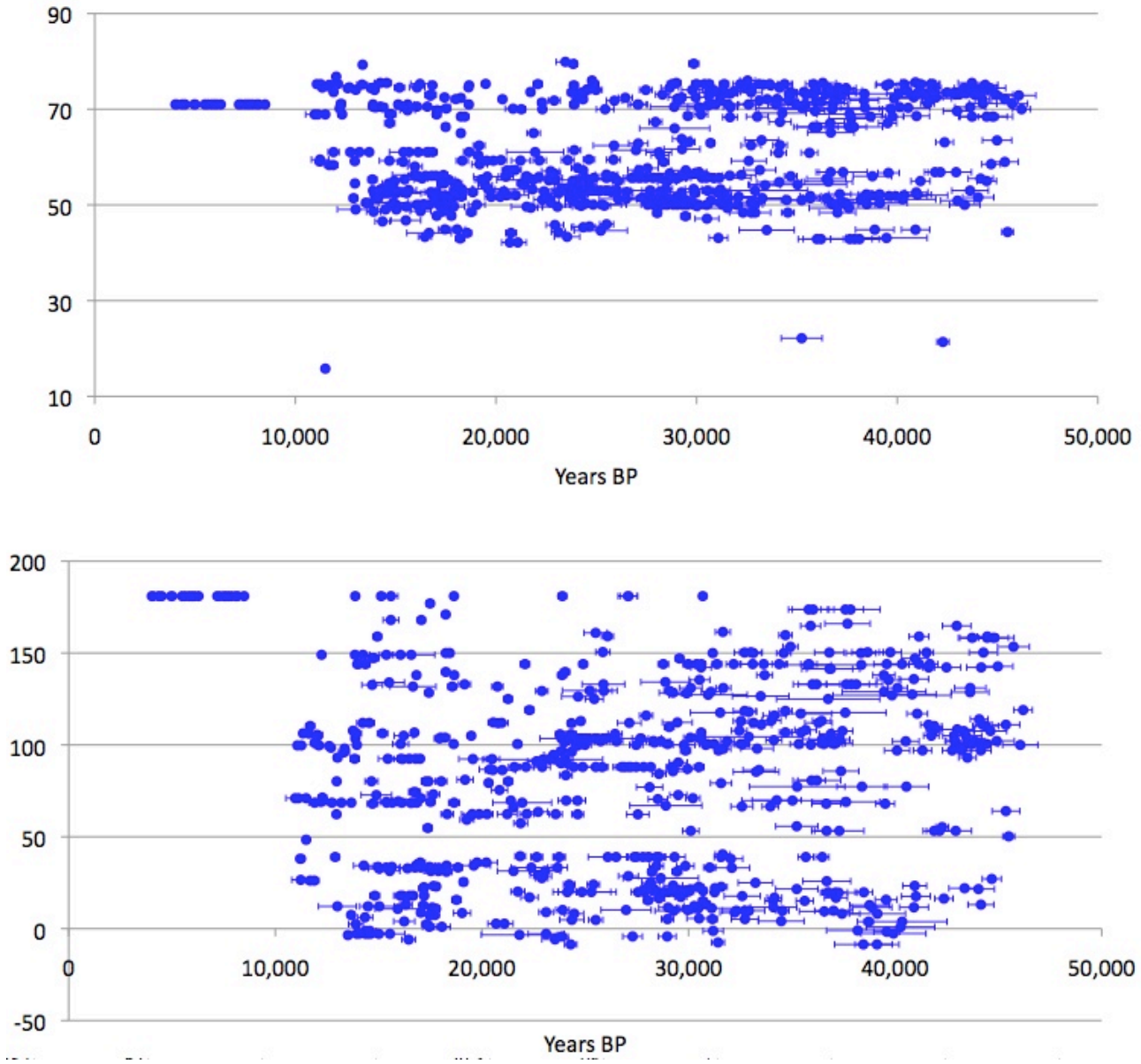

Supplementary Fig. 2.3. The woolly mammoth fossil record plotted against latitude (top) and longitude coordinates (bottom). The species was present throughout Siberia right up until its disappearance from the fossil record. X-axis in calendar years BP, 1-sigma errors of the calibrated dates are included.

2.3 Sequence generation

Stringent ancient DNA protocols were followed to avoid contamination from modern DNA and to assure reliability of results. All DNA extractions and PCR set-ups were performed in a dedicated ancient DNA facility isolated from multi-copy PCR work. PCR amplification, cloning and sequencing were performed at a separate DNA facility.

Ancient DNA sequences were obtained using the extraction procedures reported in [73].

DNA was PCR amplified using overlapping fragments ranging in length from 80–560 bp, depending on the condition of the specimen, and the species being sequenced. Primers were designed to span the entire HVR-1 of the mitochondrial control region. PCR amplifications were performed in 25 µl volumes, using 1xPCR buffer, 2 mM of $MgSO_4$, 2.0 mg/ml Bovine Serum Albumin (BSA), 0.4 µM of each primer, 1 µM of dNTPs, and 5U of High Fidelity Platinum Taq (Invitrogen, Carlsbad, CA). Cycling conditions were: 94˚C for 2 min, 50–70 cycles of 94˚C for 30 sec, 43–63˚C for 30 sec, and 68˚C for 45 sec, followed by 72˚C for 7 min. We included blank extraction controls and blank PCR controls in each reaction. Primer sequences and PCR-annealing temperatures are listed in Supplementary Table S2.1.

PCR products were subsequently purified with either the Invitek PCRapace PCR Purification Kit (Invitek, Berlin, Germany) or the QIAquick PCR purification kit (Qiagen, Valencia, CA), according to manufacturers' instructions. At least two independent PCRs were carried out for each fragment, and the products were either direct sequenced or cloned using TOPO TA cloning kit for sequencing (Invitrogen), with a minimum of six clones sequenced for each fragment. The overlapping of the PCR fragments resulted in a high degree of sequence replication. The sequences were obtained through the commercial service offered by Macrogen (Macrogen, Seoul, South Korea) and by in-house sequencing at Department of Biology, University of Copenhagen, Denmark. DNA sequences were subsequently edited by eye and aligned using Se-Al version 2.0A11 (A. Rambaut, University of Edinburgh). To investigate and account contamination and for errors caused by damage or sequencing, 79% of all consensus sequences were replicated.

The data sets resulted in 274 new mtDNA sequences, including 55 woolly rhinoceros, 115 wild horse and 104 reindeer. Sequences have been submitted to GenBank with the accession numbers JN570760-JN571033, corresponding sample numbers are listed in Supplementary Tables S6.2, S6.3 and S6.4.

Supplementary Table S2.1. Primer sequences and annealing temperatures for woolly rhinoceros, horse and reindeer.

Woolly rhinoceros	Primer name	Primer sequence (5'-3')	Annealing temp. (°C)
	1AF/WR15422F	CCCTAACTTCACCATCAACACCC	55
	1aF/WR15500F2	CACTCCCTTCTTAAACCASAAG	55
	1BF/WR15562F	TATACCAGGTATGTATATCG	55
	1AR/WR15600R	CATGCTTATATGCATGGGGC	55
	1CF2/WR15714F2	TTGATTRATATTGCATAGTAC	55
	1BR3/WR15727R3	GACTYRAATGGGGTATGTACG	55
	1cR/WR15792R	CGCGGCTTGGTGATTAAGCGC	55
	1CR/WR15812R	GAGAGGGTTGATGATTTCCC	55
	1bzF(1AR)	GCCCCATGCATATAAGCATG	55
	1bzR(1CF)	GTACTATGCAATATYAATCAAC	55
	2AF/WR16614F	GCCAAACCCCAAAAACAAG	55
	2aF/WR16635F	GACTAGGTATATAATTACACGC	55
	2BF/WR16704F2	CCCTTCTTTTGATACCAACATGC	55
	2AR3/WR16724R3	CTAGAGGGGTAYGAGTCTAYGTG	55
	2bR/WR16813R	GCTACATTAACAGGTGTATTTG	55

Horse	Primer pairs	Primer sequence (5'-3')	Annealing temp. (°C)
	L1	GCCATCAACTCCCAAAGCT	
	H1	ACATGCTTATTATTCATGG	56
	L2	CCCACCTGACATGCAATAT	
	H2	TGTTGACTGGAAATGATTTG	56
	L3	TCGTGCATACCCCATCCAA	
	H3	CCTGAAGTAGGAACCAGATG	56
	L4	CCATGAATAATAAGCATGT	
	H3	CCTGAAGTAGGAACCAGATG	56
	EQ168-187F	CGTGCATTAAATTGTTTGCC	
	EQCR2bii	CATGGGAGGTGATATGCGTG	56
	EQCR3ai	CGTGCATACCCCATCCAAGTC	
	EQCR3bi	GAACCAGATGCCAGGTATAG	56
	EQCR1F	TCCTCGCTCCGGGCCCAT	
	EQCR136R	TGTGAGCATGGGCTGATTAGTC	60
	EQCR51F	CTGGCATCTGGTTCTTTCTTCAG	
	EQCR210R	CTTTGACGGCCATAGCTGAGT	60
	EQCR163F	ACTGTGGTTTCATGCATTTG	
	EQCR296R	TTGCTGATGCGGAGTAATAA	56
	EQCRend184F	ATCTTGCCAAACCCCAAAAACAAG	
	EQCRend342R	TCTAGGGGGATGCCTGTCTATGG	63
	EQ4F	CATCAACACCCAAAGCTGAA	
	EQ4R	CGAYGTACATAGGCCATTCAT	56
	EQ5F	CATACCCACCTGACATrCAA	
	EQ5R	GACTTGGATGGGGTATGCAC	56

Reindeer	Primer pairs	Primer sequence (5'-3')	Annealing temp. (°C)
	CP1_F	GTCAACATGCGTATCCCG	51
	CP2_R	RTGAGATGGCCCTGAAGAAA	
	Rtp2_F	TCTCCCTAAGACTCAAGGAAG	
	Rtp2_R	GGCTATTGAGTGCAGAACTG	48

Rtp3_F	TCCACAAAATTCAAGAGCCTT	
Rtp3_Rshort	TAGCCGTACAGGACCATA	50
98F	AAGTTCTAATTAAACTATTCCCTG	43
231R	ATATAATATGGCTATTGAGTGC	
67F	TATAGCYCCACTATCAACACCC	47
228R	ATATAAYATGGCTATTGAGTGC	
38F	CCAATCTCCCTAAGACTCAAGG	49
219R	CTGTATTAAATTHTTRAAGGTTTTTRGA	
172F	AAAAACCTTYAADAATTTAATACAGT	46
350R	TGGGRYATRTARTTTAATGTACTATTAT	
186F	CCTTCARGAATTTAATACAGTTCTGC	52
373R	CARGTACTTGCTTATAAGCATGGGG	
272F	GGTCCTGTACGRYTATAGTAC	40
476R	CCCCTAGATCACGAGCT	
442_F	GYCAACATGCGTATCCCG	50
603_R	GCCCTGAAGAAAGAACC	

SECTION S3: Megafauna ancient DNA sequence analysis

3.1 Data retrieval and filtering

In addition to the 274 new mitochondrial DNA (mtDNA) control region sequences of woolly rhinoceros, wild horse and reindeer generated for this study (Supplementary Information section S2), we retrieved mtDNA control region sequences of mammoth (*Mammuthus primigenius*), bison (*Bison priscus/Bison bison*), and musk ox (*Ovibos moschatus*) from GenBank (Supplementary Fig. S2.1). We also augmented the horse and reindeer data sets with additional modern and ancient sequences from GenBank (Supplementary Tables S6.3, S6.4). To summarise the global diversity of modern horse breeds, we collected 140 sequences from 28 domestic breeds (*Equus caballus*), which all had at least five sequences available: Akhak Teke, Arabian, Baise, Belgian, Caspian, Cheju, Chinese, Cleveland, Clydesdale, Debao, Exmoor, Friesian, Garrano, Haflinger, Irish, Kerry, Lusitano, Mesenskay, Mongolian, Noriker, Orlov, Pottoka, Pura, Shetland, Sorraia, Vyatskaya, Yakut, and Thoroughbred. Similarly, to summarise the global diversity of modern wild reindeer, we collected all the wild reindeer sequences available in GenBank. We grouped these into regions representing Europe, Northeast Siberia, Alaska/Yukon and the Canadian Archipelago. Due to a lack of frequency information for the limited number of sequences from the rest of the US and Canada, we grouped these together as a fifth region. Four sequences were randomly selected from each region, yielding a total of 20 modern wild reindeer sequences. In addition, we sequenced seven new modern mtDNA sequences from Urals/western Siberia and Taimyr Peninsula (Supplementary Table S6.4), as no sequences > 210 bp were available from either of these regions in GenBank (sequences published by [74] were not included as they are < 150 bp long).

We calibrated the radiocarbon dates of the sequences prior to analysis. This enabled direct comparison with the range sizes (Supplementary Information section S1), which are estimated in calendar years. Hence, prior to analysis, all published sequences with infinite radiocarbon dates or with finite radiocarbon dates too old to be calibrated using the IntCal09 curve[47] (> *c*. 43,000 radiocarbon years BP, depending on the range of the radiocarbon error) were discarded from the data sets.

Sequence data sets from each species were aligned using MUSCLE[75] and checked manually using SeaView v4.2.11[76]. Sequences with substantial levels of missing data after processing at (nucleotide) sites that were polymorphic among the rest of the sequences, were automatically pruned from the data sets using a home-made Perl script. Similarly, sites with a substantial level of missing or ambiguous sites (Y, R, N, ?) were discarded from the remaining sequence subsets. These filtering steps resulted in both the removal of sequences with large numbers of ambiguous/missing

bases and shorter alignments. The final mtDNA CR data sets were: woolly rhinoceros (55 seq, 348bp), mammoth (82 seq, 705bp), horse (151 seq, 288bp; 136 seq when modern domestics are excluded), reindeer (162 seq, 415bp), bison (140 seq, 549bp) and musk ox (128 seq, 633bp) (Supplementary Table S3.1), with the data sets of mammoth, bison and musk ox being reduced from those previously reported[73,77,78] (Supplementary Table S3.2).

Supplementary Table S3.1. Summary statistics of the six megafauna DNA data sets. The Eurasian horse data set is represented both with and without the modern domestic samples. Table includes information on time bins used in the ABC and isolation-by-distance (IBD) analyses and number of sequences included in each time bin. Note that the temporal span of the time bins and sample size of each differs between the two analytical methods, as we used a minimum of three samples per time bin in ABC and a minimum of three sample localities per time bin in IBD. Because we had fewer sample localities than samples, time bins from the ABC analysis were pooled in the IBD analysis in some instances. S represents the number of polymorphic sites, π represents nucleotide diversity. The IBD p-values were determined from a randomization test with the next time-bin.

WOOLLY RHINOCEROS			**Summary Statistics**					**IBD (within region)**	
Region	**Time bin (kyr BP)**	**Seq #**	**S**	**π (per locus)**	**Tajima D**	**Haplotypic diversity**	**Fst**	**Correlation coefficient**	**p**
West of 90ºE	0-19	4	24	0.037	-0.072	1	-	-	-
	19-26	5	16	0.020	-0.840	0.9	-	-	-
	>34	4	12	0.019	0.187	1	-	-	-
East of 102ºE	0-19	9	29	0.030	-0.184	1	0.265	-	-
	19-26	10	42	0.045	0.210	0.867	0.276	-	-
	26-34	9	29	0.024	-1.045	0.972	-	-	-
	>34	14	29	0.017	-1.548	0.824	0.500	-	-
pan-Eurasian	0-19	13	41	0.038	-0.054	1	-	-0.08	-
	19-26	15	42	0.042	0.564	0.924	-	0.07	0.160
	26-34	9	19	0.024	-1.045	0.972	-	0.19	0.400
	>34	18	39	0.024	-1.548	0.895	-	0.13	0.323

Sequence Length: 348bp
Mutation Rate Prior: Normal 0.00103355,0.000325 (substitution per generation per locus)
Generation Time: 7 years

WOOLLY MAMMOTH			**Summary Statistics**					**IBD (within continent)**	
Continent	**Time bin (kyr BP)**	**Seq #**	**S**	**π (per locus)**	**Tajima D**	**Haplotypic diversity**	**Fst**	**Correlation coefficient**	**p**
Europe	0-19	13	19	0.007	-1.067	1	0.273	0.20	-
	19-26	9	4	0.003	1.766	0.806	0.255	-0.17	0.007
	26-34	12	11	0.004	-1.080	0.939	0.531	0.14	0.048
	>34	14	30	0.011	-0.742	0.956	0.260	0.42	0.321
America	0-19	3	10	0.009	ND	1	-	0.41	-

	19-26	5	12	0.008	0.050	0.9	-		
	26-34	8	9	0.004	-0.564	0.893	-	0.64	0.032
	>34	18	23	0.008	-0.810	0.967	-	0.08	0.003

Sequence Length: 705bp
Mutation Rate Prior: Normal 0.001053,0.0003666 (substitution per generation per locus)
Generation Time: 20 years

HORSE			**Summary Statistics**					**IBD (within continent)**	
Continent	**Time bin (kyr BP)**	**Seq #**	**S**	**π (per locus)**	**Tajima D**	**Haplotypic diversity**	**Fst**	**Correlation coefficient**	**p**
Europe (incl domestic)	0-11	31	37	0.02668	-0.4135	0.989	0.264		
	11-19	8	17	0.01984	-0.6626	1	0.223		
	19-26	4	12	0.02199	-0.3269	1	0.335		
	26-34	8	15	0.01637	-0.9471	0.964	0.321		
	>34	5	13	0.02083	-0.2793	1	0.131		
Europe (excl domestic)	0-19	10	21	0.021	-0.848	1	0.245	−0.141021	-
	19-26	4	12	0.022	-0.327	1	0.335	0.2857	0.074
	26-34	8	15	0.016	-0.947	0.964	0.321		
	>34	5	13	0.021	-0.279	1	0.131	-0.4023	0.024
America	11-19	23	33	0.027	-0.474	0.972	-	−0.04187	-
	19-26	52	38	0.024	-0.587	0.949	-	-0.0647	0.371
	26-34	18	20	0.025	0.997	0.922	-	0.1739	0.029
	>34	8	19	0.029	0.780	0.929	-	0.0223	0.091

Sequence Length: 288bp
Mutation Rate Prior: Normal 0.0003988,0.00017 (substitution per generation per locus)
Generation Time: 5 years

REINDEER			**Summary Statistics**					**IBD (within continent)**	
Continent	**Time bin (kyr BP)**	**Seq #**	**S**	**Nucleotide diversity (per locus)**	**Tajima D**	**Haplotypic diversity**	**Fst**	**Correlation coefficient**	**p**
Europe	0-11	31	37	0.017	-0.884	0.994	0.056	0.21	-
	19-26	14	32	0.020	-0.831	0.989	0.103	0.04	0.252
	19-26	19	39	0.021	-0.947	1	0.122	-0.12	0.365
	26-34	12	27	0.017	-0.994	1	0.095	-0.01	0.382
	>34	10	23	0.014	-1.255	1	0.123	0.05	0.269
America	0-11	58	54	0.016	-1.415	0.976	-	0.1290	-
	Nov-26	8	15	0.012	-0.631	0.964	-	-0.3215	0.044
	26-34	6	19	0.018	-0.590	1	-	0.6973	0.025
	>34	4	15	0.020	0.395	1	-		

Sequence Length: 415bp
Mutation Rate Prior: Normal 0.00060125,0.00016 (substitution per generation per locus)
Generation Time: 4 years

BISON			**Summary Statistics**					**IBD (within continent)**	
Continent	**Time bin (kyr BP)**	**Seq #**	**S**	**π (per locus)**	**Tajima D**	**Haplotypic diversity**	**Fst$**	**Correlation coefficient**	**p**
Europe	>17	7	29	0.0205	-0.2882	1.000	-	-	-
America	0-11	55	48	0.0159	-0.5781	0.877	0.528	0.03	-
	11-19	27	51	0.0259	0.2812	0.986	0.243	0.10	0.110
	19-26	16	50	0.0228	-0.7125	0.992	0.235	0.21	0.259
	26-34	13	42	0.0223	-0.4288	0.987	0.139	0.48	0.168
	>34	22	58	0.0223	-0.9194	0.996	0.210	0.14	0.033

Sequence Length: 549bp
Mutation Rate Prior: Normal 0.00102443,0.00025 (substitution per generation per locus)
Generation Time: 3 years
$ between each American time-bin and the unique Eurasian time-bin

MUSK OX			Summary Statistics					IBD (within continent)	
Continent	Time bin (kyr BP)	Seq #	S	π (per locus)	Tajima D	Haplotypic diversity	Fst$	Correlation coefficient	p
Europe	0-11	5	36	0.025	-0.643	1	0.521	0.26	-
	11-19	17	60	0.028	-0.045	0.985	0.511		
	19-26	31	92	0.022	-1.477	1	0.645	-0.19	0.047
	26-34	22	57	0.015	-1.597	1	-	0.27	0.000
	34-50	3	22	0.023	ND	1	-		
America	0-26	50	87	0.010	-2.434	0.913	-	-	-

Sequence Length: 633bp
Mutation Rate Prior: Normal 0.00097355,0.0002 (substitution per generation per locus)
Generation Time: 2 years
$ between each Eurasian time-bin and the unique American time-bin

Supplementary Table S3.2. Differences in sample size between original published (unfiltered) and filtered data sets of woolly mammoth, bison and musk ox.

	Unfiltered		Filtered		Reduction of data set			
	Sample size	Seq length	Sample size	Seq length	Sample size	Sample size %	Seq length	Seq length %*
Woolly mammoth	160	705	82	705	78	49	0	0
Bison	220	685	140	549	80	36	136	20
Musk ox	162	682	128	633	34	21	49	7

* Relative to the sequence length before filtering

3.2 Genetic analysis

Summary statistics

We grouped the sequence data sets of each species into geographic and temporal bins to calculate summary statistics for the serial coalescent simulations. Sequences were separated into Eurasia or North America and assigned to sequential time bins within each continent (Supplementary Table S3.1). Because woolly rhinoceros was found exclusively in Eurasia, we (i) analysed a single Eurasian time-series; and (ii) grouped samples west of 90ºE and east of 102ºE in two separate geographic units, as no wolly rhinoceros have ever been recovered in between.

Summary statistics were computed using Arlequin 3.5[79] (Tajima's D and Fst) and dnaSP v5[80] (number of segregating sites, nucleotide diversity per site and haplotypic diversity). Time bins were selected to test for different population models of demographic expansion or decline at various time points during the past 50,000 years and to test for possible shifts in geographic structure using isolation-by-distance. Due to variations among species in the temporal coverage of samples, the

number of sequences in each continent and within each time bin differed among data sets. Time bins were designed to include a minimum number of three sequences each (average = 15.8, range 3–58).

To avoid over-representation of modern domestic horse sequences in subsequent analyses and to minimise computation time for serial-coalescent simulations and Bayesian skyrides, we generated random subsets of the data available on GenBank. In horse, we generated ten random data sets of 13 sequences from the subset of 140 sequences selected from Genbank. Two of the new sequences generated in this study were recovered from Neolithic Eurasian horses (specimens JW191 and JW25; Supplementary Table S6.3) and were added to the domestic data set, and we subsequently estimated summary statistics independently for each of the ten data sets. The final summary statistic vector for Eurasian Neolithic horses (time bin 11–0 kyr BP) was determined as the average of the summary statistics recovered from the ten independent data sets of 15 sequences. The procedure used for the incorporation of modern reindeer is discussed in section S3.1 above.

Isolation-by-distance (IBD)

We tested for temporal changes in the level of isolation-by-distance (IBD) within each species by calculating the correlation between pairwise genetic and geographic distances within and between consecutive time bins (Supplementary Table S3.3). Each time bin included a minimum of three geographically distinct sample localities; hence, the number of sequences in each time bin differed among species due to different sampling regimes (Supplementary Fig. S3.1). Of note, the temporal span of the time bins differed from those used in the ABC analysis because some of the ABC time bins were pooled for the IBD analysis due to small locality number; e.g., we pooled samples from >34 kyr BP (n = 4) and 34–26 kyr BP (n = 6) in North American reindeer, as they represented two localities each.

Geographic distances were estimated from latitude and longitude using the haversine formula and a spherical-earth approximation, ignoring hills. We corrected the pairwise-distance estimates among sequences for differences in calendar age of the samples following [81] and used the mutation rate average used in the serial-coalescent simulations (Supplementary Table S3.1). Hence, if two specimens were separated in time and space, only geographic distance and not sample age contributed to their genetic distance, assuming a constant clock and constant population size. Correlation coefficients were estimated in the R statistical package[64] for each time bin and the significance of change in correlation between two successive time bins was tested through a randomisation approach using 10,000 pseudo-replicates. Briefly, for two successive time bins with

N_A and N_B sequences, pseudo-replicates were generated randomly by sampling (without replacement) N_A and N_B sequences from the merged pool of N_A and N_B sequences, and the difference in correlation coefficients was recorded. The re-sampling procedure provided an empirical estimate of the difference between correlation coefficients, assuming no change in population structure; the observed difference in correlation coefficients was compared against the re-sampling distribution to test for significance at the 5%-level (one-sided test). Pseudo-replicates were generated using a home-made Perl script and distributions were analysed using R.

Supplementary Table S3.3. Changes in isolation-by-distance through time for the continental populations in Eurasia and North America and for the gobal data (EurA + NA). The correlation coefficients observed between geographic distances and pairwise genetic distances are reported for each megafauna species and for each time bin where a minimum number of five sequences were available (top line of each population panel). Genetic distances were estimated after correcting for time differences between sequence pairs. The significance of the changes in correlation coefficients between two successive time periods was tested through a randomization procedure and corresponding p-values are indicated. Significant tests (5%-level) are marked with an asterisk. Time bins are in thousands of years before present.

Species	Continent	>34	34-26	26-19	19-11	11-0
Woolly rhinoceros	Eurasia	0.46	0.38	0	0.42	
				0.038*		
			0.031*			
		0.128				
Woolly mammoth	Eurasia	0.82	0.14	-0.09	0.37	
				0.231		
			0.172			
		0.203				
	North America	0.02	0.55		0.47	
				0.452		
		0.017*				
	EurA + NA	0.44	0.65	0.35	0.49	
				0.238		
			0.111			
		0.157				
Horse	Eurasia	0		0.17	0.05	
				0.357		
		0.345				
	North America	0.23	0.22	−0.07	0.02	
				0.197		
			0.004*			
		0.102				
	EurA + NA	0	0.22	0.15	0.13	
				0.466		
			0.209			

		0.125				
Reindeer	Eurasia	-0.21	0.20	0.02	-0.04	0.12
					0.218	
				0.396		
			0.399			
		0.065				
	North America	0.82		-0.32		0.11
					0.099	
		0.003*				
	EurA + NA	0.20	0.31	0.09	-0.08	0.14
					0.078	
				0.044*		
			0.472			
		0.146				
Musk ox	Eurasia	0.02		-0.19		0.20
				0.014*		
		0*				
	EurA + NA	0.02		0.06	0.31	0.07
					0.016*	
				0.129		
		0.387				
Bison	North America	0.12	0.17	0.02	0.31	0.77
					0*	
				0.076		
			0.123			
		0.128				
	EurA + NA	0.40	0.04	0.02	0.30	0.77
					0*	
				0.099		
			0.365			
		0.045*				

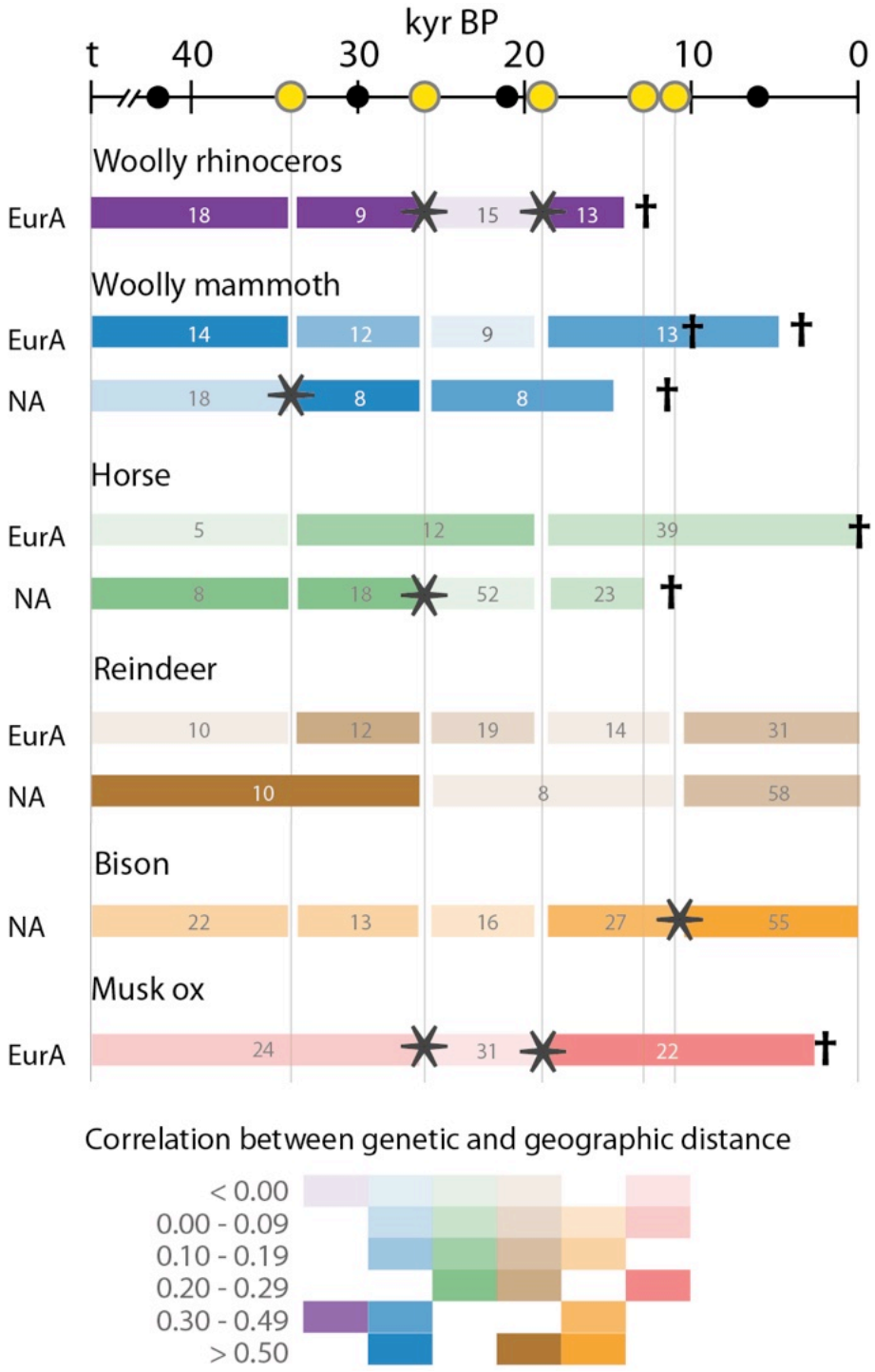

Supplementary Figure S3.1. Isolation-by-distance analysis of continental populations in Eurasia (EurA) and North America (NA). Correlation between genetic (calculated as nucleotide diversity corrected for temporal age) and geographic distance among samples within each time bin is indicated by the colour intensity, with values shown in Supplementary Table S3.3. The darker the colour, the stronger the correlation between geographic and genetic distance. Sample size of each time bin is indicated and an asterisk marks significant change in isolation-by-distance between consecutive bins. Crosses mark species extinction times; mainland (older) and island (younger) mammoth extinctions are included.

Approximate Bayesian Computation (ABC) and model selection

Serial-coalescent simulations (1,000,000 iterations per model) were performed using Bayesian Serial SimCoal (http://www.stanford.edu/group/hadlylab/ssc/) on a series of nine to 16 population models per species (Supplementary Fig. S3.2, Supplementary Table S3.4). Simulations were run on three data sets: (i) Eurasia; (ii) North America; and (iii) global. For woolly rhinoceros, simulations were run only for Eurasia, as the species was never found in North America. We tested a total of 217 models, resulting in 217 million serial-coalescent simulations. The K2P+Γ mutation model was used in all simulations, using the average of the posterior distributions for kappa (transition/transversion ratio) and alpha (gamma shape) estimated by BEAST. Similarly, we used the normal posterior distributions recovered from BEAST as a prior for the mutation rates (Supplementary Table S3.1). Using the age of first reproduction as a rough proxy for generation time, we assumed that generation times were: woolly rhinoceros (seven years, based on extant rhinoceros species), mammoth (20 years, based on extant elephants[78]), wild horse (five years, based on Przewalski's horse[82]), reindeer (four years[83]), bison (three years[84]) and musk ox (two years[73]).

In all models, the effective population size at first generation was randomly sampled at each iteration from a uniform prior ranging from 1,000 to 100,000 individuals. The first model consisted of a panmictic deme with constant effective population size (Supplementary Fig. S3.2). In a second series of models, we simulated an instantaneous demographic expansion (uninformative prior, up to 10-fold) or decline (uninformative prior, down to 0.1-fold) occurring at a fixed and unique time in the past (34, 26, 19, 12.9, 11 kyr BP). These time points were chosen for the following reasons. They represented midpoints between the periods from which we have palaeoclimatic data and potential range size estimates of each species (42, 30, 21, 6 kyr BP). Also, some of them represented periods of putative climatic change, such as the beginning of the Last Glacial Maximum (LGM; 26 kyr BP), the end of the LGM (19 kyr BP), the onset of the Younger Dryas (12.9 kyr BP), and the beginning of the Holocene (11 kyr BP). Two additional models, an instantaneous expansion at 26 kyr BP followed by a decline at 19 kyr BP, and the reverse scenario (population decline at 26 kyr BP followed by an expansion at 19 kyr BP), were considered; these models were introduced to mimic demographic events possibly driven by climatic changes around the time of the LGM. With a final set of models, we aimed a final set of models at testing population subdivision between continents at 19 kyr BP (the end of the LGM) or at 11 kyr BP (the inundation of the Bering land bridge, which put an end to gene flow between continents). For woolly rhinoceros, which did not colonise the Americas, we assumed subpopulations to be west of 90ºE and east of 102ºE. Alternatively, we assumed that population subdivision was of an older date (uniform prior, 60–75 kyr BP), followed by different episodes of isolation and migration between continents. No

symmetry in migration rates was assumed and migration frequencies were randomly sampled from a uniform distribution of 0-0.01 per generation.

Approximate Bayesian Computation (ABC) analyses were performed for each model using nucleotide diversity, Tajima's D, haplotypic diversity, and Fst (except in single-continent analyses) as a vector of summary statistics. We used a tolerance region of 0.1% of all simulations and the R makepd4() function. Note that, to match the Bayesian Serial SimCoal output, the observed haplotypic diversity values were converted and multiplied by a factor (n-1)/n, with n being the number of sequences considered in a given time bin. Finally, the posterior probability of all N_M models was estimated using categorical regression and the R calmod() function following Beaumont[85]. This procedure takes advantage of the weighted regression framework and treats a model indicator as a categorical variable that can take values ranging from 1 to N_M. R functions for ABC and categorical regression are available online at http://www.rubic.rdg.ac.uk/~mab/stuff/. Support values of the models tested in each continental population and the global species data sets are shown in Supplementary Table S3.4.

To test if the number of samples within each time bin influenced the associated estimate of nucleotide diversity, we used Spearman's ranked correlation coefficient and the R statistical package[64]. Similarly, we tested the correlation between the temporal distribution of samples and nucleotide diversity. This was done by calculating the temporal distance from each sample within a time bin to the median sample age of that time bin, and correcting for sample size. Plots of nucleotide diversity against sample size and temporal span are shown in Supplementary Figs S3.3 and S3.4. We did not find any correlation.

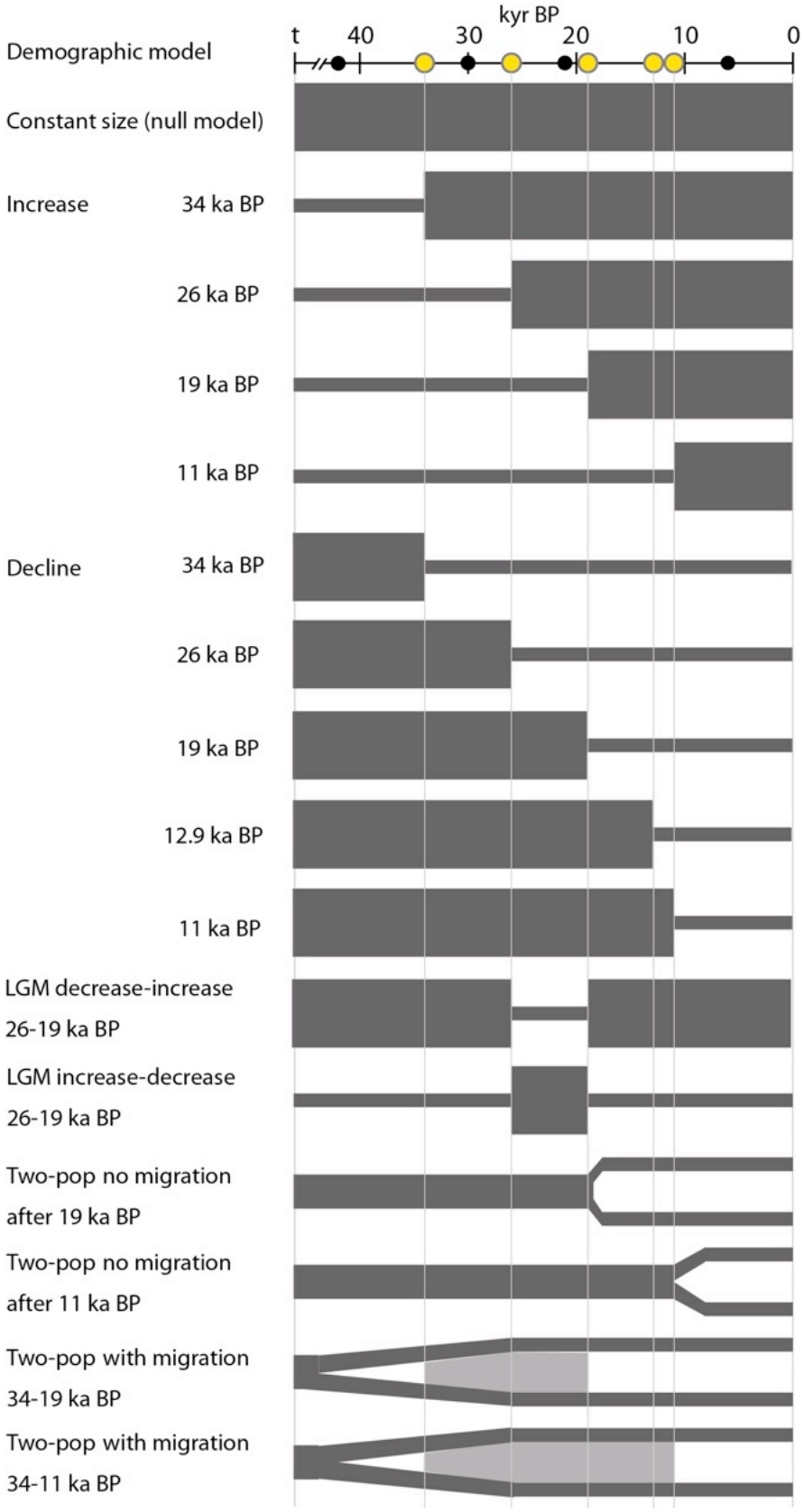

Supplementary Figure S3.2. Simulated demographic models tested against the observed data using the ABC model-selection approach. A maximum of 16 models were tested per species. Migrations between continents is indicated in light grey. Results in Supplementary Table S3.4.

Supplementary Table S3.4. Simulated demographic models tested against the observed data using the ABC model-selection approach. Models were run for Eurasia, North America and the global data set. A maximum of 16 different models were simulated for each species; two-population models were only analysed with the global data and encompass Eurasia and North America as separate populations, with or without migration (Supplementary Fig. S3.2). Support values for the different models are shown, and sum to 1 across all models within each data set. Values > 0.2 are in bold. Horses were analysed both with and without domestics.

		Eurasia						**North America**				**Global**						
Model	**Time (kyr BP)**	Woolly rhinoceros	Woolly mammoth	Horse	Horse + dom	Reindeer	Musk ox	Woolly mammoth	Horse	Reindeer	Bison	Woolly rhinoceros*	Woolly mammoth	Horse	Horse + dom	Reindeer	Bison	Musk ox
Constant size		0.09	0.07	0.08	0.06	0.06	0.03	0.10	0.04	0.03	0.02	0.04	0.00	0.04	0.05	0.05	0.02	0.00
Increase	**34**	**0.26**	0.14	**0.34**	**0.35**	**0.44**	**0.73**	**0.21**	**0.27**	0.12	0.00	**0.26**	0.01	**0.29**	**0.29**	**0.44**	0.00	n/a
	26	**0.31**	**0.26**	**0.22**	**0.25**	0.11	0.08	**0.24**	**0.48**	0.20	0.00	**0.35**	0.01	**0.36**	**0.34**	0.09	0.00	0.00
	19	**0.24**	**0.21**	0.14	0.17	0.08	0.02	**0.24**	0.11	**0.29**	0.00	0.08	0.01	0.09	0.10	0.07	0.00	0.00
	11	n/a	0.18	0.11	0.12	0.19	0.04	n/a	n/a	**0.30**	n/a	n/a	0.01	0.09	0.07	0.17	0.00	0.00
Decline	**34**	0.00	0.02	0.00	0.00	0.00	0.00	0.03	0.00	0.00	0.00	0.00	0.00	0.00	0.00	0.00	0.00	0.00
	26	0.00	0.01	0.00	0.00	0.00	0.00	0.02	0.00	0.00	0.01	0.00	0.00	0.00	0.00	0.00	0.00	0.00
	39	0.01	0.01	0.02	0.00	0.01	0.00	0.03	0.01	0.00	0.05	0.00	0.00	0.01	0.00	0.01	0.04	0.00
	12.9	n/a	0.01	0.02	0.00	0.01	0.01	0.02	n/a	0.00	**0.37**	n/a	0.00	0.02	0.01	0.01	**0.58**	0.00
	11	n/a	0.02	0.02	0.01	0.01	0.01	n/a	n/a	0.00	**0.50**	n/a	0.00	0.01	0.00	0.03	**0.22**	0.00
Increase-decline	**26-19**	0.02	0.04	0.04	0.03	0.07	0.07	0.05	0.09	0.02	0.05	0.01	0.01	0.09	0.09	0.06	0.08	0.01
Decline-increase	**26-19**	0.07	0.04	0.02	0.01	0.02	0.00	0.06	0.00	0.03	0.00	0.02	0.00	0.00	0.00	0.02	0.00	0.00
Two-pop	**34**	Two-population model, Eurasia only. No migration										**0.21**	n/a	n/a	n/a	n/a	n/a	n/a
	26											0.02	n/a	n/a	n/a	n/a	n/a	n/a
	19											0.00	n/a	n/a	n/a	n/a	n/a	n/a
	11											n/a	n/a	n/a	n/a	n/a	n/a	n/a

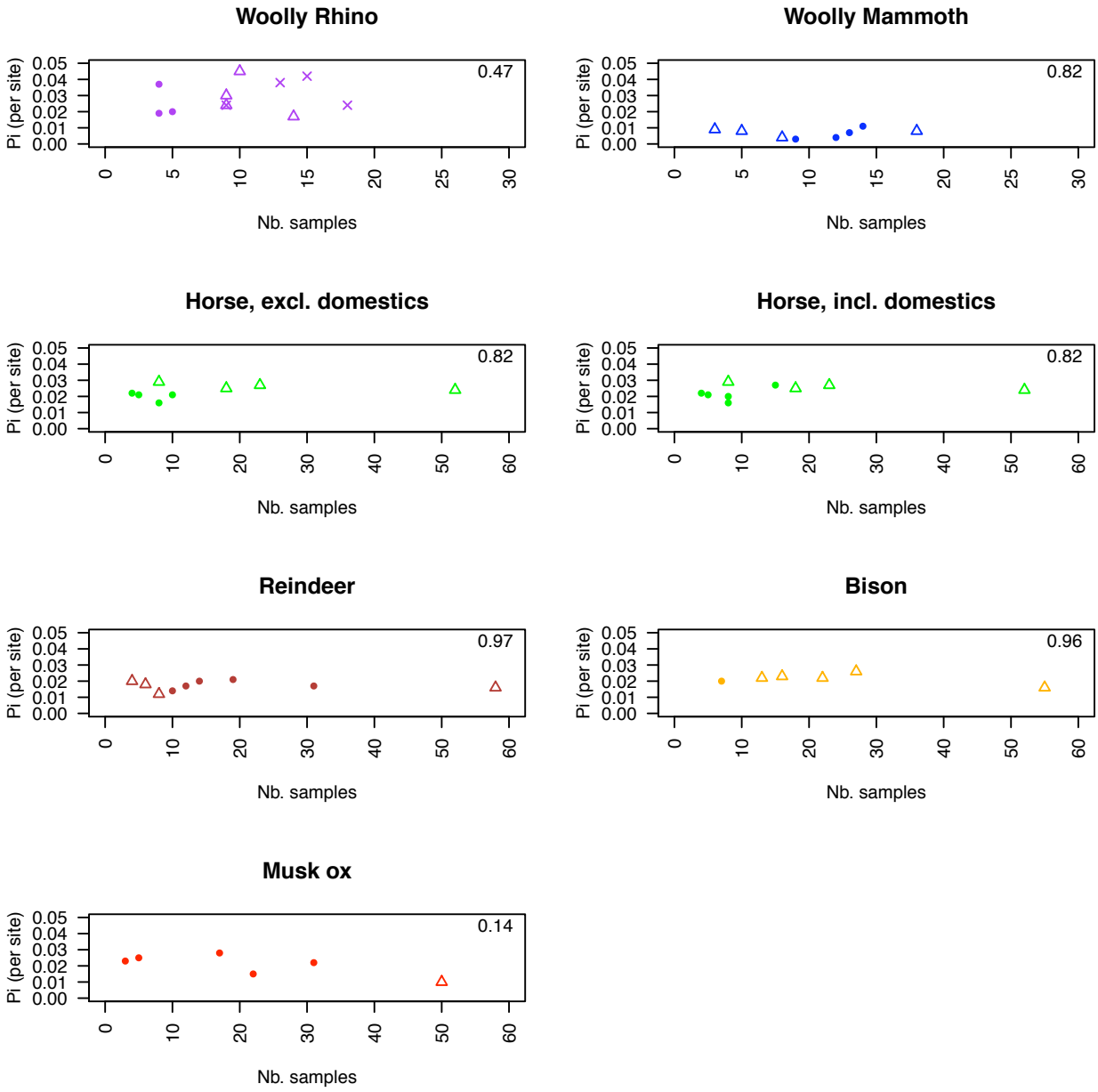

Supplementary Fig. S3.3. Plots of sample size against nucleotide diversity (π) for each time bin; data from Supplementary Table S3.1. Dots represent Eurasia, triangles represent North America. In woolly rhinoceros, which is not present in North America, the two populations are from west of 90ºE (dots) and east of 102ºE (triangles); crosses represent the pooled Eurasian data. The p-value of Spearman's correlation test is indicated in the top right-hand corner of each plot, and is based on all data points within each species.

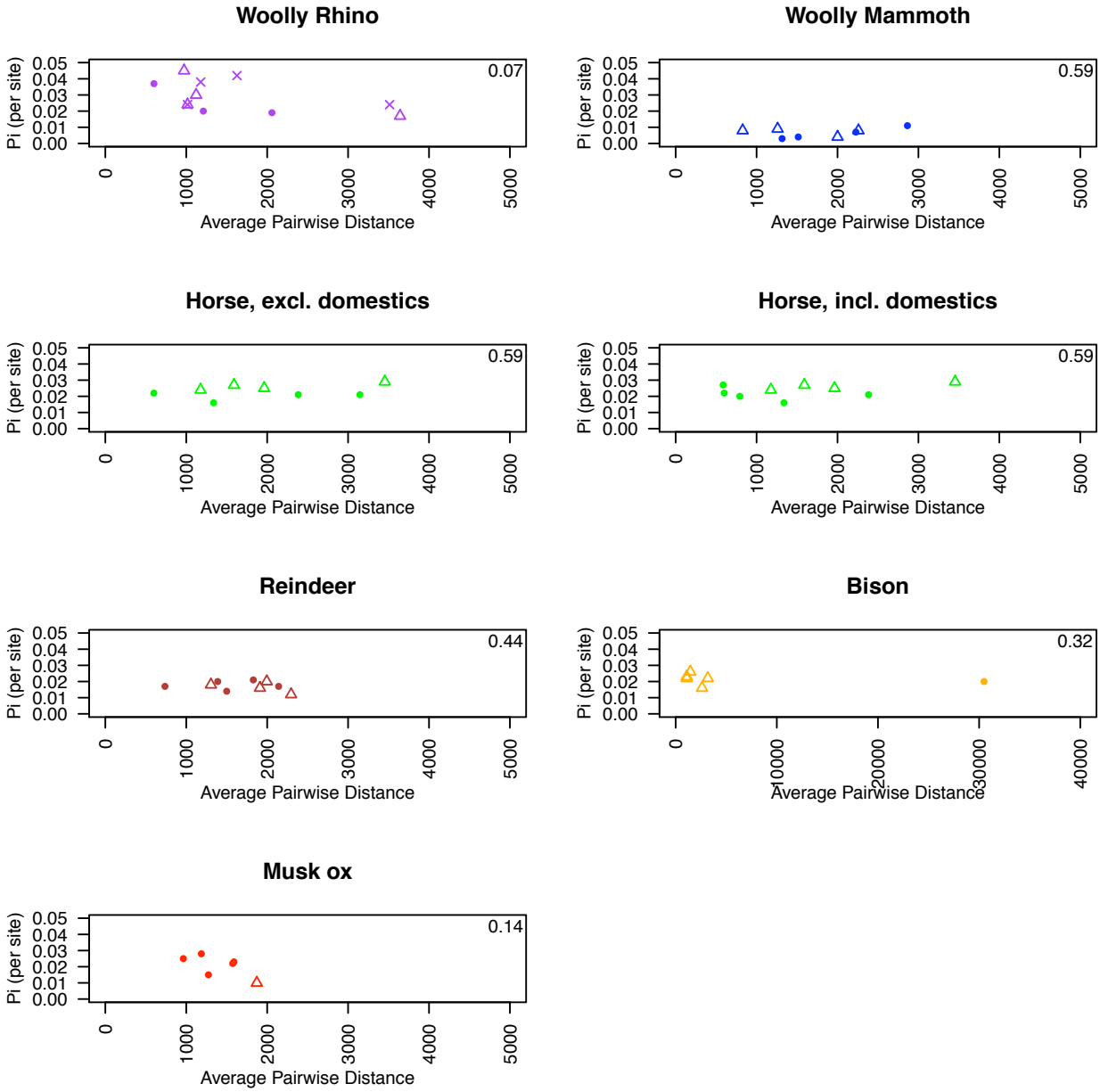

Supplementary Fig. S3.4. Plots of temporal span of samples within each time bin (average pairwise distance is in calendar years) against nucleotide diversity (π); data from Supplementary Table S3.1. The temporal span was calculated by summing the distance between each sample within a time bin and the temporal median, and dividing by the number of samples. Dots represent Eurasia, triangles represent North America. In woolly rhinoceros, which is not present in North America, the two populations are from west of 90ºE (dots) and east of 102ºE (triangles); crosses represent the pooled Eurasian data. The p-value of Spearman's correlation test is indicated in the top right-hand corner of each plot, and is based on all data points within each species.

Bayesian skyride plots

To explore the evolutionary history of the six species, we estimated the genealogical relationships of the sequences using the Bayesian phylogenetic inference package BEAST v1.5.4[86], which allows the simultaneous estimation of demographic and evolutionary parameters. For each data set we performed analyses both with and without the post-mortem damage (PMD) model, which accounts for additional substitutions at the terminal branches that may be due to DNA damage[87]. For each model, we assume the HKY+Γ model of nucleotide substitution and the strict molecular clock, with the evolutionary rate calibrated using the age (calibrated radiocarbon date or sampling date) of each sequence in the data set. For all analyses, two MCMC chains were run for 30–200 million iterations each, with samples drawn from the posterior every 5,000 iterations. Convergence to stationarity and mixing were evaluated using Tracer[88]. The first 10% of runs were discarded as burn-in and the remainder of posterior samples from the two runs were combined. As a coalescent prior we assumed the skyride demographic model[89], which accommodates uncertainty in the demographic and phylogeographic history of each species. Although in many cases a constant population size model may be the simplest model to use, the skyride model is the most flexible coalescent model currently available in the BEAST package. In addition, the skyride model allows the estimation of theta, which approximates the effective population size, confounded by population structure, throughout the history of the sampled genealogies. Theta is proportional to the effective population size unless there is substantial structure or if sampling is biased[90,91,92]. For some taxa, other demographic models, such as the constant population size and exponential growth/decline model, were also evaluated. In all cases, comparison between models was performed using Bayes factors[93].

3.3 Results and discussion

Data sets

Although some analyses were more flexible than others in terms of missing data, it was necessary to prune all the data sets in terms both of number of sequences and the number of (nucleotide) sites as described in section 3.1. First, to compare the genetic data and the results of the species distribution models (Supplementary Information section S1), it was necessary to calibrate the radiocarbon dates generated from each fossil to reflect calendar years, and samples > *c*. 43,000 radiocarbon years before present (BP) were discarded as they fell beyond the IntCal09 calibration curve[47]. This resulted in a significant decrease in the number of specimens in some data sets. In musk ox, for example, almost all northeast Siberian sequences (which include a distinct genetic clade[73]), were excluded from our analyses as they could not be calibrated. Second, the Serial

SimCoal software does not accept missing sites, and we therefore filtered the data for these prior to analysis (see section S3.1). To ensure that the results from the three different analytical approaches (IBD, ABC, and BEAST) were directly comparable, we used the filtered data sets in all analyses. For differences in number of sequences and sites between the published and filtered data sets used in our analyses, see Supplementary Table S3.2.

Isolation-by-distance

We find a significant increase in IBD in Eurasian woolly rhinoceros and musk ox after 19 kyr BP, and in North American bison after 11 kyr BP (Supplementary Fig. S3.1, Supplementary Table S3.3). Although not significant, Eurasian mammoth also show an increase in the correlation between genetic and geographic distance after 19 kyr BP. Eurasian and North American reindeer and Eurasian wild horse show no changes in IBD over time, and IBD decreases in North American horse prior to the LGM. We note that although we interpret high levels of IBD as increased structuring within populations, temporal changes in genetic diversity could also be caused by local extinctions and replacements by genetically divergent populations.

Approximate Bayesian Computation and model selection

In eight of the nine continental populations, we find maximal support for models of population expansion using the ABC model-selection approach (Supplementary Table S3.4). The intensities of the increases range from 2.5 to 10-fold across populations; distribution plots of intensity estimates for the best-fit model are shown in Supplementary Figure S3.5. Bison is the only species with a well-supported signal of decline; in all other populations, models of decline are supported by posterior probabilities of ≤ 0.03, where the support across all given models sums to 1 (Supplementary Table S3.4). The posterior probability values of the expansion models are 4–10x the values of the models of decline. In woolly rhinoceros and North American mammoth, models of expansion at 35/34, 26 and 19 kyr BP yield similar levels of support, and we are therefore unable to conclude the exact timing of the event. Similarly, we find high levels of support for population expansion at 19 and 11 kyr BP in North American reindeer. In Eurasian reindeer and musk ox, we find high support (0.44 and 0.73, respectively) for an expansion at 34 kyr BP. Interestingly, in the global populations of woolly mammoth and musk ox, we find highest support for two-population models with migration between Eurasia and North America, where the onset of migrations coincides with the timing of expansion in the continental populations (Supplementary Table S3.4). Furthermore, the end of migration at 11 kyr BP in musk ox coincides with the inundation of the

Bering land bridge, which prevented migration between continents. We could not test this timing (11 kyr BP) in mammoth, due to a lack of younger samples from North America. The estimates of effective population size at first generation were similar across populations within species (Fig. 3 in main text). Distribution plots of Ne estimates of the best-fit model are included in Supplementary Figure S3.5. We ran the ancient horse data set both with and without the modern domestic sequences, and results remained consistent (Supplementary Table S3.4).

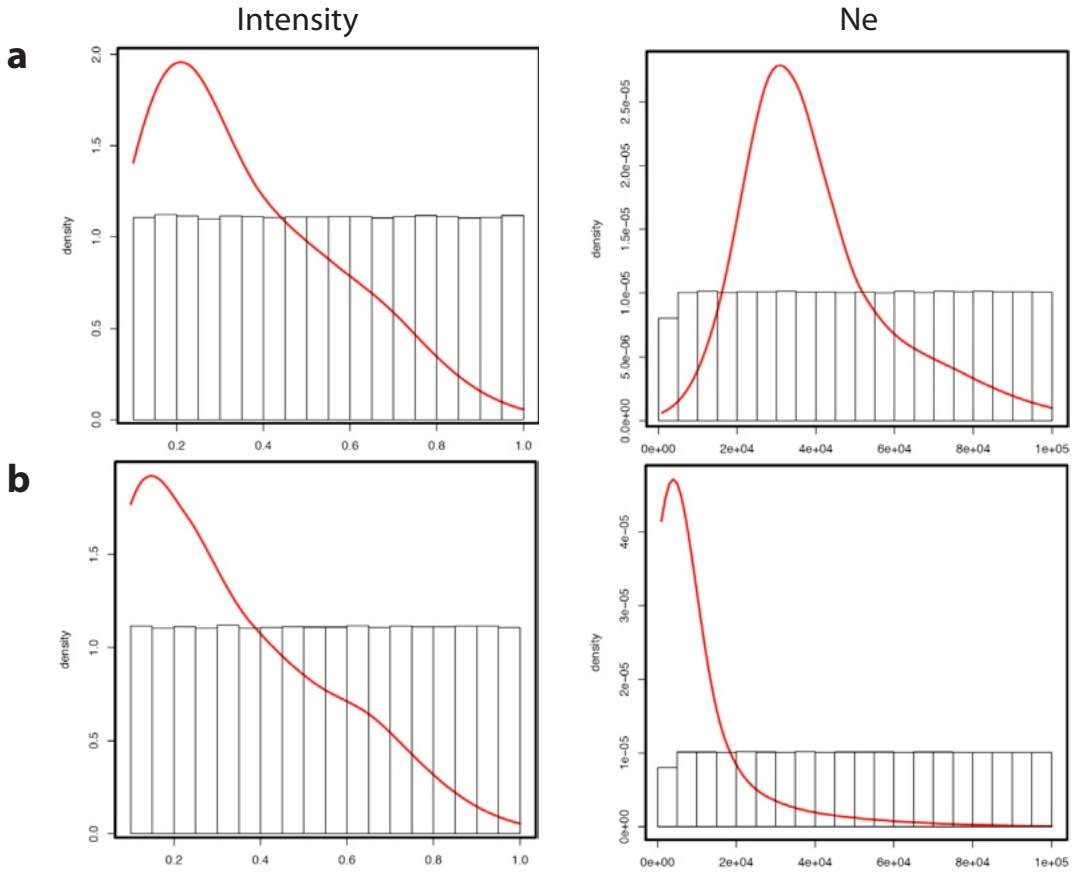

Supplementary Figure S3.5a. Density plots of the parameter estimates in the ABC model-selection approach in the Eurasian populations. Parameter estimates of intensity and effective population size (Ne) are shown for the model with highest support. (a) Woolly rhinoceros, population increase at 26 kyr BP, (b) Woolly mammoth, population increase at 26 kyr BP, (c) Horse, population increase at 34 kyr BP, (d) Reindeer, population increase at 34 kyr BP, (e) Musk ox, population increase at 34 kyr BP. Support for all demographic models tested are shown in Supplementary Table S3.4.

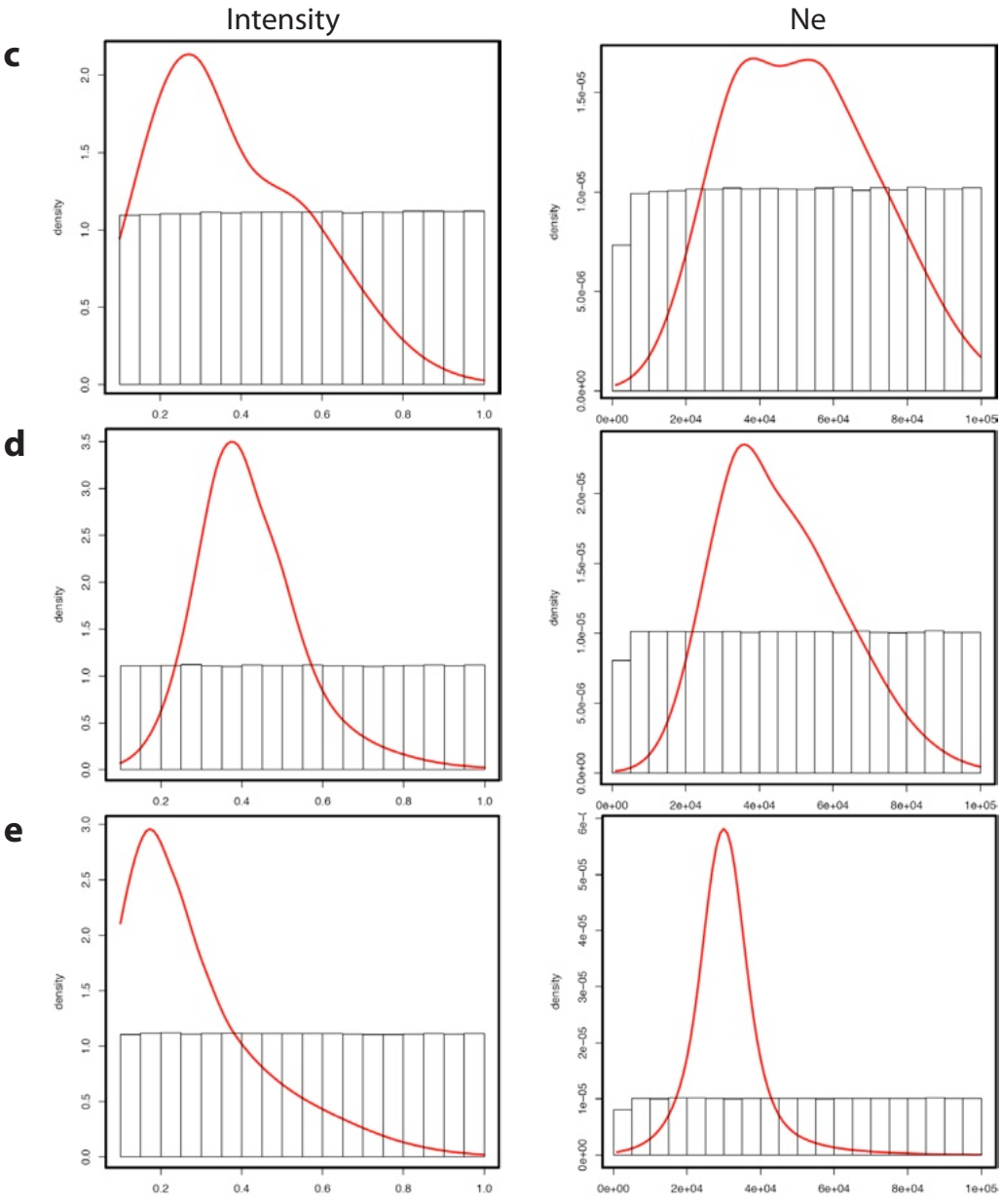

Supplementary Figure S3.5a. Continued.

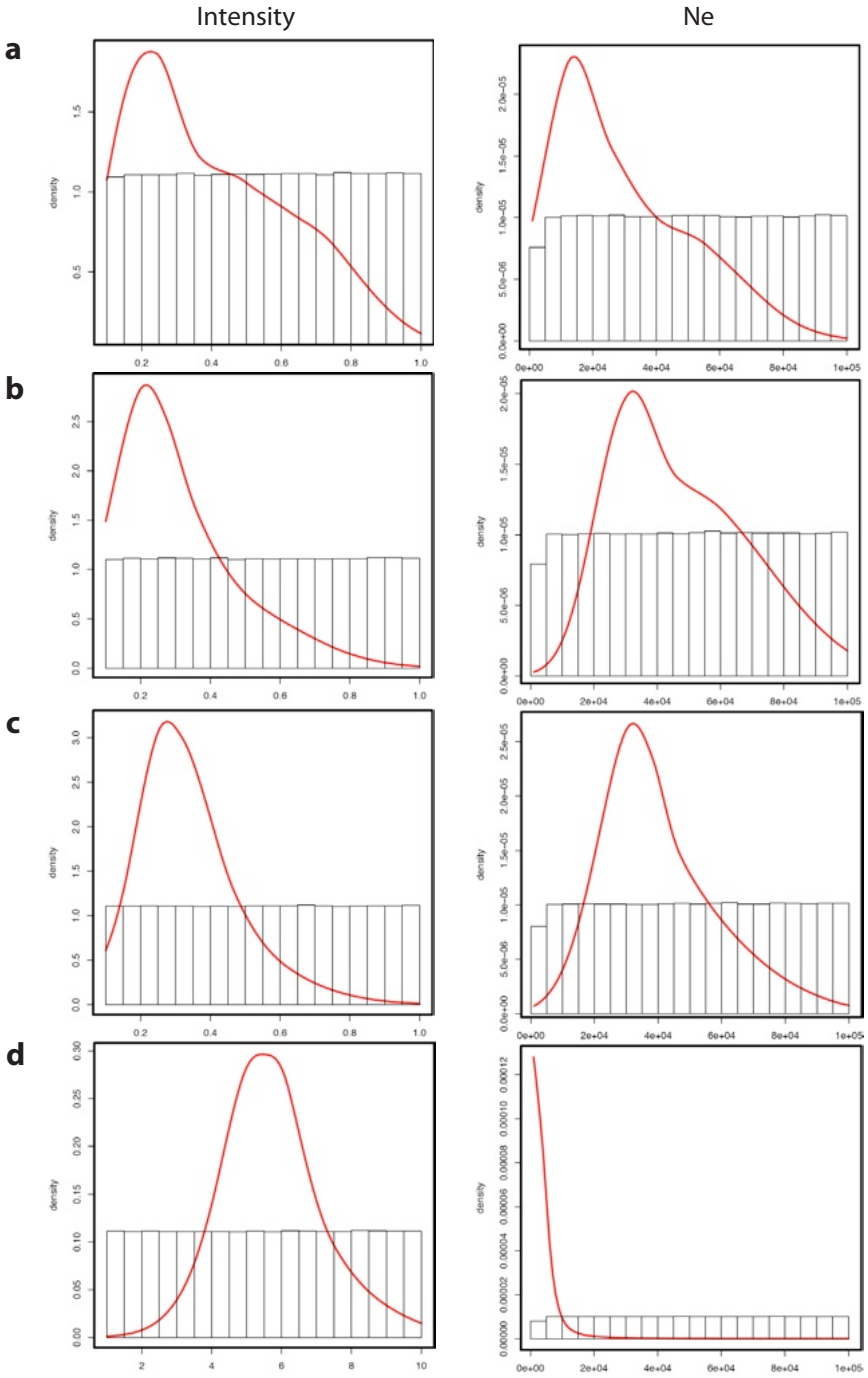

Supplementary Figure S3.5b. Density plots of the parameter estimates in the ABC model-selection approach in the North American populations. Parameter estimates of intensity and effective population size (Ne) are shown for the model with highest support. (a) Woolly mammoth, population increase at 26 kyr BP, (b) Horse, population increase at 26 kyr BP, (c) Reindeer, population increase at 11 kyr BP, d) Bison, population decline at 11 kyr BP. Support for all demographic models tested are shown in Supplementary Table S3.4.

Bayesian skyride plots

All skyrides can be seen in Figure 2 of the main text and in Supplementary Figures S3.6 and S3.7. For bison and musk ox (Fig. 2 in main text), the skyride estimates of changes in diversity through time differ slightly from those reported previously[73,78,94]. This is due to our data-filtering approach, where sequences and missing sites were pruned prior to the analysis. The additional signals of expansion reported in the published studies of bison and musk ox both occurred prior to 43,000 radiocarbon years BP. Because we exclude the older samples, we do not recover the expansion signal. However, as the time period falls outside the scope of our study, which is focused on changes that occur within the most recent 50,000 years, our results are not influenced by this omission.

For horses, excluding the domestic sequences resulted in no change to the estimated demographic trajectory (Supplementary Fig. S3.7).

For some data sets, visual inspection of the skyride plots suggests that a constant population size demographic model would be a reasonable fit to the data. Bayes Factor tests (data not shown) indicate that constant population size models are a better fit to both the mammoth and woolly rhinoceros. However, because these data sets comprise samples from both a broad temporal and geographic extent, it is likely that they violate, at least during some of their evolutionary history, the assumption of panmixia made by the coalescent models used in BEAST. The skyride plot provides the most flexibility of the coalescent models currently implemented in BEAST, and therefore is the most likely to accommodate the temporal changes in structure that likely characterised each of these species. The results of these analyses (wide confidence intervals and an inability to reject simpler, constant-size model) indicate that several of the data sets simply contain too little evolutionary information to be characterised using this approach.

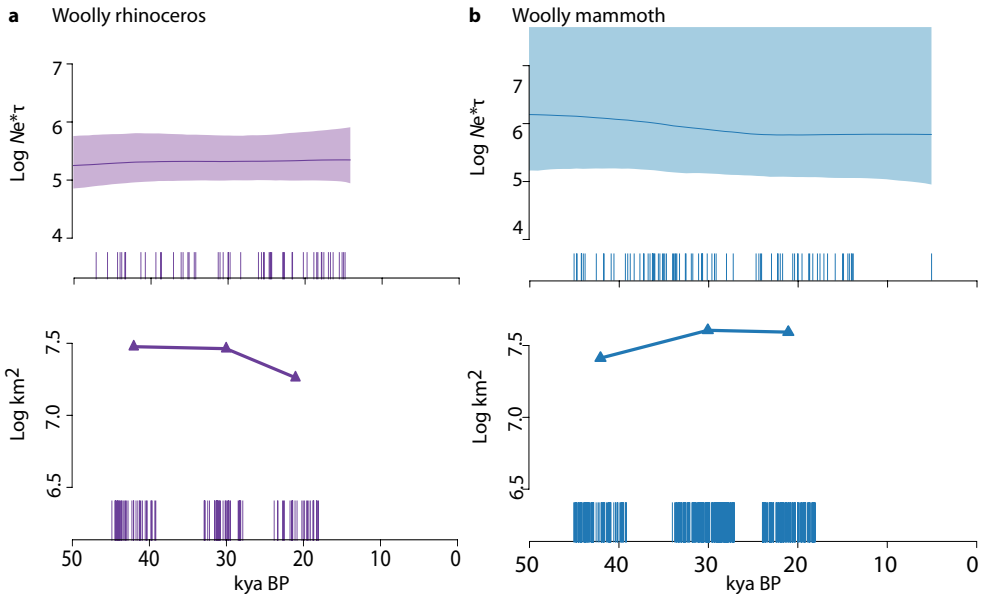

Supplementary Figure S3.6. Temporal changes in global effective population size and generation time (Ne * τ) and potential range size in (a) woolly rhinoceros and (b) woolly mammoth. Each species panel includes the demographic trajectory of the past 50,000 years inferred from BEAST and the area of potential range size (km^2) at 42, 30 and 21 estimated using species distribution models; range sizes could not be calculated at 6 kyr BP due to insufficient fossil localities (Fig. 1 in main text; Supplementary Information section S1). We assume a generation time of seven years in woolly rhinoceros and 20 years in woolly mammoth. Radiocarbon-dated samples used in each approach are shown as vertical lines below each panel; each line represents one dated individual.

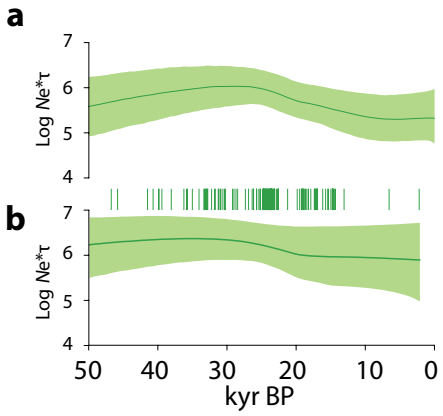

Supplementary Figure S3.7. Temporal changes in global effective population size and generation time (Ne * τ) in wild horse (a) including modern domestics (b) excluding modern domestics. Radiocarbon-dated samples used in the analysis are shown as vertical lines below the skyride in (a). We assume a generation time of five years.

SECTION S4: Gene-climate correlation

4.1 Method

The relationship between temporal changes in potential range size and changes in genetic diversity, used as a proxy for effective population size, over the past 50,000 years was evaluated in a Bayesian hierarchical modelling framework. The range size estimates were based on the results from species distribution models for four time periods with available climatic conditions (42, 30, 21 and 6 kyr BP; Supplementary Information section S1). The estimates of genetic diversity were extracted from the skyride analysis of genetic diversity based on the ancient DNA samples (Supplementary Information section S3). We estimated the relationship for the four species from which we had potential range size estimates for all four time periods: horse, reindeer, bison and musk ox. We were not able to estimate the potential range sizes of woolly rhinoceros and woolly mammoth at 6 kyr BP, as woolly rhinoceros went extinct *c*. 13 kyr BP and we did not have sufficient fossil localities for woolly mammoth at 6 kyr BP, when it was restricted to small island relict populations (Supplementary Information section S1).

Genetic diverstity estimates from BEAST are reported as a set of lines, where each line is an independent estimate of the trend in genetic diversity for the sampled population (Supplementary Fig. S4.1).These are usually summarized (e.g., by Tracer[88]) as a mean with a relatively large 95% Bayesian probability interval. However, it would be misleading to base further regression analysis on these mean values, as it would underestimate the uncertainty of the genetic diversity estimates.

To incorporate this uncertainty, we sampled 1,000 individual skyrides from the posterior distribution, available from the BEAST log files. For each of these, we calculated the mean genetic diversity of 6 ka intervals centred around the dates for which we had simulations of global climate (45–39, 33–27, 24–18 and 9–3 kyr BP; Supplementary Information section S1). We then carried out 5,000 individual Bayesian hierarchical linear regressions of these values on the estimated range sizes, and combined the resulting posterior distributions of the regression parameters to yield the final parameter estimates.

To incorporate the uncertainty in the projections of range size due to potential bias in the fossil record, we generated ten species distribution models for each species/time period, randomly sub-sampling 90% of the fossil localities for each of 10 model runs (see Supplementary Information section S1) using climate variables from GENESIS2. For each of these ten models, plus the full

model (all localities), we measured the size of the projected range. Within each of the 5,000 individual linear regressions, the climatic range size at each time point was sampled randomly from the set of potential range sizes.

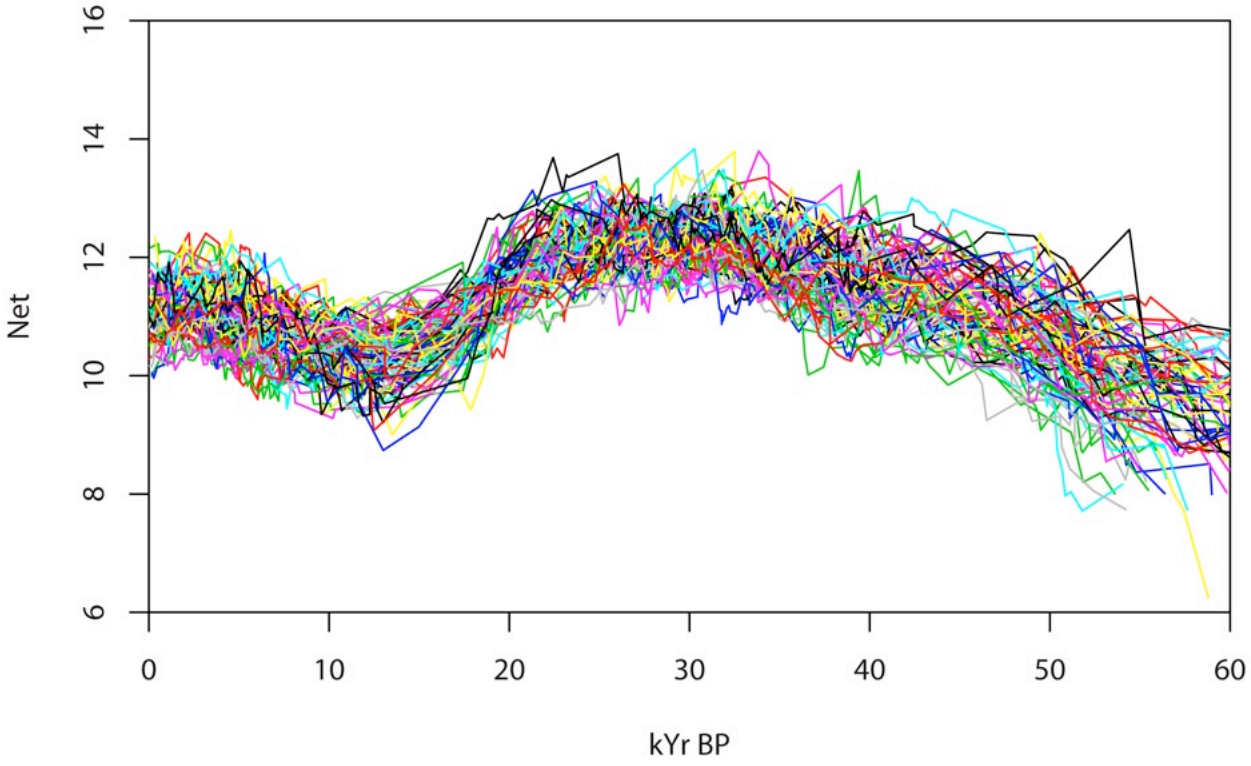

Supplementary Figure S4.1. Fifty randomly selected skylines for musk ox extracted from BEAST. Though there is an apparent overall trend, there is also considerable variation in the trajectory of each line.

The WinBUGS model used a common prior for the regression slopes for all four species, and independent priors for the intercepts. The biological rationale for this model is that although species exhibit positive temporal relationships between range size and abundance, the exact parameters of this relationship have been found to vary between different species[95]. Thus, points for different species may not simply be pooled. Using a hierarchical model for the regression slope allows a combined analysis of the regression slopes without enforcing a common intercept.

The WinBugs model used was:

```
Model
{
        for (i in 1:N)
        {
                pops[i] ~ dnorm(mu[i], tau)
                mu[i] <- alpha[species[i]] * bioms[i] + beta[species[i]]
        }

        for (j in 1:Nspec)
        {
                alpha[j] ~ dnorm(mu.alpha, tau.alpha)
                beta[j] ~ dnorm(0, 1.0E-6)
        }
        tau ~ dgamma(0.001, 0.001)
        sigma <- 1/sqrt(tau)
        sigma.alpha ~ dunif(0,100)
        tau.alpha <- 1/(sigma.alpha*sigma.alpha)
        mu.alpha ~ dnorm(0, 1.0E-6)
}
```

In WinBUGS, the Gibbs sampler was run in three individual chains for 50,000 iterations. The first 25,000 iterations were discarded as burn-in, and the remaining 25,000 were thinned by 1:25 to 1,000. Of these three chains of 1,000 values, 200 iterations were picked randomly and saved, resulting in 200 values times 5,000 skylines = 1,000,000 simulated values from the posterior distributions. These values represent a full sample of the posterior distribution for the relationship between the two variables, and incorporate error estimates from both the skyride analysis and the SDM-projected climatic range sizes.

4.2 Results

The results of a Bayesian analysis are probability distributions that reflect the degree of belief in the estimated parameters. To make the results comparable to the results of standard frequentist regression tests, we report the proportion of the posterior density of the slopes that is lower than zero. This is comparable to the p-value from a standard one-tailed t-test. The results are summarized in Supplementary Table S4.1 and Supplementary Figure S4.2.

Supplementary Table S4.1. Summary of the posterior parameters of the Bayesian hierarchical model. SE is the standard deviation of the posterior distribution. Here p represents the proportion of values that are below 0, and is comparable to the p-value from a standard one-tailed test. Range data are modelled using the GENESIS2 climatic simulations.

	Slope	SE	p	Intercept	SE
Horse	1.335	0.889	0.049	-8.829	14.675
Reindeer	0.561	0.463	0.101	5.452	7.451
Bison	1.974	0.983	0.011	-18.013	15.124
Musk ox	0.889	0.520	0.042	-2.957	8.505

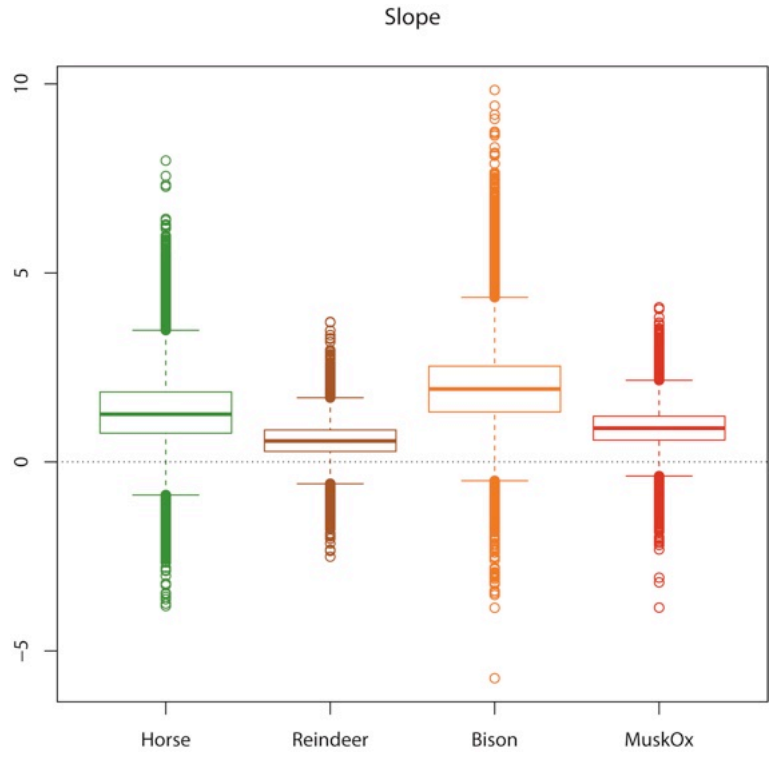

Supplementary Figure S4.2. Relationship between Ne*τ and range size (modelled with GENESIS2), summarized as posterior probability distributions of regression slopes from a Bayesian hierarchical regression. The proportion of probability densities below zero (analogous to a one-tailed p-value) can be seen in Supplementary Table S4.1.

The distributions of the six megafauna herbivores, reconstructed using SDMs for the periods 42, 30, 21 and 6 kyr BP, decreased in size from 30 kyr BP to the present for all species, although the severity of decline varies substantially among taxa (Supplementary Fig. S1.3). These trends are mirrored by genetic diversity in four of the six species, where there is a strong positive correlation

for horse, bison and musk ox, and a positive relationship for reindeer (Supplementary Fig. S4.3). Of note, due to the large confidence intervals, the slope for reindeer would not be considered significant when the posterior distribution is compared to a one-tailed significance value of 0.05. A positive correlation between range size and genetic diversity is consistent with ecological theory: the relationship between geographic distribution (range size) and species abundance is one of the best-documented patterns in macroecology[96]. These findings support the validity of climatic range as a proxy for range size, and of genetic diversity as a proxy for effective population size. The observation that effective population size is dependent on climate also strongly supports a role for climate in driving the population dynamics of megafauna species.

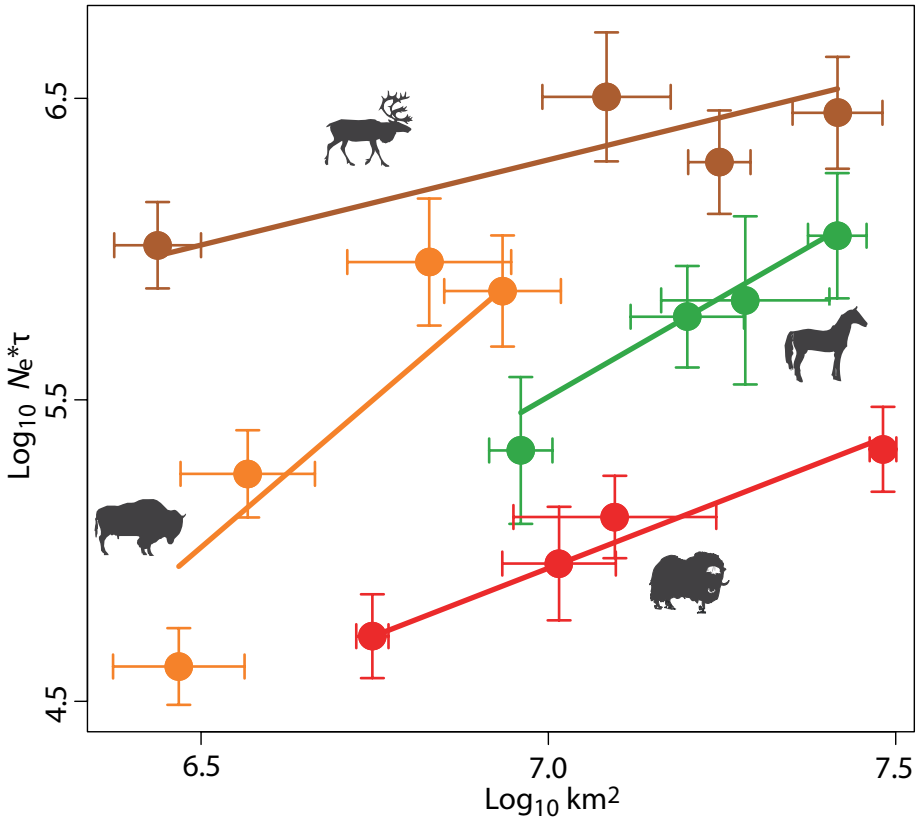

Supplementary Figure S4.3. Correlation between Ne*τ and range size for the four species for which we had sufficient data for a correlation analysis, modelled using GENESIS2. Genetic diversity is shown as the mean and standard deviation of the 1,000 values used in the regression analysis. The mean values of slope and intercept (Supplementary Table S4.1) were used to draw the trendlines. Error bars represent measures of uncertainty: range sizes calculated using ten random 90% subsets of fossil localities per period (horizontal bars) and posterior probabilities of Ne*τ (vertical bars) (S1 and S4).

To assess whether the analysis was robust with the inclusion of the data available for woolly rhinoceros and woolly mammoth, for which we did not have range size estimates at 6 kyr BP, we repeated the analysis with the three potential range size data points (42, 30, 21 kyr BP) for these two species. As expected, due to wide probability intervals of the skyrides for woolly rhinoceros and woolly mammoth (Supplementary Fig. S3.6), no relationship was detected for these two species, and the results for the remaining four species did not change.

4.3 Assessing effect of AOGCM choice

To specifically assess the effect of AOGCM choice on species' ranges (horse, reindeer, bison and musk ox) and the subsequent relationship between range size and effective population size, we also measured potential ranges modelled with an alternative Atmospheric-Ocean coupled General Circulation Model, HadCM3. The correlation between these alternative range size estimates and the estimates of genetic diversity is comparable to those for GENESIS2, and are shown in Supplementary Table S4.2 and Supplementary Figures S4.4 and S4.5. The species distribution model was run for the full set of fossil localities only (i.e. no subsampling was performed), and the genetic diversity data was represented by 1,000 different BEAST trees.

Supplementary Table S4.2. Summary of the posterior parameters of the Bayesian hierarchical model. SE is the standard deviation of the posterior distribution. Here p represents the the proportion of values that are below 0, and is comparable to the p-value from a standard one-tailed test. Range data are modelled using HadCM3.

	Slope	SE	p	Intercept	SE
Horse	0.915	0.540	0.047	-1.637	8.754
Reindeer	0.714	0.556	0.098	3.053	8.923
Bison	1.026	0.421	0.009	-3.478	6.530
Musk Ox	1.149	0.785	0.048	-6.730	12.529

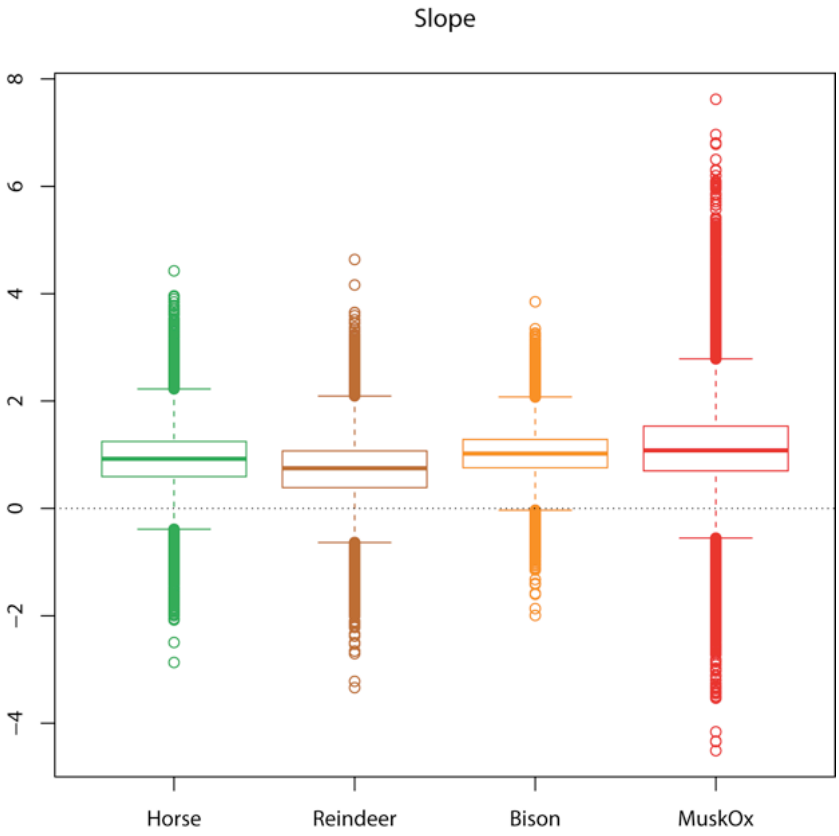

Supplementary Figure S4.4. Relationship between Ne*τ and range size (modelled with HadCM3), summarized as posterior probability distributions of regression slopes from a Bayesian hierarchical regression. The proportion of probability densities below zero (analogous to a one-tailed p-value) can be seen in Supplementary Table S4.2.

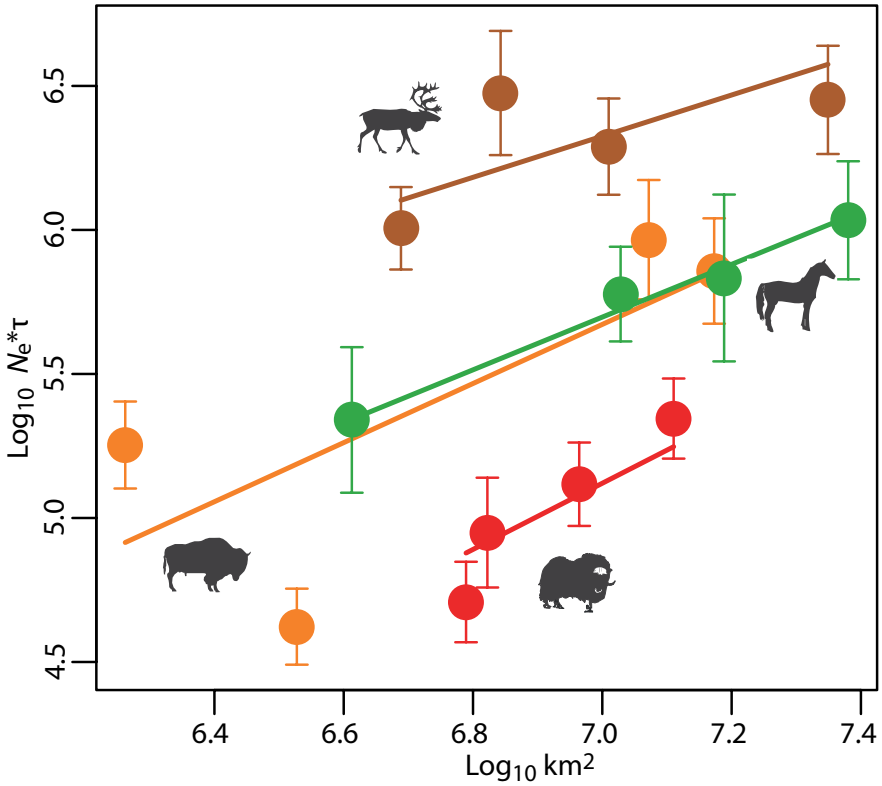

Supplementary Figure S4.5. The relationship between Ne*τ and range size for the four species for which we had sufficient data for a correlation analysis, modelled using HadCM3. Genetic diversity is shown as the mean and standard deviation of the 1,000 values used in the regression analysis. The mean values of slope and intercept (Supplementary Table S4.2) were used to draw the trendlines.

4.4 Influence of sample distribution and -size on results

The positive correlation observed between geographic range and genetic diversity could potentially be caused by the spatial distribution of samples and sample size, so the wider the distribution, the more palaeohabitats covered and consequently the larger the forecasted range. Similarly, the genetic diversity may increase with the number of samples and the geographic range covered. To investigate the effect of sample distribution, we calculated the mean pairwise geographic distance between all samples within each of the four time bins (45–39, 33–27, 24–18 and 9–3 kyr BP). Geographic distances were calculated between the LAT/LON coordinates using the Haversine formula and ignoring hills. For species present in both North America and Eurasia, pairwise distances between continents were rooted through Beringia (LAT 66.07, LON -168.92) to avoid crossing of the North Pole. To account for differences in sample size between time bins, we

averaged the pairwise distances by the number of samples. However, due to differences in the number of samples from each locality, we also averaged the geographic distances within each time bin by number of unique localities. As a third measure of spatial distribution, we calculated the distance between the two furthermost samples within each timebin. To asses the influence of sample number (disregarding spatial distribution), we estimated the correlation between estimates and sample size.

The distribution measures were compared to the mean values of genetic diversity and potential range size estimated for each time bin. To ensure that comparisons with our results were unbiased, we used the same WinBUGS hierarchical regression model to perform the correlations, and summarized our results by the proportion of the posterior distribution of slope values that are below 0 (see above). The results are presented in Supplementary Table S4.3. All posterior probability intervals include 0, indicating that the relationship between population and range size is unaffected by any relationship with the geographic distribution and number of samples.

Supplementary Table S4.3. Summary of Bayesian hierarchical linear regression models between measures of sampling (rows) and genetic diversity or range size (columns). Numbers indicate the proporation of the posterior density for the regression slope that lies below 0, and is thus comparable to the "p"-values given for the effective population size - range size correlation and to one-sided p values in frequentist statistics.

	Potential range size	Genetic diversity
Mean pairwise distance		
All samples	0.175	0.154
Unique localities	0.096	0.149
Maximum distance	0.209	0.197
Number of samples	0.246	0.225

To investigate whether the inclusion of 16 non-directly dates reindeer and bison samples (Supplementary Information section S1) influenced the positive relationship between range size and genetic diversity, we repeated the correlation analysis using GENESIS2 range sizes estimated with those data excluded. The significance of the correlation was not affected (Supplementary Table S4.4).

Supplementary Table S4.4. Summary of the posterior parameters of the Bayesian hierarchical model, with range sizes estimated using only directly-dated fossils for all species. Range data are modelled using GENESIS2. Here p is the proportion of probability densities below zero and is analogous to a one-tailed p-value.

	Slope	SE	p	Intercept	SE
Horse	1.410	0.830	0.039	-10.191	13.760
Reindeer	0.512	0.405	0.092	6.158	6.577
Bison	1.934	0.702	0.003	-17.434	10.840
Musk Ox	0.909	0.473	0.029	-3.241	7.728

SECTION S5: Temporal and spatial overlap of humans and megafauna

5.1 Introduction

To compare the temporal and geographic distribution of humans and megafauna in Europe and Siberia, we use dated faunal remains and radiocarbon determinations from human occupations for which we have latitude and longitude data. The basic premise is that the frequencies of dated sites or faunal remains can be used as a rough proxy for human or fauna population size at different points in time[97,98,99]. Differences in their geographic and temporal distribution were used to investigate whether humans and megafauna occupied similar areas at similar points in time and whether higher frequencies of humans were associated with lower frequencies of faunas, as one might expect if humans were directly or indirectly impacting the large animals.

5.2 Data collection

Fanual materials (n=2,996) come from a number of sources. Half (n=1,439) are directly-dated specimens used in this paper (Supplementary Information sections S1, S2) or summarized in [97,98,100,101]. An additional 1,557 specimens come from indirectly-dated palaeontological deposits and archaeofaunas. In Europe, these are primarily from sources compiled as part of the Stage 3 Project[102]. In Siberia, they come from sources cited in Supplementary Table S6.5. The indirectly-dated faunal material was included for multiple reasons. Firstly, the integrity of these data were good (see handling of samples below) and were comparable to the European human data. Secondly, had we not included the indirectly-dated information, we would ignore large amounts of data indicating the presence of the six megafauna species at particular points in time and in conjunction with humans. If we ignored these because they are not directly dated, our sample of direct material would be biased. Finally, including the indirectly-dated specimens considerably increased our samples sizes; without these data included, musk ox in Europe and bison in Siberia were uninformative, due to the rarity of their occurrences in the fossil record.

These indirect dates apply only to determinations of geographic overlap and temporal trends in radiocarbon frequencies as outlined in this section, and are presented within the main text. We also provide a replicate analysis using directly-dated only material for comparison, with similar results (Supplementary Fig. S5.2). The potential range size estimates used in the analysis of overlap between humans and megafauna ranges at 42, 30 and 21 kyr BP used directly-dated materials only

(except 16 indirect dates, discussed in Supplementary Information section S1), and provide another, quasi-independent assessment of these same patterns.

Indirectly-dated megafauna specimens from Europe

In Europe, data were selected from the Stage 3 database provided they met a number of criteria. 1) Ages had to be associated with the presence of one of the five key taxa being studied in Europe (woolly rhinoceros, woolly mammoth, horse, reindeer and musk ox). 2) All ages had to be clearly identified as being radiocarbon determinations (standard or AMS) or, in a few cases, had to come from organic materials that could reasonably be inferred to have been radiocarbon-dated; luminescence and uranium-thorium dates were excluded. 3) Each radiocarbon age had to have associated latitude and longitude information, lab codes and reported errors less than 10% of mean ages. All ages greater than 45,000 radiocarbon years before present were also excluded. 4) Any radiocarbon determinations that were directly associated with a given taxon were identified and assigned correctly. For example, a deposit containing horse, reindeer and woolly rhinoceros might be placed at 27,000 BP based on the dating of a horse tibia. The horse would be identified as "directly dated" and tallied with the directly dated specimens, while the other two taxa would be assigned an age of 27,000 BP but be considered "indirectly dated". These indirect radiocarbon ages were then combined with the directly-dated material and compared to trends in human radiocarbon frequencies. Note because of the temporal focus of the Stage 3 Project, the data on early European faunas (prior to 20–18 kyr BP) is actually somewhat richer than that for later periods.

Archaeofaunal data from Europe and Siberia

A further subset of purely archaeological faunas was also identified and their temporal trends examined (Figure 4 in main text). In the case of the Stage 3 data from Europe, radiocarbon ages were tallied only when associated with archaeological stone tool industries. To make the data comparable to the Siberian dataset, information was summarized by occupation (n=380) rather than individual radiocarbon age, with occupations assigned primarily on the basis of excavation layers identified in the Stage 3 database. When detailed information on individual sites and excavations was lacking, multiple radiocarbon ages within occupations were averaged, but not weighted or pooled.

The Siberian data were compiled from 98 radiocarbon-dated cultural occupations of 68 Upper Palaeolithic archaeological sites, each of which listed at least one of the six megafuna species. The

data and references are listed in Supplementary Table S6.5. An important note is that the radiocarbon dates presented are again not necessarily direct dates on a megafauna specimen, but are dates from materials (e.g., charcoal or even some other animal bone) associated with the listed species. The sites range in age from *c*. 41–12 thousand calendar years ago (kyr BP) and geographically come from the Ob', Yenisei, and Lena River basins as well as the eastern Transbaikal and far northeast Russia. All of these cultural occupations are interpreted to represent Upper Palaeolithic occupations. Middle Palaeolithic occupations were excluded. There are a few other notable Upper Palaeolithic assemblages with rich faunal records that were not included in the analysis; these are sites or occupations with no associated radiocarbon ages (e.g., the later Upper Palaeolithic occupations at the Krasnyi Iar sites, layer 8 at Diuktai Cave), only infinite dates (e.g., Makarovo-4), or problematic radiocarbon chronologies (e.g., Mogochino, Studenoe-1).

All taxonomic identifications were done by primary investigators of the archaeological sites. In most cases, published archaeological reports describing these sites provide only "kitchen lists" of faunal taxa present, while detailed statistics like number of individual specimens present (NISP) or minimum number of individuals (MNI) are not reported (although there are some notable exceptions, for example[103,104,105,106]; information included in Supplementary Table S6.5). Identifications reported in the primary literature are often at the genus level, which is not a problem for *Coelodonta*, *Mammuthus*, *Bison*, and *Rangifer*, but it means that some of the remains identified as *Equus* could include *E. hemionus*, the Asiatic wild ass. Similarly for musk ox, multiple species may occur, including *Ovibos moschatus* and *O. pallantis* ([106,107]).

Dates were gathered from the primary literature, including dates on animal bone, charcoal and other organic materials associated with Palaeolithic artifacts or features. Dates from non-cultural layers (e.g., from above or below a cultural layer) or from problematic materials (e.g., soil organics) were omitted, as were obviously aberrant dates (i.e., those that were clearly discordant from other dates in the same occupation, or were not in accord with other occupations of the same site). Multiple dates from the same occupations were averaged, using the method described by [108]. This was done to keep occupations with multiple dates (for example, Mal'ta, which has 13 radiocarbon dates for the same cultural layer) from weighing more heavily in the analysis than occupations with single dates. Latitude and longitude data were obtained using published descriptions of site locations and Google Earth.

Human data

Siberian human occupations come from [109]. The authors provide list of 516 georeferenced radiocarbon dates from 129 archaeological sites, along with summaries by individually-dated component. The radiocarbon ages for each occupational component were used here (n=233).

European human radiocarbon ages come from the INQUA Palaeolithic Radiocarbon Database, v. 11[67]. These data represent over 7,000 radiocarbon determinations from more than 1,500 sites. Due to the size and diverse nature of the INQUA data set, radiocarbon ages were not aggregated by archaeological occupation as done in Siberia. The data were cleaned for obvious errors, however, including: a) using only ages between 45,000 and 7,500 ^{14}C years BP, b) excluding all ages without latitude and longitude data, c) excluding all ages without associated ^{14}C errors, d) excluding all ages without lab codes, e) excluding dates of palaeontological deposits and f) excluding any determination with an error greater than 10% of the mean. A handful of discordant dates were also removed, mostly very young dates from purportedly old deposits. Although most sites have only a handful of ages, a few sites have many. These few sites are long, continuously occupied stratigraphic sequences, and the multiple ^{14}C determinations generally span the EpiPalaeolithic to Middle Palaeolithic (*c*. 45–12,000 ^{14}C years BP) rather than being clustered in individual occupations. They are not biased geographically, and include sites in England, Spain, France, Germany and Russia.

This yielded a total of 5,875 ages from over 1,461 sites in Europe. These include those produced by both anatomically modern *Homo sapiens sapiens* and archaic *Homo sapiens neanderthalensis*, the latter typically being associated with Middle Palaeolithic, Mousterian stone-tool industries. Although the Neandertals disappeared from most of Europe by 30,000 years ago, current interpretations suggest they were top-tier predators and should therefore have impacted megafauna populations when and where they were present[110,111,112].

While we were unable to aggregate the European human data as done in Siberia, we were able to assess the use of individual determinations by comparing patterns in the data provided by[68]. In that case, frequencies of individual ^{14}C determinations and dated components per 500-year interval are very tightly correlated ($r=.907$, $t=17.2$, $df=64$, $p<.001$; Supplementary Fig. S5.1) and the same is expected to hold true for Europe.

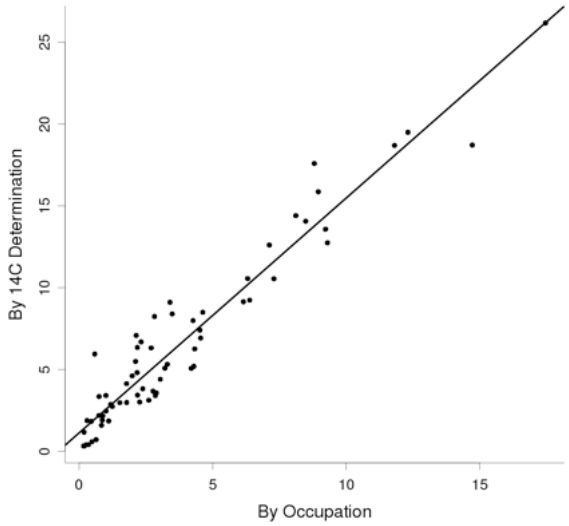

Supplementary Figure S5.1. Comparison of ^{14}C trends by aggregation method. Data points represent the binned, calibrated radiocarbon probabilities per 500-year interval for each data set (dated occupation; individual ^{14}C determinations). Periods with high numbers of individual radiocarbon dates also have high numbers of independent, dated occupations.

5.3 Data analysis

Summarizing radiocarbon frequencies and geographic data

To compare frequencies of different taxonomic groups, radiocarbon ages for all dated components, individual radiocarbon ages (European humans), or dated megafauna were summed in 500-calendar-year intervals from 50,000–0 BP (blocks 0-499 BP; 500-999 BP; 1,000-1,499 BP; etc.). Rather than using dated midpoints, the various radiocarbon ages were first calibrated using Calib 6.0 and the IntCal09 calibration curve[113]. A script was then used to collapse the year-by-year probabilities output by Calib 6.0 (options, write distribution files = "yes") into 500-year blocks using R[64]. This allowed us to use moderately-sized time intervals without worrying about larger errors associated with many determinations, the correct assignment of ages that fall close to interval divisions, or the non-normal distribution of the underlying, calibrated dates.

Mean latitudes and longitudes and their standard deviations were also calculated using the probability of a determination falling into a 500-year interval to weight its contribution. Thus dates that were highly likely to fall in a particular interval contributed heavily to estimates of the average latitude/longitude, while a determination that had a small possibility of falling in an interval

contributed little. Graphs of mean latitude and longitude for dated faunas and archaeological sites from Europe and Siberia are shown in Supplementary Figure S5.2. The area shared by humans and faunas at specific time intervals was approximated by identifying the latitudinal and longitudinal extent of the region held in common between them per interval (using mean lat/long ± 1sd), calculating its area, and expressing it as a percentage of the area occupied by the a given taxon (again at mean lat/long ± 1sd). These data and variation in location is discussed in the primary text and shown in Figure 4.

Timespan of comparison

Radiocarbon data were initially binned and mean latitudes and longitudes calculated across the entire IntCal09 sequence (50,000–0 calendar years BP), but trends in calibrated radiocarbon frequencies were compared across a smaller time range. First, no data were considered for periods beyond 45 kyr BP. Underlying ^{14}C data were too few for most taxa and regions, and the reliability of such dates more questionable. The younger end of the sequence was held at 12 kyr BP, the period by which most of the megafauna other than reindeer had substantially declined and the frequency of Palaeolithic occupations also drops off. Supplementary Figures S5.3 and S5.4 show the temporal distribution of binned, calibrated radiocarbon frequencies for the two regions using directly dated faunas only and with indirectly dated faunas included.

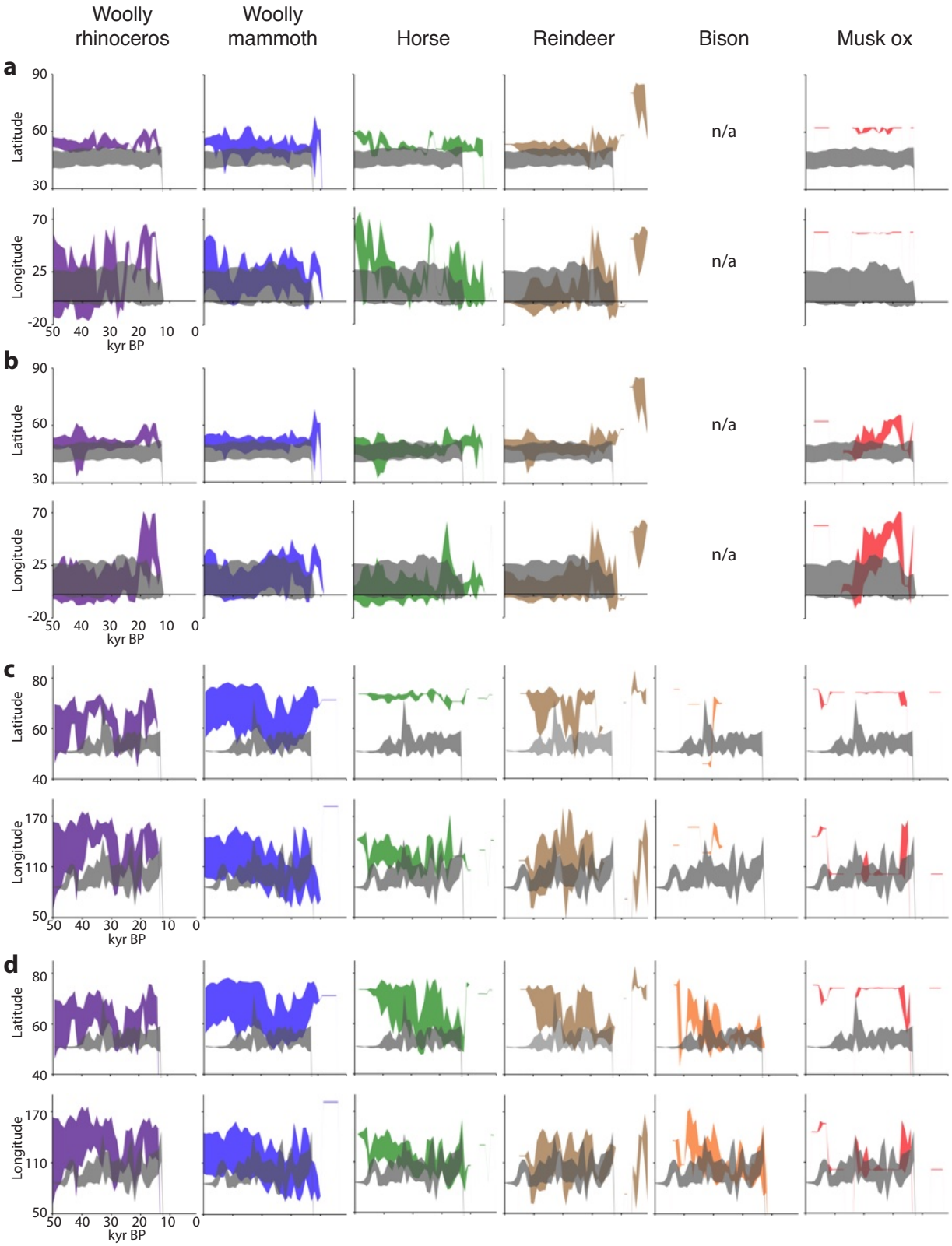

Supplementary Figure S5.2. Plots showing latitudinal and longitudinal overlap between megafauna (coloured shading) and human (grey shading) calibrated radiocarbon ages, A. Europe direct dates only, B. Europe indirect dates added, C. Siberia direct dates only, D. Siberia indirect dates added. Error bars are ± 1s.d.

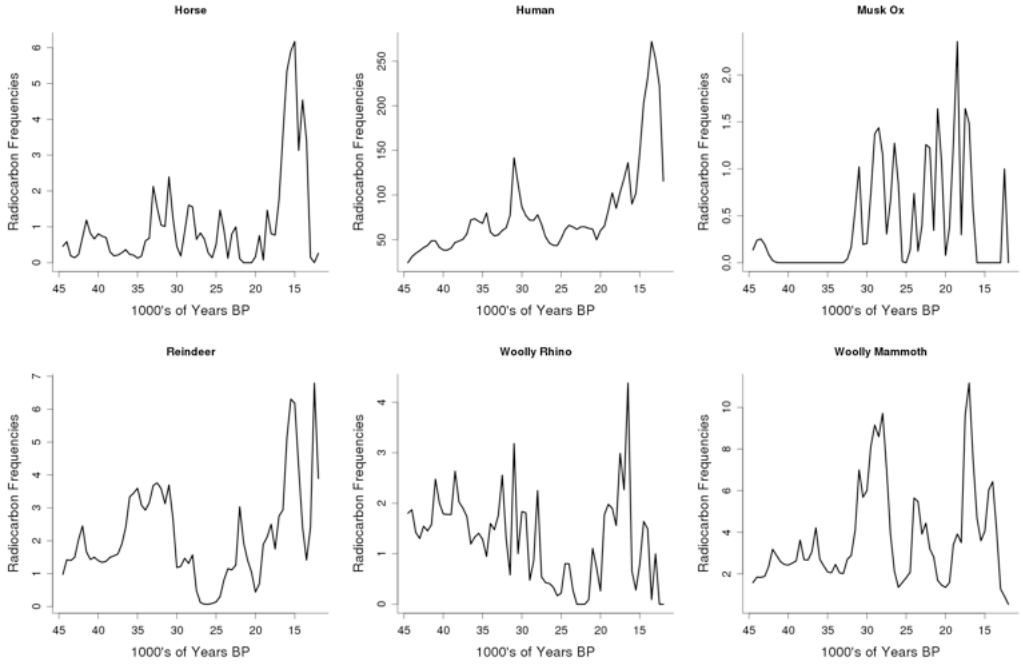

Supplementary Figure S5.3a. European radiocarbon frequencies, humans and directly dated faunas only.

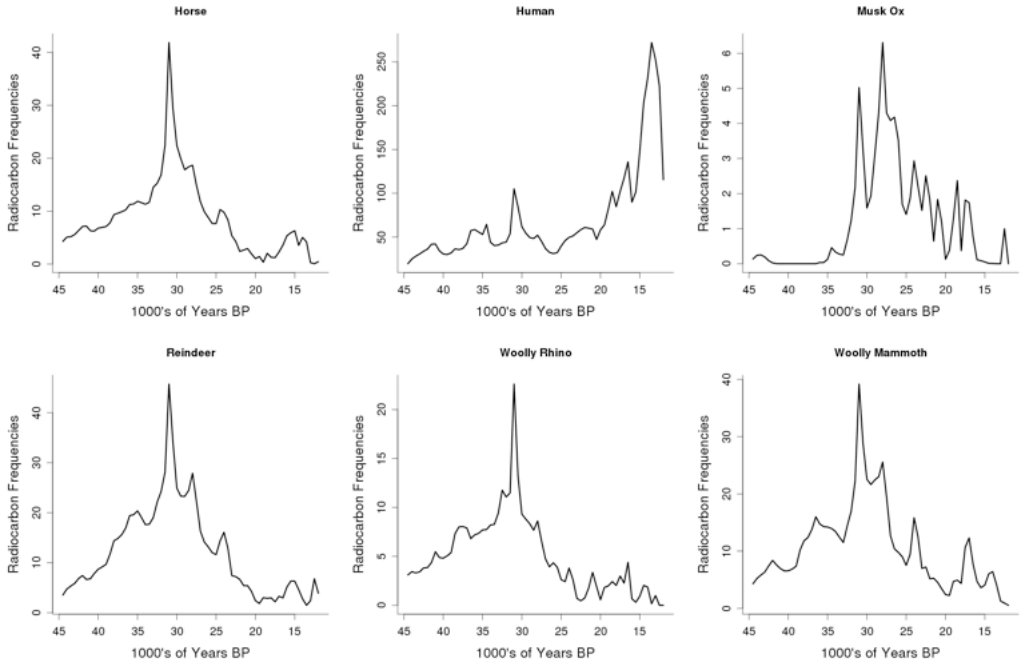

Supplementary Figure S5.3b. European radiocarbon frequencies, indirectly dated faunas included.

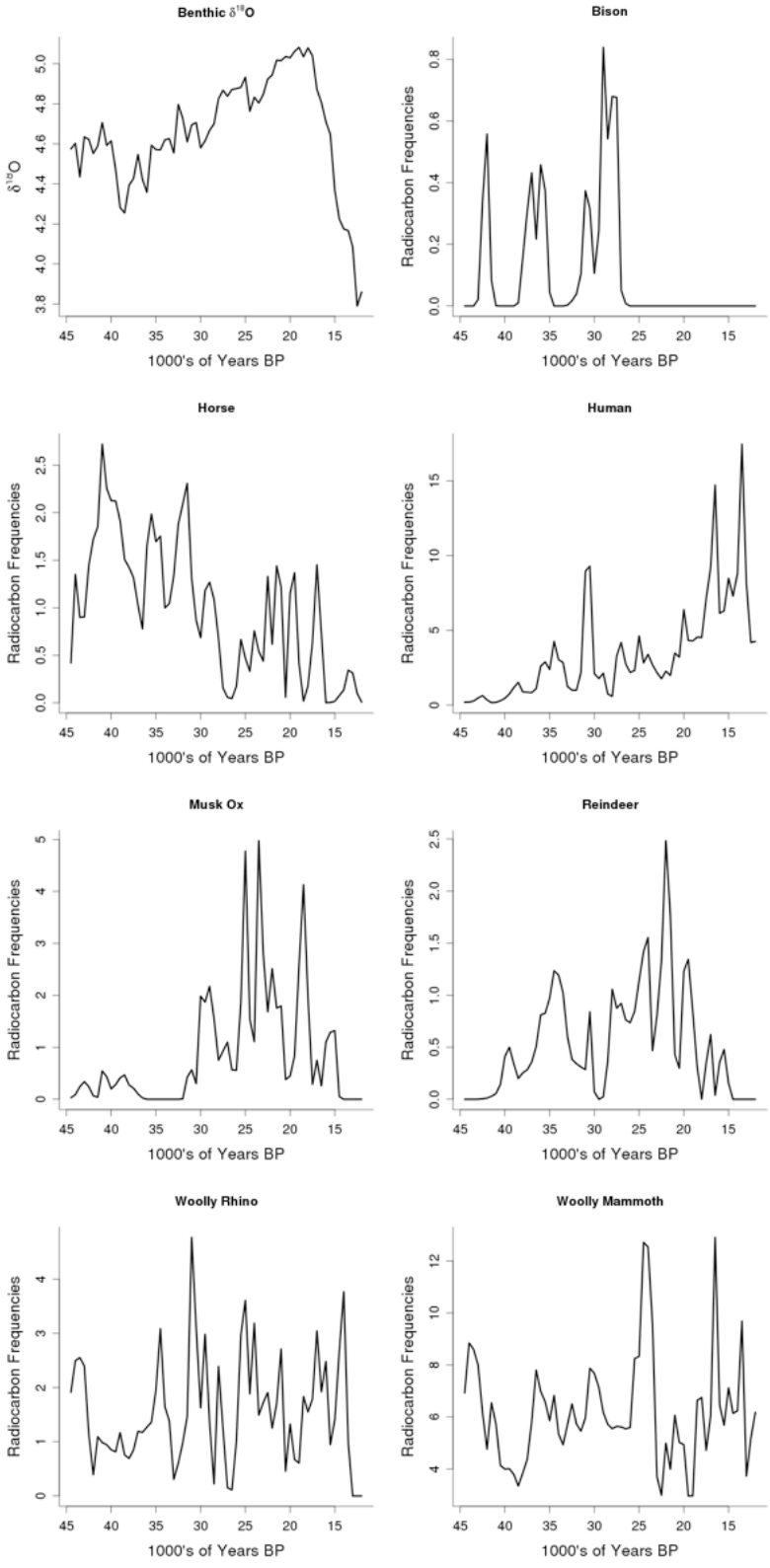

Supplementary Figure S5.4a. Siberian radiocarbon frequencies, humans and directly dated faunas only. The first panel shows the paeleoclimate data for the corresponding period.

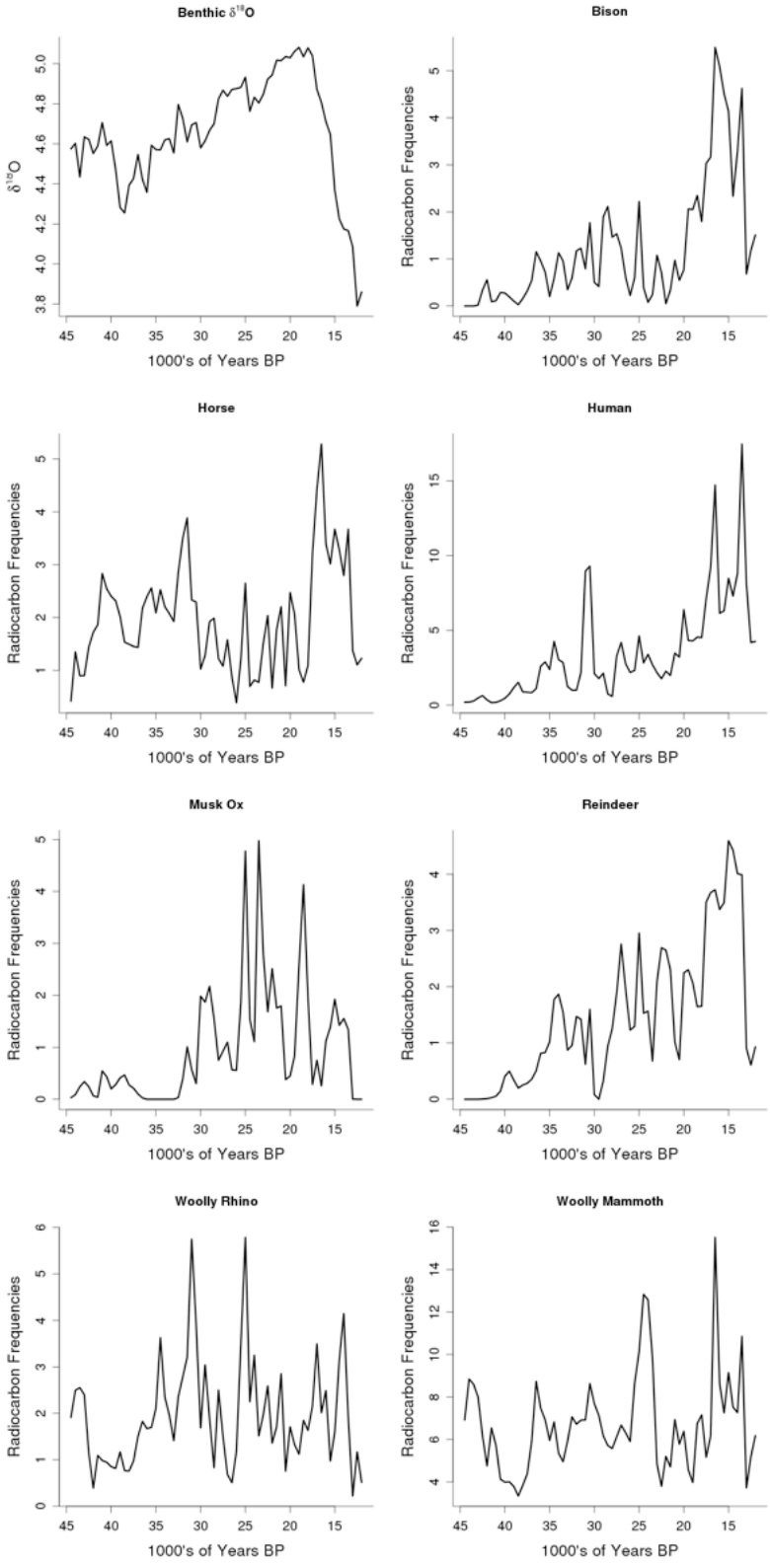

Supplementary Figure S5.4b. Siberian radiocarbon frequencies, indirectly dated faunas included. The first panel shows the paeleoclimate data for the corresponding period.

5.4 Comparing radiocarbon frequencies of humans and megafauna

We compare radiocarbon frequencies among taxa after accounting for the possible effects of taphonomy and climate, following methods outlined in [97,98] and [114]. Our chosen climate proxy was Shackleton's 24MD952042 North Atlantic benthic ^{18}O core, corrected to the SFCP2005 timescale[115,116] (variable, ^{18}O; first panel in Fig. S5.4a,b). This is the same fine-grained proxy used in the previously cited studies, is appropriate for comparing trends in geographically widespread locations and mirrors but is less noisy than the Greenland ice-cores.

To incorporate issues of taphonomy and preservation in the human data, we used the model proposed by [117]. Their formula calculates an expected number of observations at time *t* for a constant, random phenomenon suffering solely taphonomic losses. We converted this to an estimate of the proportion of original observations surviving at each 500-year interval midpoint (12,250 calendar years BP; 12,750 calendar years BP; etc.) as N_t/N_0. These values scale between 0 and 1, decline in a curvilinear fashion, and were used as predictors in our regression models (variable, Surv). Fits were slightly better than simple log transforms, with somewhat more variation across intermediate values but a reduced tendency to overestimate extremes. While this approach differs from that advocated by the original authors, we argue that it is more appropriate in cases such as ours, where similar taphonomic histories cannot be assumed for all sequences[118].

As an ancillary measure, we also calculated the absolute difference (variable, AbsDif) between radiocarbon and calendar years for each interval using the IntCal09 curve. For example, the period from 29–28.5 kyr BP corresponds to 24,146–23,743 ^{14}C years BP (ignoring error). The corresponding radiocarbon interval is thus 403 years long, or 97 years shorter than the corresponding calendar span. This interval would have a measure of "-97". Exactly equal intervals would have a value of "0" assigned, etc. These measures were meant to provide a check on possible over- or underrepresentation of parts of the calendar due to differences in atmospheric ^{14}C production. A file containing the benthic ^{18}O sequence, calculated survivorship and ^{14}C/calendar differences is provided in the supplemental archive ("climtaph.csv").

Comparison among taxa in Siberia and Europe were based on partial correlations after controlling for the three variables just mentioned. This was done using the residuals from a multiple regression of calibrated radiocarbon frequency (variable, ^{14}C; the binned sums) against each main effect and allowing for a survivorship by climate interaction (^{14}C~ Surv + ^{18}O + AbsDif +Surv:^{18}O). We then looked at how human frequencies compared with those of other faunas. In Europe, comparisons

using indirectly dated faunas were done only after excluding 676 radiocarbon determination from the INQUA human database that were also found in the Stage 3 archaeofaunas.

While not perfect, the overall behaviour of the models is good to very good in most cases, although the actual amount of variation explained by the taphonomic and climate variables varies substantially and the residuals in some taxa and regions still deviate from normal. Examples of such deviations includes higher than expected frequencies of human occupations at the Pleistocene-Holocene boundary, high frequencies of several indirectly-dated European faunas around 32 kyr BP (Fig. S5.3b), and the irregular behavior of several directly dated taxa such as European musk ox and, to a lesser extent, European horse and Siberian bison. In the latter cases this clearly results from the substantial gaps in the ^{14}C record (Supplementary Fig. S5.3a) and one should be cautious when drawing inferences from these data.

Partial correlation coefficients for humans versus European and Siberian faunas are presented in Supplementary Table S5.1. After controlling for the possible influence of climate and taphonomic losses, there appears to be little relationship between humans and any of the faunas other than mammoth and perhaps Siberian musk ox (Figure S5.5a,c). There is also little relationship among changes in the frequencies of dated faunas. Again, part of this is due to the small sample sizes of many directly dated taxa.

If the indirectly dated materials are included, changes in the frequency of dated faunas and humans in Europe become more positively correlated (Supplementary Table S5.1b; Supplementary Fig. S5.5b,d) and higher yet for OIS 3 material only (45–22 kyr BP). Correlations among faunas other than musk ox also become very high (.85 <= r <= .95). In Siberia, residual radiocarbon frequencies of humans and faunas other than musk ox also become moderately but positively correlated, echoing previously reported patterns identified for humans and woolly mammoths[97,98]. The relationship with humans reflects the incorporation of archaeological faunas, particularly the OIS 3 faunas in Europe, while the higher correlations among faunas reflect the fact that many of these animals regularly co-occur within particular archaeological deposits. The frequencies of archaeological faunas and non-faunal archaeological deposits remain highly correlated throughout OIS 3, including both broad increases from 45 kyr BP to roughly 30 kyr BP and general declines between 30 and 22 kyr BP (r=.82), and it would be interesting to see if these continued past the Last Glacial Maximum. While suggestive of some common driver for humans and faunas, this strong, positive relationship cannot be read as absolute proof that both humans and faunas were more common at certain times, since people might be expected to preferentially incorporate larger animals even if the latter were in decline.

Regardless, these changes are not the clear-cut indicator one would expect if people were negatively impacting these megafauna; more human occupations do not appear to lead to fewer occurences of any taxon. These results are not necessarily surprising given the often limited overlap in their ranges (Fig. 4 in main text, Supplementary Fig. S5.2). Humans and musk ox tend to be found in very different regions of Europe and Siberia, and in Siberia woolly rhino and woolly mammoth appear to shift their ranges northward even as human distribution remains fairly constant through 12,000 kyr BP. Opportunities for humans to impact these taxa may have been limited as a result. These results do not deny humans a role in the eventual extinction of any taxon and will merit reconsideration as additional remains are uncovered. However, they do cast doubt on whether such extinctions occurred solely as a consequence of human impact.

Supplementary Table S5.1a. Partial correlations between the frequency of dated humans and faunas per 500-year time period after controlling for climate and taphonomy. Residuals based on the model described in the text using directly dated faunas only.

	Woolly Rhino	Woolly Mammoth	Horse	Reindeer	Bison	Musk ox
Europe	.222	.415	.232	.010		.034
Siberia	.334	.374	.040	.027	.084	-.249

Supplementary Table S5.1b. Partial correlations between the frequency of dated humans and faunas per 500-year time period after controlling for climate and taphonomy. Residuals based on the model described in the text using directly and indirectly dated faunas.

	Woolly Rhino	Woolly Mammoth	Horse	Reindeer	Bison	Musk ox
Europe	.526	.540	.523	.471		.285
Siberia	.421	.448	.528	.525	.525	-.148

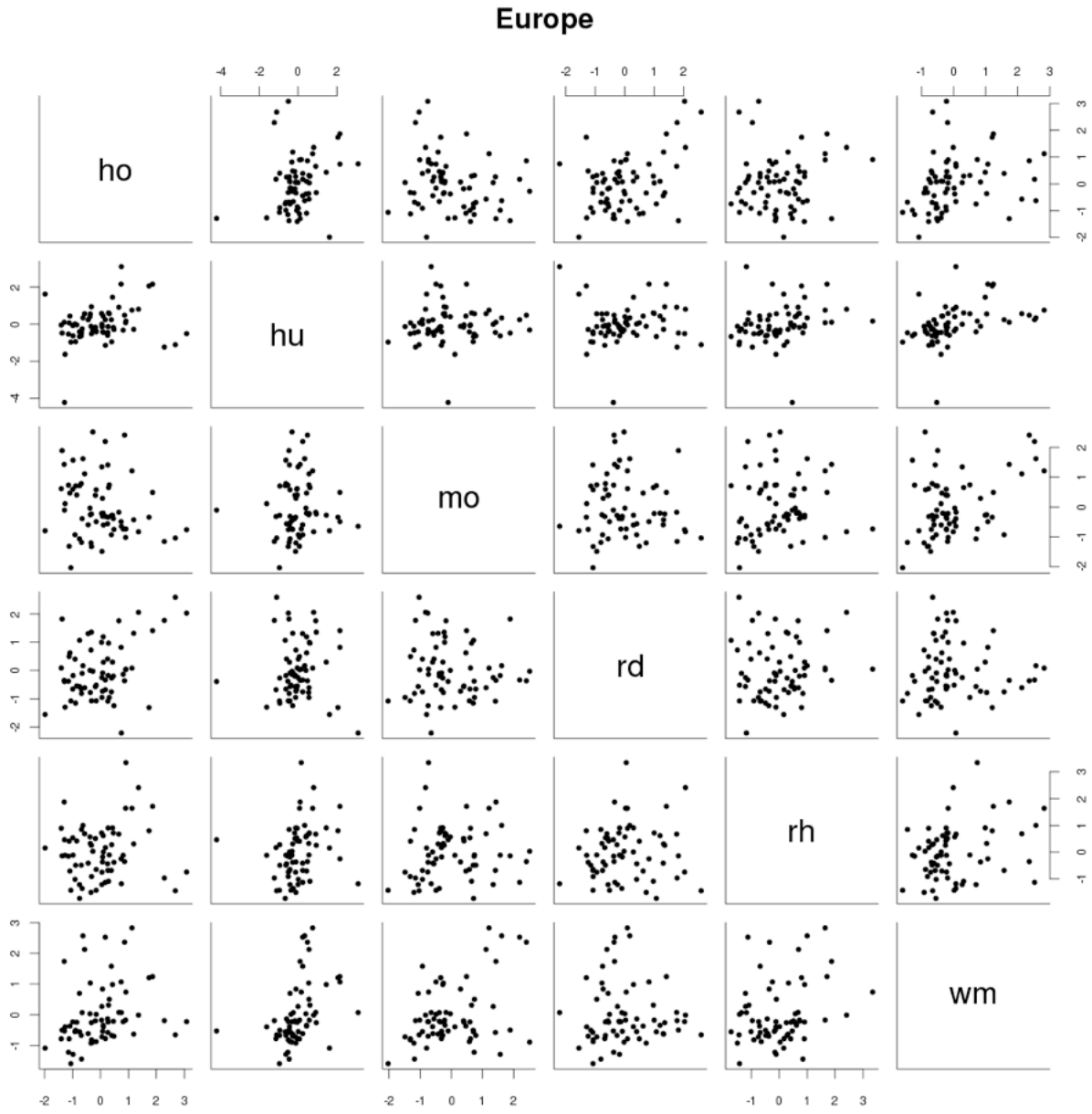

Supplementary Figure S5.5a. Scatterplot of residual ^{14}C frequencies for Europe. "ho" horse; "hu" human; "mo" musk ox; "rd" reindeer; "rh" woolly rhino; "wm" woolly mammoth. Directly dated material only.

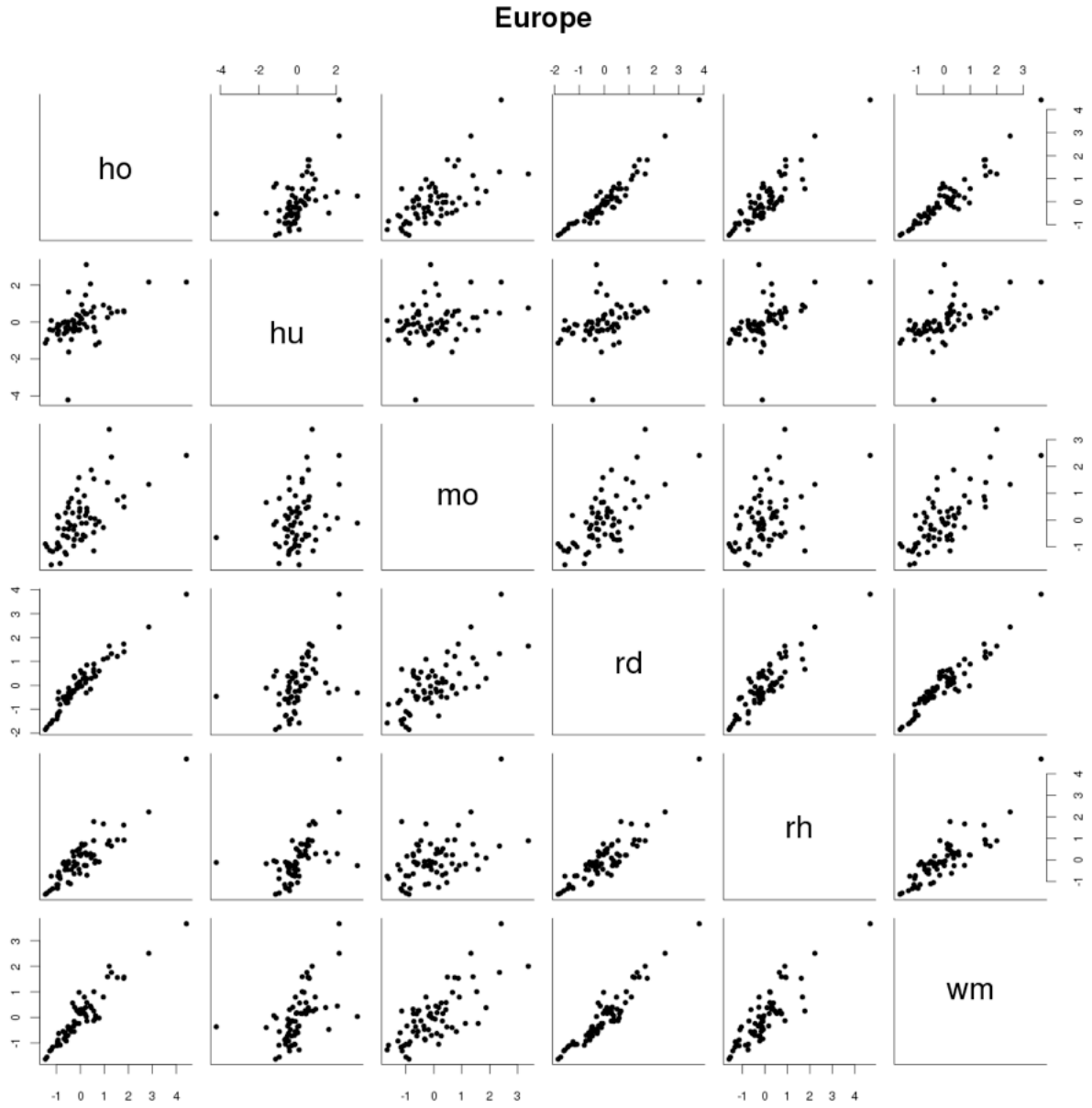

Supplementary Figure S5.5b. Scatterplot of residual ^{14}C frequencies for Europe. "bi" bison; "ho" horse; "hu" human; "mo" musk ox; "rd" reindeer; "rh" woolly rhino; "wm" woolly mammoth. Indirect dates included.

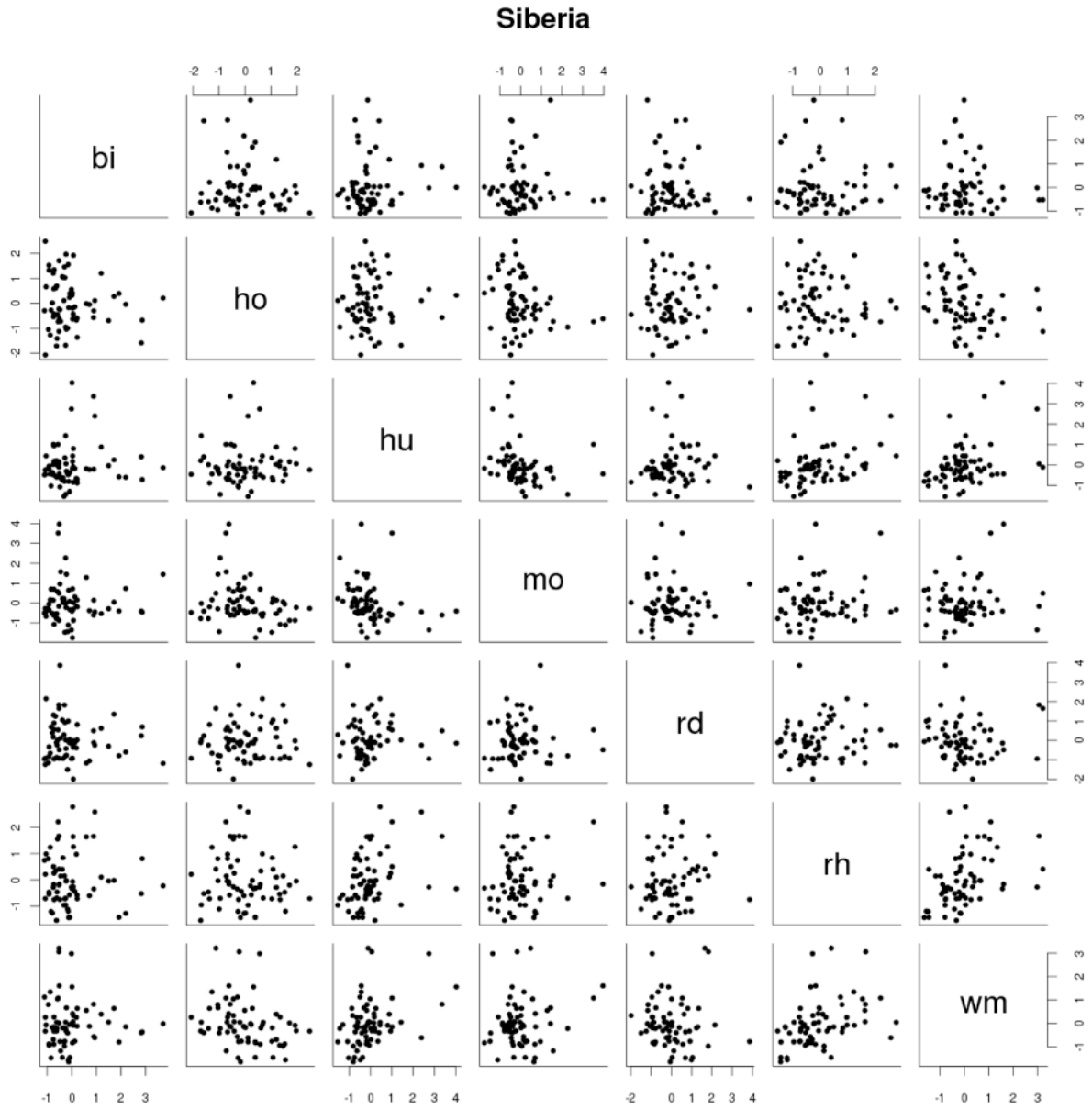

Supplementary Figure S5.5c. Scatterplot of residual ^{14}C frequencies for Siberia. "bi" bison; "ho" horse; "hu" human; "mo" musk ox; "rd" reindeer; "rh" woolly rhino; "wm" woolly mammoth. Direct dates only.

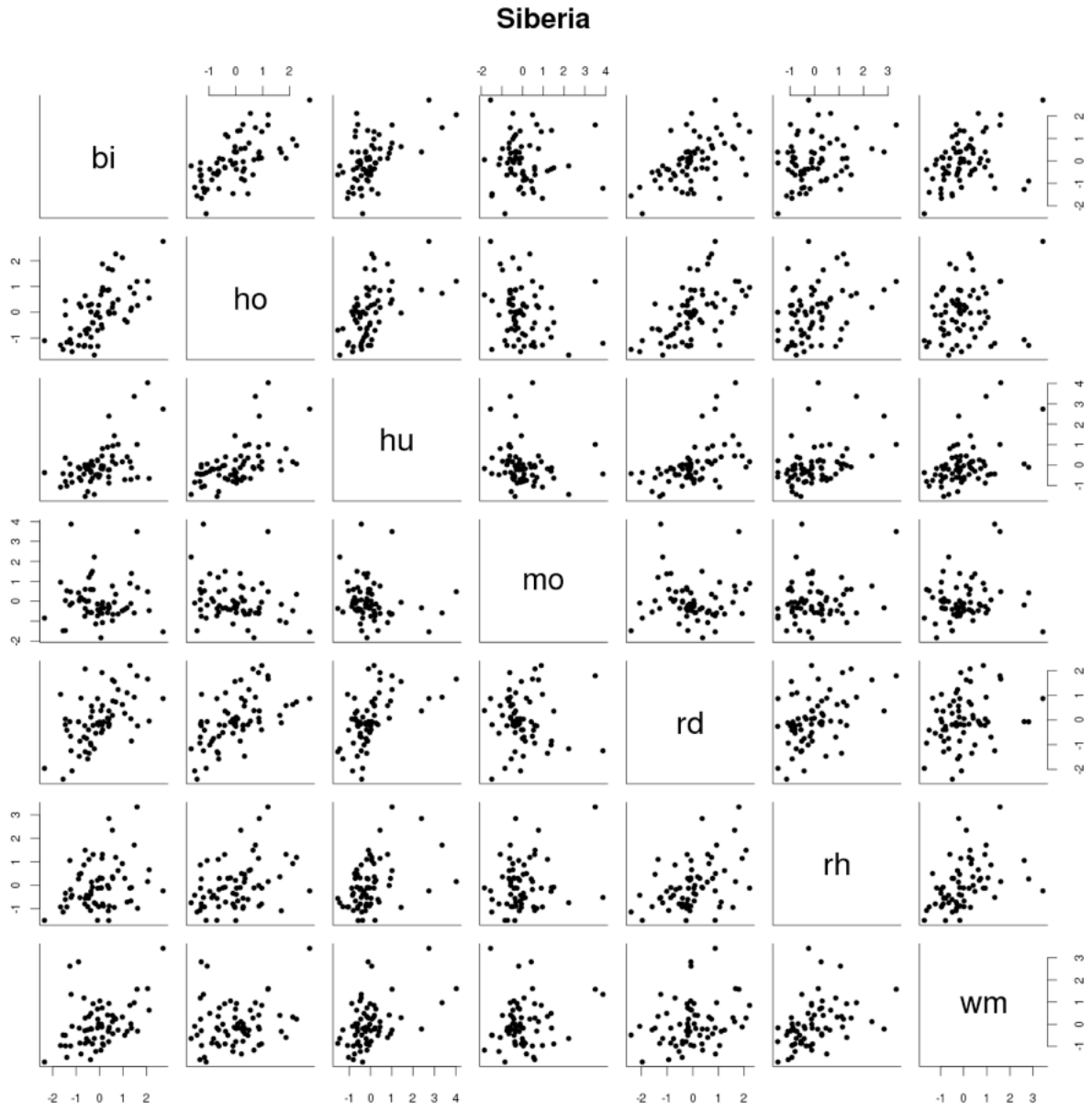

Supplementary Figure S5.5d. Scatterplot of residual ^{14}C frequencies for Siberia. "bi" bison; "ho" horse; "hu" human; "mo" musk ox; "rd" reindeer; "rh" woolly rhino; "wm" woolly mammoth. Indirect dates included.

REFERENCES

[1] Lomolino, M. V. & Heaney, L. R., eds. *Frontiers of Biogeography: New Directions in the Geography of Nature*. Sinauer Associates, Sunderland, Massachusetts (2004)

[2] Diniz-Filho, J. A. F. *et al*. Partitioning and mapping uncertainties in ensembles of forecasts of
[2] Diniz-Filho, J. A. F. *et al*. Partitioning and mapping uncertainties in ensembles of forecasts of
species turnover under climate change. *Ecography* **32**, 897-906 (2009)

[3] Nogués-Bravo, D., Rodríguez, J., Hortal, J., Batra, P. & Araújo, M. B. Climate change, humans, and the extinction of the woolly mammoth. *PLOS Biol*. **6**, e79 (2008)

[4] Grinnell, J. The niche-relationships of the California Thrasher. *Auk* **34**, 427-433 (1917)

[5] Hutchinson, G. E. Concluding remarks. *Cold Spring Harbor Symp. Quant. Biol.* **22**, 145-159 (1957)

[6] Soberón, J. Grinellian and Eltonian niches and geographic distributions of species. *Ecol. Lett*. **10**, 1115-1123 (2007)

[7] Whittaker, R. H. Vegetation of the Great Smoky Mountains. *Ecol. Monogr*. **26**, 1-80 (1956)

[8] Whittaker, R. H. Direct Gradient Analysis. In: Whittaker, R. H., ed. *Handbook of Vegetation Science 5: Coordination and Classification of Communities.* The Hague: Junk Publishers, 9-50 (1973)

[9] Austin, M. P. Models for the analysis of species' response to environmental gradients. *Vegetatio* **69**, 35-45 (1987)

[10] Austin, M. P. Spatial prediction of species distribution: an interface between ecological theory and statistical modelling. *Ecol. Model*. **157**, 101-118 (2002)

[11] Colwell, R. K. & Rangel, T. F. Hutchinson's duality: the once and future niche. *P. Nat. Acad. Sci.***106** (Supplement 2), 19651-19658 (2009)

[12] Purvis, A., Gittleman, J. L., Cowlishaw, G. & Mace, G. M. Predicting extinction risk in declining species. *Proc. R. Soc. Lond. B* **267**, 1947-1952 (2000)

[13] Elith, J., *et al*. Novel methods improve prediction of species' distributions from occurrence data. *Ecography* **29**, 129–151 (2006)

[14] Nogués-Bravo, D. Predicting the past distribution of species climatic niches. *Global Ecol. Biogeogr.* **18**, 521-531 (2009)

[15] Pearson, R. G. & Dawson, T. P. Predicting the impacts of climate change on the distribution of species: are bioclimate envelope models useful? *Global Ecol. Biogeogr.* **12**, 361-371 (2003)

[16] Williams, J. W., Jackson, S. T. & Kutzbach, J. E. Projected distributions of novel and disappearing climates by 2100 AD. *P. Nat. Acad. Sci.* **104**, 5738-5742, (2007)

[17] Sowers, T. & Bender, M. Climate records covering the last deglaciation. *Science* **269**, 210–214 (1995)

[18] Bonfils, C. J., Lewden, D. & Taylor, K. E. Summary documentation of the PMIP models. Available: http://pmip.lsce.ipsl.fr/docs/. Accessed 27 February 2008 (1998)

[19] CLIMAP Project Members. Seasonal reconstructions of the Earth's surface at the Last Glacial Maximum. In: *Map Series, Technical Report MC-36*. Boulder (Colorado): Geological Society of America (1981)

[20] Barron, E. J., & Pollard, D. High-resolution climate simulations of Oxygen Isotope Stage 3 in Europe. *Quaternary Res*. **58**, 296–309 (2002)

[21] Pollard, D., Bergengren, J. C., Stillwell-Soller, L. M., Felzer, B. & Thompson, S. L. Climate simulations for 10000 and 6000 years BP using the GENESIS global climate model. *Palaeoclimates- Data Model.* **2**, 183–218 (1998)

[22] Berger, A. L. Long-term variations of daily insolation and Quaternary climatic changes. *J Atmos. Sci.* **35**, 2362–2367 (1978)

[23] Berger, A., & Loutre, M. F. Insolation values for the climate of the last 10 million years. *Quaternary Sci. Rev.* **10**, 297–317 (1991)

[24] Hoar, M. R. Palutikof, J. P. & Thorne, M. C. Model intercomparison for the present day, the mid-Holocene, and the Last Glacial Maximum over western *Europe. J. Geophys. Res.* **109**, D08104.1-D08104.25 (2004)

[25] Alfano, M. J., Barron, E. J., Pollard, D., Huntley, B. & Allen, J. R. M. Comparison of climate model results with European vegetation and permafrost during oxygen isotope stage three. *Quaternary Res.* **59**, 97-107 (2003)

[26] Thompson, S. L. & Pollard, D. Greenland and Antarctic mass balances for present and doubled atomospheric CO_2 from the GENESIS version-2 global model. *J. Climate* **10**, 871–900 (1997)

[27] Barnola, J.-M., Raynaud, D., Korotkevich, Y. S. & Lorius, C. Vostok ice core provides 160,000-year record of atmospheric CO2. *Nature* **329**, 408-414 (1987)

[28] Neftel, A., Oeschger, H., Staffelbach, T. & Stauffer, B. CO2 record in the Byrd ice core 50,000–5,000 years B.P. *Nature* **331**, 609–611 (1988)

[29] Singarayer, J. S. & Valdes, P. J. High-latitude climate sensitivity to ice-sheet forcing over the last 120 kyr. *Quaternary Sci. Rev.* **29**, 43-55 (2010)

[30] Gordon, C. *et al*. The simulation of SST, sea ice extents and ocean heat transports in a version of the Hadley Centre coupled model without flux adjustments. *Clim. Dynam*. **16**, 147–168 (2000)

[31] Gregory, J. M. & Mitchell, J. F. B. The climate response to CO2 of the Hadley Centre Coupled AOGCM with and without flux adjustment. *Geophys. Res. Lett*. **24**, 1943–1946 (1997)

[32] Edwards, J. M. & Slingo, A. Studies with a flexible new radiation code.1. Choosing a configuration for a large-scale model. *Q. J. Royal Met. Soc.* **122**, 689–719 (1996)

[33] Cusack, S., Slingo, A., Edwards, J. M. & Wild, M. The radiative impact of a simple aerosol climatology on the Hadley Centre GCM. *Q. J. Royal Met. Soc.* **124**, 2517–2526 (1998)

[34] Gregory, D., Kershaw, R. & Inness, P. M. Parameterisation of momentum transport by convection: II. Tests in single column and general circulation models. *Q. J. Royal Met. Soc.* **123**, 1153–1183 (1997)

[35] Cox, P., Betts, R., Bunton, C., Essery, R., Rowntree, P. R., & Smith, J. The impact of new land-surface physics on the GCM simulation and climate sensitivity. *Clim. Dynam*. **15**, 183-203 (1999)

[36] Gent, P. R. & McWilliams, J. C. Isopycnal mixing in ocean circulation models. *J. Phys. Oceanogr.* **20**, 150–155 (1990)

[37] Cattle, H. & Crossley, J. Modelling arctic climate change. *Phil. Trans. R. Soc. Lond. A* **352**, 201-213 (1995)

[38] Petit, J. R. *et al*. Climate and atmospheric history of the past 420 000 years from the Vostok Ice Core, Antarctica. *Nature* **399**, 429–436 (1999)

[39] Spahni, R. *et al*. Variations of atmospheric methane and nitrous oxide during the last 650 000 years from Antarctic ice cores. *Science* **310**, 1317–1321 (2005)

[40] Parrenin, F. *et al*. The EDC3 agescale for the EPICA dome C ice core. *Clim. Past* **3**, 485–497 (2007)

[41] Peltier, W. R. Global glacial isostasy and the surface of the iceage Earth: the ICE-5G (VM2) model and GRACE. *Annu. Rev. Earth Planet Sci*. **32**, 111–149 (2004)

[42] Peltier, W. R. & Fairbanks, R. G. Global glacial ice volume and Last Glacial Maximum duration from an extended Barbados sea level record. *Quat. Sci. Rev*. **25**, 3322–3337 (2006)

[43] Martinsen, D. G., *et al*. Age dating and orbital theory of the ice ages: development of a high resolution 0–300,000-year chronostratigraphy. *Quat. Res*. **27**, 1–30 (1987)

[44] Hewitt, C. D., *et al*. The effect of a large freshwater perturbation on the glacial North Atlantic Ocean using a coupled general circulation model. *J. Clim*. **19**, 4436–4447 (2006)

[45] Braconnot, P., *et al*. Results of PMIP2 coupled simulations of the Mid-Holocene and Last Glacial Maximum–Part 1: experiments and large-scale features. *Clim. Past* **3**, 261–277, doi:10.5194/cp-3-261-2007 (2007)

[46] Beaumont, L. J., Hughes, L. & Poulsen, M. Predicting species distributions: use of climatic parameters in BIOCLIM and its impact on predictions of species' current and future distributions. *Ecol. Mod.* **186**, 251-270 (2005)

[47] Reimer, P. J., *et al*. IntCal09 and Marine09 radiocarbon age calibration curves, 0–50,000 years cal BP. *Radiocarbon* **51**, 1111–1150 (2009)

[48] Barnosky, A. D. & Lindsey, E. L. Timing of Quaternary megafaunal extinction in South America in relation to human arrival and climate change. *Quatern. Int*. **217**, 10-29 (2010)

[49] Kuzmin, Y. V. & Orlova, L. A. Radiocarbon chronology and environment of wooly mammoth (*Mammuthus primigenius* Blum.) in northern Asia: results and perspectives. *Earth Sci. Rev.* **68**, 133-169 (2004)

[50] Vartanyan, S. L., Arslanov, K. A., Karhu, J. A., Possnert, G. & Sulerzhitsky, L. D. Collection of radiocarbon dates on the mammoths (*Mammuthus primigenius*) and other genera of Wrangel Island, northeast Siberia, Russia. *Quaternary Res.* **70**, 51-59 (2008)

[51] Guthrie, R. D. Radiocarbon evidence of mid-Holocene mammoths stranded on an Alaskan Bering Sea island. *Nature* **429**, 746-749 (2004)

[52] Farber, O. & Kadmon, R. Assessment of alternative approaches for bioclimatic modelling with special emphasis on the Mahalanobis distance. *Ecol. Mod.***160**, 115-130 (2003)

[53] Anderson, R. P., Lew, D. & Peterson, A. T. Evaluating predictive models of species' distributions: criteria for selecting optimal models. *Ecol. Mod.* **162**, 211-232 (2003)

[54] Phillips, S. J., Anderson, R. P. & Schapire, R. E. Maximum entropy modelling of species geographic distributions. *Ecol. Mod.* **190**, 231-259 (2006)

[55] Lobo, J. M., Jiménez-Valverde, A. & Hortal, J. The uncertain nature of absences and their importance in species distribution modelling. *Ecography* **33**, 103-114 (2010)

[56] Lobo, J. M. & Tognelli, M. F. Exploring the effects of quantity and location of pseudo-absences and sampling biases on the performance of distribution models with limited point occurrence data. *J. Nat. Conserv*. **19**, 1-7 (2011)

[57] Varela, S. J. M., Lobo, J., Rodríguez, J., & Batra, P. Were the Late Pleistocene climatic changes responsible for the disappearance of the European spotted hyena populations? Hindcasting a species geographic distribution across time. *Quaternary Sci. Rev.* **29**, 2027-2035 (2010)

[58] Tsoar, A., Allouche, O., Steinitz, O., Rotem, D. & Kadmon, R. A comparative evaluation of presence-only methods for modelling species distribution. *Diversity Distrib*. **13**, 397-405 (2007)

[59] Varela, S., Rodríguez, J. & Lobo, J. M. Is current climatic equilibrium a guarantee for the transferability of distribution model predictions? A case study of the spotted hyena. *J. Biogeogr.* **36**, 1645-1655 (2009)

[60] Martínez-Meyer, E., Peterson, A. T. & Hargrove, W. W. Ecological niches as stable distributional constraints on mammal species, with implications for Pleistocene extinctions and climate change projections for biodiversity. *Global Ecol. Biogeogr.* **13**, 305-314 (2004)

[61] Souza Muñoz, M. *et al.* openModeller: a generic approach to species' potential distribution modelling. *GeoInformatica* **1-25**, DOI 10.1007/s10707-009-0090-7(2009)

[62] Lobo, J. M., Jiménez-Valverde, A. & Real, R. AUC: a misleading measure of the performance of predictive distribution models. *Global Ecol. Biogeogr.* **17**, 145-151 (2008)

[63] Pearce, J. & Ferrier, S. An evaluation of alternative algorithms for fitting species distribution models using logistic regression. *Ecol. Mod.* **128**, 127-147 (2000)

[64] R Development Core Team. R: A language and environment for statistical computing. R Foundation for Statistical Computing, Vienna, Austria. ISBN 3-900051-07-0, URL http://www.R-project.org (2010)

[65] Bivand, R. S., Pebesma, E. J. & Gomez-Rubio, V. Applied spatial data analysis with R. Springer, NY. http://www.asdar-book.org/ (2008)

[66] Kuhn, T. S., McFarlane, K. A., Groves, P., Mooers, A. O. & Shapiro, B. Modern and ancient DNA reveal recent partial replacement of caribou in the southwest Yukon. *Mol. Ecol.* **19**, 1312–1323 (2010)

[67] INQUA. *International Union for Quaternary Research (INQUA) Radiocarbon Palaeolithic Database Europe, v.11*. (http://www.kuleuven.be/geography/frg/projects/14c-palaeolithic/download) (2010)

[68] Hamilton, M. J. & Briggs, B. Archaeological support for the three-stage expansion of modern humans across northeastern Eurasia and into the Americas. *PLOS One* **5(8)**, 1-9 (2010)

[69] Araújo, M. B. & Pearson, R. G. Equilibrium of species' distributions with climate. *Ecography* **28**, 693-695 (2005)

[70] Svenning, J.-C. & Skov, F. Could tree diversity pattern in Europe be generated by postglacial dispersal limitation? *Ecol. Let*. **10**, 453-460 (2007)

[71] Elias, S. A. & Crocker, B. The Bering Land Bridge: a moisture barrier to the dispersal of steppe-tundra biota? *Quaternary Sci. Rev.* **27**, 2473-2483 (2008)

[72] Weinstock, J. *et al*. Evolution, systematics, and phylogeography of Pleistocene horses in the New World: a molecular perspective. *PLoS Biol.* **3**: e241 (2005)

[73] Campos, P.F. *et al.* Ancient DNA analyses exclude humans as the driving force behind late Pleistocene musk ox (*Ovibos moschatus*) population dynamics. *P. Nat. Acad. Sci.***107**, 5675–5680 (2010)

[74] Gravlund, P., Meldgaard, M., Paabo, S. & Arctander, P. Polyphyletic origin of the small-bodied, high-arctic subspecies of tundra reindeer (*Rangifer tarandus*). *Mol. Phylogenet. Evol.* **10**, 151–159 (1998)

[75] Edgar, R. C. MUSCLE: multiple sequence alignment with high accuracy and high throughput. *Nucleic Acids Res.* **32**, 1792-1797 (2004)

[76] Gouy, M., Guindon, S. & Gascuel, O. SeaView version 4: a multiplatform graphical user interface for sequence alignment and phylogenetic tree building. *Mol. Biol. Evol.* **27**, 221–224 (2010)

[77] Shapiro, B. *et al.* Rise and fall of the Beringian steppe bison. *Science* **306**, 1561-1565 (2004)

[78] Debruyne, R. *et al*. Out of America: ancient DNA evidence for a new world origin of late Quaternary woolly mammoths. *Curr. Biol.* **18**, 1320–1326 (2008)

[79] Excoffier, L. & Lischer, H. E. Arlequin suite ver 3.5: a new series of programs to perform population genetics analyses under Linux and Windows. *Mol. Ecol. Res.* **10**, 564–567 (2010)

[80] Librado, P. & Rozas, J. DnaSP v5: A software for comprehensive analysis of DNA polymorphism data. *Bioinformatics* **25**, 1451–1452 (2009)

[81] Depaulis, F., Orlando, L. & Hänni, C. Using classical population genetics tools with heterochroneous data: time matters! *PLoS ONE* **4**, e5541 (2009)

[82] Boyd, L. & Haupt, K.A. *Przewalski's horse: the history and biology of an endangered species*. Albany: State University of New York Press (1984)

[83] Boulet, M., Couturier, S., Côté, S. D., Otto, R. & Bernatchez, L. Integrative use of spatial, genetic, and demographic analyses for investigating genetic connectivity between migratory, montane, and sedentary caribou herds. *Mol. Ecol.* **16**, 4223–42 (2007)

[84] Halbert, N. D., Ward, T. J., Schnabel, R. D., Taylor, J.F. & Derr, J.N. Conservation genomics; disequilibrium mapping of domestic cattle chromosomal segments in North American bison populations. *Mol. Ecol.* **14**, 2343–2362 (2005)

[85] Beaumont, M. Joint determination of topology, divergence time and immigration in population trees. pp. 134-154. In *Simulations, Genetics and Human Prehistory*, S. Matsumura, P. Forster and C. Renfrew (eds.) Cambridge: McDonald Institute for Archaeological Research (2008)

[86] Drummond, A. J. & Rambaut, A. BEAST: Bayesian evolutionary analysis by sampling trees. *BMC Evol. Biol.* **7**, 214 (2007)

[87] Drummond, A. J., Ho, S. Y. W., Phillips, M. J. & Rambaut, A. Relaxed phylogenetics and dating with confidence. *PLoS Biology* **4,** e88 (2006)

[88] Rambaut, A. & Drummond, A. J. Tracer v1.4, Available from: http://beast.bio.ed.ac.uk/Tracer (2007). Accessed April 2010.

[89] Minin, V. N., Bloomquist, E. W. & Suchard, M. A. Smooth skyride through a rough skyline: Bayesian coalescent-based inference of population dynamics. *Mol. Biol. Evol.* **25**, 1459-1471 (2008)

[90] Pannell, J. R. Coalescence in a metapopulation with recurrent local extinction and recolonization. *Evolution* **57**, 949-961 (2003)

[91] Navascués, M., Depaulis, F. & Emerson, B. C. Combining contemporary and ancient DNA in population genetic and phylogeographical studies. *Mol. Ecol. Res.* **10**, 760-772 (2010)

[92] Ho, S. Y. W. & Shapiro, B. Skyline-plot methods for estimating demographic history from nucleotide sequences. *Mol. Ecol. Res.* **11**, 423-432 (2011)

[93] Suchard, M. A., Weiss, R. E. & Sinsheimer, J. S. Bayesian selection of continuous-time Markov chain evolutionary models. *Mol. Biol. Evol.* **18**, 1001-1013 (2001)

[94] Drummond, A. J., Rambaut, A., Shapiro, B. & Pybus, O. G. Bayesian coalescent inference of past population dynamics from molecular sequences. *Mol. Biol. Evol*. **22**, 1185–1192 (2005)

[95] Webb, T. J., Noble, D. & Freckleton, R. P. Abundance–occupancy dynamics in a human dominated environment: linking interspecific and intraspecific trends in British farmland and woodland birds. *J. Anim. Ecol.* **76**, 123 (2007)

[96] Borregaard, M. K. & Rahbek, C. Causality of the relationship between geographic distribution and species abundance. *Q. Rev. Biol.* **85**, 3-25 (2010)

[97] Ugan, A. & Byers, D. Geographic and temporal trends in proboscidean and human radiocarbon histories during the late Pleistocene. *Quaternary Sci. Rev.* **26**, 3058–3080 (2007)

[98] Ugan, A. & Byers, D. A global perspective on the spatiotemporal pattern of the Late Pleistocene human and woolly mammoth radiocarbon record. *Quatern. Int*. **191**, 69–81 (2008)

[99] Dye, T. & Komori, E. A pre-censal population history of Hawai'i. *New Zeal. J. Archaeol.* **14**, 113–128 (1992)

[100] Ukkonen, P., Arppe, L., Houmark-Nielsen, M., Kjær, K. H. & Karhu, J. A. MIS 3 mammoth remains from Sweden—implications for faunal history, palaeoclimate and glaciation chronology. *Quaternary Sci. Rev.* **26**, 3081–3098 (2007)

[101] Nadachowski, A., Lipeckia, G., Wojtala, P. & Miękdo, B. (2011). Radiocarbon chronology of woolly mammoth (Mammuthus primigenius) from Poland. *Quatern. Int*. doi:10.1016/j.quaint.2011.03.011

[102] van Andel, T.H. & Davies, W.D. (editors). *Neanderthals and Modern Humans in the European Landscape of the Last Glaciation - Archaeological Results of the Stage 3 Project*. The McDonald Institute for Archaeological Research, Cambridge (2003)

[103] Ermolova, N. M. *Teriofauna Doliny Angary v Pozdnem Antropogene* (Nauka, Novosibirsk, 1978) [in Russian]

[104] Germonpre, M. & Lbova, L. Mammalian remains from the Upper Palaeolithic Site Kamenka, Buryatia (Siberia). *J. Archaeol. Sci.* **23**, 35-57 (1996)

[105] Ovodov, N. D. in *Prirodnaia Sreda i Drevnii Chelovek v Pozdnem Antropogene* (Nauka, Ulan-Ude, 1987), pp. 122–40 [in Russian]

[106] Ineshin, E. M., & Teten'kin, A. V. *Chelovek i Prirodnaia Sreda Severa Baikal'skoi Sibiri v Pozdnem Pleistotsene. Mestonakhozhdenie Bol'shoi Iakor' I* (Nauka, Novosibirsk, 2010) [in Russian]

[107] Mochanov, IU. A. *Drevneishie Etapy Zaseleniia Chelovekom Severo-Vostochnoi Azii* (Nauka, Novosibirsk, 1977) [in Russian]

[108] Long, A., & Rippeteau, B. Testing contemporaneity and averaging radiocarbon dates. *Am. Antiquity* **39**, 205-215 (1974)

[109] Hamilton, M. J., Buchanon, B. & O'Rourke, D. Archaeological Support for the Three-Stage Expansion of Modern Humans across Northeastern Eurasia and into the Americas. *PLoS ONE* **5**, e12472 (2010)

[110] Bocherens, H., *et al*. New isotopic evidence for dietary habits of Neandertals from Belgium. *J. Hum. Evol.* **40**, 497–505 (2001)

[111] Adler, D., Bar-Oz, G., Belfer-Cohen, A. & Bar-Yosef, O. Ahead of the game: Middle and Upper Paleolithic hunting behaviors in the southern Caucasus. *Curr. Anthr.* **47**, 89–118 (2006)

[112] Richards, M., *et al*. Isotopic dietary analysis of a Neanderthal and associated faunas from the site of Jonzac (Charente-Maritime), France. *J. Hum. Evol.* **55**, 179–185 (2008)

[113] Stuiver, M. & Reimer, P. J. Extended ^{14}C database and revised CALIB radiocarbon calibration program. *Radiocarbon* **35**, 215–230 (1993)

[114] Surovell, T. A. & Brantingham, P. J. A note on the use of temporal frequency distributions in studies of prehistoric demography. *J. Archaeol. Sci.* **24**, 1868–1877 (2007)

[115] Shackleton, N. J., Hall, M. A., &Vincent, E. Phase relationships between millennial-scale events 64,000–24,000 years ago. *Palaeoceanography* **15**, 565–569 (2000)

[116] Shackleton, N. J., Fairbanks, R. G., Chiu, T. C. & Parrenin, F. Absolute calibration of the Greenland time scale: implications for Antarctic time scales and for d^{14}C. *Quaternary Sci. Rev.* **23**, 1513–1522 (2004)

[117] Surovell, T., Finley, J., Smith, G., Brantingham, P. & Kelly, R. Correcting temporal frequency distributions for taphonomic bias. *J. Archaeol. Sci.* **36**, 1715–1724 (2009)

[118] Ballenger, J. & Mabry, J. Temporal frequency distributions of alluvium in the American Southwest: taphonomic, paleohydraulic, and demographic implications. *J. Arch. Sci.* **38**, 1314–1325 (2011)

SECTION S6: Data tables and sample information

Table S6.1. Dated fossil localities of the six megafauna species used to build the species distribution models; woolly rhinoceros (WR), woolly mammoth (MAM), wild horse (HRS), reindeer (RD), bison (BIS) and musk ox (MOX). Most specimens are directly dated; n/a in the AMS ID column indicates indirectly-dated specimens. In addition, woolly rhinoceros, horse and reindeer fossils with calibrated ages within 45–39, 33–27, 24–18 and 9–3 kyr BP from Supplementary Tables S6.2, S6.3 and S6.4 were included in the analysis. References follow below the table.

Species	AMS ID	14C date	14C SE	IntCal09 date	IntCal 09 SE	LAT	LON	Country	Locality	Ref
BIS	OxA-11169	3,155	36	3,383	39	44.50	-108.20	U.S.A.	Natural Trap Cave, WY	1
BIS	OxA-11271	3,220	45	3,438	51	44.50	-108.20	U.S.A.	Natural Trap Cave, WY	1
BIS	OxA-11618	3,298	37	3,524	47	53.28	-110.00	Canada	Lloydminster, AB	1
BIS	Beta-1627	3,600	70	3,910	102	51.08	-114.08	Canada	Hitching Post Ranch, Calgary, AB	1
BIS	Beta 65662	4,495	60	5,149	107	66.65	-143.72	U.S.A.	Black R. Yukon Flats, AK	1
BIS	OxA-11579	4,660	38	5,402	59	49.63	-110.21	Canada	Stampede Site, Cypress Hills, AB	1
BIS	OxA-11610	5,205	45	5,965	68	53.34	-113.31	Canada	Edmonton, AB	1
BIS	OxA-11624	5,845	45	6,661	61	51.08	-114.08	Canada	Horse Hills Pit, Edmonton, AB	1
BIS	OxA-11165	6,110	45	6,991	83	70.52	-128.35	Canada	Baillie Island, NWT	1
BIS	OxA-11585	6,775	40	7,626	29	51.08	-114.08	Canada	Tuscany Site, Calgary, AB	1
BIS	OxA-11589	7,060	45	7,891	46	49.63	-110.21	Canada	Stampede Site, Cypress Hills, AB	1
BIS	OxA-11581	7,105	45	7,938	45	49.63	-110.21	Canada	Stampede Site, Cypress Hills, AB	1
BIS	OxA-11614	7,115	50	7,945	49	49.63	-110.21	Canada	Stampede Site, Cypress Hills, AB	1
BIS	OxA-11583	7,310	45	8,108	55	51.08	-114.08	Canada	Tuscany Site, Calgary, AB	1
BIS	OxA-11622	7,475	45	8,295	55	51.08	-114.08	Canada	Tuscany Site, Calgary, AB	1
BIS	OxA-11223	16,685	80	19,822	177	66.26	-161.35	U.S.A.	Elephant Point, AK	1
BIS	CAMS 53777	17,160	80	20,362	200	70.81	-154.41	U.S.A.	Ikpikpuk R., North Slope, AK	1
BIS	OxA-10542	17,960	90	21,426	149	64.06	-141.89	U.S.A.	Lost Chicken Cr., Chicken, AK	1
BIS	n/a	19,150	280	22,876	361	65.46	-147.38	U.S.A.	Upper Cleary Cr., Fairbanks, AK	1
BIS	n/a	19,360	280	23,072	382	64.84	-147.96	U.S.A.	Ester Cr., Fairbanks, AK	1
BIS	CAMS 53772	19,420	100	23,136	253	70.81	-154.41	U.S.A.	Ikpikpuk R., North Slope, AK	1
BIS	OxA-11247	19,420	100	23,136	253	60.81	-149.43	U.S.A.	Seward Peninsula, Alder Cr., AK	1
BIS	OxA-11139	19,540	120	23,361	266	64.06	-141.89	U.S.A.	Lost Chicken Cr., Chicken, AK	1
BIS	n/a	19,570	290	23,367	420	64.84	-147.96	U.S.A.	Ester Cr., Fairbanks, AK	1
BIS	OxA-12068	20,020	150	23,925	230	44.50	-108.20	U.S.A.	Natural Trap Cave, WY	1
BIS	OxA-11629	23,040	120	27,896	254	69.90	133.90	Russia	Yana-Indigirka lowland, Siberia	1
BIS	n/a	23,380	460	28,209	574	64.84	-147.96	U.S.A.	Ester Cr., Fairbanks, AK	1
BIS	CAMS 53901	23,680	170	28,427	254	70.81	-154.41	U.S.A.	Ikpikpuk R., North Slope, AK	1
BIS	OxA-11194	23,780	140	28,549	253	71.16	153.45	Russia	Kolyma lowland, Bol. Khomus-Yuryakh R., Siberia	1
BIS	CAMS 53764	24,500	180	29,335	277	70.81	-154.41	U.S.A.	Ikpikpuk R., North Slope, AK	1
BIS	OxA-11959	24,570	90	29,426	149	68.20	157.67	Russia	Kolyma lowland, Siberia	1

BIS	CAMS 53899	25,980	230	30,745	201	70.81	-154.41	U.S.A.	Ikpikpuk R., North Slope, AK	1
BIS	OxA-11227	26,210	170	30,918	161	64.06	-141.89	U.S.A.	Lost Chicken Cr., Chicken, AK	1
BIS	Beta 110938	26,300	300	30,937	217	65.12	-153.34	U.S.A.	Palisaides, AK	1
BIS	OxA-11131	26,460	160	31,075	112	64.06	-141.89	U.S.A.	Lost Chicken Cr., Chicken, AK	1
BIS	AECV:140 2c	26,560	670	31,107	635	45.80	126.67	China	Yanjiagang site, Harbin	1
BIS	OxA-11193	27,060	190	31,331	120	63.90	-139.00	Canada	Hester Cr., Dawson City, YT	1
BIS	CAMS 53758	27,400	260	31,556	286	70.81	-154.41	U.S.A.	Ikpikpuk R., North Slope, AK	1
BIS	CAMS 53768	27,590	280	31,760	360	70.81	-154.41	U.S.A.	Ikpikpuk R., North Slope, AK	1
BIS	n/a	27,440	790	32,035	849	64.84	-147.96	U.S.A.	Ester Cr., Fairbanks, AK	1
BIS	CAMS 53892	28,120	290	32,357	436	70.81	-154.41	U.S.A.	Ikpikpuk R., North Slope, AK	1
BIS	OxA-11613	34,050	450	39,044	668	53.50	-113.10	Canada	Cons. Pit 48, Edmonton, AB	1
BIS	n/a	33,880	1,900	39,065	2,118	65.57	-148.38	U.S.A.	Lower Eldorado Cr., Fairbanks, AK	1
BIS	OxA-11991	34,470	200	39,424	387	64.05	-139.53	Canada	Evergreen Cr., Dawson City, YT	1
BIS	CAMS 53894	35,580	550	40,733	617	70.81	-154.41	U.S.A.	Ikpikpuk R., North Slope, AK	1
BIS	CAMS 53782	35,710	730	40,808	747	70.81	-154.41	U.S.A.	Ikpikpuk R., North Slope, AK	1
BIS	CAMS 53900	36,320	780	41,375	697	70.81	-154.41	U.S.A.	Ikpikpuk R., North Slope, AK	1
BIS	OxA-11196	37,550	400	42,244	303	60.81	-149.43	U.S.A.	Seward Peninsula, Alder Cr., AK	1
BIS	CAMS 53893	37,460	890	42,248	680	70.81	-154.41	U.S.A.	Ikpikpuk R., North Slope, AK	1
BIS	OxA-11224	37,810	380	42,406	293	75.37	135.59	Russia	Novosibirsk Islands, Zimovye R., Siberia	1
BIS	CAMS 53769	38,700	1,000	43,150	761	70.81	-154.41	U.S.A.	Ikpikpuk R., North Slope, AK	1
BIS	CAMS 53779	38,800	1,100	43,245	839	70.81	-154.41	U.S.A.	Ikpikpuk R., North Slope, AK	1
BIS	OxA-10683	39,200	550	43,433	456	65.04	-147.11	U.S.A.	Fairbanks Cr., Fairbanks, AK	1
BIS	CAMS 53781	39,800	1,200	43,942	964	70.81	-154.41	U.S.A.	Ikpikpuk R., North Slope, AK	1
BIS	CAMS 53761	39,850	1,200	43,976	968	70.81	-154.41	U.S.A.	Ikpikpuk R., North Slope, AK	1
BIS	OxA-11275	40,800	600	44,607	468	66.65	-143.72	U.S.A.	Black R.. Yukon Flats, AK	1
HRS	GIN-3243	3,250	60	3,477	68	71.60	87.00	Russia	Agapa River, Taimyr	2
HRS	GIN-10256	4,610	40	5,387	95	71.80	129.30	Russia	Bykovsky Peninsula, Lena Delta	2
HRS	Erl-11271	4,686	46	5,409	75	48.15	10.95	Germany	Pestenacker	3
HRS	Erl-11268	4,742	57	5,482	82	48.40	11.45	Germany	Ziegelberg	3
HRS	UtC-11461	4,770	51	5,509	75	48.41	9.91	Germany	Ehrenstein	4
HRS	Erl-11266	4,783	46	5,516	66	48.13	10.96	Germany	Unfriedshausen	3
HRS	ETH-9346	4,810	66	5,526	83	49.12	8.58	Germany	Bruchsal	5
HRS	Erl-11267	4,818	48	5,528	62	48.40	11.45	Germany	Ziegelberg	3
HRS	Erl-11272	4,840	47	5,585	61	48.15	10.95	Germany	Pestenacker	3
HRS	Erl-11265	4,870	46	5,612	53	48.13	10.96	Germany	Unfriedshausen	3
HRS	KIA-35736	4,975	31	5,696	52	48.77	2.44	France	Bercy, Paris	6
HRS	UtC-11460	5,010	51	5,751	77	47.80	9.10	Germany	Sipplingen	4
HRS	UtC-11462	5,070	61	5,812	71	48.41	9.91	Germany	Ehrenstein	4
HRS	KIA-35913	5,185	31	5,940	34	54.03	10.50	Germany	Heidmoor/Seedorf	7
HRS	KIA-4216	5,270	41	6,058	73	54.26	10.76	Germany	Wangels	8
HRS	UtC-11453	5,306	46	6,087	72	49.95	9.63	Germany	Aulendorf	4
HRS	KIA-30008	5,314	36	6,090	64	54.10	10.81	Germany	Neustadt/Holstein	6
HRS	KIA 10334	5,319	35	6,094	64	52.76	18.15	Poland	Żegotki 5	9
HRS	ETH-11029	5,455	61	6,249	75	49.12	8.58	Germany	Bruchsal	10
HRS	KIA 10336	5,495	36	6,295	44	52.73	18.68	Poland	Siniarzewo	9
HRS	K-2651-a	5,550	96	6,352	103	56.15	10.11	Denmark	Braband	11

HRS	KIA-35738	5,600	26	6,363	34	55.40	9.80	Denmark	Tybrind Vig	6
HRS	KIA-35737	5,698	74	6,493	88	57.93	27.17	Estonia	Kääpa	6
HRS	KIA 9561	5,794	71	6,593	84	54.25	11.03	Germany	Rosenhof	9
HRS	KIA 10344	5,903	34	6,721	40	52.15	11.22	Germany	Eilsleben	9
HRS	KIA 10331	5,999	35	6,838	49	54.38	16.32	Poland	Dąbki	9
HRS	KIA 10335	6,111	36	6,988	76	52.81	17.70	Poland	Bożejewice	9
HRS	OxA-1134	6,250	131	7,149	154	50.48	7.48	Germany	Niederbieber	12
HRS	OxA-1131	7,010	91	7,839	87	37.18	-3.24	Spain	Cueva de la Carigüela	13
HRS	KIA-35735	7,385	36	8,223	63	59.50	26.57	Estonia	Kunda	6
HRS	OxA-8996	7,970	81	8,828	121	49.73	2.15	Belgium	Place Saint-Lambert	14
HRS	OxA-9017	15,440	80	18,670	84	42.37	1.84	Spain	Montllas open air site, Prats	15
HRS	GIN-10233	16,380	120	19,527	177	71.80	129.30	Russia	Lena Delta, Bykovsky P	2
HRS	GIN-10668	16,800	170	19,955	230	73.50	142.20	Russia	N.S.I., Bol. Lyakhovsky Is	2
HRS	GIN-11133	17,000	150	20,182	250	73.54	100.49	Russia	Bol'shaya Balakhnaya	2
HRS	Beta-148659	17,950	60	21,416	108	74.60	102.60	Russia	Taimyr Lake	2
HRS	GrA-17351	18,090	80	21,572	186	74.60	108.70	Russia	Arlakh Lake	2
HRS	GIN-3140б	18,300	200	21,855	252	73.50	104.00	Russia	Bolshaya Balakhnya R Taimyr	2
HRS	GIN-8252	19,100	120	22,787	260	76.00	138.00	Russia	Kotelniy Is N.S.I.	2
HRS	OxA-6927	23,580	320	28,385	380	51.55	-4.24	U.K.	Paviland Cave [Goat's Hole]	16
HRS	OxA-1790	23,670	400	28,515	455	51.55	-4.24	U.K.	Paviland Cave [Goat's Hole]	16
HRS	GIN-9879	23,850	700	28,737	773	71.80	129.30	Russia	Bykovsky Peninsula, N-E Siberia	2
HRS	GIN-11132	23,900	400	28,769	432	73.50	100.40	Russia	Bol'shaya Balakhnaya	2
HRS	GIN-6426	24,000	400	28,857	427	70.50	120.00	Russia	Anabar-Olenyok	2
HRS	Beta-148660	24,690	110	29,516	181	74.50	100.50	Russia	Taimyr L, Cape Sabler	2
HRS	GIN-1817a	25,200	200	29,993	245	75.00	100.00	Russia	Engelgardt L Taimyr	2
HRS	OxA-6928	25,940	420	30,682	343	51.55	-4.24	U.K.	Paviland Cave [Goat's Hole]	16
HRS	GIN-3142б	26,400	300	31,004	210	73.50	104.00	Russia	Bolshaya Balakhnya R Taimyr	2
HRS	GIN-3841b	27,900	300	32,111	421	74.53	100.53	Russia	Taimyr L, Cape Sabler	2
HRS	GIN-8219	28,180	270	32,424	424	72.00	116.00	Russia	Anabar-Olenyok	2
HRS	GIN-5732	28,300	400	32,601	596	73.00	106.00	Russia	Khatanga R, Kozhevnikov B	2
HRS	GIN-10257	28,400	300	32,715	497	71.80	129.30	Russia	Bykovsky Peninsula, N-E Siberia	2
HRS	GIN-10232	34,100	400	39,102	586	71.80	129.30	Russia	Bykovsky Peninsula, N-E Siberia	2
HRS	GIN-11083	34,200	500	39,255	690	72.30	126.10	Russia	Lena R, Olenekskaya Channel, Byor-Khaya	2
HRS	GIN-10268	34,600	100	39,592	343	71.81	129.35	Russia	Lena Delta, Bykovsky P	2
HRS	GIN-3141v	34,600	1,200	39,676	1,302	73.50	104.00	Russia	Bolshaya Balakhnya R Taimyr	2
HRS	GIN-9043	34,700	1,900	39,846	2,067	72.82	141.31	Russia	Laptev Sea coast (east)	2
HRS	GIN-10254	34,800	700	39,901	781	71.80	129.30	Russia	Bykovsky Peninsula, N-E Siberia	2
HRS	GIN-10667	35,100	1,200	40,159	1,230	73.50	142.20	Russia	N.S.I., Bol. Lyakhovsky Is	2
HRS	GIN-10691	35,000	100	40,173	332	73.50	142.20	Russia	N.S.I., Bol. Lyakhovsky Is	2
HRS	GIN-9873	35,800	500	40,973	523	71.80	129.30	Russia	Bykovsky Peninsula, N-E Siberia	2
HRS	GIN-10269	35,900	600	41,038	602	71.80	129.30	Russia	Bykovsky Peninsula, N-E Siberia	2
HRS	GIN-10252	35,800	100	41,050	202	71.81	129.35	Russia	Lena Delta, Bykovsky P	2
HRS	GIN-3119	36,300	900	41,337	822	73.50	104.00	Russia	Bolshaya Balakhnya R Taimyr	2
HRS	GIN-8221	36,300	640	41,382	556	72.00	116.00	Russia	Anabar-Olenyok	2
HRS	Beta-148622	36,770	610	41,735	462	73.04	106.58	Russia	Khatanga Talalakh L	2
HRS	GIN-10673	37,200	800	42,051	605	73.50	142.20	Russia	N.S.I., Bol. Lyakhovsky Is	2
HRS	GIN-10661	38,000	100	42,511	178	73.50	142.20	Russia	N.S.I., Bol. Lyakhovsky Is	2
HRS	GIN-6430	38,100	800	42,670	612	70.50	122.00	Russia	Anabar-Olenyok	2

HRS	GIN-4965	38,700	1,000	43,150	761	70.50	134.50	Russia	Omoloy-Yana Yana R basin, Kular Range region	2
HRS	GIN-3519	39,600	500	43,709	417	73.60	118.00	Russia	Anabar-Olenyok , Laptev Sea coast	2
HRS	GIN-3823	40,200	1,200	44,221	998	73.30	97.00	Russia	Logata R Taimyr	2
HRS	GIN-11135	40,400	100	44,334	170	73.60	101.13	Russia	Kupchiktakh L, Taimyr	2
HRS	GIN-10693	41,000	1,600	44,994	1,524	73.50	142.20	Russia	N.S.I., Bol. Lyakhovsky Is	2
MAM	GIN-3518	14,800	50	18,000	227	72.12	104.00	Russia	Ulakhan-Yuriakh River	17
MAM	SOAN-111A	14,800	150	18,036	266	54.50	80.20	Russia	Volchya Griva (2)	17
MAM	Ly-434	14,850	350	18,063	403	44.90	1.02	France	La Croze-sur-Suran 1	18
MAM	AA-27374	14,940	170	18,213	228	43.00	104.00	Russia	Angara River Basin	18
MAM	GIN-5370	15,100	70	18,248	164	65.00	171.00	Russia	Mayn River	17
MAM	GIN-8255	15,000	70	18,250	162	72.36	139.73	Russia	Shirokostan Peninsula	17
MAM	GIN-6023	15,130	50	18,256	168	68.45	150.00	Russia	Kolyma River	18
MAM	OxA-719	15,100	200	18,281	226	51.75	33.08	Russia	Mezin	18
MAM	OxA-716	15,100	250	18,283	270	52.83	30.97	Russia	Berdyzh	18
MAM	Lu-358	15,110	530	18,291	572	53.33	34.33	Rus/Ukr	Timonovka I	18
MAM	SOAN-4462	15,150	280	18,318	302	59.24	62.34	Russia	Gari	17
MAM	GIN-6024bis	15,200	80	18,438	189	68.45	150.00	Russia	Kolyma River	18
MAM	Ki-1130	15,300	140	18,563	211	44.15	131.78	Russia	Khorol	17
MAM	GIN-8258	15,400	100	18,647	115	71.00	-179.00	Russia	Wrangel Island	17
MAM	SOAN-5065	15,420	215	18,654	263	61.05	68.57	Russia	Lugovskoye	17
MAM	LU-1671	15,420	100	18,660	106	75.00	138.00	Russia	Kotelny Island	17
MAM	GrA-4891	15,560	200	18,770	227	48.52	15.68	Austria	Schönberg Am Kamp	18
MAM	LU-127	15,660	180	18,846	211	52.67	33.28	Russia	Yudinovo	18
MAM	HV-1961	15,810	410	19,042	414	50.07	8.53	Germany	Kelsterbach	18
MAM	Hela-321	15,910	155	19,108	178	60.37	25.43	Finland	Helsinki, Herttoniemi	18
MAM	IM-887	16,000	300	19,161	295	62.42	133.00	Russia	Khayrgas	17
MAM	SOAN-3835	16,000	385	19,185	389	58.50	81.05	Russia	Bolshoi Istok	18
MAM	SOAN-4804	16,130	310	19,270	334	55.29	59.29	Russia	Nikolskaya Cave	17
MAM	AA 14866	16,168	209	19,280	252	64.40	-147.00	Alaska	Cleary Creek	19
MAM	IERZH-165	16,300	300	19,465	357	54.10	61.40	Russia	Troitskaya	17
MAM	GIN-3130	16,330	100	19,486	164	75.30	105.00	Russia	Bolshaya Balachnya River	17
MAM	SOAN-4461	16,320	450	19,528	507	59.24	62.34	Russia	Gari	17
MAM	GIN-6093	16,300	600	19,564	682	55.92	92.33	Russia	Listvenka	17
MAM	GIN-2002	16,300	700	19,607	805	53.33	34.33	Rus/Ukr	Timonovka I	18
MAM	QC-886	16,565	270	19,763	308	51.70	36.00	Russia	Avdeevo	18
MAM	SOAN-4843	16,700	240	19,870	277	59.24	62.34	Russia	Gari	17
MAM	QC-621	16,960	420	20,217	537	51.70	36.00	Russia	Avdeevo	18
MAM	SOAN-4844	17,050	160	20,248	282	59.38	62.33	Russia	Evalga	17
MAM	SOAN-5044	17,100	390	20,388	515	52.85	86.68	Russia	Ushlep 6	17
MAM	SOAN-5084	17,200	230	20,493	367	55.92	92.33	Russia	Listvenka	17
MAM	SOAN-3504	17,220	245	20,530	376	52.01	86.32	Russia	Isha River	17
MAM	GIN-8983	17,290	100	20,553	249	57.23	112.25	Russia	Kaverga River	17
MAM	Gif-6418	17,320	290	20,684	396	42.17	2.74	Spain	L'Arbreda B Superior	18
MAM	Ki-1301	17,400	150	20,752	268	44.15	131.78	Russia	Khorol	17
MAM	GIN-10908	17,450	100	20,784	240	57.22	111.83	Russia	Niryakyan River	17
MAM	GIN-7576	17,500	300	20,851	389	70.11	75.46	Russia	Parisento River	17
MAM	SOAN-4418	17,610	200	20,957	304	57.30	112.00	Russia	Tesa River	17
MAM	SOAN-3503	17,600	500	20,989	631	52.01	86.32	Russia	Isha River	17
MAM	Gif-6419	17,720	290	21,091	416	42.17	2.74	Spain	L'Arbreda B Superior	18

MAM	SOAN-4463	17,810	320	21,224	465	59.27	62.33	Russia	Rychkovo	17
MAM	GIN-5042	17,780	80	21,266	202	70.00	125.00	Russia	Lower Lena River	17
MAM	GIN-11463	17,800	100	21,277	214	54.50	80.20	Russia	Volchya Griva (2)	17
MAM	LE-1432A	17,930	100	21,400	163	54.25	69.73	Russia	Gagarino	18
MAM	SOAN-2211	18,050	95	21,524	190	56.00	65.92	Russia	Shikaevka 2	17
MAM	KI-1055	18,020	600	21,530	773	49.63	31.40	Russia	Mezhirich	18
MAM	SOAN-3610	18,040	175	21,569	281	55.64	88.00	Russia	Shestakovo	17
MAM	Beta-148646	18,190	60	21,722	179	73.60	100.48	Russia	Bolshaya Balakhnya River	17
MAM	OxA-3694	18,160	260	21,738	337	49.42	20.17	Poland	Oblazowa Cave	20
MAM	Birm-1460	18,000	1,400	21,818	1,847	53.26	-3.37	U.K.	Cae Gwyn Cave	18
MAM	GIN-3727	18,300	200	21,855	252	55.27	39.45	E_Europe	Zaraisk	18
MAM	TA-121	18,320	280	21,873	333	65.02	57.38	E_Europe	Byzovaya	18
MAM	SOAN-3838	18,250	1,100	21,952	1,421	61.05	68.57	Russia	Lugovskoye	17
MAM	GIN-8229	18,500	120	22,087	224	75.26	144.00	Russia	Faddeyevsky Island	17
MAM	SOAN-4945	18,580	240	22,136	348	55.85	88.05	Russia	Kochegur	17
MAM	SOAN-4845	18,600	230	22,163	343	59.30	62.38	Russia	Berezovy Mys	17
MAM	GIN-5046	18,680	120	22,292	194	71.40	119.00	Russia	Bur River	17
MAM	GIN-6099	18,700	100	22,312	161	70.00	119.00	Russia	Amydai River	17
MAM	LU-361	18,690	770	22,392	981	52.85	33.23	Russia	Pogon	18
MAM	LE-3834	18,930	320	22,641	438	55.15	91.10	Russia	Tarachikha	17
MAM	LE-2950	19,010	120	22,655	265	51.29	39.00	Russia	Kostienki I	21
MAM	SOAN-4815	18,990	340	22,723	447	57.07	63.57	Russia	Komsomolsky	17
MAM	OxA-697	19,000	300	22,733	400	50.55	29.23	Russia	Randomyshl	18
MAM	LE-2946B	19,200	200	22,901	298	56.58	27.50	E_Europe	Leski	18
MAM	SOAN-3609	19,190	310	22,918	391	55.64	88.00	Russia	Shestakovo	17
MAM	OxA-718	19,200	350	22,936	435	45.82	28.58	E_Europe	Kirillovka	18
MAM	GIN-2862	18,600	2,000	22,946	2,902	55.20	92.05	Russia	Shlenka	17
MAM	KI-1056	19,280	600	23,064	737	49.63	31.40	Russia	Mezhirich	18
MAM	R-2533	19,400	230	23,106	348	44.38	8.98	Italy	Arene Candidae, Schicht P7	18
MAM	Giff-1110	19,300	700	23,108	870	52.44	-2.83	U.K.	Condover, Shrosphire	18
MAM	GIN-2859	19,500	200	23,271	337	53.55	92.00	Russia	Middle Yenisei River	17
MAM	UCIAMS-11211	19,530	80	23,355	233	39.89	-98.03	Kansas	Lovewell Reservoir	22
MAM	LU-654A	19,640	330	23,460	460	79.90	94.58	Russia	Oktyabrskoi Revolutsii Island	17
MAM	OxA-10122	19,700	500	23,541	636	43.35	-5.83	Spain	Cueto de la Mina	18
MAM	GIN-2861	19,700	200	23,561	311	53.55	92.00	Russia	Middle Yenisei River	17
MAM	SOAN-4464	19,710	205	23,572	315	59.38	62.33	Russia	Evalga	17
MAM	OxA-698	19,800	350	23,664	474	52.00	33.27	Russia	Novgorod-Severskii	18
MAM	LE-2949	19,860	200	23,737	281	51.29	39.00	Russia	Kostienki I	21
MAM	UtC-8137	19,910	130	23,780	214	73.53	105.82	Russia	Bolshaya Balachnya River	17
MAM	GIN-3016	19,960	80	23,834	184	55.05	90.00	Russia	Chulym River	17
MAM	LU-688	19,970	110	23,852	205	79.47	96.75	Russia	Oktyabrskoi Revolutsii Island	17
MAM	GIN-7705	19,900	800	23,855	1,045	53.00	103.50	Russia	Mal'ta (Belaya River)	17
MAM	OxA-7112	19,980	220	23,878	292	51.55	-4.24	U.K.	Paviland Cave [Goat's Hole]	16
MAM	LU-1970	19,990	110	23,880	206	75.00	138.00	Russia	Kotelny Island	17
MAM	LU-2807	20,000	110	23,894	206	71.00	-179.00	Russia	Wrangel Island	17
MAM	GIN-8259	22,400	300	27,066	474	71.00	-179.00	Russia	Wrangel Island	17
MAM	Hela-281	22,420	315	27,090	482	62.85	28.62	Finland	Nilsia, Syvari	18
MAM	GIN-8257	22,400	200	27,096	403	71.00	-179.00	Russia	Wrangel Island	17

MAM	LU-104	22,410	200	27,115	400	55.64	88.00	Russia	Shestakovo	17
MAM	SOAN-4416	22,480	420	27,136	569	57.30	112.00	Russia	Mama Tributary, Vitim Basin, Tesa R.	17
MAM	SOAN-1467	22,450	200	27,178	385	55.64	88.00	Russia	Kiya River	17
MAM	SOAN-4177	22,500	280	27,200	438	55.64	88.00	Russia	Tesa River	17
MAM	OxA-7108	22,620	340	27,293	475	51.55	-4.24	U.K.	Paviland Cave [Goat's Hole]	23
MAM	LE-2969	22,700	250	27,383	383	51.29	39.00	Russia	Kostienki I	21
MAM	LE-2800	22,760	250	27,451	385	51.29	39.00	Russia	Kostienki I	21
MAM	GrA-15880	22,750	160	27,463	324	55.64	88.00	Russia	Shestakovo	17
MAM	GIN-3089	22,750	150	27,468	320	74.03	100.00	Russia	Baskura Peninsula	17
MAM	OxA-4114	22,780	250	27,478	387	51.39	39.04	Russia	Kostienki XIV [Markina Gora]	20
MAM	SOAN-4802	22,860	410	27,549	541	57.68	62.20	Russia	Tavda River	17
MAM	GIN-8888	22,900	240	27,667	393	53.00	103.50	Russia	Mal'ta (Belaya River)	18
MAM	AA 14868	23,015	449	27,754	588	64.94	-147.65	Alaska	Goldstream	19
MAM	LE-3276	23,010	300	27,798	439	51.29	39.00	Russia	Kostienki I	21
MAM	SOAN-1386	22,990	170	27,829	334	55.64	88.00	Russia	Shestakovo	17
MAM	Poz-124	23,020	180	27,861	335	50.07	19.95	Poland	Krakow-Spadzista Street	18
MAM	GrN-6636	23,040	170	27,888	316	50.07	19.95	Poland	Krakow-Spadzista Street	18
MAM	GIN-3232	23,100	200	27,951	323	67.35	116.00	Russia	Tyung River	17
MAM	AA 14864	23,222	453	28,025	587	64.94	-147.65	Alaska	Goldstream	19
MAM	GrA-5005	23,180	120	28,036	205	48.32	15.40	Austria	Willendorf II	16
MAM	LE-3289	23,260	680	28,047	838	51.42	39.00	Russia	Kostenki	18
MAM	LE-3287	23,260	420	28,077	543	51.29	39.00	Russia	Kostenki	16
MAM	IERiZh-176	23,300	500	28,114	633	61.00	77.00	Russia	Agansky Uval	18
MAM	GrN-13235	23,330	110	28,168	176	55.64	88.00	Russia	Shestakovo	17
MAM	Hela-282	23,340	350	28,170	435	60.39	25.18	Finland	Helsinki, Toolo	18
MAM	LU-104	23,430	180	28,230	202	52.83	30.97	Russia	Berdyzh	18
MAM	GIN-2763a	23,500	300	28,302	351	73.06	102.16	Russia	Bederbo-Tarida River	17
MAM	GIN-5886	23,600	200	28,352	257	59.00	101.30	Russia	Middle Angara River	17
MAM	LU-358	23,660	270	28,451	343	53.33	34.12	Russia	Khotylevo II	18
MAM	LE-3283	23,640	320	28,477	1,050	51.29	39.00	Russia	Kostienki I	21
MAM	Poz-1248	23,750	140	28,507	246	50.07	19.95	Poland	Krakow-Spadzista Street	18
MAM	KIGN-397f	23,670	410	28,517	465	54.87	70.50	Russia	Uspenka	17
MAM	Poz-1251	23,770	160	28,545	271	50.07	19.95	Poland	Krakow-Spadzista Street	18
MAM	LE-2951	23,770	200	28,566	305	51.29	39.00	Russia	Kostienki I	21
MAM	SOAN-3634	23,760	245	28,573	335	55.12	84.24	Russia	Kudelin Kluch	17
MAM	GIN-7992	23,800	150	28,584	265	43.00	33.00	Russia	Kostyonki Site, near Voronezh	18
MAM	LE-2946A	23,770	1,540	28,659	1,824	56.58	27.50	E_Europe	Leski	18
MAM	GIN-1296B	23,800	400	28,665	441	74.50	102.00	Russia	Sabler Cape	17
MAM	AA 14881	23,808	487	28,684	529	64.87	-146.84	Alaska	Gilmore Creek	19
MAM	GIN-8244	23,940	150	28,780	254	75.26	144.00	Russia	Faddeyevsky Island	17
MAM	Poz-225	23,980	280	28,840	331	50.07	19.95	Poland	Krakow-Spadzista Street	18
MAM	Poz-268	24,000	300	28,857	342	50.07	19.95	Poland	Krakow-Spadzista Street	18
MAM	GIN-7166	24,000	1,100	28,882	1,188	70.50	134.23	Russia	Omolon River, Kular Settlement	17
MAM	IERiZh-63	24,000	1,500	28,904	1,745	66.00	67.00	Russia	430th KM	18
MAM	OxA-7111	24,140	400	28,969	429	51.55	-4.24	U.K.	Paviland Cave [Goat's Hole]	23
MAM	Beta-148639	24,170	110	28,987	226	75.50	100.50	Russia	Trautfetter River	17
MAM	Beta-148651	24,250	110	29,066	234	72.25	109.75	Russia	Munchirdakh Lake	18
MAM	GrA-10935	24,360	150	29,183	253	55.90	87.95	Russia	Shestakovo	18
MAM	SOAN-119	24,400	650	29,250	668	52.63	85.67	Russia	Biya River	17
MAM	IM-835	24,400	650	29,250	668	72.47	128.42	Russia	Sobo-Sise Island	17

MAM	Hela-295	24,450	385	29,256	458	63.80	23.48	Finland	Lohtaja	18
MAM	K-3806	24,400	900	29,273	896	61.67	9.68	Norway	Kvam	18
MAM	GIN-7999	24,500	450	29,324	513	51.29	39.00	Russia	Kostienki VIII [Tel'manskaya site]	16
MAM	LE-2624	24,600	150	29,442	232	47.65	31.10	Russia	Anetovka	18
MAM	SOAN-4422	24,600	730	29,459	722	57.23	112.25	Russia	Kaverga River	17
MAM	SOAN-2712	24,650	305	29,504	410	50.50	72.75	Kazakhstan	Batpak	17
MAM	SOAN-4401	24,650	340	29,504	436	56.30	90.40	Russia	Achinsk	17
MAM	GIN-2160	24,900	500	29,781	524	74.03	100.00	Russia	Baskura Peninsula	17
MAM	IGAN-73	24,960	400	29,850	418	53.33	34.12	Russia	Khotylevo II	18
MAM	LU-749B	24,960	210	29,860	245	79.52	96.92	Russia	Oktyabrskoi Revolutsii Island	17
MAM	GrA-13506	25,040	200	29,909	235	52.45	128.11	Russia	Uralovka	17
MAM	LE-612	25,100	500	29,953	492	72.50	87.00	Russia	Pyasina River	17
MAM	K-3699	25,110	440	29,962	435	56.72	10.12	Denmark	Hadsund	18
MAM	GIN-8227	25,180	150	29,981	220	75.26	144.00	Russia	Faddeyevsky Island	17
MAM	GIN-8246	25,200	180	29,992	235	75.26	144.00	Russia	Faddeyevsky Island	17
MAM	GIN-6143	25,300	400	30,108	395	56.85	53.23	E_Europe	Lower Kama River	18
MAM	GIN-3502	25,300	600	30,109	548	70.45	131.00	Russia	Laptev Sea Coast	17
MAM	AA 14870	25,362	584	30,166	527	64.40	-147.00	Alaska	Cleary Creek	19
MAM	GIN-2210	25,400	300	30,214	344	68.92	71.00	Russia	Yuribey River	17
MAM	K-3809	25,480	560	30,275	496	56.02	12.35	Denmark	Ostrupgaard	18
MAM	GIN-8532	25,540	170	30,396	245	75.26	144.00	Russia	Faddeevsky Island	17
MAM	GrA13238	25,660	200	30,509	235	55.90	87.95	Russia	Shestakovo	18
MAM	Ly-1863	25,800	700	30,515	593	47.14	5.57	France	Gr de la Mere Clochette	16
MAM	GIN-11465	25,800	600	30,532	497	70.72	135.42	Russia	Yana River	18
MAM	Ox-A6190	25,700	260	30,542	279	53.00	103.50	Russia	Mal'ta (Belaya River)	18
MAM	Beta-148634	25,800	130	30,615	165	72.83	106.75	Russia	Sopochnaya	17
MAM	GIN-4710B	25,800	200	30,623	202	75.26	144.00	Russia	Faddeyevsky Island	17
MAM	SR-6086	26,000	120	30,777	155	46.99	-104.19	Montana	Beaver Creek	24
MAM	Beta-148665	26,100	170	30,839	169	74.03	100.00	Russia	Baskura Peninsula	17
MAM	GIN-11127	26,200	150	30,919	152	73.60	100.48	Russia	Bolshaya Balakhnya River	17
MAM	Mo-215	26,000	1,600	30,951	1,890	71.05	127.30	Russia	Chekurovka	17
MAM	LU-125	26,470	420	31,025	294	52.67	33.28	Russia	Yudinovo	18
MAM	WB7β-41	26,560	550	31,086	462	43.11	128.91	China	Mingyuegou	17
MAM	OxA-1205	26,700	550	31,193	489	53.26	-1.20	U.K.	Pin Hole Cave	25
MAM	GIN-1216	26,700	700	31,238	701	73.60	100.48	Russia	Bolshaya Balakhnya River	17
MAM	GIN-8224	27,100	300	31,375	231	75.26	144.00	Russia	Faddeyevsky Island	17
MAM	OxA-3607	27,150	350	31,427	315	52.10	-7.50	Ireland	Shandon Cave	26
MAM	GIN-3836	27,300	200	31,452	179	73.35	97.00	Russia	Logata River	17
MAM	PV-0175	26,695	1,300	31,533	1,443	49.35	117.58	China	Zhalainuoer	17
MAM	GIN-2021b	27,200	500	31,574	510	71.02	79.20	Russia	Yambuto Lake	17
MAM	OxA-9039	27,460	310	31,653	361	56.13	40.48	Russia	Sungir' [Vladimir]	27
MAM	AA-38235	27,470	310	31,663	364	68.33	161.50	Russia	Maly Anui River	17
MAM	GIN-3929	27,500	300	31,685	360	73.28	97.88	Russia	Kubalakh River	17
MAM	GIN-3505	27,500	300	31,685	360	70.45	131.00	Russia	Laptev Sea Coast	17
MAM	GIN-5880	27,700	500	32,049	578	50.00	38.00	Russia	Sungir', Vladimir Region	18
MAM	KI-1051	27,500	800	32,096	861	51.75	33.08	Russia	Mazin	18
MAM	GIN-4710	28,000	200	32,183	360	75.26	144.00	Russia	Faddeyevsky Island	17
MAM	K-4192	27,810	610	32,232	709	56.28	8.80	Denmark	Stengardens Grusgrav 2	18
MAM	OxA-5229	27,950	550	32,316	674	48.40	9.77	Germany	Das Geissenklosterle	18
MAM	Beta-148662	28,270	210	32,541	377	76.00	113.00	Russia	Taymyr Peninsula	18
MAM	GIN-8545	28,300	350	32,585	535	71.00	66.50	Russia	Yamal Peninsula	17
MAM	K-3808	28,120	760	32,600	871	59.20	17.73	Denmark	Ronninge 1	18

MAM	Beta-148643	28,310	170	32,606	344	74.32	100.33	Russia	Taymyr Lake	17
MAM	GIN-5696	28,400	300	32,715	497	62.45	150.30	Russia	Srednekan River	17
MAM	GIN-8220	28,400	340	32,719	550	73.55	118.50	Russia	Terpyi-Tumus Peninsula	17
MAM	KIA-13081	28,400	200	32,732	370	48.38	9.75	Germany	Sirgenstein	18
MAM	SOAN-2222	27,615	2,015	32,913	2,611	53.00	104.40	Russia	Irkutsk	17
MAM	SOAN-3440	28,525	200	32,917	374	50.11	118.00	Russia	Urtuiskoe	17
MAM	OxA-5228	28,500	550	32,919	764	48.40	9.77	Germany	Das Geissenklosterle	18
MAM	OxA-4235	34,100	840	39,124	1,063	52.22	-8.58	Ireland	Castlepook Cave	26
MAM	OxA-6920	34,100	1,200	39,141	1,357	50.42	8.14	Germany	Wildscheuer cave	28
MAM	GIN-8254	34,400	400	39,454	533	75.00	138.00	Russia	Kotelny Island	17
MAM	WB-78-42	34,310	1,850	39,465	2,026	43.11	128.91	China	Mingyuegou	18
MAM	Birm-466	34,500	500	39,594	623	51.87	-1.68	U.K.	Little Rissington	18
MAM	GIN-8247	34,500	500	39,594	623	75.26	144.00	Russia	Faddeyevsky Island	17
MAM	GIN-8711	34,600	470	39,686	588	70.08	135.33	Russia	Mus-Khaya	17
MAM	GIN-4434	34,700	400	39,768	536	68.45	150.45	Russia	Duvanny Yar	17
MAM	OxA-1564	34,850	1,500	39,921	1,572	51.84	-2.66	U.K.	King Arthur's Cave	16
MAM	GIN-3821	35,000	500	40,092	617	73.35	97.00	Russia	Logata River	17
MAM	GIN-3503	35,000	300	40,114	480	70.45	131.00	Russia	Laptev Sea Coast	18
MAM	OxA-1610	35,200	1,600	40,263	1,657	51.17	0.89	U.K.	Conningbrook Pit	29
MAM	GIN-8243	35,210	500	40,335	615	75.26	144.00	Russia	Faddeyevsky Island	17
MAM	GIN-8223	35,800	700	40,908	712	75.63	135.83	Russia	Belkovsky Island	17
MAM	OxA-10521	35,800	690	40,911	703	44.83	11.62	Italy	Settepolesini di Bodeno	18
MAM	LU-504	35,830	630	40,960	644	68.58	147.08	Russia	Terekhtyakh River	17
MAM	Lu-879	36,000	1,550	41,025	1,534	57.91	12.04	Sweden	Dosebacka mammoth	18
MAM	GIN-8262	35,900	500	41,067	500	73.60	117.00	Russia	Anabaro-Olenek interfluve	17
MAM	GIN-8238	36,000	500	41,158	477	75.26	144.00	Russia	Faddeevsky Island	17
MAM	GIN-3425	36,000	500	41,158	477	55.00	159.00	Russia	Kamchatka River, Nikolka	17
MAM	GIN-3822	36,200	500	41,325	437	73.35	97.00	Russia	Logata River	17
MAM	SOAN-1005	36,450	420	41,518	335	71.20	150.30	Russia	Shandrin River	17
MAM	GIN-5751	36,600	500	41,617	384	72.10	111.00	Russia	Anabarka River	17
MAM	GIN-8243a	36,700	500	41,685	377	75.26	144.00	Russia	Faddeyevsky Island	17
MAM	GIN-3122	36,800	500	41,753	373	75.30	105.00	Russia	Bolshaya Balachnya River	18
MAM	Beta-148630	36,950	450	41,851	336	74.42	107.58	Russia	Arylakh Lake	17
MAM	GIN-6141	37,000	500	41,888	369	56.85	53.23	E_Europe	Lower Kama River	18
MAM	GIN-5750	37,000	500	41,888	369	73.37	110.25	Russia	Semiriskay River	17
MAM	Beta-148666	37,080	460	41,939	342	72.50	109.00	Russia	Popigay River	17
MAM	GIN-6142	37,300	1,000	42,148	794	56.85	53.23	E_Europe	Lower Kama River	18
MAM	GIN-3231	37,600	400	42,276	303	21.38	55.30	Belarus	Viliya River, Neman	18
MAM	GIN-3817	38,300	600	42,761	473	73.35	97.00	Russia	Logata River	17
MAM	GIN-942	38,000	1,500	42,779	1,288	72.16	103.00	Russia	Khatanga River	17
MAM	GIN-3118	38,400	700	42,858	551	73.50	105.00	Russia	Bolshaya Balachnya River	17
MAM	GIN-2763B	38,500	500	42,883	414	73.06	102.16	Russia	Bederbo-Tarida River	17
MAM	GIN-3136	38,500	600	42,906	486	73.06	102.16	Russia	Bederbo-Tarida River	17
MAM	GIN-6148	38,400	1,000	42,935	764	56.85	53.23	E_Europe	Lower Kama River	18
MAM	GIN-8250	38,500	900	42,981	691	69.60	164.80	Russia	Keinguveem River	17
MAM	SOAN-1625	38,460	1,100	43,004	842	50.90	108.48	Russia	Kandabaevo	17
MAM	GIN-3476	38,800	400	43,087	361	73.08	98.75	Russia	Nemu-Dika-Tarida River	17
MAM	GIN-3831	38,900	600	43,212	494	73.35	97.00	Russia	Logata River	17
MAM	GIN-1491	38,800	1,300	43,298	1,031	75.63	101.80	Russia	Trautfetter River	17
MAM	Beta-148664	39,050	580	43,325	478	74.42	107.58	Russia	Arylakh Lake	17
MAM	GIN-3120/P	39,100	1,000	43,432	758	73.30	105.00	Russia	Bolshaya Balachnya River	17

MAM	GIN-3071	39,300	500	43,500	423	74.05	93.10	Russia	Baikura-Neru Bay, Lake Taymyr	17
MAM	GIN-11127a	39,300	600	43,512	483	73.60	100.55	Russia	Bolshaya Balachnya River	17
MAM	GrA-13487	39,340	1,170	43,630	909	53.00	128.68	Russia	Oktyabrsky	17
MAM	GIN-3517	39,400	1,000	43,634	758	70.45	131.00	Russia	Laptev Sea Coast	17
MAM	Beta-148638	39,560	910	43,725	690	75.50	100.50	Russia	Trautfetter River	17
MAM	LU-718A	39,570	870	43,725	661	68.45	158.30	Russia	Kirgilyakh River	17
MAM	LU-718B	39,590	770	43,726	591	68.45	158.30	Russia	Kirgilyakh River	17
MAM	GIN-3135	39,800	600	43,850	481	73.06	102.16	Russia	Bederbo-Tarida River	17
MAM	GIN-5726A	40,100	500	44,069	428	73.54	114.00	Russia	Anabar Gulf	17
MAM	GIN-3804	40,200	600	44,146	493	73.35	97.00	Russia	Logata River	17
MAM	GIN-11134	40,200	600	44,146	493	73.53	100.48	Russia	Bolshaya Balachnya River	17
MAM	GIN-5025	40,300	400	44,239	361	72.10	111.00	Russia	Anabarka River	17
MAM	LU-595	40,350	880	44,274	687	71.20	150.30	Russia	Shandrin River	17
MAM	GIN-1818/P	40,500	800	44,383	628	75.10	110.30	Russia	Engelgard Lake	17
MAM	Beta-148645	40,560	700	44,427	555	74.53	100.50	Russia	Sabler Cape	17
MAM	MAG-366A	40,600	700	44,458	553	68.45	158.30	Russia	Kirgilyakh River	17
MAM	GIN-3407	40,600	600	44,460	483	55.00	159.00	Russia	Kamchatka River, Polovinka	17
MAM	Beta-148648	40,790	970	44,614	785	74.42	107.58	Russia	Arylakh Lake	17
MAM	MAG-576	41,000	900	44,761	717	68.45	158.30	Russia	Kirgilyakh River	17
MAM	MAG-366B	41,000	1,100	44,796	958	68.45	158.30	Russia	Kirgilyakh River	17
MAM	GIN-2744B	41,200	1,000	44,921	848	73.06	102.16	Russia	Bederbo-Tarida River	17
MOX	GIN-25529	2,900	60	3,046	94	76.75	110.50	Russia	Pronchishchev Coast	30
MOX	OxA-17063	2,918	28	3,063	58	74.00	101.00	Russia	Taimyr	31
MOX	GIN-2945	2,920	50	3,073	83	77.63	104.24	Russia	Chelyuskin C	30
MOX	AAR11733	3,097	39	3,321	47	82.49	-35.86	Greenland	Pearyland	31
MOX	I-10985	3,280	90	3,518	103	64.02	-140.87	Canada	Miller Creek, Sixtymile Area, Yukon	32
MOX	AAR11744	3,372	43	3,613	62	74.00	101.00	Russia	Taimyr	31
MOX	K-3365	3,590	60	3,896	90	82.22	-33.37	Greenland	Martins Site, NMS	32
MOX	K-3531	3,670	80	4,006	115	83.12	-33.80	Greenland	Adam C. Knuth Site, Hvalterrasserne, Frigg Fjord	32
MOX	K-3362	3,800	85	4,195	128	81.98	-26.12	Greenland	Kap Peter Henrik, IPS	32
MOX	K-3364	3,830	85	4,237	125	82.15	-30.15	Greenland	Midternaes, JBF	32
MOX	K-3366	3,870	85	4,289	123	81.57	-61.55	Greenland	Solbakken, HLV	32
MOX	OxA-17064	4,082	30	4,577	96	74.00	101.00	Russia	Taimyr	31
MOX	AAR12025	4,687	46	5,410	75	82.49	-35.86	Greenland	Pearyland	31
MOX	AAR12042	4,753	49	5,501	79	75.77	-99.78	Canada	Bathhurst Island	31
MOX	AAR11749	5,364	49	6,148	82	74.00	101.00	Russia	Taimyr	31
MOX	I-10919	6,725	130	7,594	114	75.50	-99.00	Canada	Goodser Inlet, Bathurst I., NU	32
MOX	AAR12082	15,020	90	18,250	166	74.00	101.00	Russia	Taimyr	31
MOX	AAR12085	15,100	100	18,259	172	74.00	101.00	Russia	Taimyr	31
MOX	AAR12081	15,300	90	18,580	166	74.00	101.00	Russia	Taimyr	31
MOX	AAR12084	15,380	100	18,634	125	74.00	101.00	Russia	Taimyr	31
MOX	BI 93435	15,610	80	18,768	94	72.00	116.00	Russia	Anabar R., Yakutia	33
MOX	AAR11711	15,680	90	18,819	142	62.00	58.67	Russia	Medvezhya Cave, Urals	31
MOX	Beta-148653	15,710	50	18,837	120	74.00	101.00	Russia	Taimyr	30
MOX	AAR12061	15,720	100	18,863	171	62.00	58.67	Russia	Medvezhya Cave, Urals	31
MOX	AAR11728	15,750	100	18,901	179	62.00	58.67	Russia	Medvezhya Cave, Urals	31
MOX	OxA-17065	15,770	55	18,904	157	74.00	101.00	Russia	Taimyr	31

MOX	Beta-148653	15,800	50	18,949	159	74.54	101.64	Russia	Taimyr Lake, Cape Sabler	30
MOX	OxA-17068	15,875	60	19,096	149	74.00	101.00	Russia	Taimyr	31
MOX	AAR12077	16,010	100	19,156	153	74.00	101.00	Russia	Taimyr	31
MOX	GIN-3239	16,080	100	19,199	158	71.60	87.00	Russia	Agapa River, Taimyr	30
MOX	OxA-17072	16,295	60	19,451	124	74.00	101.00	Russia	Taimyr	31
MOX	AAR11747	16,310	110	19,468	184	62.00	58.67	Russia	Medvezhya Cave, Urals	31
MOX	AAR12052	16,810	150	19,967	218	74.00	101.00	Russia	Taimyr	31
MOX	OxA-17070	17,265	65	20,475	229	69.58	-139.08	Canada	Herschel Island	31
MOX	AAR11713	17,520	110	20,859	249	62.00	58.67	Russia	Medvezhya Cave, Urals	31
MOX	AAR12056	17,660	120	21,056	266	59.42	57.77	Russia	Tayn Cave, Urals	31
MOX	AAR11748	17,690	120	21,103	265	74.00	101.00	Russia	Taimyr	31
MOX	GIN-1815	17,800	300	21,207	445	75.98	99.78	Russia	Lower Taimyr R	30
MOX	GIN-3140v	17,800	160	21,236	288	74.54	101.64	Russia	Taimyr Lake, Cape Sabler	30
MOX	OxA-17074	17,900	65	21,380	119	74.00	101.00	Russia	Taimyr	31
MOX	AAR12054	17,930	120	21,401	202	59.42	57.77	Russia	Tayn Cave, Urals	31
MOX	AAR11717	18,100	110	21,624	210	74.00	101.00	Russia	Taimyr	31
MOX	BM-725	18,213	310	21,781	388	52.23	-0.82	U.K.	Clifford Hill, Northamptonshire	34
MOX	Beta-148628	18,310	70	21,854	187	74.00	101.00	Russia	Taimyr	33
MOX	BI 48628	18,310	70	21,854	187	74.54	101.64	Russia	Taimyr L., Taimyr Pen.	33
MOX	Beta-148628	18,370	70	21,917	196	74.54	101.64	Russia	Taimyr L., S of Sabler C	30
MOX	AAR12086	18,600	140	22,197	233	74.00	101.00	Russia	Taimyr	31
MOX	AAR11766	18,630	130	22,237	216	62.00	58.67	Russia	Medvezhya Cave, Urals	31
MOX	AAR12080	18,750	120	22,357	207	74.00	101.00	Russia	Taimyr	31
MOX	AAR11753	18,830	170	22,460	294	74.00	101.00	Russia	Taimyr	31
MOX	AAR12060	18,960	130	22,594	269	62.00	58.67	Russia	Medvezhya Cave, Urals	31
MOX	OxA-17078	19,140	70	22,816	242	62.00	58.67	Russia	Medvezhya Cave, Urals	31
MOX	Beta-148627	19,230	80	22,922	237	74.00	101.00	Russia	Taimyr	33
MOX	BI 48627	19,230	80	22,922	237	74.54	101.64	Russia	Taimyr L., Taimyr Pen.	33
MOX	AAR12073	19,310	140	23,008	267	74.00	101.00	Russia	Taimyr	31
MOX	Beta-148627	19,310	80	23,016	235	74.54	101.64	Russia	Taimyr Lake, Cape Sabler	30
MOX	AAR11759	19,570	130	23,404	267	74.00	101.00	Russia	Taimyr	31
MOX	Beta-148654	19,640	70	23,500	179	73.54	100.49	Russia	Bol'shaya Balakhnaya	30
MOX	Beta-148652	19,640	70	23,500	179	74.54	101.64	Russia	Taimyr L., coast opposite Kupffer Is	33
MOX	Beta-148654	19,710	70	23,578	160	73.54	100.49	Russia	Bol'shaya Balakhnaya	30
MOX	OxA-17148	19,780	75	23,644	155	74.00	101.00	Russia	Taimyr	31
MOX	AAR12068	19,790	160	23,659	238	74.00	101.00	Russia	Taimyr	31
MOX	AAR12065	19,840	140	23,706	214	74.00	101.00	Russia	Taimyr	31
MOX	AAR11767	19,860	130	23,725	206	74.00	101.00	Russia	Taimyr	31
MOX	OxA-17075	19,925	80	23,790	178	74.54	101.64	Russia	Taimyr Lake, Cape Sabler	31
MOX	Beta-156194	22,370	80	27,029	335	74.54	101.64	Russia	Taimyr L., coast opposite Kupffer Is	30
MOX	OxA-17084	22,470	90	27,250	291	62.00	58.67	Russia	Medvezhya Cave, Urals	31
MOX	GrA-17605	22,530	220	27,251	377	72.40	106.00	Russia	Popygai R	30
MOX	BI 48652	22,550	100	27,297	278	74.00	101.00	Russia	Taimyr	33
MOX	AAR12071	22,630	180	27,333	325	74.00	101.00	Russia	Taimyr	31
MOX	AAR12064	23,220	180	28,079	242	74.00	101.00	Russia	Taimyr	31
MOX	OxA-17081	23,430	100	28,230	166	59.42	57.77	Russia	Tayn Cave, Urals	31
MOX	Beta-13869	23,720	80	28,457	177	52.65	-113.65	Canada	Gee Pits at Ponoka, AB	32
MOX	AAR11768	23,860	190	28,693	294	62.00	58.67	Russia	Medvezhya Cave, Urals	31
MOX	AAR12069	24,000	210	28,855	281	74.00	101.00	Russia	Taimyr	31
MOX	OxA-17061	24,150	110	28,969	224	73.30	141.30	Russia	Bolshoy Lyakhovsky Island	31
MOX	AAR12059	24,150	210	28,970	268	62.00	58.67	Russia	Medvezhya Cave, Urals	31

MOX	AAR12053	24,160	210	28,977	268	69.58	-139.08	Canada	Herschel Island	31
MOX	AAR11745	24,270	160	29,073	252	74.00	101.00	Russia	Taimyr	31
MOX	OxA-17080	24,310	110	29,142	238	62.00	58.67	Russia	Medvezhya Cave, Urals	31
MOX	Beta-148657	24,660	110	29,491	173	74.14	98.44	Russia	Upper Taimyr R	30
MOX	OxA-17082	24,870	110	29,731	217	59.42	57.77	Russia	Tayn Cave, Urals	31
MOX	AAR11770	24,940	230	29,847	260	74.00	101.00	Russia	Taimyr	31
MOX	AAR11721	25,310	240	30,091	292	74.00	101.00	Russia	Taimyr	31
MOX	OxA-17150	25,300	110	30,092	230	74.00	101.00	Russia	Taimyr	31
MOX	AAR11715	25,490	230	30,333	308	74.00	101.00	Russia	Taimyr	31
MOX	AAR11716	26,700	350	31,177	228	59.42	57.77	Russia	Tayn Cave, Urals	31
MOX	Beta-148656	27,440	150	31,530	174	74.54	101.64	Russia	Taimyr Lake, Cape Sabler	30
MOX	AAR11762	27,500	300	31,685	360	62.00	58.67	Russia	Medvezhya Cave, Urals	31
MOX	AAR-4188	28,490	350	32,855	586	56.02	12.18	Denmark	Bannebjerg, Helsinge, N. Sjælland	35
MOX	AAR12076	34,150	600	39,196	824	74.00	101.00	Russia	Taimyr	31
MOX	OxA-17077	35,830	240	41,057	276	74.00	101.00	Russia	Taimyr	31
MOX	UtC-10156	36,700	700	41,684	551	74.92	106.58	Russia	Bikada R	30
MOX	AAR12023	38,350	900	42,873	690	64.05	-139.44	Canada	Klondike	31
MOX	AAR11740	39,000	700	43,308	554	69.35	154.97	Russia	Omoloy R., Yana Lowland	31
MOX	AAR11734	39,900	1,000	43,966	770	62.00	58.67	Russia	Medvezhya Cave, Urals	31
MOX	Beta-173287	40,220	670	44,163	538	69.90	-131.17	Canada	McKinley Bay, Northwest Territories	32
MOX	BI 93436	40,270	450	44,210	396	73.30	141.30	Russia	Bol'shoi Lyakhovski I., New Siberian Is.	33
RD	GX-21987G	2,925	80	3,085	116	80.25	53.12	Russia	Hooker Island, Frans Josef Land	36
RD	GX-20445G	3,030	65	3,233	93	80.34	52.46	Russia	Scot Keltie, Frans Josef Land	36
RD	Ua-3104	3,140	95	3,357	120	80.80	48.06	Russia	Alexander Island, Frans Josef Land	36
RD	Ua-3103	3,295	95	3,534	110	80.80	48.06	Russia	Alexander Island, Frans Josef Land	36
RD	OxA-2790	3,350	70	3,588	90	55.73	13.50	Sweden	Harlosa	37
RD	OxA-4012	3,435	70	3,698	94	55.73	13.50	Sweden	Harlosa	37
RD	Ua-3105	3,605	105	3,920	148	80.80	48.06	Russia	Alexander Island, Frans Josef Land	36
RD	GX-21285G	3,640	135	3,974	189	80.34	52.46	Russia	Scot Keltie, Frans Josef Land	36
RD	OxA-3884	3,665	75	3,998	108	55.73	13.50	Sweden	Harlosa	37
RD	Ua-3106	3,777	70	4,158	114	80.80	48.06	Russia	Alexander Island, Frans Josef Land	36
RD	St-13090	3,870	70	4,292	102	80.80	48.06	Russia	Alexander Island, Frans Josef Land	36
RD	GX-21986G	3,925	85	4,356	132	80.25	53.12	Russia	Hooker Island, Frans Josef Land	36
RD	GX-21982G	4,240	85	4,756	130	80.25	53.12	Russia	Hooker Island, Frans Josef Land	36
RD	GX-20444G	4,280	65	4,851	108	81.08	65.05	Russia	Graham Bell Island, Frans Josef Land	36
RD	GX-21984G	4,425	85	5,052	135	80.25	53.12	Russia	Hooker Island, Frans Josef Land	36
RD	GX-21985G	5,500	110	6,295	129	80.25	53.12	Russia	Hooker Island, Frans Josef Land	36
RD	GX-21988G	5,660	100	6,458	108	80.25	53.12	Russia	Hooker Island, Frans Josef Land	36
RD	n/a	14,930	70	18,264	183	43.43	-5.05	Spain	Tito Bustillo, Asturias	38
RD	OxA-9060	15,240	100	18,516	196	48.45	27.47	Ukraine	Molodovo	45
RD	VERA-3345	15,460	60	18,680	74	46.70	14.73	Austria	Griffener Tropfsteinhöhle	45
RD	n/a	17,320	290	20,684	396	42.12	2.77	Spain	L'Arbreda, Gerona	38
RD	n/a	17,720	290	21,091	416	42.12	2.77	Spain	L'Arbreda, Gerona	38
RD	OxA-7500	17,820	200	21,248	342	50.08	8.33	Germany	Wiesbaden-Igstadt	28
RD	OxA-7501	18,220	180	21,792	243	50.08	8.32	Germany	Wiesbaden-Igstadt	28
RD	OxA-4125	18,510	200	22,053	281	48.25	27.17	Moldova	Ciuntu	45
RD	OxA-6808	18,670	160	22,271	264	50.08	8.32	Germany	Wiesbaden-Igstadt	45

RD	OxA-6809	18,670	160	22,271	264	50.08	8.33	Germany	Wiesbaden-Igstadt	45
RD	GIN-9875	18,850	360	22,534	494	71.79	129.40	Russia	Lena Delta, Bykovsky P	2
RD	GIN-9888	18,900	600	22,630	753	71.79	129.40	Russia	Lena Delta, Bykovsky P	2
RD	OxA-4118	19,220	180	22,917	286	48.08	27.25	Moldova	Brinzeni I	20
RD	OxA-6985	19,980	220	23,878	292	51.55	-4.25	U.K.	Paviland, Gower	16
RD	OxA-1490	23,340	350	28,170	435	51.67	-4.73	U.K.	Little Hoyle	39
RD	OxA-8309	23,420	220	28,226	239	50.22	4.83	Belgium	Trou da Somme (Hastiere)	40
RD	OxA-203	23,980	320	28,839	360	46.17	4.73	France	Vergisson II	45
RD	OxA-5805	24,560	340	29,388	438	51.23	-2.67	U.K.	Hyena Den, Wookey Hole	41
RD	SRR-2104	24,590	790	29,452	771	58.11	-4.94	U.K.	Reindeer cave	45
RD	OxA-5721	24,680	360	29,542	446	48.92	11.83	Germany	Klausenhohlen	42
RD	SRR-2103	25,360	810	30,138	727	58.11	-4.94	U.K.	Reindeer cave	45
RD	GIN-9869	26,060	190	30,805	180	71.79	129.40	Russia	Lena Delta, Bykovsky P	2
RD	OxA-6226	26,200	600	30,818	488	51.67	-4.73	U.K.	Hoyle's Mouth	45
RD	OxA-6594	26,320	360	30,934	250	50.22	4.90	Belgium	Trou Magrite	45
RD	OxA-6227	26,500	550	31,041	452	51.67	-4.73	U.K.	Hoyle's Mouth	45
RD	OxA-5226	26,540	460	31,069	341	48.40	9.77	Germany	Geissen Klosterle Cave	16
RD	OxA-4122	26,600	370	31,117	249	48.08	27.25	Moldova	Brinzeni I	20
RD	OxA-4855	27,000	550	31,431	542	48.40	9.77	Germany	Geissenklosterle	45
RD	OxA-4436	27,780	400	32,051	491	50.47	-3.50	U.K.	Kent's Cavern	41
RD	OxA-5693	27,820	500	32,162	598	50.47	-3.50	U.K.	Kent's Cavern, Devon	41
RD	OxA-X-2199-15	27,940	390	32,207	504	48.87	15.47	Austria	Alberndorf	45
RD	OxA-3705	28,000	370	32,258	494	52.17	-8.42	Ireland	Foley Cave	42
RD	OxA-5227	28,050	550	32,409	693	48.40	9.77	Germany	Geissenklösterle	16
RD	OxA-3984	28,240	390	32,524	568	58.11	-4.94	U.K.	Reindeer cave	43
RD	OxA-7391	28,340	420	32,660	629	50.42	8.13	Germany	Wildscheuer Cave	28
RD	OxA-6433	34,950	950	40,033	1,002	46.17	4.73	France	Vergisson II	45
RD	OxA-4236	35,200	950	40,269	967	52.22	-8.58	Ireland	Castlepook Cave	42
RD	Erl-6746	35,499	436	40,692	527	51.76	10.84	Germany	Baumannshöhle	45
RD	OxA-3417	37,200	1,300	42,106	1,128	53.26	-1.20	U.K.	Cresswell Crags	43
RD	OxA-3406	37,450	1,050	42,268	833	53.26	-1.19	U.K.	Pin Hole cave	43
RD	OxA-11980	37,760	340	42,371	271	53.26	-1.19	U.K.	Pin Hole cave	45
RD	OxA-13598	37,900	1,000	42,580	768	50.47	-3.50	U.K.	Kent's Cavern	45
RD	OxA-2032	38,000	1,000	42,651	767	54.07	-1.87	U.K.	Stump Cross Cave	45
RD	OxA-4230	38,650	1,400	43,223	1,143	52.22	-8.58	Ireland	Castlepook Cave	42
RD	OxA-7870	38,800	1,400	43,329	1,145	46.17	4.73	France	Vergisson II	45
RD	OxA-13888	40,000	700	43,998	552	50.47	-3.50	U.K.	Kent's Cavern	45
RD	OxA-11797	40,650	500	44,500	408	53.26	-1.19	U.K.	Pin Hole cave	45
WR	GIN-6024	15,130	90	18,266	175	71.16	153.45	Russia	Bolshoi Khomus-Yuriakh River	44
WR	GIN-6020	15,850	80	19,072	160	69.87	147.58	Russia	Indigirka River	44
WR	GIN-9594	19,500	120	23,295	271	62.00	132.50	Russia	Churapcha	44
WR	A.Lister/A Stuart in prep			28,327		50.45	5.00	Belgium	Third Cave, Goyet	45
WR	IM-239	26,030	200	30,783	185	63.17	133.75	Russia	Ikhine 2	44
WR	A.Lister/A Stuart in prep			30,903		62.77	148.16	Russia	Magadan	45
WR	GIN-6005	26,900	400	31,296	315	68.20	157.67	Russia	Kolyma River	44
WR	GIN-3209	27,300	300	31,502	301	68.00	162.17	Russia	Maly Anui River	44
WR	GIN-6018	27,300	300	31,502	301	68.00	162.17	Russia	Maly Anui River	44
WR	A.Lister/A Stuart in prep			32,736		59.10	31.10	Russia	Lyuban', Novgorod Region	45
WR	OxA-3449	34,500	800	39,606	945	50.47	-3.50	U.K.	Kent's Cavern, Devon	16
WR	OxA-3450	34,620	820	39,728	937	50.47	-3.50	U.K.	Kent's Cavern, Devon	16
WR	OxA-14715	35,150	330	40,314	495	50.46	-3.50	U.K.	Kent's Cavern, Devon	46

WR	OxA-14701	35,650	330	40,877	378	50.46	-3.50	U.K.	Kent's Cavern, Devon	46
WR	OxA-13921	36,040	330	41,223	319	50.46	-3.50	U.K.	Kent's Cavern, Devon	46
WR	OxA-14201	36,370	320	41,469	272	50.46	-3.50	U.K.	Kent's Cavern, Devon	46
WR	GIN-6009	37,100	1,100	42,004	920	69.03	156.00	Russia	Bolshaya Chukochya River	44
WR	OxA-13965	37,200	550	42,027	400	50.46	-3.50	U.K.	Kent's Cavern, Devon	46
WR	OxA-14196	37,540	370	42,235	286	53.29	-1.19	U.K.	Ash Tree Cave, Derbyshire	46
WR	GIN-6011	39,900	500	43,916	422	67.27	155.87	Russia	Dzhelon-Siene	44
WR	GIN-6012	40,000	500	43,991	425	67.20	132.90	Russia	Yana River headwaters	44
WR	OxA-10804	40,200	700	44,148	557	51.29	-2.85	U.K.	Picken's Hole, Somerset	46
WR	OxA-15484	40,550	400	44,430	343	53.26	-1.20	U.K.	Robin Hood Cave, Creswell	46

Supplementary Table S6.1 references

[1] Shapiro, B., *et al*. Rise and fall of the Beringian steppe bison. *Science* **306**, 1561-1565 (2004)

[2] Sher, A.V., Kuzmina, S.A., Kuznetsova, T.V. & Sulerzhitsky, L.D. New insights into the Weichselian environment and climate of the East Siberian Arctic, derived from fossil insects, plants, and mammals. *Quaternary Sci. Rev*. **24**, 533-569 (2005)

[3] Metzger, M., Obermaier, H., Schlager, S., Weber, C. & Steppan, K. Jungsteinzeitliche Wildpferde in Süddeutschland – Paläogenetik, Morphometrie und Nahrungsökologie. *Beiträge zur Archäozoologie und Prähistorischen Anthropologie* **7**, 31-40 (2009)

[4] Steppan, K. Die Tierknochenfunde aus der Schicht 9 von Sipplingen-Osthafen. In: Kieselbach, P. & Kolb, M. (eds.): *Siedlungen der Pfyner Kultur im Osten der Pfahlbaubucht von Sipplingen, Bodenseekreis. Band 2: Naturwissenschaftliche Untersuchungen.* Hemmenhofener Skripte 4/2, 87-96 (2004)

[5] Steppan, K. Mittelholozäne Wildpferde am nördlichen Oberrhein? Beiträge zur Archäozoologie und Prähistorischen Anthropologie. *Forschungen und Berichte zur Vor- und Frühgeschichte in Baden-Württemberg* **53**, 251-255 (1994)

[6] Sommer, R. S., Benecke, N., Lougas, L., Nelle, O. & Schmölcke, U. Holocene colonization pattern of the wild horse (*Equus ferus*) in Europe: a matter of landscape openness? *J. Quat. Sci.*, accepted. (2011)

[7] Lage, W. Schleifknochen versus Schabbahnknochen: Untersuchungen zur Verwendung steinzeitlicher Langknochen von Großsäugern mit konkaven Arbeitsbahnen. *Schriften des Naturwissenschaftlichen Vereins für Schleswig-Holstein* **71**, 26-40 (2009)

[8] Hartz S. & Lübke, H. New Evidence for a Chronostratigraphic Division of the Ertebølle Culture and the Earliest Funnel Beaker Culture on the Southern Mecklenburg Bay. In: Kind, C.-J. (Ed.), *After the Ice Age. Settlements, subsistence and social development in the Mesolithic of Central Europe.* Konrad Theiss Verlag, Stuttgart, 59-74 (2006)

[9] Benecke, N. Zu den Anfängen der Pferdehaltung in Eurasien. Aktuelle archäozoologische Beiträge aus drei Regionen. *Ethnographisch-Archäologische Zeitschrift* **43**, 186-226 (2002)

[10] Steppan, K. Taphonomie - Zoologie - Chronologie - Technologie - Ökonomie. Die Säugetierreste aus den jungsteinzeitlichen Grabenwerken in Bruchsal/Landkreis Karlsruhe. *Materialhefte zur Archäologie in Baden-Württemberg* **66**. Stuttgart (2003)

[11] Davidsen, K. *The Final TRB Culture in Denmark.* Akademisk Forlag, Copenhagen (1978)

[12] Street, M. *Analysis of Late Palaeolithic and Mesolithic faunal Assemblages in the northern Rhineland, Germany*. Ph.D. thesis. University of Birmingham (1993)

[13] Hedges, R.E.M., Housley, R. A., Law, I.A., Perry, C. & Gowlett, J.A.J. Radiocarbon Dates Ffrom the Oxford AMS system: Archaeometry Datalist 6. *Archaeometry* **29**, 289-306 (1987)

[14] Stevens, R.E. & Hedges, R.E.M. Carbon and nitrogen stable isotope analysis of northwest European HRS bone and tooth collagen, 40,000 BP - present: Palaeoclimatic interpretations. *Quaternary Sci. Rev.* **23**, 977-991 (2004)

[15] Ramsey, C.B., Pettitt, P.B., Hedges, R.E.M., Hodgins, G.W.L. & Owen, D.C. Radiocarbon dates from the Oxford AMS system: Archaeometry Datelist 30. *Archaeometry* **42**, 459-479 (2000)

[16] Stage Three Project Database (http://www.esc.cam.ac.uk/oistage3/Details/Homepage.html) Accessed 5 Jan 2011

[17] Kuzmin, Y.V. & Orlova, L.A. Radiocarbon chronology and environment of woolly mammoth (*Mammuthus primigenius* Blum.) in northern Asia: results and perspectives. *Earth-Sci. Rev.* **68**, 133–169 (2004)

[18] Ugan, A. & Byers, D. Geographic and temporal trends in proboscidean and human radiocarbon histories during the late Pleistocene. *Quaternary Sci. Rev.* **26**, 3058–3080 (2007)

[19] Barnes, I., Shapiro, B., Lister, A., Kuznetsova, T., Sher, A., Guthrie, D. & Thomas, M.G. Genetic structure and extinction of the woolly mammoth, *Mammuthus primigenius*. *Curr. Biol*. **17**, 1072–1075 (2007)

[20] Hedges, R.E.M., Housley, R.A., Pettitt, P.B., Ramsey, C.B. & Van Klinken, G.J. Radiocarbon dates from the Oxford AMS System: Archaeometry datelist 21. *Archaeometry* **38**, 181-207 (1996)

[21] Velichko, A.A. & Zelikson, E.M. Landscape, climate and mammoth food resources in the East European Plain during the Late Paleolithic epoch. *Quatern. Int*. **126**, 137-151 (2005)

[22] Holen, S.R. The age and taphonomy of mammoth (*Mammuthus*) at Lovewell Reservoir, Jewell County, Kansas, USA. *Quatern. Int.* **169-170**, 51-63 (2007)

[23] Jacobi, R.M. & Higham, T.F.G. The ''Red Lady'' ages gracefully: new ultrafiltration AMS determinations from Paviland. *J. Hum. Evol.* **55**, 898–907 (2008)

[24] Hill, C.L. Stratigraphic and geochronologic contexts of mammoth (*Mammuthus*) and other Pleistocene fauna, Upper Missouri Basin (northern Great Plains and Rocky Mountains), U.S.A. *Quatern. Int.* **142–143**, 87–106 (2006)

[25] Hedges, R.E.M., Housley, R.A., Law, I.A. & Perry, C. Radiocarbon dates from the Oxford AMS System: Archaeometry datelist 7. *Archaeometry* **30**, 155-164 (1988)

[26] Woodman, P., McCarthy, M. & Monaghan, N. The Irish Quaternary fauna project. *Quaternary Sci. Rev*. **16**, 129-159 (1997)

[27] Kuzmin, Y. V., Burr, G. S., Jull, A. J. T., and Sulerzhitsky, L. D., AMS 14C age of the Upper Palaeolithic skeletons from Sungir site, Central Russian Plain. *Nucl. Instrum. Meth. B* **223**, 731–734 (2004)

[28] Hedges, R.E.M., Pettitt, P.B., Ramsey, C.B. & Van Klinken, G.J. Radiocarbon dates from the Oxford AMS System: Archaeometry datelist 26. *Archaeometry* **40**, 437-455 (1998)

[29] Hedges, R.E.M., Housley, R.A., Law, I.A. & Bronk, C.R. Radiocarbon dates from the Oxford AMS System: Archaeometry Datelist 9. *Archaeometry* **31**, 207-234 (1989)

[30] MacPhee, R.D.E., *et. al*. Radiocarbon chronologies and extinction dynamics of the Late Quaternary mammalian megafauna of the Taimyr Peninsula, Russian Federation. *J. Archaeol. Sci.* **29**, 1017-1042 (2002)

[31] Campos, P. F. *et al.* Ancient DNA analyses exclude humans as the driving force behind late Pleistocene musk ox (*Ovibos moschatus*) population dynamics. *P. Nat. Acad. Sci.* **107**, 5675–5680 (2010)

[32] Harington, C.R. *Annotated Bibliography of Quaternary Vertebrates of Northern North America*. University of Toronto Press, Toronto, Canada. 539 pp.

[33] MacPhee, R.D.E., Tikhonov, A.N., Mol, D. & Greenwood, A.D. Late Quaternary loss of genetic diversity in muskox (*Ovibos)*. *BMC Evolutionary Biology* **5**, 49 (2005)

[34] Stuart, A. J. Mammalian extinctions in the Late Pleistocene of Northern Eurasia and North America. *Biol. Rev. (Camb.)* **66**, 453-562 (1991)

[35] Aaris-Sørensen, K. Diversity and dynamics of the mammalian fauna in Denmark throughout the last glacial-interglacial cycle, 115-0 kyr BP. *Fossils and Strata* **57**, 1-59 (2009)

[36] Forman, S.L., Lubinski, D. & Weihe, R.R. The Holocene occurrence of reindeer on Franz Josef Land, Russia. *Holocene* **10**, 763-768 (2000)

[37] Hedges, R.E.M., Housley, R.A., P.B., Ramsey, C.B. & Van Klinken, G.J. Radiocarbon dates from the Oxford AMS System: Archaeometry Datelist 20. *Archaeometry* **37**, 417-430 (1995)

[38] Álvarez-Lao, D.J. & García, N. Geographical distribution of Pleistocene cold-adapted large mammal faunas in the Iberian Peninsula, *Quatern. Int.* **233**, 159-170 (2011)

[39] Hedges, R.E.M., Housley, R.A., Ramsey, C.B. & and Van Klinken, G.J. Radiocarbon dates from the Oxford AMS system: Archaeometry Datelist 17. *Archaeometry* **35**, 305-326 (1993)

[40] Ramsey, C.B., Higham, T.H.F., Owen, D.C., Pike, A.W.G. & Hedges, R.E.M. Radiocarbon dates from the Oxford AMS system: Archaeometry Datelist 31. *Archaeometry* **44**, 1-149 (2002)

[41] Hedges, R.E.M., Pettitt, P.B., Ramsey, C.B. & Van Klinken, G.J.. Radiocarbon dates from the Oxford AMS system: Archaeometry Datelist 22. *Archaeometry* **38**, 391-415 (1996)

[42] Hedges, R.E.M., Pettitt, P.B., Ramsey, C.B. & Van Klinken, G.J. Radiocarbon dates from the Oxford AMS system: Archaeometry datelist 23. *Archaeometry* **39**, 247-262 (1997)

[43] Hedges, R.E.M., Housley, R.A., Ramsey, C.B. & van Klinken, G.J. Radiocarbon dates from the Oxford AMS system: Archaeometry Datelist 18. *Archaeometry* **36**, 337-374 (1994)

[44] Orlova, L.A., Kuzmin, Y.V. & Dementiev, V.N. A review of the evidence for extinction chronologies for five species of Upper Pleistocene megafauna in Siberia. *Radiocarbon* **46**, 301-314 (2004)

[45] Lister, A.M. & Stuart, A. J., in preparation

[46] Jacobi, R.M., Rose, J., MacLeod, A. & Higham, T.F.G. Revised radiocarbon ages on woolly rhinoceros (*Coelodonta antiquitatis*) from western central Scotland: significance for timing the extinction of woolly rhinoceros in Britain and the onset of the LGM in central Scotland. *Quaternary Sci. Rev*. **28**, 2551–2556 (2009)

Supplementary Table S6.2. Woolly rhinoceros (*Coelodonta antiquitatis*) sample information, listed by calibrated radiocarbon age. Data include radiocarbon age, locality information, and institution currently housing the sample. BC denotes radiocarbon dates beyond the calibration curve. Information on new radiocarbon dates and the GenBank accession numbers of new sequences (JN570760–JN570863) are included. Institution abbreviations used in Supplementary Tables S6.2, S6.3 and S6.4 are listed below.

AMNH: American Museum of Natural History, New York, USA
CGG: Center for GeoGenetics, Natural History Museum, University of Copenhagen, Denmark
CMC: Canadian Museum of Civilization, Gatineau, Quebec, Canada
CMN: Canadian Museum of Nature, Gatineau, Quebec, Canada
EPQ: Department Of Early Prehistory and Quaternary Ecology, Tuebingen
GIN RAS: Geological Institute, Moscow, Russian Academy of Sciences, Russia
GYW: Government of Yukon, Dept. Turism and Culture, Whitehorse
IPAE RAS: Zoological museum of Institute of Plant and Animal Ecology, Ekaterinburg, Russian Academy of Sciences, Russia
KIC: Khatanga Ice Cave, Taimyr Peninsula, Russia
KU: Kansas University
MPI EVA: Max Plank Institute, Leipzig, Germany
PIN RAS: Paleontological Institute, Moscow, Russian Academy of Sciences, Russia
ZIN RAS: Zoological Institute, St. Petersburg, Russian Academy of Sciences, Russia
ZMK: Zoological Museum, University of Copenhagen, Denmark

AMS ID	New date	Sample ID	Museum	Lab ID	New seq	14C date	14C SE	IntCal09 date	IntCal09 SE	LAT	LON	Country	Region	Locality
AAR-11027	x	321	GIN RAS	WR198	-	12,190	60	14,040	141	61.00	130.00	Russia	East Siberia, Lena R. (middle) Basin	Lena-Amga
OxA-20097	x	169-38	PIN RAS	WR320	-	12,280	45	14,164	210	68.70	158.70	Russia	NE Siberia, Kolyma Lowland	Ust'-Omolon
OxA-20096	x	164-59	PIN RAS	WR319	-	12,355	50	14,384	229	68.23	161.92	Russia	NE Siberia, Kolyma Lowland	Molotkovskiy Kamen'
AAR-11028	x	313/1084	GIN RAS	WR199	JN570894	12,460	90	14,572	259	70.20	126.00	Russia	East Siberia, Lena R. (lower) Basin	Govorovo, Lena
OxA-15913	x	3658-3	PIN RAS	WR075	JN570876	12,550	50	14,763	224	67.64	146.77	Russia	NE Siberia, Indigirka River	Orto-Tirekhtyakh.R.
AAR-11029	x	600/398	GIN RAS	WR200	JN570895	12,650	65	14,961	209	69.20	123.00	Russia	East Siberia, Lena R. (lower) Basin	Molodo
AAR-11042	x	436-1	GIN RAS	WR222	-	12,675	65	15,006	205	59.91	56.35	Russia	European Rissia, east	Gremyachevo

AAR-11048	x	202-0919	PIN RAS	WR295	JN570911	12,840	75	15,323	263	73.40	142.40	Russia	NE Siberia	Bol. Lyakhovskiy Isl.
OxA-15857	x	20298	ZIN RAS	WR150	JN570883	13,205	50	16,127	322	54.00	105.80	Russia	Middle Siberia (south)	Lena Upper
OxA-16310	x	4160	ZIN RAS	WR168	-	13,235	55	16,194	321			Russia	European Russia	n/a
AAR-11053	x	ASH7-SVT	Sher	WR300	JN570914	13,355	75	16,478	288	65.12	172.80	Russia	Chukotka, South	Otrozhniy
Lister/Stuart in prep	-	12603/UR.42	n/a	WR283	JN570909	Lister/Stuart in prep		16,739	116	57.45	61.45	Russia	The Urals	Grotto Pershinsky 1
OxA-15854	x	22437	ZIN RAS	WR136	-	14,120	50	17,162	159	50.35	106.44	Russia	Tranbaikalia	Kyakhta
OxA-16258	x	F-3	SIAM	WR087	JN570879	14,245	65	17,327	169	69.40	155.00	Russia	NE Siberia, Kolyma Lowland	Alazeya R.
AAR-11056	x	GIN-21	GIN RAS	WR305	-	14,390	80	17,504	188	54.00	110.10	Russia	Transbaikalia	Barguzin R.
Lister/Stuart in prep	-	12595/UR.30	n/a	WR278	JN570908	Lister/Stuart in prep		17,585	186	60.40	60.05	Russia	The Urals	Grotto Nikolsky
OxA-15850	x	3020-357	PIN RAS	WR072	JN570874	14,500	50	17,654	167	66.90	148.90	Russia	NE Siberia, Kolyma Lowland	Doyda R.
Lister/Stuart in prep	-	13031/UR.79	n/a	WR274	JN570907	Lister/Stuart in prep		18,103	224	61.20	58.38	Russia	The Urals	Grotto Surya 7
GIN-6023	-	165-77	PIN RAS	WR051	JN570866	15,130	50	18,256	168	70.07	153.49	Russia	NE Siberia, Indigirka Lowland	Loc. 88LB
Lister/Stuart in prep	-	12897/UR.38	n/a	WR273	JN570906	Lister/Stuart in prep		18,626	104	55.18	58.63	Russia	The Urals	Grotto Sikiyaz - Tamak 7
OxA-15859	x	30851	ZIN RAS	WR155	-	16,340	60	19,487	112	53.00	41.50	Russia	European Russia (center)	Tsna R.
Lister/Stuart in prep	-	12602/UR.40	n/a	WR269	JN570905	Lister/Stuart in prep		19,508	133	58.67	57.57	Russia	The Urals	Grotto Holodny
AAR-11020	x	10698	ZIN RAS	WR127a	-	16,680	80	19,816	176	56.30	42.14	Russia	Central EUR Russia	Vyazniki
AAR-11022	x	4368/148	GIN RAS	WR189	JN570893	16,820	90	19,992	188	57.00	74.50	Russia	West Siberia, Irtysh R. Basin	Irtysh-3
AAR-11030	x	EWCHINA#4	CGG	WR202	-	16,975	75	20,172	146	46.47	126.03	China	Qingang province	Hongqi site
OxA-15858	x	4058	ZIN RAS	WR153	-	17,075	65	20,275	139			n/a		patria? Kunstkamer
OxA-15806	x	1940	ZIN RAS	WR041	-	17,470	80	20,798	231	55.60	31.20	Russia	West European Russia	Smolensk Region
OxA-20101	x	PIN 3751-150	PIN RAS	WR324	-	17,640	65	21,058	245	70.72	135.42	Russia	NE Siberia, Yana Lowland	Yana, Mus-Khaya
AAR-11059	x	GIN-24	GIN RAS	WR308	JN570916	17,920	110	21,391	182	55.00	90.97	Russia	Central Siberia, south	Yanovo
AAR-11033	x	50/3	GIN RAS	WR211	JN570896	17,990	100	21,457	176	55.02	90.97	Russia	East Siberia (south)	Yanovo
OxA-16308	x	31806	ZIN RAS	WR162	-	18,030	70	21,485	149	54.50	76.50	Russia	West Siberia	Irtysh River
AAR-11024	x	359	GIN RAS	WR194	-	18,160	100	21,708	200	62.91	134.14	Russia	East Siberia, Aldan R. Basin	Mamontova Gora
AAR-11039	x	1135	GIN RAS	WR219	JN570899	18,840	110	22,441	233	69.20	166.50	Russia	Chukotka	Rauchua
OxA-16307	x	3655	ZIN RAS	WR147	JN570882	19,000	75	22,604	247	53.77	102.66	Russia	Middle Siberia (south)	Unga R.
OxA-16309	x	10739	ZIN RAS	WR166	JN570884	19,020	80	22,635	250	51.50	109.50	Russia	Transbaikalia	Khilok river

OxA-15811	x	32186	ZIN RAS	WR050	-	19,500	90	23,305	247	66.00	152.00	Russia	NE Siberia, Kolyma R. Basin	Lower Kolyma
OxA-15861	x	33195	ZIN RAS	WR163	-	19,905	75	23,767	169	50.77	116.10	Russia	Transbaikalia	Mirnaya
OxA-15852	x	23812	ZIN RAS	WR129	JN570881	20,170	80	24,098	154	54.00	49.10	Russia	European Russia (east)	Cheremshan R., Tunguz Peninsula
OxA-16311	x	21851 (2)	ZIN RAS	WR176	JN570887	20,290	80	24,211	156	52.86	103.55	Russia	Middle Siberia (south)	Mal'ta
Lister/Stuart in prep	-	13578/ILC.11 (PIN 3915-32, GIN-6021)	PIN RAS	WR266	JN570904	Lister/Stuart in prep		24,301	182	70.61	142.80	Russia	NE Siberia	Khroma River, Loc.4012
GIN-6021	-	3915-32	PIN RAS	WR094	-	20,400	200	24,346	281	70.60	142.90	Russia	NE Siberia, Indigirka Lowland	Khroma R., Loc. 4012 (OK) = 737 (TB)
OxA-16312	x	21851 (6)	ZIN RAS	WR181	JN570889	20,480	90	24,436	190	52.86	103.55	Russia	Middle Siberia (south)	Mal'ta
OxA-15863	x	21851 (10)	ZIN RAS	WR182	JN570890	21,010	80	25,055	188	52.86	103.55	Russia	Middle Siberia (south)	Mal'ta
OxA-20109	x	21851 (4)	ZIN RAS	WR178	JN570888	21,090	90	25,171	190	52.86	103.55	Russia	Middle Siberia (south)	Mal'ta
OxA-20107	x	21851 (1)	ZIN RAS	WR180	-	21,160	90	25,268	189	52.86	103.55	Russia	Middle Siberia (south)	Mal'ta
OxA-15862	x	21851(5)	ZIN RAS	WR175	JN570886	21,300	80	25,433	209	52.86	103.55	Russia	Middle Siberia (south)	Mal'ta
OxA-16302	x	10687/1687	ZIN RAS	WR110	-	21,400	100	25,600	229	62.00	129.70	Russia	Siberia, Central Yakutia	Yakutsk
OxA-15917	x	21851 (8)	ZIN RAS	WR183	JN570891	21,560	90	25,823	211	52.86	103.55	Russia	Middle Siberia (south)	Mal'ta
AAR-11062	x	GIN-27	GIN RAS	WR311	-	21,660	160	25,953	301	51.18	108.31	Russia	Transbaikalia	Nikolskaya
OxA-15856	x	4157	ZIN RAS	WR143	-	21,660	90	25,971	201	58.60	43.69	Russia	European Russia	n/a
OxA-20108	x	21851 (9)	ZIN RAS	WR179	-	21,690	90	26,011	200	52.86	103.55	Russia	Middle Siberia (south)	Mal'ta
AAR-11058	x	GIN-23	GIN RAS	WR307	-	23,000	170	27,841	331	51.26	107.26	Russia	Transbaikalia	Barykino
OxA-15860	x	4188	ZIN RAS	WR161	-	23,270	100	28,119	181	57.68	66.20	Russia	West Siberia (south-west)	Tavda River
AAR-11060	x	GIN-25	GIN RAS	WR309	JN570917	23,270	180	28,123	225	68.32	161.72	Russia	NE Siberia, Kolyma R. Basin	Mal. Anyuy R., Krasivoye
AAR-11061	x	GIN-26	GIN RAS	WR310	-	23,500	190	28,273	217	50.10	119.18	Russia	Transbaikalia	Argun'
OxA-15911	x	F-45	SIAM	WR061	JN570867	24,670	110	29,499	175	70.74	136.21	Russia	NE Siberia, Yana Lowland	Kazachye, near the village
OxA-15874	x	3914-5	PIN RAS	WR068	JN570871	24,860	100	29,707	213	68.19	146.60	Russia	NE Siberia, Indigirka Lowland	Badyarikha
AAR-11051	x	Galgan I -1	PIN RAS	WR298	JN570913	24,830	210	29,738	272	59.70	161.10	Russia	Kamchatka	Galgan I archeological site
OxA-15916	x	3491-898	PIN RAS	WR088	JN570880	24,880	110	29,746	217	68.65	159.15	Russia	NE Siberia, Kolyma lower	Duvannyy Yar, whole
OxA-16303	x	10693	ZIN RAS	WR115	-	25,040	120	29,914	208	54.60	44.80	Russia	European Russia (east)	Irset R.

OxA-16300	x	10696	ZIN RAS	WR107	-	25,320	130	30,130	239	55.42	55.56	Russia	The Urals, Southern (Bashkiria)	Birsk
OxA-15849	x	3342-101	PIN RAS	WR070	JN570873	25,550	110	30,402	171	67.58	160.78	Russia	NE Siberia, Kolyma Lowland	Khetachan Creek mine
AAR-11041	x	612-2	GIN RAS	WR221	JN570900	26,100	300	30,807	228	60.80	114.00	Russia	East Siberia (center)	Nyuya
AAR-11047	x	34893	ZIN RAS	WR292	JN570910	26,440	250	31,044	176	62.77	148.16	Russia	NE Siberia, SE	Kirgilyakh Baby Mammoth site
OxA-20091	x	F-1099	SIAM	WR314	-	26,570	120	31,126	82	68.52	147.10	Russia	NE Siberia, Indigirka River	Tirekhtyakh
OxA-16259	x	3658-17	PIN RAS	WR091	-	26,680	130	31,170	84	65.88	150.31	Russia	NE Siberia, Kolyma middle course	Sa-Sabanyt R. (left lower Zyryanka)
OxA-15807	x	SP1357	ZIN RAS	WR042	-	26,990	180	31,300	110	51.41	39.05	Russia	European Russia	Kostenki
AAR-11052	x	Galgan I -2	PIN RAS	WR299	-	27,950	300	32,168	427	59.70	161.10	Russia	Kamchatka	Galgan I archeological site
OxA-20095	x	161-135	PIN RAS	WR318	-	28,160	190	32,393	359	70.56	149.71	Russia	NE Siberia, Indigirka Lowland	Keremesit R., Lower Camp Site (1503)
OxA-20103	x	10736	ZIN RAS	WR289	-	28,450	180	32,815	348	59.10	31.10	Russia	EUR Russia, NW	Lyuban'
OxA-15853	x	10717	ZIN RAS	WR132	-	29,110	150	33,789	346			n/a	n/a	patria? Donator?
OxA-15846	x	3915-137	PIN RAS	WR067	JN570870	29,260	140	33,955	325	70.60	147.60	Russia	NE Siberia, Indigirka lower	A.-Allaikha, ANV-II site
AAR-11049	x	202-0203	PIN RAS	WR296	JN570912	29,550	350	34,155	414	72.10	142.50	Russia	NE Siberia	Shirokostan Peninsula
OxA-15912	x	3657-142	PIN RAS	WR074	JN570875	30,240	170	34,823	137	70.60	147.60	Russia	NE Siberia, Indigirka lower	A.-Allaikha, ANV-II site
OxA-20098	x	169-86	PIN RAS	WR321	-	30,350	170	34,874	153	68.32	161.72	Russia	NE Siberia, Kolyma Lowland	Krasivoye
AAR-11035	x	359/102	GIN RAS	WR215	JN570898	30,500	250	34,978	348	62.90	134.10	Russia	East Siberia, Aldan R. Basin	Mamontova Gora
AAR-11036	x	359/90	GIN RAS	WR216	-	30,950	250	35,505	419	62.90	134.10	Russia	East Siberia, Aldan R. Basin	Mamontova Gora
OxA-15808	x	SP1360	ZIN RAS	WR045	JN570864	31,070	190	35,607	385	62.00	58.67	Russia	Urals (north)	Medvezhya Cave
OxA-15730	x	3658-13	PIN RAS	WR062	JN570868	31,500	200	35,857	368	68.60	147.06	Russia	NE Siberia, Indigirka Lowland	Tirekhtyakh
OxA-16323	x	F-36	SIAM	WR080	JN570878	32,380	220	36,848	301	67.94	142.42	Russia	NE Siberia, Indigirka Lowland	Selennyakh
OxA-15855	x	35594	ZIN RAS	WR137	-	32,690	200	37,176	388	71.10	180.00	Russia	NE Siberia, Chukotka	Wrangel Island
OxA-20100	x	171-6	PIN RAS	WR323	-	33,150	220	37,891	439	69.29	154.72	Russia	NE Siberia, Kolyma Lowland	Alazeya, Sergeev Ruchey
Lister/Stuart in prep	-	12560/UR.37	n/a	WR252	JN570903	Lister/Stuart in prep		38,445	847	60.40	60.05	Russia	The Urals	Grotto Cheremuhovo 1-4

Lister/Stuart in prep	-	12605/UR.44	n/a	WR250	JN570902	Lister/Stuart in prep		38,500	477	58.20	58.17	Russia	The Urals	Grotto Kumishsky
OxA-16687	x	50B	ZIN RAS	WR184	JN570892	34,200	240	39,134	371	52.86	103.55	Russia	Middle Siberia (south)	Mal'ta
OxA-20102	x	198-001	PIN RAS	WR325	-	34,320	230	39,258	384	64.74	171.20	Russia	Chukotka, SW	Main Yar
OxA-16685	x	15131	ZIN RAS	WR140	-	34,700	260	39,746	437	53.06	51.30	Russia	European Russia (east)	Bogatoe
OxA-16686	x	20077	ZIN RAS	WR144	-	35,110	280	40,276	460	50.40	107.42	Russia	Tranbaikalia	Tamir
AAR-11054	x	ASH8-Main	Sher	WR301	JN570915	35,400	650	40,509	712	65.00	176.00	Russia	Chukotka, South	Anadyr'
AAR-11034	x	358/6	GIN RAS	WR214	JN570897	35,900	450	41,080	449	62.82	134.51	Russia	East Siberia, Aldan R. Basin	Krest-Khaldzhay
AAR-11043	x	SLWS-4	n/a	WR224	-	37,800	900	42,487	686			China	Inner Mongolia	Salawusu
Oxa-15851	x	10712	ZIN RAS	WR118	-	38,330	310	42,737	266	55.75	40.75	Russia	European Russia (center)	n/a
OxA-16314	x	4734	ZIN RAS	WR174	JN570885	38,790	350	43,067	323	71.00	136.00	Russia	NE Siberia, Yana Lowland	Yana R. downstream
OxA-15810	x	4733	ZIN RAS	WR049	JN570865	38,900	400	43,166	366	69.00	135.00	Russia	NE Siberia, Yana R.	Yana
OxA-16301	x	10703	ZIN RAS	WR108	-	39,380	370	43,543	349	56.45	53.80	Russia	European Russia (east), Udmurtia	Sarapul
OxA-18755	x	Y-24	n/a	WR333	JN570918	39,410	390	43,568	359	69.00	162.00	Russia	Cherskiy	Rodinka Mountain
Lister/Stuart in prep	-	11787/CE.13	n/a	WR244	JN570901	Lister/Stuart in prep		43,786	512	48.56	10.19	Germany	Vogelherd Cave	Vogelherd Cave
GIN-6012	-	3915-308	PIN RAS	WR093	-	40,000	500	43,991	425	67.20	132.90	Russia	NE Siberia, Yana R., Verkhoyansk District	Sartang R., Loc.3821
OxA-20090	x	F-602	SIAM	WR064	JN570869	40,150	650	44,108	524	68.69	161.65	Russia	NE Siberia, Kolyma lower	Gold field "Drevniy"
OxA-20094	x	F-355	SIAM	WR317	-	40,250	400	44,199	363	68.52	147.10	Russia	NE Siberia, Indigirka River	Tirekhtyakh
OxA-20106	x	4362/103-579	GIN RAS	WR188	-	40,400	1,100	44,344	901	56.00	83.84	Russia	West Siberia, Ob' R. Basin	Voronovo, Ob' R.
OxA-15798	x	SP168	MPI EVA	WR035	-	40,500	450	44,391	384	51.50	6.70	Germany	Northern Rhein-Westfalien	Herne West
OxA-20104	x	EWCHINA#3	CGG	WR201	-	41,150	500	44,835	377	46.47	126.03	China	Qingang province	Hongqi site
OxA-16306	x	3946	ZIN RAS	WR139	-	41,450	500	45,022	379	58.01	40.87	Russia	European Russia (center)	Ustye River
OxA-15809	x	20120	ZIN RAS	WR048	-	41,800	550	45,251	420	50.40	106.40	Russia	Transbaikalia	Kyakhta
OxA-16256	x	F-71	SIAM	WR079	JN570877	42,050	500	45,412	397	69.28	146.85	Russia	NE Siberia, Indigirka River	Indigirka, right bank
OxA-15804 &15805	x	SP1193	MPI EVA	WR030	-	43,650	650	46,779	829	51.30	83.00	Russia	Altay	Strashnaya cave
OxA-15802	x	SP1191-1	MPI EVA	WR027	-	43,750	600	46,851	795	51.30	83.00	Russia	Altay	Strashnaya cave
OxA-15848	x	3491-895	PIN RAS	WR069	JN570872	43,850	500	46,889	713	68.65	159.15	Russia	NE Siberia, Kolyma lower	Duvannyy Yar, whole

OxA-20089	x	198-2	PIN RAS	WR055	-	46,450	750	BC	73.30	143.40	Russia	New Siberian Islands	Bolshoy Lyakhovsky Island
OxA-15731	x	F-603	SIAM	WR065	-	49,700	1,100	BC	68.69	161.65	Russia	NE Siberia, Kolyma lower	Gold field "Drevniy"
OxA-15910	x	3914-48	PIN RAS	WR073	-	53,300	1,500	BC	66.18	151.65	Russia	NE Siberia, Kolyma Lowland	Irelyakh R.
OxA-15914	x	F-38	SIAM	WR078	-	46,300	700	BC	68.52	147.10	Russia	NE Siberia, Indigirka River	Tirekhtyakh
OxA-16324	x	F-31	SIAM	WR081	-	44,650	600	BC	70.40	152.30	Russia	NE Siberia, Indigirka Lowland	Sundrun
OxA-15915	x	F-49	SIAM	WR082	-	49,900	1,000	BC	70.50	156.80	Russia	NE Siberia, Kolyma Lowland	Kuropatochya Bol. R.
OxA-16257	x	3100-170	PIN RAS	WR086	-	44,450	650	BC	69.76	157.63	Russia	NE Siberia, Kolyma Lowland	Chukochya Bol. R., Loc. N 39
OxA-16294	x	SP1390	n/a	WR096	-	47,400	1,200	BC	55.10	5.00	Netherlands	NW Europe, North Sea	North Sea
OxA-16295	x	SP1391	n/a	WR097	-	45,200	1,000	BC	55.30	4.00	Netherlands	NW Europe, North Sea	North Sea
OxA-16296	x	SP1392	n/a	WR098	-	47,900	1,200	BC	55.50	6.00	Netherlands	NW Europe, North Sea	North Sea
OxA-16297	x	SP1393	n/a	WR099	-	48,100	1,100	BC	55.70	4.00	Netherlands	NW Europe, North Sea	North Sea
OxA-16299	x	SP1396	n/a	WR102	-	47,100	1,200	BC	55.90	6.00	Netherlands	NW Europe, North Sea	North Sea
OxA-16304	x	10708	ZIN RAS	WR134	-	45,800	800	BC	57.38	65.03	Russia	West Siberia (south-west)	Salairka
AAR-11023	x	4362/99-579	GIN RAS	WR190	-	45,300	1,200	BC	57.94	70.30	Russia	West Siberia, Irtysh R. Basin	Ishchetskaya, Irtysh R.
AAR-11026	x	990/4-902/26	GIN RAS	WR196	-	43,300	950	BC	63.00	134.00	Russia	East Siberia, Aldan R. Basin	Mamontova Gora, Aldan R.
AAR-11038	x	GIN 361/189	GIN RAS	WR218	-	43,000	1,550	BC	63.31	131.84	Russia	East Siberia, Aldan R. Basin	Tanda
AAR-11040	x	GIN 114/12	GIN RAS	WR220	-	42,150	1,450	BC	63.00	117.00	Russia	East Siberia, Vilyuy R. Basin	Sokolinyy
AAR-11045	x	10729	ZIN RAS	WR290	-	41,000	1,250	BC	53.65	111.93	Russia	East Siberia, south	Dzhilinda
AAR-11050	x	202-0413	PIN RAS	WR297	-	44,750	1,900	BC	73.32	141.37	Russia	NE Siberia	Bol. Lyakhovskiy Isl.
AAR-11063	x	GIN-28	GIN RAS	WR312	-	42,750	1,550	BC	54.53	84.86	Russia	Altay	Novokamenka, Vydrikha R.
OxA-20092	x	F-0354	SIAM	WR315	-	50,500	1,300	BC	68.52	147.10	Russia	NE Siberia, Indigirka River	Tirekhtyakh
OxA-20093	x	F-0351	SIAM	WR316	-	48,800	1,000	BC	68.52	147.10	Russia	NE Siberia, Indigirka River	Tirekhtyakh
OxA-20099	x	169-085	PIN RAS	WR322	-	48,300	900	BC	68.32	161.72	Russia	NE Siberia, Kolyma Lowland	Krasivoye
OxA-15799	x	SP1183-2	MPI EVA	WR002	-	>58,600		Infinite	51.60	82.80	Russia	Altay	Logovo Gieny Cave
OxA-15800	x	SP1183-4	MPI EVA	WR004	-	>50,900		Infinite	51.60	82.80	Russia	Altay	Logovo Gieny Cave

OxA-15801	x	SP1183-6	MPI EVA	WR006	-	>51,700	Infinite	51.60	82.80	Russia	Altay	Logovo Gieny Cave
OxA-15803	x	SP1192	MPI EVA	WR029	-	>51,800	Infinite	51.30	83.00	Russia	Altay	Strashnaya cave
OxA-15947	x	F-2	SIAM	WR089	-	>53,900	Infinite	68.69	161.65	Russia	NE Siberia, Kolyma lower	Gold field "Drevniy"
OxA-16298	x	SP1395	n/a	WR101	-	>43,500	Infinite	55.80	5.00	Netherlands	NW Europe, North Sea	North Sea
AAR-11021	x	771/201-9	GIN RAS	WR185	-	>44,000	Infinite	63.29	107.41	Russia	Middle Siberia, Yenissey R. Basin	Nizhnyaya Tunguska
AAR-11025	x	453	GIN RAS	WR195	-	>50,000	Infinite	52.01	86.79	Russia	Altay	Isha
AAR-11031	x	EWCHINA#7	CGG	WR205	-	>44,000	Infinite	46.47	126.03	China	Qingang province	Hongqi site
AAR-11032	x	661/250	GIN RAS	WR208	-	>49,000	Infinite	54.56	91.34	Russia	East Siberia (south), Yenissey R. Basin	Bellyk
AAR-11037	x	GIN 361 No.56	GIN RAS	WR217	-	>46,000	Infinite	63.40	133.00	Russia	East Siberia, Aldan R. Basin	Aldan
AAR-11044	x	31521	ZIN RAS	WR287	-	>50,000	Infinite	59.98	42.75	Russia	North Eur Russia	Tot'ma
AAR-11046	x	10706	ZIN RAS	WR291	-	>46,000	Infinite	-	-	Russia	Chukotka	Chukotskiy Nos Cape
AAR-11055	x	GIN-19	GIN RAS	WR303	-	>52,000	Infinite	52.08	115.99	Russia	Transbaikalia	Ostrovki
AAR-11057	x	GIN-22	GIN RAS	WR306	-	>47,000	Infinite	50.36	108.74	Russia	Transbaikalia	Chikoy
AAR-11064	x	GIN-29	GIN RAS	WR313	-	>49,000	Infinite	51.00	108.00	Russia	Transbaikalia	Transbaikalia

Supplementary Table S6.3. Horse *(Equus ferus)* sample information, listed by calibrated radiocarbon age. Data include radiocarbon age, locality information, and institution currently housing the sample. Information on new radiocarbon dates and GenBank accession numbers of new sequences (JN570919–JN571033) are included. Some DNA sequences were generated from specimens with published radiocarbon dates; these references follow below the table.

AMS ID	New date	Collection no	Museum	Lab ID	New seq	14C date	14C SE	IntCal09 date	IntCal 09 SE	LAT	LON	Country	Region	Locality	Ref
GIN-10687	-	BL-O 279-R	IEM RAS	JW25	JN570962	2,220	50	2,230	64	73.30	141.30	Russia	Novosibirsk Islands, N-E Siberia	Zimovye River mouth	5
OxA-13847	x	PIN M9-6	PIN RAS	JW191	JN570956	5,778	34	6,581	48	71.80	129.30	Russia	Lena River Delta, N-E Siberia	Mamontovy Khayata	1
OxA-14270	-	P89.21.1	Royal Alberta Museum	JW174	DQ007594	11,200	90	13,092	121	53.50	-113.50	Canada	Alberta, Canada	Grand Prairie	6
CAMS-119982	x	F:AM 142429	AMNH	JAL294	JN570941	12,310	100	14,338	272	64.40	-147.30	U.S.A.	Fairbanks, Alaska	Goldstream	1
AA-37609	-	-	-	-	AF326670	12,380	120	14,459	282	64.40	-147.30	U.S.A.	Fairbanks, Alaska	Ester Creek	3
AA26819	-	A-144-9422	AMNH	JW184	JN570955	12,510	130	14,644	292	64.40	-147.30	U.S.A.	Fairbanks, Alaska	Ester Creek	4
CAMS-145101	x	F:AM 143628	AMNH	JAL276	JN570930	12,510	45	14,681	233	64.40	-147.30	U.S.A.	Fairbanks, Alaska	Upper Cleary	1
AA26810	-	A-6159	AMNH	JW348	JN570983	12,560	140	14,714	316	53.30	-113.10	U.S.A.	Fairbanks, Alaska	Fox	4
OxA-13669	-	NHMS n/a	NHMS	JW177	DQ007611 DQ007558	12,545	50	14,751	226	47.40	8.50	Germany	Germany, Europe	Petersfels	6
OxA-13670	-	NHMS n/a	NHMS	JW175	DQ007609 DQ007556	12,550	60	14,752	234	48.20	9.40	Germany	Germany, Europe	Hohlefels	6
CAMS-145091	x	F:AM 143621	AMNH	JAL249	JN570922	12,560	45	14,792	215	64.40	-147.30	U.S.A.	Fairbanks, Alaska	Lower Goldstream	1
CAMS-145092	x	F:AM 143622	AMNH	JAL252	JN570923	12,670	60	15,001	196	64.40	-147.30	U.S.A.	Fairbanks, Alaska	Goldstream	1
AA-37614	-	-	-	-	AF326675	12,840	140	15,381	396	64.40	-147.30	U.S.A.	Fairbanks, Alaska	Ester Creek	3
AA26829	-	A-4339	AMNH	JW356	JN570991	12,860	140	15,423	393	65.40	-147.10	U.S.A.	Fairbanks, Alaska	Fairbanks Creek	4
CAMS-145095	x	F:AM 143625	AMNH	JAL268	JN570925	13,055	50	15,764	331	64.40	-147.30	U.S.A.	Fairbanks, Alaska	Goldstream	1
AA26811	-	Bx334-2870	AMNH	JW579	JN571004	13,270	150	16,182	398	64.40	-148.00	U.S.A.	Fairbanks, Alaska	Cripple Creek	4
OxA-13671	x	IPT-6671	EPQ	JW266	JN570963	13,845	50	16,928	92	48.50	10.20	Germany	Germany, Europe	Vogelherd IV	1
OxA-14363	x	EK 994/708	IPAE	JW305	JN570972	13,900	50	16,964	102	59.00	58.80	Russia	Surya, Urals	Sur'ya 5	1
OxA-13758	x	PIN 3658-121	PIN RAS	JW194	JN570957	13,935	55	16,990	113	68.30	157.70	Russia	Kolyma lowlands, N-E Siberia	Alyoshkina Zaimka, Loc. 3298	1
AA26809	-	A-276	AMNH	JW374	JN570993	13,940	55	16,994	114	59.00	58.80	Russia	Urals	Sur'ya 5	4
AA26805	-	A-144-6987	AMNH	JW355	JN570990	14,000	160	17,089	203	64.40	-147.30	U.S.A.	Fairbanks, Alaska	Ester Creek	4
AA26817	-	A-237-10198	AMNH	JW585	JN571007	14,120	180	17,219	232	64.50	-147.40	U.S.A.	Fairbanks, Alaska	Goldstream	4

OxA-14364	x	EK 994/1	IPAE	JW345	JN570982	14,195	50	17,268	162	59.00	58.80	Russia	Urals	Sur'ya 5	1
AA26840	-	A-5598-2402	AMNH	JW353	JN570988	14,260	160	17,358	230	64.40	-148.00	U.S.A.	Fairbanks, Alaska	Fairbanks Creek	4
OxA-16361	x	A-274	AMNH	JW557	JN571000	14,300	160	17,399	233	65.00	-147.40	U.S.A.	Fairbanks, Alaska	Cleary	1
OxA-17691	x	MgV3-85-74	CMC	JW617	JN571025	14,715	55	17,899	185	67.10	-140.50	Canada	N. Yukon	Bluefish Cave 3	1
AA26852	-	A-160-6810	AMNH	JW593	JN571010	14,990	190	18,234	229	64.40	-147.30	U.S.A.	Fairbanks, Alaska	Ester Creek	4
Beta-109267	-	n/a		JW69	JN571026	15,090	70	18,257	171	56.60	-133.30	U.S.A.	Fairbanks, Alaska	Gerstle River Quarry	2
OxA-14372	x	EK 994/22	IPAE	JW342	JN570981	15,200	60	18,484	184	59.00	58.80	Russia	Urals	Sur'ya 5	1
CAMS-119977	x	F:AM 142424	AMNH	JAL275	JN570929	15,460	100	18,686	95	64.40	-147.30	U.S.A.	Fairbanks, Alaska	BC	1
AA26812	-	A-114-5278	AMNH	JW354	JN570989	15,570	190	18,775	214	64.50	-147.30	U.S.A.	Fairbanks, Alaska	Engineer Creek	4
AA26808	-	A-144-6306	AMNH	JW574	JN571003	15,750	190	18,954	215	64.40	-147.30	U.S.A.	Fairbanks, Alaska	Ester Creek	4
CAMS-145109	x	F:AM 143638	AMNH	JAL301	JN570943	15,810	70	18,989	164	64.40	-147.30	U.S.A.	Fairbanks, Alaska	Goldstream	1
CAMS-120068	x	F:AM 60032	AMNH	JAL328	JN570951	15,850	100	19,073	167	64.40	-147.30	U.S.A.	Fairbanks, Alaska	Goldstream	1
AA26820	-	A-144-9414	AMNH	JW584	JN571006	15,920	190	19,109	195	64.40	-147.30	U.S.A.	Fairbanks, Alaska	Ester Creek	4
CAMS-145104	x	F:AM 143631	AMNH	JAL282	JN570933	15,920	70	19,122	146	64.40	-147.30	U.S.A.	Fairbanks, Alaska	Upper Cleary	1
AA26837	-	A-6150	AMNH	JW564	JN571002	16,130	240	19,247	268	64.50	-147.60	U.S.A.	Fairbanks, Alaska	Fox	4
AA26845	-	A-114-6909	AMNH	JW592	JN571009	16,150	210	19,260	247	64.40	-147.30	U.S.A.	Fairbanks, Alaska	Ester Creek	4
CAMS-119968	x	F:AM 60004	AMNH	JAL239	JN570920	16,370	100	19,514	154	64.40	-147.30	U.S.A.	Fairbanks, Alaska	Ester Creek	1
AA26807	-	A-940	AMNH	JW583	JN571005	16,700	220	19,866	256	65.00	-147.20	U.S.A.	Fairbanks, Alaska	Cleary	4
CAMS-145098	x	F:AM 143627	AMNH	JAL274	JN570928	17,770	80	21,254	208	64.40	-147.30	U.S.A.	Fairbanks, Alaska	Cleary	1
AA26839	-	A-160-6819	AMNH	JW387	JN570995	18,890	280	22,580	405	64.40	-147.30	U.S.A.	Fairbanks, Alaska	Ester Creek	4
AA26821	-	Bx-278-5635	AMNH	JW296	JN570968	18,910	280	22,607	400	65.40	-147.10	U.S.A.	Fairbanks, Alaska	Fairbanks Creek	4
CAMS-120058	x	F:AM 60023	AMNH	JAL316	JN570949	19,000	100	22,623	257	64.40	-147.30	U.S.A.	Alaska	El Dorado	1
OxA-14299	x	PIN 3751-51	PIN RAS	JW207	JN570960	19,045	75	22,672	248	69.90	133.90	Russia	Yana River Basin, N-E Siberia	Mus.-Khaya, Loc. 2210	1
AA26824	-	A-114-6801	AMNH	JW298	JN570970	19,120	290	22,852	372	64.40	-147.30	U.S.A.	Fairbanks, Alaska	Ester Creek	4
AA26801	-	A-216-6190	AMNH	JW600	JN571014	19,390	290	23,106	396	64.50	-147.40	U.S.A.	Fairbanks, Alaska	Goldstream	4
AA26836	-	A-114-5336	AMNH	JW294	JN570967	19,450	280	23,183	397	64.40	-147.30	U.S.A.	Fairbanks, Alaska	Engineer Creek	4
AA26823	-	A-155-6052	AMNH	JW297	JN570969	19,460	320	23,205	434	64.40	-147.30	U.S.A.	Fairbanks, Alaska	Ester Creek	4
AA26816	-	A-506	AMNH	JW386	JN570994	19,470	290	23,216	409	65.40	-147.10	U.S.A.	Fairbanks, Alaska	Fairbanks Creek	4
AA26827	-	A-1537	AMNH	JW591	JN571008	19,560	300	23,351	428	65.30	-147.10	U.S.A.	Fairbanks, Alaska	Fish Creek	4
CAMS-120059	x	F:AM 60027	AMNH	JAL318	JN570950	19,590	100	23,437	230	64.40	-147.30	U.S.A.	Fairbanks, Alaska	Fairbanks Creek	1
CAMS-145097	x	F:AM 143626	AMNH	JAL273	JN570927	19,630	100	23,489	212	64.40	-147.30	U.S.A.	Fairbanks, Alaska	Goldstream	1
CAMS-145096	x	F:AM 143647	AMNH	JAL272	JN570926	19,720	100	23,589	180	64.40	-147.30	U.S.A.	Fairbanks, Alaska	Goldstream	1
CAMS-145103	x	F:AM 143630	AMNH	JAL281	JN570932	19,760	100	23,627	174	64.40	-147.30	U.S.A.	Fairbanks, Alaska	Goldstream	1
CAMS-145108	x	F:AM 143637	AMNH	JAL292	JN570939	19,780	100	23,645	173	64.40	-147.30	U.S.A.	Fairbanks, Alaska	Lower Goldstream	1
AA26849	-	A-414	AMNH	JW525	JN570998	19,790	335	23,653	458	64.40	-147.30	U.S.A.	Fairbanks, Alaska	Ester Creek	4

AA-37611	-	-	-	-	AF326672	19,800	280	23,671	391	64.40	-147.30	U.S.A.	Fairbanks, Alaska	Ester Creek	3
CAMS-145116	x	F:AM 60042	AMNH	JAL313	JN570948	19,810	100	23,673	173	64.40	-147.30	U.S.A.	Fairbanks, Alaska	Goldstream	1
CAMS-145093	x	F:AM 143623	AMNH	JAL260	JN570924	19,830	100	23,692	175	64.40	-147.30	U.S.A.	Alaska	Point Barrow	1
AA26841	-	A-559-4237	AMNH	JW299	JN570971	19,830	330	23,703	447	65.40	-147.10	U.S.A.	Fairbanks, Alaska	Fairbanks Creek	4
AA26863	-	A-5642	AMNH	JW352	JN570987	19,835	155	23,704	231	64.50	-147.40	U.S.A.	Fairbanks, Alaska	Fairbanks Creek	4
AA26834	-	A-237-6189	AMNH	JW563	JN571001	19,835	155	23,704	231	65.90	-147.10	U.S.A.	Fairbanks, Alaska	Fairbanks Creek	4
CAMS-119983	x	F:AM 142429	AMNH	JAL295	JN570942	19,950	100	23,824	197	64.40	-147.30	U.S.A.	Fairbanks, Alaska	Goldstream	1
CAMS-119980	x	F:AM 142427	AMNH	JAL288	JN570937	19,960	100	23,837	198	64.40	-147.30	U.S.A.	Fairbanks, Alaska	Lower Goldstream	1
AAR-11188	x	YG-3-20210	GYW	PH7	JN571033	19,990	140	23,883	226	64.00	-139.20	Canada	Dawson area, Yukon	Hunker Creek	1
GIN-10688	-	BL-O 128	IEM RAS	JW27	JN570964	20,100	170	24,024	236	73.30	141.30	Russia	Novosibirsk Islands, N-E Siberia	Zimovye River mouth	5
CAMS-145105	x	F:AM 143632	AMNH	JAL283	JN570934	20,150	110	24,080	177	64.40	-147.30	U.S.A.	Fairbanks, Alaska	Cleary	1
AA26813	-	A-1013	AMNH	JW349	JN570984	20,170	329	24,099	412	64.50	-147.40	U.S.A.	Fairbanks, Alaska	Goldstream	4
AA-37608	-	-	-	-	AF326669	20,200	310	24,129	388	65.40	-147.10	U.S.A.	Fairbanks, Alaska	Fairbanks Creek	3
CAMS-145102	x	F:AM 143629	AMNH	JAL279	JN570931	20,210	110	24,130	170	64.40	-147.30	U.S.A.	Fairbanks, Alaska	Lower Goldstream	1
CAMS-145106	x	F:AM 143634	AMNH	JAL287	JN570936	20,430	90	24,374	185	64.40	-147.30	U.S.A.	Fairbanks, Alaska	Gil	1
AA26862	-	A-463-3144	AMNH	JW597	JN571012	20,410	320	24,374	405	64.50	-147.30	U.S.A.	Fairbanks, Alaska	Engineer Creek	4
OxA-14384	x	EK 994/710	IPAE	JW306	JN570973	20,430	110	24,375	204	59.00	58.80	Russia	Urals	Sur'ya 5	1
CAMS-119978	x	F:AM 142425	AMNH	JAL284	JN570935	20,440	100	24,387	196	64.40	-147.30	U.S.A.	Fairbanks, Alaska	Lower Goldstream	1
AA26869	-	A-144-6509	AMNH	JW512	JN570996	20,420	325	24,388	412	64.40	-147.30	U.S.A.	Fairbanks, Alaska	Ester Creek	4
AA26866	-	A-559-4332	AMNH	JW351	JN570986	20,545	345	24,546	443	65.40	-147.10	U.S.A.	Fairbanks, Alaska	Ester Creek	4
AA26857	-	A-802	AMNH	JW598	JN571013	20,580	160	24,584	230	64.50	-147.30	U.S.A.	Fairbanks, Alaska	Engineer Creek	4
AA-37613	-	F:AM 6171	AMNH	-	AF326674	20,670	350	24,695	458	64.50	-147.40	U.S.A.	Fairbanks, Alaska	Goldstream	3
CAMS-145113	x	F:AM 143648	AMNH	JAL310	JN570946	20,720	110	24,712	172	64.40	-147.30	U.S.A.	Alaska	Chatom	1
CAMS-145107	x	F:AM 143635	AMNH	JAL290	JN570938	20,730	90	24,720	161	64.40	-147.30	U.S.A.	Fairbanks, Alaska	Upper Cleary	1
OxA-14367	x	EK 994/145	IPAE	JW338	JN570979	20,730	110	24,721	172	59.00	58.80	Russia	Urals	Sur'ya 5	1
CAMS-145110	x	F:AM 143639	AMNH	JAL307	JN570944	20,810	120	24,792	188	64.40	-147.30	U.S.A.	Fairbanks, Alaska	Cleary	1
AA26850	-	A-4-4-2145	AMNH	JW601	JN571015	20,840	350	24,895	471	64.40	-148.00	U.S.A.	Fairbanks, Alaska	Cripple Creek	4
OxA-17690	x	2MgV2-16-9-10	CMC	JW616	JN571024	21,100	80	25,182	180	67.10	-140.50	Canada	N. Yukon	Bluefish Cave 2	1
OxA-14125	x	KU-42625	KU	JW157	JN570952	21,130	90	25,229	188	44.50	-108.20	U.S.A.	Wyoming	Natural Trap Cave	1
CAMS-119981	x	F:AM 142428	AMNH	JAL293	JN570940	21,280	100	25,412	217	64.40	-147.30	U.S.A.	Fairbanks, Alaska	Lower Goldstream	1
OxA-14156	x	KU-51467	KU	JW160	JN570953	21,500	290	25,724	435	44.50	-108.20	U.S.A.	Wyoming	Natural Trap Cave	1

CAMS-145114	x	n/a	AMNH	JAL311	JN570947	21,520	130	25,752	253	64.40	-147.30	U.S.A.	Fairbanks, Alaska	Upper Cleary	1
AA26844	-	A-7211	AMNH	JW513	JN570997	21,800	370	26,178	590	64.90	-147.60	U.S.A.	Fairbanks, Alaska	Fox	4
CAMS-119989	x	F:AM 142435	AMNH	JAL309	JN570945	21,840	100	26,195	233	64.40	-147.30	U.S.A.	Fairbanks, Alaska	Goldstream	1
AAR-11182	x	YG	GYW	PH1	JN571027	21,950	170	26,386	290	64.00	-139.10	Canada	Dawson area, Yukon	last Chance Creek	1
AA26814	-	I-36	AMNH	JW596	JN571011	22,300	410	26,905	587	64.50	-147.40	U.S.A.	Fairbanks, Alaska	Goldstream	4
AA26848	-	A-160-6805	AMNH	JW350	JN570985	22,710	440	27,364	572	64.40	-147.30	U.S.A.	Fairbanks, Alaska	Ester Creek	4
OxA-14385	x	EK 994/711	IPAE	JW314	JN570976	23,740	100	28,482	199	59.00	58.80	Russia	Urals	Sur'ya 5	1
OxA-17686	x	YT03-40	GYW	JW613	JN571022	23,920	100	28,724	225	64.80	-139.40	Canada	Dawson area, Yukon	Dawson area	1
OxA-14307	x	EK 994/214	IPAE	JW313	JN570975	24,200	110	29,015	228	59.00	58.80	Russia	Urals	Sur'ya 5	1
AA-37612	-	-	-	-	AF326673	24,400	500	29,223	545	64.40	-147.30	U.S.A.	Fairbanks, Alaska	Ester Creek	3
AAR-11185	x	IK-01-060		PH4	JN571030	25,460	230	30,298	309	69.70	-153.80	U.S.A.	N. Alaska	North Slope, Ikpikpuk River	1
AAR-11183	x	YG	GYW	PH2	JN571028	25,490	230	30,333	308	63.90	-138.90	Canada	Dawson area, Yukon	Gold Bottom	1
OxA-16428	x	I-979	AMNH	JW548	JN570999	25,800	130	30,615	165	64.80	-147.70	U.S.A.	Fairbanks, Alaska	Ester Creek	1
AAR-11187	x	YG-5-121	GYW	PH6	JN571032	26,250	300	30,903	219	64.00	-139.20	Canada	Dawson area, Yukon	Hunker Creek	1
AA26859	-	A-517-1358	AMNH	JW357	JN570992	26,450	320	31,032	219	65.40	-147.10	U.S.A.	Fairbanks, Alaska	Fairbanks Creek	4
OxA-17685	x	YT03-46	GYW	JW612	JN571021	26,880	120	31,251	86	63.90	-139.30	Canada	Dawson area, Yukon	Irish Gulch	1
AA-37610	-	F:AM 6206	AMNH	-	AF326671	26,710	800	31,289	836	64.40	-147.30	U.S.A.	Fairbanks, Alaska	Ester Creek	3
OxA-14120	x	PIN Bkh-2002-30	PIN RAS	JW195	JN570958	27,700	140	31,764	244	72.20	126.10	Russia	Lena River Delta, N-E Siberia	Kurungnah, Buor-Khaya	1
GIN-10253	-	PIN Mkh-O 483	PIN RAS	JW203	JN570959	27,500	400	31,776	455	71.80	129.30	Russia	Lena River Delta, N-E Siberia	Mamontovy Khayata	5
OxA-14362	x	EK 994/4	IPAE	JW311	JN570974	28,060	140	32,252	322	59.00	58.80	Russia	Urals	Sur'ya 5	1
OxA-17679	x	YT03-144	GYW	JW604	JN571016	28,430	140	32,803	311	63.90	-139.30	Canada	Dawson area, Yukon	Irish Gulch	1
AA-37607	-	F:AM 4695	AMNH	-	AF326668	28,340	850	32,846	952	65.40	-147.10	U.S.A.	Fairbanks, Alaska	Gold Hill	3
OxA-17680	x	YT	GYW	JW605	JN571017	28,530	140	32,948	291	64.80	-139.40	Canada	Dawson area, Yukon	Dawson area	1
OxA-14304	x	EK 994/18	IPAE	JW316	JN570978	28,600	140	33,035	278	59.00	58.80	Russia	Urals	Sur'ya 5	1
OxA-14552	x	EK 994/3	IPAE	JW315	JN570977	28,640	160	33,080	313	59.00	58.80	Russia	Urals	Sur'ya 5	1
OxA-17681	x	YT03-254	GYW	JW606	JN571018	28,780	140	33,261	319	63.90	-139.30	Canada	Dawson area, Yukon	Irish Gulch	1
GIN-10672	-	BL-O 847	IEM RAS	JW28	JN570965	28,800	1,100	33,372	1,221	73.30	141.30	Russia	Novosibirsk Islands, N-E Siberia	Alyoshkina Zaimka	5
AAR-11186	x	YG-29-120	GYW	PH5	JN571031	29,450	350	34,070	416	64.00	-139.20	Canada	Dawson area, Yukon	Hunker Creek	1

AAR-11198	x	YG-5-50	GYW	PH38	JN571029	30,450	400	35,033	487	64.00	-139.20	Canada	Dawson area, Yukon	Hunker Creek	1
OxA-13675	-	PIN Bkh-2002-042	PIN RAS	JW190	DQ007577 1	31,220	180	35,735	360	72.20	126.10	Russia	Lena River Delta, N-E Siberia	Kurungnah, Buor-Khaya	6
OxA-17683	x	YT03-122	GYW	JW608	JN571019	31,540	170	35,880	362	63.70	-139.10	Canada	Dawson area, Yukon	Quartz Creek	1
OxA-17684	x	YT03-185	GYW	JW609	JN571020	31,680	180	36,258	372	64.80	-139.40	Canada	Dawson area, Yukon	n/a	1
OxA-14301	x	PIN 169-43	PIN RAS	JW209	JN570961	33,320	230	38,078	414	68.30	157.70	Russia	Kolyma lowlands, N-E Siberia	Omolon River mouth, Loc. 9	1
OxA-14380	x	EK 994/332	IPAE	JW341	JN570980	34,460	240	39,436	411	59.00	58.80	Russia	Urals	Sur'ya 5	1
CAMS-145090	x	F:AM 71464	AMNH	JAL246	JN570921	34,780	650	39,880	737	64.40	-147.30	U.S.A.	Nome dist., Alaska	Rainbow Mine	1
GIN-10699	-	BL-O 244	IEM RAS	JW29	JN570966	34,800	1,000	39,886	1,079	73.30	141.30	Russia	Novosibirsk Islands, N-E Siberia	Zimovye River mouth	5
CAMS-91789	x	n/a		IK009	JN570919	35,500	400	40,708	491	70.82	-154.30	U.S.A.	N. Alaska	North Slope, Ikpikpuk River	1
OxA-17687	x	YT110-13	GYW	JW614	JN571023	36,450	270	41,523	237	63.90	-139.30	Canada	Dawson area, Yukon	Irish Gulch	1
OxA-12906	x	EK 994/217	IPAE	JW17	JN570954	42,550	800	45,848	799	59.00	58.80	Russia	Urals	Sur'ya 5	1
OxA-13030	-	CMN-49368	CMN	JW98	DQ007557 DQ007610	43,900	180	46,760	416	67.30	-139.40	Canada	N. Yukon	Old Crow, Loc. 22	6

Supplementary Table S6.3 references

[1]This study

[2]Holmes, C.E. Archaeological testing and evaluation of the gerstle River Quarry, East-Central Alaska, 1996. Division of Parks and Outdoor Recreation, Alaska Department of Natural Resources, Office of History and Aracheology Report Number **85**, 1–18 (1998)

[3]Vila *et al*. Widespread origins of domestic horse lineages. *Science* **291**, 474–477 (2001)

[4]Guthrie, R. D., Rapid body size decline in Alaskan Pleistocene horses before extinction. *Nature* **426**, 169–171 (2003)

[5]Sher, A. V., Kuzmina, S. A., Kuznetsova, T. V. & Sulerzhitsky, L. D. New insights into the Weichselian environment and climate of the East Siberian Arctic, derived from fossil insects, plants, and mammals. *Quat. Sci. Rev.* **24**, 533-569 (2005)

[6]Weinstock *et al*. Evolution, Systematics, and Phylogeography of Pleistocene Horses in the New World: A Molecular Perspective. *PLoS Biol* **3**, e241.

Supplementary Table S6.4. Reindeer (*Rangifer tarandus*) sample information, listed by calibrated radiocarbon age. Data include radiocarbon age, locality information and institution currently housing the sample. BC denotes radiocarbon dates beyond the calibration curve. Information on new radiocarbon dates and GenBank accession numbers of new sequences (JN570760–JN570863) are included. GenBank accession numbers of previously published sequences used in the genetic analysis are included. References follow below the table.

AMS ID	New date	Collection no	Museum	Lab ID	New seq	14C date	14C SE	IntCal09 date	IntCal09 SE	LAT	LON	Country	Region	Ref
AA85585	x	3658-142	PIN RAS	289	-	133	43	0	0	69.96	147.56	Russia	Indigirka	1
AA83759	x	Ellef Ringnes Isl.	Private	308	-	0	0	0	0	78.78	-103.55	Canada	Canadian Arctic Archipelago	1
AA83779	x	620	KIC	1100	JN570796	0	0	0	0	74.00	101.00	Russia	Taimyr	1
AA83780	x	618	KIC	1101	-	0	0	0	0	74.00	101.00	Russia	Taimyr	1
AA83781	x	619	KIC	1103	JN570797	0	0	0	0	74.00	101.00	Russia	Taimyr	1
AA85594	x	616	KIC	1105	-	0	0	0	0	74.00	101.00	Russia	Taimyr	1
AA84492	x	614	KIC	1116	JN570807	0	0	0	0	74.00	101.00	Russia	Taimyr	1
AA83786	x	639	KIC	1118	-	0	0	0	0	74.00	101.00	Russia	Taimyr	1
AA84475	x	633	KIC	1125	-	0	0	0	0	74.00	101.00	Russia	Taimyr	1
AA83788	x	628	KIC	1127	-	0	0	0	0	74.00	101.00	Russia	Taimyr	1
AA84493	x	647	KIC	1129	-	0	0	0	0	74.00	101.00	Russia	Taimyr	1
AA83789	x	516	KIC	1131	-	0	0	0	0	74.00	101.00	Russia	Taimyr	1
AA84476	x	552	KIC	1152	-	0	0	0	0	74.00	101.00	Russia	Taimyr	1
AA83793	x	547	KIC	1155	JN570816	89	49	0	0	74.00	101.00	Russia	Taimyr	1
AA83794	x	700	KIC	1156	-	0	0	0	0	74.00	101.00	Russia	Taimyr	1
AA83796	x	749	KIC	1160	-	130	49	0	0	74.00	101.00	Russia	Taimyr	1
AA83798	x	747	KIC	1163	-	121	49	0	0	74.00	101.00	Russia	Taimyr	1
AA83799	x	1019	KIC	1168	-	0	0	0	0	74.00	101.00	Russia	Taimyr	1
AA83800	x	1021	KIC	1171	-	0	0	0	0	74.00	101.00	Russia	Taimyr	1
AA83810	x	CMN17521	CMN	1671	-	115	44	0	0	64.08	-139.43	Canada	Loy Lake	1
AA84483	x	CMN 17521	CMN	4396	-	220	120	0	0	64.08	-139.43	Canada	Dawson Area Loy Lake	1
AA85596	x	A-295-5223	AMNH	4808	-	112	44	0	0	64.83	-147.64	Canada	Fairbanks Ck	1
-	-	-	-	-	AF096422	0	0	0	0	52.81	-73.44	Canada	Quebec	3
-	-	-	-	-	AF096428	0	0	0	0	50.36	-85.36	Canada	Southeast Canada	3
-	-	-	-	-	AF096434	0	0	0	0	52.81	-73.44	Canada	Quebec	3
-	-	-	-	-	AF096443	0	0	0	0	52.09	-117.08	Canada	Southwest Canada	3
-	-	-	-	-	AY178677	0	0	0	0	69.81	-142.66	Alaska	Fairbanks	4
-	-	-	-	-	AY178686	0	0	0	0	75.09	-100.02	Canada	Canadian Archipelago	4
-	-	-	-	-	AY178688	0	0	0	0	78.82	18.11	Norway	Svalbard	4
-	-	-	-	-	AY178702	0	0	0	0	75.09	-100.02	Canada	Canadian Archipelago	4
-	-	-	-	-	AY178704	0	0	0	0	75.09	-100.02	Canada	Canadian Archipelago	4
-	-	-	-	-	AY178714	0	0	0	0	75.09	-100.02	Canada	Canadian Archipelago	4
-	-	-	-	-	EU653423	0	0	0	0	60.13	7.48	Norway	Hardangervidda, Langfjella	6

-	-	-	-	-	EU653483	0	0	0	0	61.47	8.74	Norway	Knutshø, Dovre/ Rondane	6
-	-	-	-	-	EU653574	0	0	0	0	61.49	145.38	Russia	Yakuts, Sakha Republic	6
-	-	-	-	-	EU653584	0	0	0	0	61.49	145.38	Russia	Yakuts, Sakha Republic	6
-	-	-	-	-	EU653587	0	0	0	0	61.49	145.38	Russia	Yakuts, Sakha Republic	6
-	-	-	-	-	EU653592	0	0	0	0	61.49	145.38	Russia	Yakuts, Sakha Republic	6
-	-	-	-	-	EU653691	0	0	0	0	64.11	29.45	Finland	Kuhmo, Kainnu	6
-	-	-	-	-	GU327544	90	40	0	0	60.31	-136.01	Alaska/Yukon	Sandpiper	5
-	-	-	-	-	GU327596	0	0	0	0	64.44	-141.03	Alaska/Yukon	Fortymile herd	5
-	-	-	-	-	GU327597	0	0	0	0	60.63	-135.58	Alaska/Yukon	Ibex herd	5
AA85597	x	1432/6	IPAE	1432-6_0	JN570767	0	0	0	0	68.13	69.09	Russia	Yamal	1
-	-	-	CGG	WPU-103-1_0	JN570792	0	0	0	0	68.95	64.92	Russia	West Polar Urals	1
-	-	-	CGG	WPU-106-1_0	JN570793	0	0	0	0	68.95	64.92	Russia	West Polar Urals	1
AA83785	x	615	KIC	1112	JN570804	138	41	140	83	74.00	101.00	Russia	Taimyr	1
AA84474	x	632	KIC	1123	JN570798	148	43	149	84	74.00	101.00	Russia	Taimyr	1
AA85588	x	1930/1	IPAE	1930-1	JN570768	156	44	157	86	70.00	71.00	Russia	Yamal	1
AA83783	x	617	KIC	1109	JN570803	162	33	174	86	74.00	101.00	Russia	Taimyr	1
AA84490	x	625	KIC	n/a	-	180	41	175	90	74.00	101.00	Russia	Taimyr	1
AA83802	x	748 /2003	KIC	1357	JN570820	195	49	178	98	74.00	101.00	Russia	Taimyr	1
B-212897	-	-	-	-	GU327578	190	40	178	92	61.04	-136.87	Alaska/Yukon	E. Thulsoo	5
B-212882	-	-	-	-	GU327579	190	40	178	92	60.58	-131.30	Alaska/Yukon	Irvine	5
AA83782	x	624	KIC	1107	JN570801	203	33	179	95	74.00	101.00	Russia	Taimyr	1
AA84472	x	634	KIC	1121	JN570810	195	53	179	101	74.00	101.00	Russia	Taimyr	1
AA84498	x	CMN 34646	CMN	n/a	-	255	43	303	113	64.08	-139.43	Canada	Dawson Area	1
AA83808	x	CMN12085	CMN	1662	JN570856	293	45	379	74	70.57	-128.22	Canada	Baillie ice. NW Territories	1
AA83797	x	746	KIC	1162	JN570818	361	50	408	59	74.00	101.00	Russia	Taimyr	1
B-162895	-	-	-	-	GU327577	360	40	408	57	60.40	-135.45	Alaska/Yukon	Alligator	5
AA83826	x	CMN 12085	CMN	4809	JN570857	375	45	428	60	70.57	-128.22	Canada	Baillie Is	1
AA83835	x	627	KIC	1113	JN570805	402	41	461	61	74.00	101.00	Russia	Taimyr	1
AA83757	x	210-44	PIN RAS	262	JN570828	500	47	530	41	75.37	135.59	Russia	Novosibirsk Islands	1
Ua-325	-	39b/1990	ZMK	ZM08	JN570862	700	100	658	83	81.60	-60.05	Greenland	Hall Land	2
B-217505	-	-	-	-	GU327568	790	40	711	31	61.29	-138.00	Alaska/Yukon	Upper Jo Jo	5
AA87167	x	75/1981	ZMK	ZM02	JN570858	928	35	849	45	64.23	-50.18	Greenland	Vesterbrygden (V51)	1
AA87166	x	15/1939	ZMK	ZM06	JN570860	943	35	853	43	65.57	-37.13	Greenland	Kap Dan	1
Ua-326	-	15/1939	ZMK	ZM07	JN570861	950	100	859	98	65.57	-37.13	Greenland	Kap Dan	2
-	-	-	-	-	GU327562	1,000	40	918	55	60.40	-135.45	Alaska/Yukon	Alligator	5
AA83768	x	48- 18987 (22)	ZIN RAS	859	JN570779	1,171	43	1,095	63	57.61	59.02	Russia	Urals, Central	1
AA84462	x	485	CGG	485	JN570836	1,303	44	1,236	46	70.54	158.91	Russia	Sibirien, Yakutien	1
AA85592	x	211-92	PIN RAS	275	JN570831	1,743	48	1,654	64	73.61	117.18	Russia	Laptev Sea Coast	1
B-162887	-	-	-	-	GU327575	1,940	40	1,890	48	60.39	-135.44	Alaska/Yukon	Friday Creek	5
B-162889	-	-	-	-	GU327574	2,320	40	2,340	71	60.39	-135.44	Alaska/Yukon	Friday Creek	5
B-162886	-	-	-	-	GU327549	2,340	40	2,355	76	60.40	-135.45	Alaska/Yukon	Alligator	5

-	-	-	-	-	GU327546	2,500	40	2,581	89	60.39	-135.44	Alaska/Yukon	Friday Crek	5
-	-	-	-	-	GU327549	2,500	40	2,581	89	60.39	-135.44	Alaska/Yukon	Friday Crek	5
-	-	-	-	-	GU327552	2,500	40	2,581	89	60.39	-135.44	Alaska/Yukon	Friday Crek	5
-	-	-	-	-	GU327565	2,500	40	2,581	89	60.39	-135.44	Alaska/Yukon	Friday Crek	5
B-162888	-	-	-	-	GU327557	2,510	40	2,586	86	60.39	-135.44	Alaska/Yukon	Friday Creek	5
B-162893	-	-	-	-	GU327576	2,550	40	2,628	85	60.39	-135.44	Alaska/Yukon	Friday Creek	5
B-212884	-	-	-	-	GU327569	2,700	40	2,804	35	60.17	-136.91	Alaska/Yukon	Vand Creek	5
AA83758	x	210-75	PIN RAS	264	JN570829	2,883	70	3,025	105	74.73	138.45	Russia	Novosibirsk Islands	1
-	-	-	-	-	GU327547	3,000	40	3,198	72	60.60	-136.26	Alaska/Yukon	Thandlat	5
B-162894	-	-	-	-	GU327561	3,140	40	3,369	47	60.60	-136.26	Alaska/Yukon	Thandlat	5
B-162885	-	-	-	-	GU327559	3,150	40	3,379	45	60.39	-135.44	Alaska/Yukon	Friday Creek	5
B-162897	-	-	-	-	GU327560	3,220	40	3,436	46	60.39	-135.44	Alaska/Yukon	Friday Creek	5
B-212894	-	-	-	-	GU327572	3,480	40	3,757	56	61.27	-138.08	Alaska/Yukon	Gladstone	5
-	x	114/1966	ZMK	ZM03	JN570859	3,565	110	3,866	151	64.37	-50.38	Greenland	Itivnera	1
AA84495	x	96	KIC	n/a	-	3,632	55	3,950	81	74.00	101.00	Russia	Taimyr	1
B-152439	-	-	-	-	GU327581	3,720	40	4,061	64	60.40	-135.45	Alaska/Yukon	Alligator	5
B-162892	-	-	-	-	GU327573	3,740	40	4,095	69	60.39	-135.44	Alaska/Yukon	Friday Creek	5
B-162882	-	-	-	-	GU327555	3,760	40	4,124	72	60.39	-135.44	Alaska/Yukon	Friday Creek	5
B-227525	-	-	-	-	GU327542	3,790	40	4,174	74	61.27	-138.08	Alaska/Yukon	Gladstone	5
B-227526	-	-	-	-	GU327543	3,820	40	4,217	78	61.27	-138.08	Alaska/Yukon	Gladstone	5
B-162884	-	-	-	-	GU327556	3,890	40	4,326	65	60.39	-135.44	Alaska/Yukon	Friday Creek	5
B-212895	-	-	-	-	GU327570	4,190	40	4,724	70	61.29	-138.00	Alaska/Yukon	L Gladstone	5
AA83790	x	715	KIC	1133	JN570813	4,516	56	5,161	99	74.00	101.00	Russia	Taimyr	1
Ua-328	-	117/1986	ZMK	ZM09	JN570863	4,660	135	5,368	186	66.50	-51.80	Greenland	Ivnajuattoq	2
AA84494	x	753	KIC	n/a	-	4,730	59	5,469	83	74.00	101.00	Russia	Taimyr	1
B-162890	-	-	-	-	GU327567	4,760	40	5,512	72	60.60	-136.26	Alaska/Yukon	Thandlat	5
B-212896	-	-	-	-	GU327571	4,830	40	5,544	54	61.27	-138.08	Alaska/Yukon	Gladstone	5
-	-	-	-	-	GU327545	5,000	40	5,731	74	61.27	-138.08	Alaska/Yukon	Gladstone	5

-	-	-	-	-	GU327550	5,000	40	5,731	74	60.74	-136.66	Alaska/Yukon	Bratneber	5
-	-	-	-	-	GU327553	5,000	40	5,731	74	61.27	-138.08	Alaska/Yukon	Gladstone	5
-	-	-	-	-	GU327554	5,000	40	5,731	74	61.27	-138.08	Alaska/Yukon	Gladstone	5
-	-	-	-	-	GU327564	5,000	40	5,731	74	61.27	-138.08	Alaska/Yukon	Gladstone	5
-	-	-	-	-	GU327566	5,000	40	5,731	74	61.27	-138.08	Alaska/Yukon	Gladstone	5
B-152440	-	-	-	-	GU327580	5,000	40	5,731	74	60.31	-136.00	Alaska/Yukon	Texas Gulch	5
B-162883	-	-	-	-	GU327558	5,710	40	6,497	57	60.34	-136.06	Alaska/Yukon	Sandpiper	5
B-162891	-	-	-	-	GU327563	6,320	40	7,250	51	60.31	-136.00	Alaska/Yukon	Texas Gulch	5
AA85589	x	1406/2	IPAE	1406-2	JN570766	7,431	77	8,256	82	70.00	72.00	Russia	Yamal	1
AA83770	x	69E- 34768	ZIN RAS	880	JN570782	10,122	99	11,732	211	62.00	58.67	Russia	Urals, Northern	1
AA84496	x	CMN 49615	CMN	4399	JN570849	11,020	110	12,904	132	64.08	-139.43	Canada	Dawson Area Hester Creek	1
AA83771	x	18E- 34768	ZIN RAS	829	JN570772	11,200	110	13,084	136	62.00	58.67	Russia	Urals, Northern	1
AA83805	x	P1S/87-54 BK-2	Landesdenkmalamt Baden-Wuerttemberg, Konstanz	1647	JN570762	12,550	130	14,701	300	47.95	8.85	Germany	Petersfels	1
AA84465	x	85E- 31608 (17)	ZIN RAS	896	JN570786	12,790	130	15,241	378	59.25	57.46	Russia	Urals, Central	1
OxA-21396	x	n/a	ZIN RAS	Zin-08	JN570795	13,100	50	15,870	332	60.00	113.80	Russia	East Siberia, south	1
AA83769	x	57E- 34768	ZIN RAS	868	JN570780	13,150	130	15,971	388	62.00	58.67	Russia	Urals, Northern	1
AA83778	x	104E- 34768	ZIN RAS	915	JN570790	13,220	130	16,103	386	62.00	58.67	Russia	Urals, Northern	1
AA83767	x	45E- 18993 (1)	ZIN RAS	856	JN570778	13,390	140	16,448	358	60.53	57.67	Russia	Ural, Chusovaya river, cave Dyrovataya	1
AA84497	x	CMN 44455	CMN	n/a	-	13,930	150	17,021	183	64.08	-139.43	Canada	Dawson Area Dominion Creek	1
AA83765	x	43E- 18993 (5)	ZIN RAS	854	JN570777	14,140	150	17,228	213	60.53	57.67	Russia	Ural, Chusovaya river, cave Dyrovataya	1
AA83775	x	86E- 31608 (12)	ZIN RAS	897	JN570787	14,215	85	17,297	179	59.25	57.46	Russia	Urals, Central	1
AA87053	x	17157 (2)	ZIN RAS	Zin-05	JN570794	14,310	150	17,408	227	55.98	92.74	Russia	Baikal	1
AA83806	x	MF(1537)10	n/a	1658	JN570763	14,430	170	17,549	257	50.09	19.91	Poland	Mammoth cave	1
AA83815	x	A-194-5925	AMNH	1683	JN570843	14,610	160	17,774	281	64.94	-147.67	USA	Engineer Creek, Alaska	1
AA83774	x	81E- 31608 (322)	ZIN RAS	892	JN570785	14,761	96	17,962	243	59.25	57.46	Russia	Urals, Central	1
AA84487	x	n/a	n/a	10411	JN570760	15,020	170	18,250	209	50.09	19.91	Poland	Mammoth Cave	1
AA84491	x	612	KIC	n/a	-	15,940	180	19,120	188	74.00	101.00	Russia	Taimyr	1
AA83761	x	27E- 34768	ZIN RAS	838	JN570773	16,010	200	19,152	202	62.00	58.67	Russia	Urals, Northern	1
AA83773	x	79E- 31608 (3)	ZIN RAS	890	JN570784	16,190	190	19,304	244	59.25	57.46	Russia	Urals, Central	1
AA83777	x	96E- 34768	ZIN RAS	907	JN570789	16,340	200	19,504	278	62.00	58.67	Russia	Ural, Medvezhya cave, 1960, Kuzmina	1
OxA-21397	x	5215	n/a	1695	JN570848	16,565	70	19,721	150	64.83	-147.65	USA	Gold-Hill, Alaska	1

AA85583	x	204-134	PIN RAS	257	JN570826	16,590	220	19,774	251	71.79	129.40	Russia	Lena Delta	1
AA85580	x	169-12	PIN RAS	241	JN570823	16,760	220	19,920	267	68.65	158.27	Russia	Yakutia, Kolyma	1
AA83801	x	94	KIC	1173	JN570819	17,120	170	20,347	311	74.00	101.00	Russia	Taimyr	1
AA83813	x	A-394-3315	AMNH	1674	JN570842	17,430	220	20,785	313	64.83	-147.65	USA	Cripple Creek, Alaska	1
AA84481	x	V-54-572	n/a	1694	JN570847	17,440	190	20,790	291	64.07	-141.90	USA	Lost Chicken, Alaska	1
AA85578	x	153-42	PIN RAS	229	JN570821	18,090	240	21,660	340	69.18	148.66	Russia	Indigirka	1
AA85579	x	161-149	PIN RAS	235	JN570822	18,500	250	22,036	330	70.56	149.71	Russia	Indigirka	1
AA84473	x	634	KIC	1122	JN570811	18,500	180	22,047	261	74.00	101.00	Russia	Taimyr	1
AA83818	x	V-54-653	n/a	1692	JN570846	18,570	250	22,123	356	64.07	-141.90	USA	Lost Chicken, Alaska	1
AA83776	x	91E- 31608 (294)	ZIN RAS	902	JN570788	18,620	250	22,189	374	59.25	57.46	Russia	Urals, Central	1
AA84469	x	613	KIC	1115	JN570806	18,770	190	22,392	321	74.00	101.00	Russia	Taimyr	1
AA85590	x	210-103	PIN RAS	258	JN570827	19,205	280	22,925	362	74.25	140.35	Russia	Novosibirsk Islands	1
AA84480	x	A-600-1535	AMNH	1690	JN570845	19,370	220	23,071	334	65.37	-164.75	USA	Atlas Creek, Alaska	1
AA84477	x	HOF01/abc5505	State Museum Natural Hicetory Stuttgart	1636	JN570761	19,420	330	23,153	436	48.38	9.75	Germany	Hohlefels cave	1
AA84501	x	550	KIC	n/a	-	19,430	280	23,154	394	74.00	101.00	Russia	Taimyr	1
AA83812	x	CMN47679	CMN	1673	JN570841	19,720	330	23,566	458	64.03	-140.73		60 mile Loc5	1
AA85582	x	200-337	PIN RAS	244	JN570825	20,500	320	24,486	409	71.79	129.40	Russia	Lena Delta	1
AA83762	x	38E- 21838 (770)	ZIN RAS	849	JN570774	20,810	330	24,851	444	51.90	103.60	Russia	Siberia, Baikal area	1
AA84468	x	611	KIC	1108	JN570802	20,840	350	24,895	471	74.00	101.00	Russia	Taimyr	1
AA83763	x	39E- 21838 (155)	ZIN RAS	850	JN570775	20,940	340	25,024	465	51.90	103.60	Russia	Siberia, Baikal area	1
AA85595	x	651	KIC	1148	JN570815	21,202	349	25,377	483	74.00	101.00	Russia	Taimyr	1
AA83764	x	40E- 21838 (100)	ZIN RAS	851	JN570776	21,220	340	25,397	472	51.90	103.60	Russia	Siberia, Baikal area	1
AA84461	x	484	CGG	484	JN570835	21,820	280	26,194	467	70.54	158.91	Russia	Sibirien, Yakutien	1
AA85593	x	875/24	IPAE	875-24	JN570781	22,410	403	27,056	562	59.27	62.21	Russia	West Siberia, southwest	1
AA84463	x	494	CGG	494	JN570837	22,690	300	27,365	431	70.54	158.91	Russia	Sibirien, Yakutien	1
AA85587	x	465	CGG	465	JN570833	23,120	440	27,897	577	70.54	158.91	Russia	Sibirien, Yakutien	1
AA83824	x	CMN 37930	CMN	4409	JN570852	23,320	450	28,143	572	64.08	-139.43	Canada	Dawson Area Loc. 45	1
OxA-21399	x	915/93, 71	IPAE	915-93-71	JN570791	23,670	120	28,403	199	58.00	69.00	Russia	West Siberia, center	1
AA83811	x	CMN49615	CMN	1672	JN570840	23,720	510	28,590	569	64.08	-139.43	Canada	Hester Creek, Yukon	1
AA84471	x	629	KIC	1119	JN570809	23,850	480	28,726	516	74.00	101.00	Russia	Taimyr	1

AA84486	x	n/a	n/a	9999	JN570855	24,700	530	29,560	570	64.08	-139.43	Canada	Dawson, Quartz Ck	1
AA83827	x	n/a	n/a	9788	JN570853	24,900	550	29,775	564	60.72	-135.05	Canada	Whitehorse, Yukon	1
AA83784	x	622	KIC	n/a	-	25,300	440	30,113	424	74.00	101.00	Russia	Taimyr	1
AA84470	x	610	KIC	1117	JN570808	25,710	600	30,462	504	74.00	101.00	Russia	Taimyr	1
AA83821	x	CMN 35558	CMN	4403	JN570851	25,800	620	30,528	514	64.08	-139.43	Canada	Dawson Area Hunker Creek	1
AA83807	x	930	n/a	1661	JN570764	26,760	680	31,283	682	50.83	20.50	Poland	Raj cave, Poland	1
AA84466	x	621	KIC	1104	JN570799	26,940	700	31,463	728	74.00	101.00	Russia	Taimyr	1
AA85584	x	3657-220	PIN RAS	287	JN570832	27,630	760	32,184	829	70.55	147.40	Russia	Indigirka	1
AA83772	x	74E- 34768	ZIN RAS	885	JN570783	27,720	760	32,261	836	62.00	58.67	Russia	Urals, Northern	1
AA83787	x	636	KIC	1126	JN570812	29,130	660	33,689	787	74.00	101.00	Russia	Taimyr	1
AA83828	x	n/a	n/a	9880	JN570854	29,260	640	33,821	747	64.08	-139.43	Canada	Quartz Ck, Yukon	1
AA83791	x	717	KIC	1135	JN570814	29,660	710	34,200	827	74.00	101.00	Russia	Taimyr	1
AA84467	x	626	KIC	1106	JN570800	30,340	530	34,991	625	74.00	101.00	Russia	Taimyr	1
AA85581	x	200-330	PIN RAS	243	JN570824	30,800	1,100	35,611	1,286	71.79	129.40	Russia	Lena Delta	1
AA87052	x	398/234	IPAE	398-234	JN570770	31,100	1,200	35,944	1,418	59.25	62.20	Russia	WestBeringia	1
AA84460	x	466	CGG	466	JN570834	31,550	860	36,171	993	70.54	158.91	Russia	Sibirien, Yakutien	1
AA83819	x	CMN 25176	CMN	4400	JN570850	31,400	1,200	36,225	1,412	64.08	-139.43	Canada	Dawson Area Hunker Creek	1
AA87051	x	1077/5	IPAE	1077-5	JN570765	31,800	1,300	36,698	1,539	55.98	92.74	Russia	WestBeringia	1
AA83795	x	548	KIC	1157	JN570817	32,360	990	37,190	1,219	74.00	101.00	Russia	Taimyr	1
AA84488	x	n/a	n/a	10790	JN570838	32,600	1,400	37,623	1,636	64.08	-139.43	Canada	Dawson area, Irish Gulch, Yukon	1
AA84464	x	17E- 34768	ZIN RAS	828	JN570771	33,900	1,600	38,995	1,758	62.00	58.67	Russia	Urals, Northern	1
AA85591	x	211-104	PIN RAS	269	JN570830	34,051	1,690	39,171	1,848	73.61	117.18	Russia	Laptev Sea Coast	1
AA83809	x	CMN25242	CMN	1668	JN570839	34,300	1,800	39,442	1,964	64.83	-147.65	Canada	Cripple Hill, Yukon (?)	1
OxA-21398	x	1930/3	IPAE	1930-3	JN570769	34,800	260	39,858	442	70.00	71.00	Russia	Yamal	1
AA84479	x	A-329-2357	AMNH	1689	JN570844	37,500	1,500	42,384	1,335	64.83	-147.65	USA	Cripple Creek, Alaska	1
OxA-21395	x	851-087	GIN RAS	307	-	46,300	750	BC		68.13	157.84	Russia	Yakutia, Kolyma	1
AA83760	x	3E- 35601	ZIN RAS	814	-	37,900	2,700	BC		51.40	39.05	Russia	European Russia, Center	1
AA83814	x	A-521-3878	AMNH	1676	-	40,700	3,800	BC		64.83	-147.65	Canada	Fairbanks area, Cripple	1
AA84484	x	CMN 35961	CMN	4398	-	37,900	2,000	BC		64.08	-139.43	Canada	Dawson Area/Hunker Creek?	1
AA83820	x	CMN 35564	CMN	4401	-	38,100	2,800	BC		64.08	-139.43	Canada	Dawson Area/Hunker Creek?	1
AA84499	x	103.92	John Storer, Withehorse	n/a	-	37,300	2,500	BC		64.08	-139.43	Alaska/Yukon	Irish Gulch	1
AA83755	x	F-0516	IAM	216	-	>41,100		Infinite		70.87	155.60	Russia	Rang Kolyma F-516	1

AA83756	x	F-0588	IAM	218	-	>41,100	Infinite	70.50	156.80	Russia	Yakutia, Kolyma	1
AA85577	x	F-1754	IAM	223	-	>40,800	Infinite	68.60	147.06	Russia	Yakutia, Indigirka	1
AA85586	x	3915-258	PIN RAS	295	-	>39,000	Infinite	71.68	148.12	Russia	Indigirka	1
AA84489	x	469	CGG	469	-	>41,100	Infinite	70.54	158.91	Russia	Sibirien, Yakutien	1
AA83816	x	V-18-3	n/a	1686	-	>41,100	Infinite	64.83	-147.65	Alaska	Fairbanks area, Ester Creek	1
AA83817	x	V-54-1731	n/a	1691	-	>38,000	Infinite	64.07	-141.90	Alaska	Lost Chicken	1
AA84482	x	CMN 47799	CMN	4164	-	>35,000	Infinite	64.03	-140.73	Canada	60-mile R. Y.T., Loc. 3	1
AA84503	x	CMN 47722	CMN	4405	-	>36,100	Infinite	64.03	-140.73	Canada	60-mile, Loc. 3	1
AA84504	x	CMN 44585	CMN	4406	-	>34,800	Infinite	64.07	-139.43	Canada	Dawson Area Hunker Creek	1
AA83822	x	CMN 45467	CMN	4407	-	>41,100	Infinite	64.07	-139.43	Canada	Dawson Area Eldorado Creek	1
AA83823	x	CMN 25242	CMN	4408	-	>41,100	Infinite	64.07	-139.43	Canada	Dawson Area Cripple Hill	1
AA83825	x	CMN 37935	CMN	4410	-	>39,700	Infinite	64.07	-139.43	Canada	Dawson Area Loc. 45	1
AA84485	x	CMN 42376	CMN	4413	-	>40,400	Infinite	64.03	-140.73	Alaska	60-mile, Loc. 3`	1

Supplementary Table S6.4 references

[1]This study

[2]Meldgaard, M. The Greenland caribou – zoogeography, taxonomy, and population dynamics. *Meddelelser om Grønland Bioscience* **29**, 1–88 (1986)

[3]Dueck, G.S. *Genetic relationships and phylogeography of woodland and Barrenground caribou*. M.Sc. thesis, University of Alberta, Canada (1998)

[4]Flagstad, Ø. & Røed, K. H. Refugial origins of reindeer (Rangifer tarandus L.) inferred from mitochondrial DNA sequences. Evolution 57, 658–670 (2003)

[5]Kuhn, T. S., McFarlane, K. A., Groves, P., Mooers, A. O. & Shapiro, B. Modern and ancient DNA reveal recent partial replacement of caribou in the southwest Yukon. *Mol. Ecol.* **19**, 1312–1323 (2010)

[6]Røed, K.H. et al. Genetic analyses reveal independent domestication origins of Eurasian reindeer. *Proc. R. Soc. B* **275**, 1849–1855 (2008)

Supplementary Table S6.5. Megafaunal taxa present in Upper Palaeolithic archaeological sites of Siberia, by calibrated radiocarbon age. Table includes information on the minimum number of megafauna individuals reported at each site (NISP). The data are presented in Figure 4 of the main text. References are listed below table.

Site	^{14}C Age	^{14}C SE		Cal BP	Cal BP (σ)	Woolly rhinoceros	Woolly mammoth	Horse	Reindeer	Bison	Musk ox	NISP	LAT	LON	Ref.‡
Ushki, layer 6	10354	31	†	12208	97			x		x		n/a	56.17	159.95	11
Ust'-Timpton, layer 6	10421	53	†	12298	119				x			2	58.7	127.12	24
Kaminnaia Cave, layer 11a	10683	137	†	12593	170	x				x?		79	51.2	84.6	9
Kaminnaia Cave, layer 11b	10860	360		12741	436	x		x		x?		426	51.2	84.6	9
Oshurkovo, layer 2	11108	69	†	12993	106			x	x			n/a	51.96	107.49	32
Makarovo-2, layer 3	11707	245	†	13581	274			x*	x?	x		n/a	54	105.84	32
Makarovo-2, layer 4	11950	50		13809	73			x				n/a	54	105.84	32
Bol'shoi Iakor'-1, layer 4B	11970	170		13833	247				x	x		31	57.82	113.98	17
Bol'shoi Iakor'-1, layer 5	12050	120		13912	174				x	x		~361	57.82	113.98	17
Berelekh	12078	21	†	13919	62	x	x	x	x	x	x	1003	70.43	143.94	24
Ust'-Kiakhta-17, layer 5	12143	62	†	13988	108			x	x?	x		n/a	50.35	106.45	31
Maininskaia, east layer 2-1	12173	93	†	14035	202					x		57	52.98	91.5	33
Maininskaia, west, layer A1	12110	220		14064	380					x		158	52.98	91.5	33
Ust'-Mil'-2, layer A	12200	170		14169	332		x	x	x	x	x?	n/a	59.64	133.1	24
Bol'shoi Iakor'-1, layer 6	12380	200		14483	359				x		x	~153	57.82	113.98	17
Tashtyk-1, layer 1	12413	88	†	14494	256			x	x			78	54.61	90.99	2

Bol'shoi Iakor'-1, layer 7	12380	250		14502	438				x		x	~322	57.82	113.98	17
Diuktai Cave, layer 7a	12480	99	†	14604	265		x	x	x	x		>72	59.3	132.6	24
Verkholenskaia Gora, layer 3	12570	180		14729	389	x		x*	x	x		~50	52.36	104.28	13
Bol'shoi Iakor'-1, layer 8	12630	230		14871	528			x	x			18	57.82	113.98	17
Kokorevo-3	12690	140		14992	382			x	x	x		363	54.93	90.94	1
Bol'shoi Iakor'-1, layer 9	12700	140		15016	387				x		x	226	57.82	113.98	17
Kokorevo-2	12710	71	†	15061	218		x	x	x			598	54.93	90.94	1
Listvenka, layer 8	12750	140		15138	402		x	x	x	x		n/a	55.95	92.4	3
Ui-2, layer 3	12910	54	†	15420	271					x		8	52.97	91.49	33
Bol'shaia Slizneva, layer 7	12930	60		15462	291		x	x	x	x		n/a	55.96	92.6	35
Novoselovo-6	12913	135	†	15523	381				x	x		9481	55.07	91.11	2
Kokorevo-1, layer 2	12993	238	†	15722	508			x*	x	x		>67	54.92	90.93	2
Golubaia-1, layer 3	13065	89	†	15800	356			x*		x		7**	52.98	91.51	5
Diuktai Cave, layer 7v	13110	90		15895	358		x	x	x	x		163	59.3	132.6	24
Listvenka, layer 10	13200	110		16077	371		x	x*	x	x		n/a	55.95	92.4	3
Ui-2, layer 2	13260	270		16079	489			x		x		29	52.97	91.49	33
Divnyi-1	13220	150		16090	401				x	x		n/a	55.08	91.31	22
Maininskaia, east, layer 4	13217	124	†	16102	382					x		65	52.98	91.5	33
Maininskaia, east, layer 3	13302	86	†	16334	332					x		73	52.98	91.5	33
Bol'shaia Slizneva, layer 8	13540	500		16388	775					x		n/a	55.96	92.6	35
Diuktai Cave, layer 7b	13317	58	†	16412	293		x	x		x		70	59.3	132.6	24

Tashtyk-2, layer 2	13550	320		16495	540			x	x		n/a	54.61	90.99	2
Afontova Gora-2	13373	46	†	16537	232		x	x*	x	x	~100	55.99	92.79	6
Listvenka, layer 12	13437	126	†	16550	310		x	x*	x	x	n/a	55.95	92.4	3
Listvenka, layer 6	13677	280	†	16740	468				x	x	n/a	55.95	92.4	3
Kokorevo-1, layer 3	13633	45	†	16787	91			x*	x	x	>97	54.92	90.93	2
Volch'ia Griva†	13679	74	†	16818	100		x	x		x	1392	55.19	75.64	28
Novoselovo-13, layer 1	14097	190	†	17199	236			x*	x	x	n/a	55.07	91.11	22
Biriusa-1	14238	52	†	17319	163			x*	x	x	n/a	55.85	92.22	21
Listvenka, layer 9	14307	78	†	17396	180			x	x	x	n/a	55.95	92.4	3
Kokorevo-4a, layers 5-3	14320	330		17469	392	x		x	x	x	n/a	54.94	90.96	4
Chernoozer'e 2	14500	50		17654	167			x			~300	55.74	73.99	28
Kurtak-3, excav. 1	14652	66	†	17825	165				x	x	n/a	55.15	91.56	22
Tashtyk-4, layer 2	14700	150		17896	280					x	n/a	54.61	90.99	2
Oznachennoe-1	14713	67	†	17898	197			x	x		n/a	53.08	91.42	5
Listvenka, layer 7	14750	250		17966	347		x		x	x	n/a	55.95	92.4	3
Novoselovo-7	15190	93	†	18330	190			x	x	x	928	55.07	91.11	2,22
Kokorevo-4b, layer 2	15460	320		18689	365				x	x	97	54.94	90.96	4
Maininskaia, east, layer 1	15500	150		18717	154					x	39	52.98	91.5	33
Ust'-Menza-2, layer 17	15900	313	†	19099	298			x	x?	x	n/a	50.23	108.63	19
Verkhne Troitskaia, layer 6	16347	99	†	19499	157	x	x		x	x	72	60.35	134.45	24
Sokhatino-4	16345	226	†	19513	300		x			x	n/a	51.99	113.46	26
Maininskaia, east, layer 5	16419	124	†	19559	176					x	107	52.98	91.5	33

Listvenka, layer 19	17013	192	†	20201	318		x	x*	x			n/a	55.95	92.4	3
Listvenka, layer 15	17080	485		20391	605		x	x*		x		n/a	55.95	92.4	3
Ezhantsy, layer 3	17150	345		20446	474	x	x	x	x	x		415	60.48	135.15	24
Ui-1, layer 2	17995	75	†	21454	138			x*		x		173	52.97	91.49	33
Shikaevka-2	18050	95		21524	190		x		x			314	55.9	65.8	28
Tomsk	18300	1000		21973	1284		x					n/a	56.46	84.93	28
Krasnyi Iar, layer 6	19100	100		22779	253	x			x			n/a	53.6	103.4	8
Shlenka	19193	89	†	22879	243		x	x	x	x		~1500	55.2	91.93	22
Tarachikha	19543	56	†	23378	209		x	x	x	x		n/a	55.05	91.04	22
Kunalei, comp. 3	21100	300		25241	423	x		x		x		n/a	50.64	107.64	18
Mal'ta	21157	37	†	25247	155	x	x	x	x	x		66**	52.83	103.55	13
Buret'	21190	100		25306	201	x	x	x*	x	x		>61	52.99	103.51	13
Novoselovo-13, layer 3	22000	700		26510	925		x		x			n/a	55.07	91.11	22
Alekseevsk	22415	480		27047	640				x			n/a	57.84	108.34	36
Igeteiskii Log	22426	171	†	27157	372	x	x	x	x			134	53.57	103.48	23
Ust'-Kova, middle comp.	22477	185	†	27217	363		x	x	x	x		>10,000	50.3	100.11	34
Kashtanka, layer 1	22635	174	†	27337	321			x	x	x		269	55.14	91.52	12
Arta-2, layer 3	23200	2000		28181	2757	x		x		x		n/a	51.19	112.3	10
Anui-2, layer 11	23431	1547		28277	1852					x		<9	51.39	84.68	10
Kuilug Khem-1, layer 4	23600	400		28435	464			x*		x		n/a	51.99	92.96	30
Sabanikha	23979	217	†	28837	289				x	x		n/a	54.61	90.96	22
Kurtak-4, layer 1	24150	137	†	28970	235	x		x		x		n/a	55.15	91.56	22
Priiskovoe	25825	290		30636	267			x		x		n/a	50.15	108.32	20
Ikhine-2, layer 2b	26177	143	†	30904	152	x	x	x	x	x		126	63.11	133.62	24
Tolbaga	27346	146	†	31465	142	x	x	x*				494	51.21	109.32	27
Yana RHS	27895	54	†	31943	249	x	x	x	x	x	x	2380	70.72	135.42	29

Ikhine-2, layer 2g	27800	500		32143	594	x	x	x	x	x	94	63.11	133.62	24
Malaia Syia	28118	196	†	32339	363	x		x*	x	x	685	54.41	89.44	25
Ust'-Mil' 2, layer B	28250	354	†	32524	527	x	x				n/a	63.11	133.62	24
Nepa-1	28410	295	†	32729	492	x		x			n/a	59.99	108.37	15
Kamenka, Complex B	28563	143	†	32989	288	x					15	51.74	108.3	14
Kamenka, Complex A	29308	166	†	34006	330			x		x	1978	51.74	108.3	14
Ikhine-2, layer 2v	29667	439	†	34234	492	x		x	x	x	32	63.11	133.62	24
Voennyi Gospital	29700	500		34254	563	x		x	x	x	n/a	52.28	104.25	23
Masterov Kliuch, comp 1	30743	845	†	35489	909			x			18	51.4	110.65	16
Ust'-Mil' 2, layer V	31800	386	†	36294	523	x	x	x		x	n/a	63.11	133.62	24
Kurtak-4, layer 2	32137	248	†	36653	311		x	x*		x	n/a	55.15	91.56	22
Varvarina Gora	32379	411	†	37003	575	x		x*			1120	51.58	108.12	27
Podzvonkaia	35249	500		40381	614			x		x	42	50.21	107.32	7

*May include *Equus hemionus*.

†Radiocarbon age is average of two or more.

‡References for faunal data.

Supplementary Table S6.5 references

[1] Abramova, Z. A. *Paleolit Eniseia: Afontovskaia Kul'tura* [in Russian] (Nauka, Leningrad, 1979a) [in Russian]

[2] Abramova, Z. A. *Paleolit Eniseia: Kokorevskaia Kul'tura* [in Russian] (Nauka, Leningrad, 1979b) [in Russian]

[3] Akimova, E. V. *et al. Paleolit Eniseia: Listvenka* [in Russian] (Institut Arkheologii i Etnografii Sibirskogo Otdeleniia Rossiiskoi Akademii Nauk, Krasnoiarsk, 2005) [in Russian]

[4] Astakov, S. N. PozdnePaleoliticheskaia stoianka Kokorevo 4. *Sovetskaia Arkheologiia* **2**, 288-294 (1966) [in Russian]

[5] Astakhov, S. N. *Paleolit Tuvy* (Sibirskoe Otdelenie, Akademiia Nauk SSSR, Krasnoiarsk, 1986) [in Russian]

[6] Astakhov, S. N. *Paleolit Eniseia: Paleoliticheskie Stoianki Afontovoi Gore v G. Krasnoiarske* (RAN, St. Petersburg, 1999) [in Russian].

[7] Caiwe, N. *et al.* Le Paleolithique superior ancient de Siberie. Les fouilles de Frans Steenhoudt et de Vasily Tashak en Bouriatie. *Bulletin Musees R D'Art D'Hist* **64**, 129-149 (1993) [in Russian]

[8] Derev'anko, A. P. *The Paleolithic of Siberia: New Discoveries and Interpretations* (University of Illinois Press, Urbana and Chicago, 1998)

[9] Derevianko, A. P. *et al. Arkheologiia, Geologiia i Paleogeografiia Pleistotsena i Golotsena Gornogo Altaia* (Izdatel'stvo Instituta Arkheologii i Etnografii SO RAN, Novosibirsk, 1998) [in Russian]

[10] Derevianko, A. P. *et al. Prirodnaia Sreda i Chelovek v Paleolite Gornogo Altaia* (Izdatel'stvo Instituta Arkheologii i Etnografii SO RAN, Novosibirsk, 2003) [in Russian]

[11] Dikov, N. N. *Arkheologicheskie Pamiatniki Kamchatki, Chukotki i Verkhnei Kolymy (Aziia na Styke s Amerikoi v Drevnosti)* (Nauka, Moscow, 1977) [in Russian]

[12] Drozdov, N. I., Chekha, V. P., & Artem'ev, E. V. in *Arkheologiia, Geologiia i Paleogeografiia Paleoliticheskikh Pamiatnikov Iuga Srednei Sibiri (Severo-Minusinskaia Vpadina, Kuznetskii Alatai i Vostochnyi Saian* (ed Derevianko, A. P., Drozdov, N. I., & Chekha, V. P.), (RAN, Krasnoiarsk, 1992) [in Russian]

[13] Ermalova, N. M. *Teriofauna Doliny Angary v Pozdnem Antropogene* (Nauka, Novosibirsk, 1978) [in Russian]

[14] Germonpre, M. & Lbova, L. Mammalian remains from the Upper Paleolithic site of Kamenka, Buryatia (Siberia). *J. Archaeolog. Science* **23**, 35-57 (1996)

[15] Goebel, T. in *Entering America: Northeast Asia and Beringia before the Last Glacial Maximum* (ed Madsen, D. B.) (University of Utah Press, Salt Lake City, pp. 311-356 (2004)

[16] Goebel , T., Waters, M. R., & Meshcherin, M. N. Masterov Kliuch and the early Upper Paleolithic of the Transbaikal, Siberia. *Asian Perspectives* **39**, 47-70 (2000)

[17] Ineshin, E. M. & Teten'kin, A. V. *Chelovek i Prirodnaia Sreda Severa Baikal'skoi Sibiri v Pozdnem Pleistotsene. Mestonakhozhdenie Bol'shoi Iakor' I* (Nauka, Novobisirsk, 2010) [in Russian]

[18] Konstantinov, M. V. in *Arkheologicheskii Poisk (Severnaia Azii)* (Nauka, Novosibirsk, pp. 16-24, 1980) [in Russian]

[19] Konstantinov, M. V. *Kamennyi Vek Vostochnogo Regiona Baikal'skoi Azii* (Izdatel'stvo ION BNTS SO RAN/Izdatel'stvo CHGPI Im. N. G. Chernyshevskogo, Ulan-Ude/Chita, 1994) [in Russian]

[20] Konstantinov, M. V. & Konstantinov, A. V. in *Problemy Khronologii i Pervobytnaia Iuzhnoi Sibiri* (Nauka, Barnaul, pp. 13-15, 1991) [in Russian]

[21] Kuzmina , I. & Sinitsyna, G. in *Pervoe Mezhdunarodnoe Mamontovoe Soveshchanie* (St. Petersburg, 1995) [in Russian]

[22] Lisitsyn, N. F. *Pozdnii Paleolit Chulymo-Eniseiskogo Mezhdurech'ia* (Trudy Tom II, Institut Istorii Material'noi Kul'tury, RAN, St. Petersburg, 2000) [in Russian]

[23] Medvedev, G. I., Savel'ev, N. A., Svinin, V. V. *Stratigrafiia, Paleogeografiia i Arkheologiia Iuga Srednei Sibiri* (Irkutskii Gosudarstvennyi Universitet, Irkutsk, 1990) [in Russian]

[24] Mochanov, I. U. A. *Drevneishie Etapy Zaseleniia Chelovekom Severo-Vostochnoi Azii* (Nauka, Novosibirsk, 1977) [in Russian]

[25] Muratov, V. M., Ovodov, N. D., Panychev, V. A., & Safarova, S. A. in *Arkheologiia Severnoi Azii* (Nauka, Novosibirsk, pp. 33-48, 1982) [in Russian]

[26] Okladnikov, A. P. & Kirillov, I. I. *Iugo-Vostochnoe Zabaikal'e v Epokhy Kamnia i Rannei Bronzy* (Nauka, Novosibirsk, 1980) [in Russian]

[27] Ovodov, N. D. in *Prirodnaia Sreda i Drevnii Chelovek v Pozdnem Antropogene* (Nauka, Ulan-Ude, pp. 122-140, 1987) [in Russian]

[28] Petrin, V. T. *Paleoliticheskie Pamitaniki Zapadno-Sibirskoi Ravniny* (Nauka, Novosibirsk, 1986) [in Russian]

[29] Pitulko, V. V. *et al.* Yana RHS site: humans in the Arctic before the last glaciation. *Science* **303**, 52-56 (2004)

[30] Semenov, V. A., Vasil'ev, S. A., Zaitseva, G. I., Kilunovskaya, M. E., & Kasparov, A. K. Kuilug-Khem 1: a new Paleolithic cave site in Tuva (south Siberia, Russia). *Current Research in the Pleistocene* **22**, 9-11 (2005)

[31] Tashak, V. I. in *100 Let Gunnskoi Arkheologii. Nomadizm Proshloe, Nastoiashchee v Global'nom Kontekste i Istoricheskoi Perspective. Gunnskii Fenomen. (Tezisy Dokladov) II Chast'*. Rossiiskaia Akademiia Nauk, Sibirskoe Otdelenie, Ulan-Ude, pp. 61-64, 1996) [in Russian]

[32] Tseitlin, S. M. *Geologiia Paleolita Severnoi Azii* (Nauka, Moscow, 1979) [in Russian]

[33] Vasil'ev, S. A. *Pozdnii Paleolit Verkhnego Eniseia* (RAN, IIMK, St. Petersburg, 1996) [in Russian]

[34] Vasil'evskii, R. S., Burilov, V. V., & Drozdov, N. I. *Arkheologicheskie Pamiatniki Severnogo Priangar'ia* (Nauka, Novosibirsk, 1988) [in Russian]

[35] Vdovin , A. S., Iamskikh, A. F., Iamskikh, G. I. U., & Ovodov, N. D. in *Arkheologiia, Geologii i Paleogeografiia Paleoliticheskikh Pamiatnikov Iuga Srednei Sibiri* (ed Derevianko, A. P., Drozdov, N. I., & Chekha, V. P.) (Nauka, Krasnoiarsk, pp. 21-34, 1992) [in Russian]

[36] Zadonin, O. V., Khomik, S. N., & Krasnoshchekov, V. V. in *Problemy Arkheologii i Etnografii Sibiri i Dal'nego Vostoka, 1*. Nauka, Krasnoiarsk, pp. 45-48, 1991) [in Russian]